Theory and Simulation of Thermodynamics and Flow Induced Order in Carbonaceous Mesophase Binary Mixtures

Mojdeh Golmohammadi

Doctor of Philosophy

Department of Chemical Engineering

McGill University
Montreal, Quebec
August 2010

DEDICATION

To my FAMILY …

to my parents & …

to my brother and sister,

for their deep, ocean like pure love and their unconditional, endless support

through my life

&

to those

who gave me the chance to fully feel and experience

both aspects of life:

joy to become happier and sadness to become wiser.

Foreword

The author chooses the manuscript-based thesis option.

Contribution of Authors

Contents of chapters 2 to 6 of the present thesis are adopted or revised from the papers that have been published or submitted for publication in scientific journals under the normal supervision of my research supervisor, Professor A.D. Rey, who is also co-author. Specific mathematical derivations of new theories are the work of Professor Rey as outlined below:

Chapter 2:

The equations derived for: the tensor order parameter of the mixture (eqn. 2.3), the entropy per molecule (Appendix A, A2.3), thermodynamic consistency check (Appendix A, A2.6) and orientation distribution function of the components and the mixture (Appendix B, A2.11) are the work of Professor Rey.

Chapter 3: The equations derived for the latten heat at the NI transition (section 3.5) is the work of Professor Rey.

Chapter 4: The equations derived for: flow induced order and flow induced alignment (Appendix A, A4.4) and dissipation function (Appendix B, A4.5) are the work of Professor Rey.

Publisher Copyright Authorization

Article

Entropic Behavior of Binary Carbonaceous Mesophases

Mojdeh Golmohammadi ✉ and **Alejandro D. Rey** * ✉

Department of Chemical Engineering, McGill University, Montreal, Quebec H3A 2B2, Canada
* Author to whom correspondence should be addressed.

(This article belongs to the Special Issue Configurational Entropy)

📄   **Download PDF Full-Text** **[392 KB, uploaded 16 September 2008 11:01 CET]**

Abstract: The Maier-Saupe model for binary mixtures of uniaxial discotic nematogens, formulated in a previous study [1], is used to compute and characterize orientational entropy [2] and orientational specific heat. These thermodynamic quantities are used to determine mixture type (ideal or non-ideal) which arise due to their different intrinsic properties, determined by the molecular weight asymmetry ΔM_w and the molecular interaction parameter β. These molecular properties are also used to characterize the critical concentration where the mixture behaves like a single component system and exhibits the minimum nematic to isotropic (NI) transition temperature (pseudo-pure mixture). A transition within the nematic phase takes place at this specific concentration. According to the Maier-Saupe model, in a single mesogen, entropy at NI transition is a universal value; in this work we quantify the mixing effect on this universal property. The results and analysis provide a new tool to characterize molecular interaction and molecular weight differences in mesogenic mixtures using standard calorimetric measurements.

Keywords: Entropy; specific heat; discotic nematic liquid crystal; molecular weight; mixture; carbonaceous mesophase.

This is a License Agreement between Mojdeh Golmohammadi ("You") and Elsevier ("Elsevier") provided by Copyright Clearance Center ("CCC"). The license consists of your order details, the terms and conditions provided by Elsevier, and the payment terms and conditions.

All payments must be made in full to CCC. For payment instructions, please see information listed at the bottom of this form.

Supplier	Elsevier Limited The Boulevard,Langford Lane Kidlington,Oxford,OX5 1GB,UK
Registered Company Number	1982084
Customer name	Mojdeh Golmohammadi
Customer address	3610, University Street
	Montreal, QC H3A2B2
License number	2478800900647
License date	Jul 30, 2010
Licensed content publisher	Elsevier
Licensed content publication	Journal of Non-Newtonian Fluid Mechanics
Licensed content title	Structure and phase transitions of carbonaceous mesophase binary mixtures under uniaxial extensional flow
Licensed content author	Mojdeh Golmohammadi, Alejandro D. Rey
Licensed content date	July 2010
Licensed content volume number	165
Licensed content issue number	13-14
Number of pages	14
Type of Use	reuse in a thesis/dissertation
Requestor type	Not specified
Intended publisher of new work	other
Portion	full article
Format	electronic
Yes	
No	
Order reference number	

Title of your thesis/dissertation	Theory and Simulation of Thermodynamics and Flow Induced Order in Carbonaceous Mesophase Binary Mixtures.
Expected completion date	Aug 2010
Estimated size (number of pages)	200
Elsevier VAT number	GB 494 6272 12
Terms and Conditions	

Copyright Clerance from Co-author

I, Alejandro D. Rey, hereby give copyright clearance of the following papers, of which I am a co-author, in the doctoral thesis of Mojdeh Golmohammadi.

- Chapter 2: Golmohammadi, M.; Rey, A.D. *A Thermodynamic Modeling of Carbonaceous Mesophase Mixtures*. Liquid Crystals 2009, 36, 1, 75-92.

- Chapter 3: Golmohammadi, M.; Rey, A.D. *Entropic Behavior of Binary Carbonaceous Mesophases*. Entropy 2008, 10, 183-199.

- Chapter 4: Golmohammadi, M.; Rey, A. D. *Structure and Phase Transitions of Carbonaceous Mesophase Binary Mixtures Under Uniaxial Extensional Flow*. Journal of Noun Newtonian Fluid Mechanics 2010, 165, 698-711.

- Chapter 5: Golmohammadi, M.; Rey, A. D. *Structural Modeling of Carbonaceous Mesophase Amphotropic Mixtures under Uniaxial Extensional Flow*. Journal of Chemical Physics 2010, 133, 034903: 1-11.

Alejandro D. Rey
James McGill Professor
Department of Chemical Engineering
McGill University
Montreal, Quebec H3A2B2, Canada
Phone: 514-398-4196
E-mail: alejandro.rey@mcgill.ca
http://people.mcgill.ca/alejandro.rey/
http://mmrg.chemeng.mcgill.ca/

Acknowledgements

Abstract

Carbonaceous mesophases (CMs) obtained from petroleum pitches and naphthalene precursors are mixtures of discotic nematic liquid crystals (DNLCs) employed to produce high performance carbon fibers (CFs). Natural pitches are usually polydisperse while synthetic ones are currently produced with very narrow molecular weight distributions.

To design and control the final structure and mechanical properties of CFs three key parameters have to be considered: (i) characteristics of the raw material including the molecular weight, molecular interactions and the concentration of each species, (ii) the processing temperature and (iii) the extensional flow applied in the fiber spinning process. Experimental synthesis, processing, and characterization of CM materials are expensive due to the required equipment and operating conditions. Hence the computational modeling methodology adopted in this thesis is a cost effective tool for these novel materials.

This thesis uses theory, mathematical modeling and computational simulations to characterize the effect of three above mentioned major factors on the orientational and molecular ordering behavior of a mixture of two monodisperse DNLCs, of relevance to the manufacturing of high performance CFs.

The statistical mechanics Maier-Saupe model which effectively predicts the molecular ordering behavior of pure discotic systems is first extended to binary mixtures and then further extended to incorporate uniaxial extensional flow effects. Thermodynamic and thermo-rheological phase diagrams of binary lyotropic/thermotropic CM mixtures are predicted by this theory and partially validated by previous theoretical results and experimental observations. The generic thermo-rheological phase diagram which specifies the orientational structure of each component and their degree of molecular orientation under extensional spinning flow is obtained. X-ray diffraction intensity and orientational specific heat are also simulated in the present thesis, verified by

available data and used as characterization tools for the orientation behavior of CM mixtures.

In summary the thesis provides a new practical route for targeted structure-property relations for high performance CFs, through the chemistry and composition of the precursors, thus extending the traditional routes based on modifications of operating conditions and process geometry. At the fundamental level, the thesis presents the first dynamical model for DNLC mixtures. The models and results of the thesis are also applicable to rod-like systems under biaxial extensional flow, and DNLC under magnetic and electric fields.

Résumé

Les mésophases de carbone (CMs) obtenu à partir de précurseurs de bitume et de naphtalène sont des mélanges de cristaux liquides nématiques discotiques (DNLCs) utilisés pour produire les fibres de carbone (CF) à hautes performances. Le bitume naturel est généralement polydispersé tandis que celui qui est synthétique est présentement produit avec des distributions étroites du poids moléculaires.

Afin de concevoir et de contrôler la structure finale et les propriétés mécaniques des CFs, trois paramètres importants doivent être pris en compte: (i) les caractéristiques de la matière première dont le poids moléculaire et les interactions moléculaires (ii) la température du processus et (iii) l'écoulement extensionnel appliqué dans le processus de filage de la fibre. La synthèse expérimentale, le traitement et la caractérisation des matériaux CM sont chers en raison de l'équipement et des conditions d'opérations requises. C'est pourquoi la méthode de modélisation numérique adoptée dans cette thèse est un outil rentable pour l'étude ces nouveaux matériaux.

Cette thèse s'appuie sur la théorie, la modélisation mathématique et des simulations numériques pour caractériser l'effet de chacun des trois facteurs principaux, mentionnés ci-dessus, sur le comportement et l'orientation moléculaires d'un mélange de deux DNLCs monodispersés, relevant pour la fabrication de CFs à hautes performances.

Le modèle de mécanique statistique de Maier-Saupe qui prédit efficacement l'arrangement moléculaire des systèmes discotiques purs est d'abord étendu aux mélanges binaires puis étendu afin d'incorporer les effets d'écoulement extensionnel uniaxiaux. Les diagrammes de phases de thermodynamique et de thermo-rhéologie des mélanges binaires de CM lyotrope / thermotrope prédis par cette théorie et partiellement validée par les résultats théoriques et les observations expérimentales précédentes. Le diagramme de phase de thermo-rhéologie générique qui spécifie la structure d'orientation de chaque composant et leur degré d'orientation moléculaire sous extension est obtenu. L'intensité de

la diffraction à rayon X ainsi que la chaleur spécifique orientée sont également simulées dans la présente thèse, vérifié par les données disponibles et utilisés comme outils de caractérisation du comportement d'orientation des mélanges de CM. En résumé, la thèse propose une nouvelle démarche pratique pour les relations ciblées propriété-structure pour les CFs à haute performance, grâce à la chimie et la composition des précurseurs, ainsi étendant les démarches traditionnelles basées sur des modifications de conditions d'exploitation et de la géométrie des processus. Au niveau fondamental, la thèse présente le premier modèle dynamique pour les mélanges DNLC. Les modèles et les résultats de cette thèse sont aussi applicables aux systèmes allongés sous écoulements extensionnel biaxial et sous l'effet de champs électriques et magnétiques.

Results Summary

The major results of this thesis are summarized into two main parts: (1) Thermodynamic predictions (the effect of temperature on the orientational behavior of discotic nematic liquid crystalline (DNLC) mixtures) and (2) Thermo-rheological predictions (the simultaneous effects of temperature and flow on the orientational behavior of DNLC mixtures), as follows:

1. Thermodynamics

   1.1. Structural Predictions

      1.1.1. Thermal dependence of the order parameter of each discotic component within the mixture;

      1.1.2. Concentration, molecular weight asymmetry and species' interaction dependency of the order parameter of each discotic component within the mixture;

      1.1.3. Classification of the orientational behavior of mixtures into ideal and non-ideal based on their phase transition temperature trends;

      1.1.4. Model of critical composition determination for minimal phase transition temperature in ideal mixtures;

      1.1.5. Derivation of a model to evaluate the interaction between the components through their orientational behavior.

   1-2. Development and Simulation of Characterization Methods

      1.2.1. Derivation of the X-ray diffraction intensity to evaluate the ordering behavior of dicotic mixtures and to determine their type of behavior (ideal or non-ideal);

      1.2.2. Derivation of the orientational specific heat to determine the nematic

         to isotropic transition temperature, T_{NI}, of the mixture and to determine their type of behavior (ideal vs. non-ideal).

2. Thermo-Rheology

2.1. Structure Prediction

    2.1.1. Obtaining the Mw dependency of the rotational diffusivity of discotic components within the mixture;

    2.1.2. Determination of the extensional flow intensity influence on the phase behavior of each discotic component within the mixture;

    2.1.3. Evaluation the lyotropic / thermotropic competition/cooperation effects of discotic mixtures under uniaxial extensional flow;

    2.2.3. Determination of the influence of species' concentration on the thermo-rheological phase diagram of the discotic mixtures.

2.2. Structural Characterization

    2.2.1. Derivation of the X-ray diffraction intensity of discotic mixtures in the presence of the extensional flow as a tool to evaluate the level of biaxiality and structural ordering for each component.

Table of Content

List of Figures

List of Tables

1   General Introduction

1.1 Organization

This introductory chapter is organized as follows. Section 1.1 provides a short introduction to the classification of liquid crystals and carbonaceous mesophases (CM) emphasizing how and why these mesophases arise. Particular attention is placed on mixtures of discotic nematic liquid crystals, since CM precursors spun into high performance carbon fibres (CFs) are never monodisperse. Section 1.2 introduces the different types of CFs with emphasis on CM-based carbon fibres, their different structures and morphologies, their applications and the main fibre manufacturing steps. Particular attention is placed on the fibre spinning process which is the processing of transforming CM precursors into CFs and the key parameters that influence the fibres' structure and mechanical properties. Section 1.3 provides an introduction to the computational material science of nematic CMs and its application to mesophase fiber spinning. This section introduces the theoretical concepts and the theoretical model used for the CM materials in the current work, modeling of the parameters involved in the theory and the computational methods used to solve the derived governing equations. It also introduces the characterization tools derived in this thesis to measure the ordering within the discotic nematic mixtures. Section 1.5 describes the need for mesophase mixture modeling and simulation. Section 1.6 specifies motivations and objectives of the thesis. Section 1.7 describes thesis scope and organization and section 1.8 provides the references.

1.2 Liquid crystals

1.2.1 Liquid crystals overview

Liquid crystals (LCs) or mesophases are anisotropic viscoelastic materials formed by anisodiametric molecules that possess orientational order and varying degrees of positional order. Figure 1- 1 displays a comparison of the orientational and positional order of a rod-like nematic liquid crystalline phase with crystalline (C) solid and liquid (I) phases[1-4].

n

Solid   Liquid Crystal   Liquid
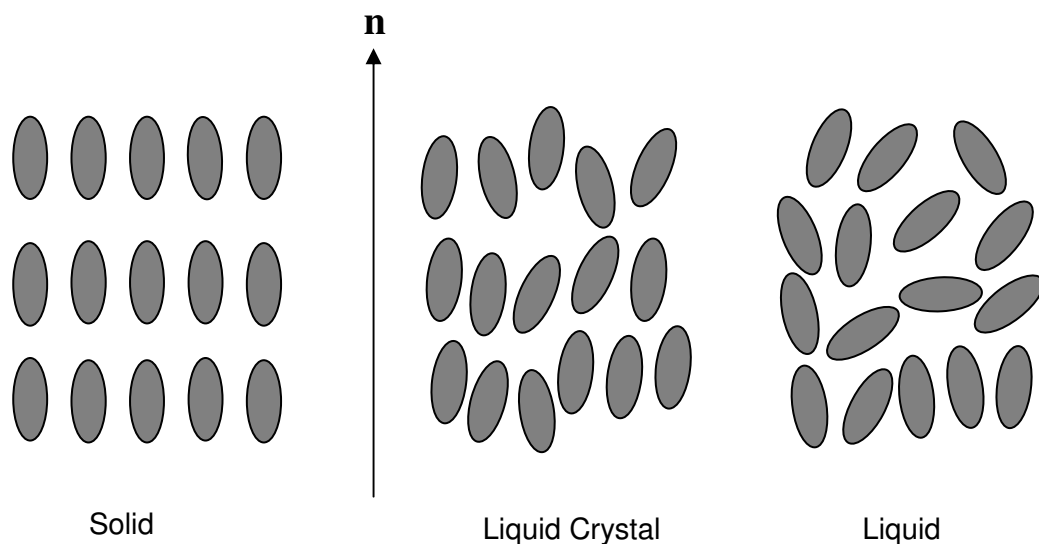
Figure 1- 1. Liquid crystal (LC) phase ordering compared to a crystalline (C) solid and an isotropic (I) liquid. Liquic crystal shows a degree of ordering, both positional and translational, between the orientation of a perfect crystal and an isotropic liquid. n which is called the director is the vector which gives the average of molecular orientation in C and LC phases: in C phase all the molecules are aligned parallel to n, though in LC the average of all the molecular orientations is along n.

The transition from isotropic liquid-liquid crystal-crystalline solid can be viewed as a sequence of symmetry breaking transitions, starting with orientation at the I/LC transition, followed by position at the LC/C . Mesophases can be classified according to (i) driving force (temperature and/or solvents) for symmetry breaking, (ii) average molecular order, (iii) molecular shape and (iv) molecular weight. When the formation of mesophase occurs due to the temperature change, it is defined as a thermotropic liquid crystal and when the formation occurs due to the concentration effects it is known as lyotropic liquid crystal[5]. Liquid crystals which are formed due to the simultaneous effects of temperature and concentration are called thermotropic/lyotropic or amphotropic liquid crystals. This thesis deals with amphotropic liquid crystals. Depending on the average molecular order or orientation, these materials are classified into three phases known as nematics, cholesterics and smectics (see Figure 1-2). Nematic liquid crystals[6] exhibits partial orientational order; in this phase the long molecular axes are preferably oriented along a particular direction called director **n**. In a cholesteric liquid crystal, the director rotates in a helical form about an axis perpendicular to the director.

Smectic liquid crystals exhibit both partial orientational order and translational order which is one dimensional positional order along the vertical axis. In this case, the director **n** shows the average orientation of the long molecular axes in each layer. This thesis deals with nematic liquid crystals.
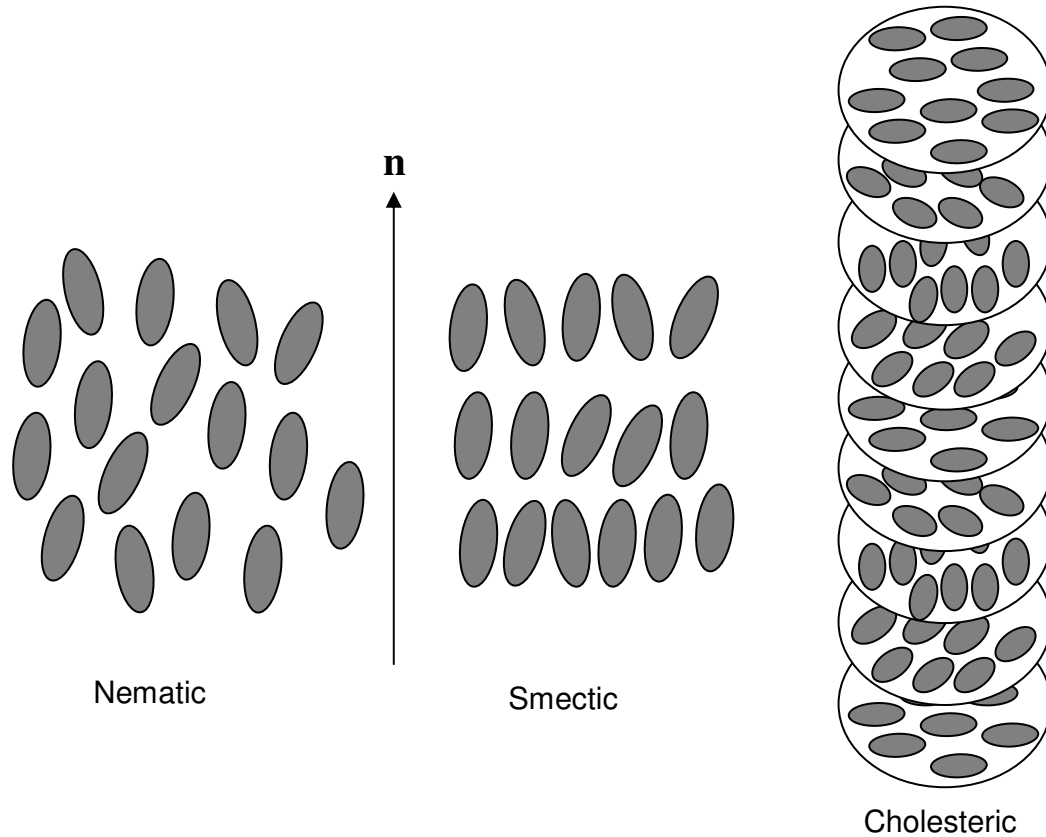
Figure 1- 2 Classification of liquid crystals based on molecular order: nematic liquid crystals exhibits partial orientational order; smectic liquid crystals exhibit both partial orientational and translational order and in a cholesteric liquid crystal, the director rotates in a helical form about an axis perpendicular to the director.

Based on molecular shape, liquid crystals can be classified as rodlike (calamitic) and disklike (discotic) as shown in Figure 1-3. The director is near parallel to the axis of rod like molecules but near perpendicular to the flat surface of the discotic molecules. This thesis focuses on disc-like molecules.[4] Depending on the molecular packing, discotic liquid crystals are classified as nematic, columnar (smectic) and chiral nematic phases. In nematic phase there is only orientational order with no positional order. In columnar phases, in addition to the orientational order present in the nematic phase most of the molecules tend to position themselves in columns

and form a set of stacked coins. In chiral[7] nematic discotic liquid crystal the director rotates in a helical fashion throughout the sample, just as in the case of rodlike cholestric liquid crystals[2]. This thesis concentrates on discotic nematic liquid crystals.
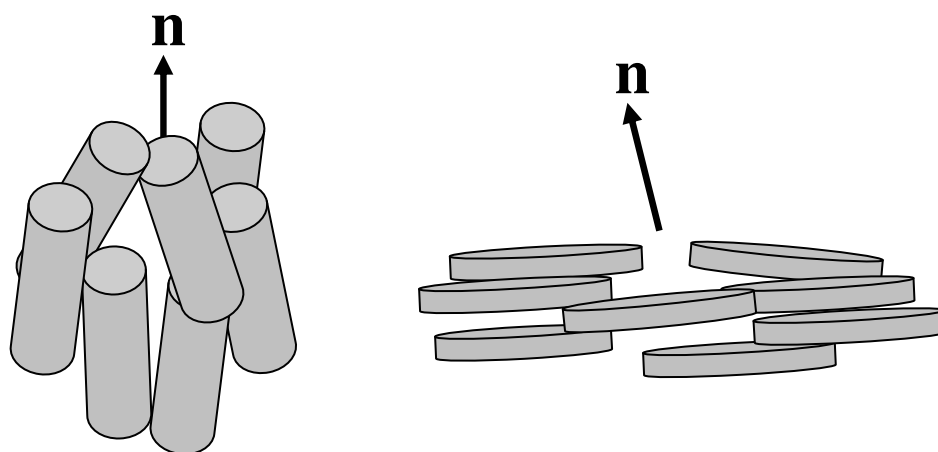
Figure 1- 3. Classification of liquid crystals based on molecular shape. The director is parallel to the axis of the rod like molecules and perpendicular to the surface of the discotic molecules.

From the molecular weight (Mw) point of view, these materials are classified into low molecular weight and polymeric liquid crystals. This thesis deals with oligomers with the Mw between the molecular weight of monomers and Mw of polymers. Their Mw ranges from 200 to 1400[8, 9].

1.2.2 Liquid crystalline mixtures

Mixtures of liquid crystalline components with different molecular weights are widely used to optimize product and device performance. For example the addition of a lower Mw component to a higher Mw material reduces the blend's melting point and viscosity and makes the melt process easier and more economical. The presence of the higher Mw component, on the other hand, provides higher degree of orientation in the presence of electric or magnetic fields[2]; it also improves the mechanical properties of the final product. Mixing is also used to broaden the temperature range of liquid crystalinity[10]. These mixtures are employed for different applications such as liquid crystalline displays (LCDs)[11], carbon-carbon (C/C) composites and carbon fibres[12] (CFs) through the fibre spinning, film stretching and injection moulding processes.

1.3 Carbon fibres

1.3.1 Introduction

Liquid crystals are functional materials and precursors for high performance structural materials. Examples of the former include display devices, optical filters[13], thermal sensors[14], lubricants[15], reaction media[16], and chemical sensors[11, 17]. Examples of the latter include high performance fibres[12, 18], films[11, 19], and composites[19].

Carbon materials are used as structural and functional materials. Examples of the former include carbon-carbon (C/C) composites and carbon fibres (CFs)[12]. Examples of the latter include carbon foams for heat transfer purposes, and as materials for purification and adsorption applications like catalysts and catalyst supports[20]. In this thesis we focus on carbonaceous mesophases precursors for the production of structural materials and more specifically for the formation of carbon fibres using the melt fibre spinning process[12, 21]. Carbon fibre, alternatively graphite fibre consists of extremely thin fibres about 0.005-0.01 mm in diameter and mostly composed of carbon rings[22]. The strength and stiffness of these fibres is superior to that of all other reinforcing fibres[12] such as glass and aluminium. The unique properties of all carbon fibres can be directly attributed to the highly anisotropic nature of the graphite crystal. The graphite crystal is composed of stacks of multi-pole sheet-like layers of carbon atoms. The crystal alignment makes the fibre very strong for its size. The density of carbon fibre is also considerably lower than the density of steel, making it ideal for applications requiring low weight[12]. The combination of these properties i.e. high modulus, high tensile strength, low weight, and low thermal expansion makes it highly usable in aerospace, civil engineering, military, and motor sports, along with other competition sports[23].

1.3.2 Carbon fibre routes

Three types of precursors including rayon, Polyacrylonitrile (PAN) and pitch (anisotropic pitch is widely refered as carbonaceous mesophase) are mostly used to produce carbon fibres in commercial processes. While rayon is mostly used in common daily applications (e.g. apparel, filling in Zippo lighters, furnishings, medical surgery products and tire cord)[24], PAN and pitch based carbon fibres are

mostly used in high tech industries because of their high mechanical performance. PAN fibre is used in industries where its strength and stiffness have enabled many low weight applications such as civil and military aircraft primary and secondary structures, solid propellant rocket motors, pressure vessels, fishing rods, tennis rackets, badminton rackets & high-tech bicycles[25]. In comparison to PAN, mesophase pitch-based carbon fibre has a higher Young modulus. As figure 1-4 shows, the modulus of mesophase pitch can be twice the modulus of PAN. It also can be 20 times greater than the modulus of the isotropic pitch. Mesophase pitch also exhibits lower to negative coefficient of thermal expansion, and higher thermal and electrical conductivity compared to PAN and hence is appropriate to be used in airplane and aerospace industries. Beside, among these three sources, yield of pitch precursor, a vital factor in both processing and the economics of commercial carbon fibres, is the highest one. A comparison of the process yield of these sources can be seen in Table 1-1. In this thesis we concentrate on pitch-based CFs.
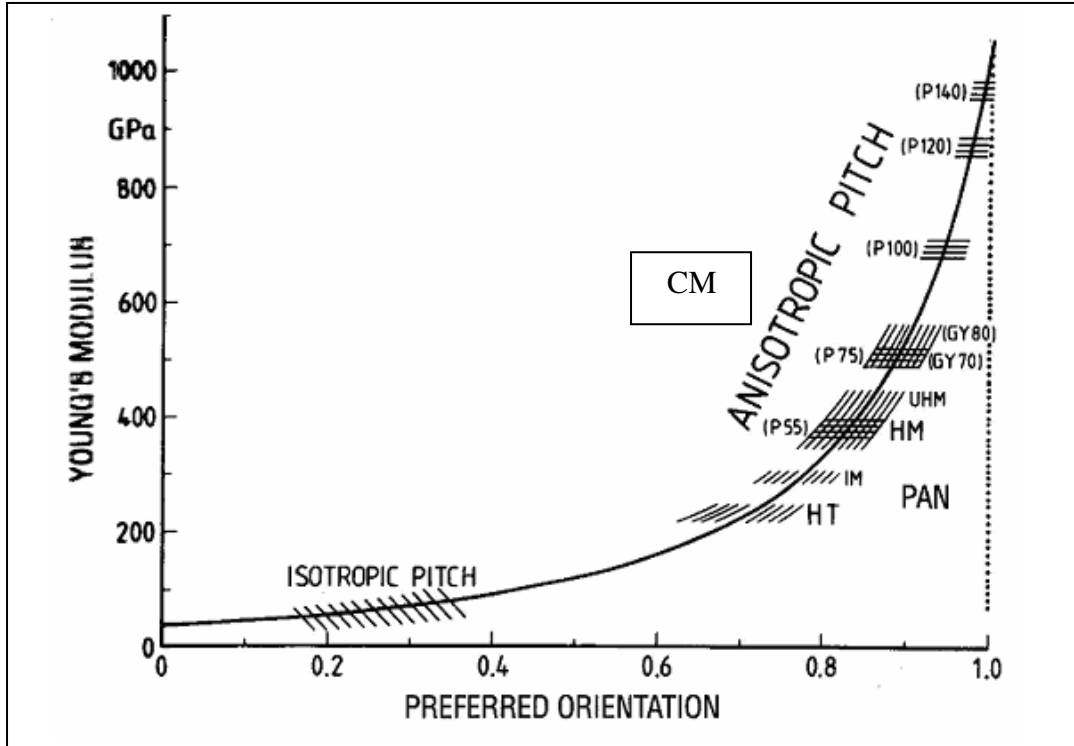
Figure 1- 4. The effect of preferred orientation on the Young's modulus of carbon fibers adapted from [12]. Anisotropic pitch exhibits the modulus about twice of the modulus of PAN and 20 times of the modulus of the isotropic pitch. Carbonaceous mesophase (CM) belongs to the anisotropic pitch category.

Table 1- 1. Carbon Yield for various carbon fiber precursors adapted from [12]

Precursor	Process yield
Rayon	20-30
PAN	45-50
Pitch	75-90

1.3.2.1 Pitch based carbon fibers

Two types of pitch-based carbon fibres are commercially available: isotropic carbon fibre which is produced from an isotropic pitch precursor and anisotropic carbon fibre which is produced from an anisotropic, mesophase precursor or carbonaceous mesophase (CM). CM is a stack of graphite sheets (see Figure 1- 5) which form the discotic nematic liquid crystals (DNLCs), presented in Fig.1-3. It is

formed during the liquid phase pyrolysis of coal or petroleum pitches and exhibits very high Young's modulus (210-620 Gpa), low to negative coefficient of thermal expansion, and high thermal and electrical conductivity. Hence, while isotropic pitch precursor is used as a catalyst or as catalyst supports only due to their functional groups[26], CMs are used to produce high performance CFs employed in aerospace industries due to their preferred orientation and their extraordinary mechanical and thermal properties.[12, 20]
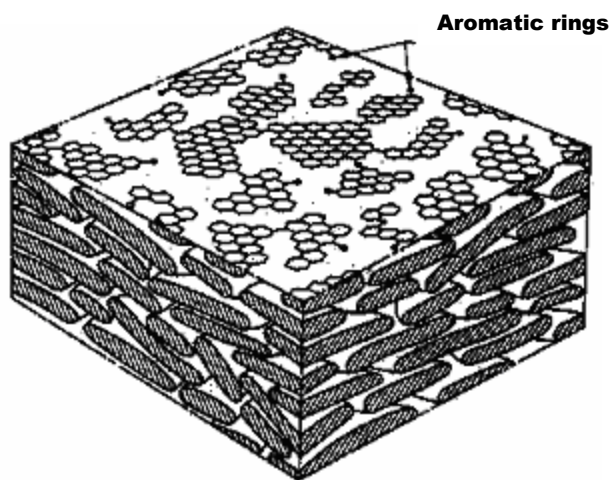
Figure 1- 5. CM as a stack of graphite sheets, adapted from [12]

1.3.2.2 Manufacturing of mesophase carbon fibers - Fiber spinning process

Mesophase carbon fibres are manufactured from mesophase pitches in mainly three steps: (i) melt spinning (ii) stabilization and (iii) heat treatment. Figure 1-6 shows the schematic representation of these three steps. In the melt spinning step, the fibres are drawn using the molten mesophase pitch to achieve preferred orientation in the as-spun fibres[12]. Typically the precursor is melted in an extruder, see Figure 1-7, which then pumps the melt into the spin pack. The molten pitch is then filtered before being extruded through a multi-holes spinneret. The pitch is subjected to a high stress as it approaches and flows through the spinneret capillaries. The associated flow-induced torque tends to orient the disk-shaped molecules in a regular transverse pattern upon emerging from the spinneret capillaries[27]. The as-spun fibres are drawn to have the improved axial orientation and are then collected on a wind-up device[21].

In the second step, oxygen is used to prevent the fibre from melting during the subsequent carbonization process. This is done to "lock in" the structure developed during the extrusion process.

Heat treatment or carbonization involves two steps; (i) around $1000^{o}C$ to reduce the rate of gas evolution and (ii) in 1200-3000 ^{o}C depending on whether high strength (lower temperatures) or high modulus (higher temperatures) carbon fibre are required[28].
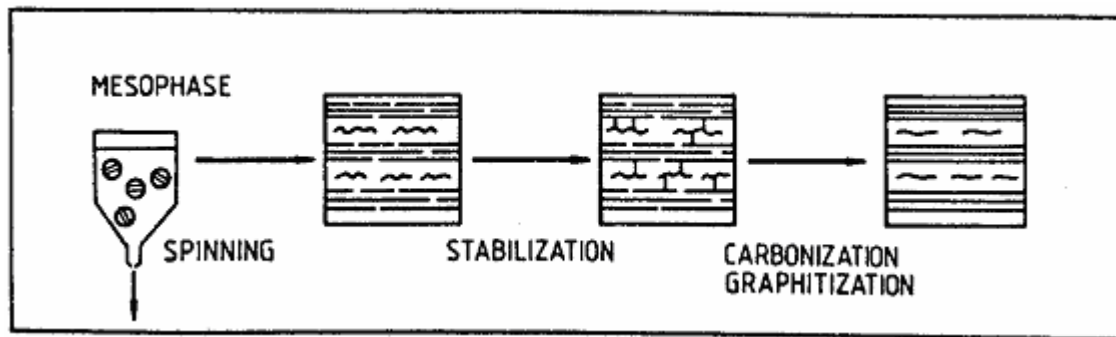
Figure 1- 6. Different steps of manufacturing of mesophase pitch-based carbon fibers, adapted from [12]. The molten pitch is spun in the fiber spinning process. It's structure then is stabilized by oxygen and then is carbonized through heat treatment.
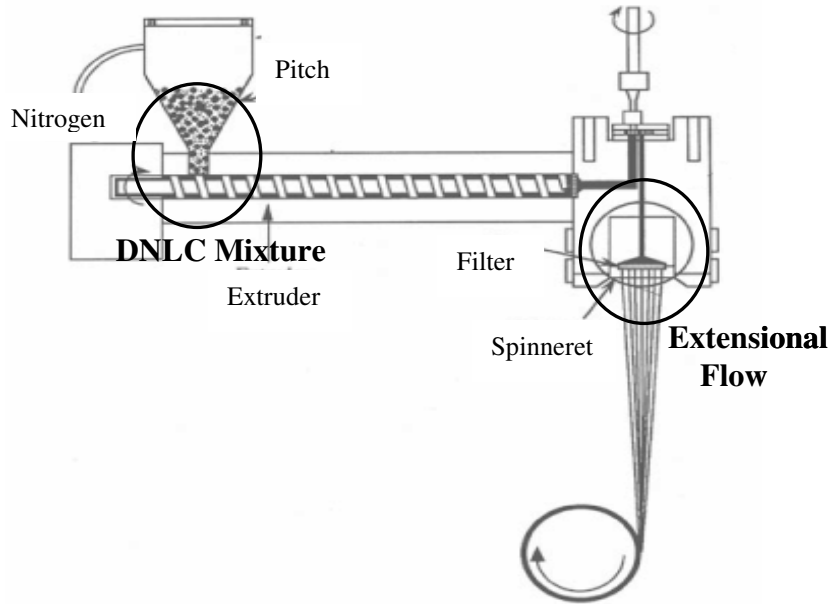
Figure 1- 7. Fiber Spinning Process. Adapted from [12] . The raw material, melt carbonaceous mesophase, is fed into the hopper, metered through the extruder and then is spun through the spinneret and collected on the wind-up device. The fiber experiences the extensional flow in the spinneret and exhibits an enhanced orientation in a regular transverse pattern.

1.3.2.3 Structure and morphology of mesophase carbon fibers

As anisotropic pitch-based carbon fibres are melt-spun from a liquid crystalline precursor (CM), a variety of microstructures with different mechanical properties can be produced merely by modifying the spinning conditions such as temperature of the spin, extensional flow intensity in the spinneret, the composition of the pitch[12] (see Figure 1-7). Two types of common structures, planar polar, PP, and planar radial, PR[29], with the corresponding mechanical properties reported in Table 1-2 are shown in Figure 1-8.

Previous investigations have proven that depending on the temperature and size of the fibre one of the two is formed.[29] As demonstrated in Table 1-2 different morphologies provide different mechanical properties making them appropriate for different applications. Hence, having a clear understanding of the physics and orientation behaviour of the CMs materials under the extensional flow and its control is very critical to tailor the CF for a specific application.

(a) PP   **(b)** PR
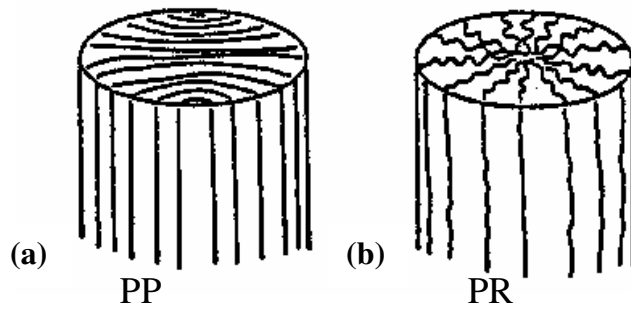
Figure 1- 8. Commercial pitch-based carbon fibers morphologies: Planar Polar structure (a) and Planar Radial structure (b) adapted from [12]. By changing the characteristics and composition of the raw material (molecular weight of the components, their interaction and their concentrations) or the processing conditions (temperature, flow intensity) different morphologies can be achieved.

Table 1- 2. Mechanical properties of two different morphologies of CFs adapted from [12]

	Tensile Strength (GPa)	Tensile Modulus (GPa)	Strain %
PP	2.4	830	0.3
PR	3.0	590	0.5

1.3.2.4 Key parameters in the fiber structure formation

As depicted in figure 1-7 and discussed in section (1.2.2.3) three major factors which determine the final structure of the fibre in fibre spinning process are:

(i) characteristics of the CM as the mixture of discotic nematic liquid crystal including polydispersity of the feed, interaction between the component and concentration of each component in the mixture;

(ii) spinning temperature which influences the phase state (nematic versus isotropic) and the orientation of the components within the mixture ;

(iii) intensity of extensional flow which again influences the phase state and the molecular orientation of each component within the mixture.

The focus of this thesis is to elucidate the roles of precursor composition (i) and operating conditions (ii, iii) on the emergence of orientational order, since this order controls many of the end product properties.

1.4 Computational material science of nematic liquid crystals applicable to CMs

1.4.1 Overview

CMs currently used to produce CFs are polydisperse materials including monomer, diamer, trimer and tetramer of aromatic molecules[30], as suggested in Figure 1-9. In previous research investigations, petroleum pitches have been used as precursors for the production of high-performance carbon materials[12]. In general, pitches of Mw, i.e., mesophase pitches, have been used for the production of high thermal conductivity carbon fibers[12] and high thermal conductivity carbon–carbon (C/C) composites[31]; the mesophases with different Mws also exhibit different orientational behavior. Pitches of low molecular weight, i.e., isotropic pitches, have been used as precursors for the production of general purpose carbon fibers, activated carbon fibers (ACF) with highly uniform surface characteristics[26], and as a low-viscosity matrix in C/C composites. Thus, the molecular weight of petroleum pitches is known to play a key role in their suitability for a given carbon
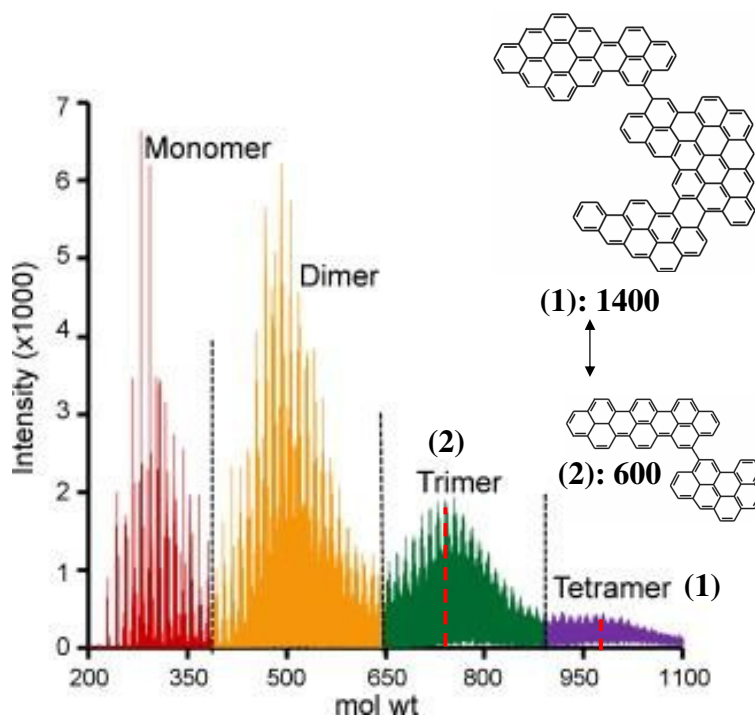
Figure 1- 9. Molecular weigh distribution of a CM sample with two typical molecules representing a trimer (Mw=600) and a tetramer (Mw=1400), adapted from [30]. Molecular weights of the components is one of the key parameters influencing the final morphology of CM based CFs.

application. However, a quantitative relationship between molecular weight and final product properties has yet to be clearly established. The separation of different Mws to obtain monodisperse samples and subsequent controlled blending to produce CFs with a set of specific thermo/mechanical properties is a topic of intense current work[30]. However, the separation process to obtain different monodisperse samples is extremely expensive[30, 32]. Preparing the mixtures with different concentrations and interactions, through surface modification for instance, followed by processing in different temperatures and under different flow conditions, as shown in figure 1-10, makes the process even more expensive.
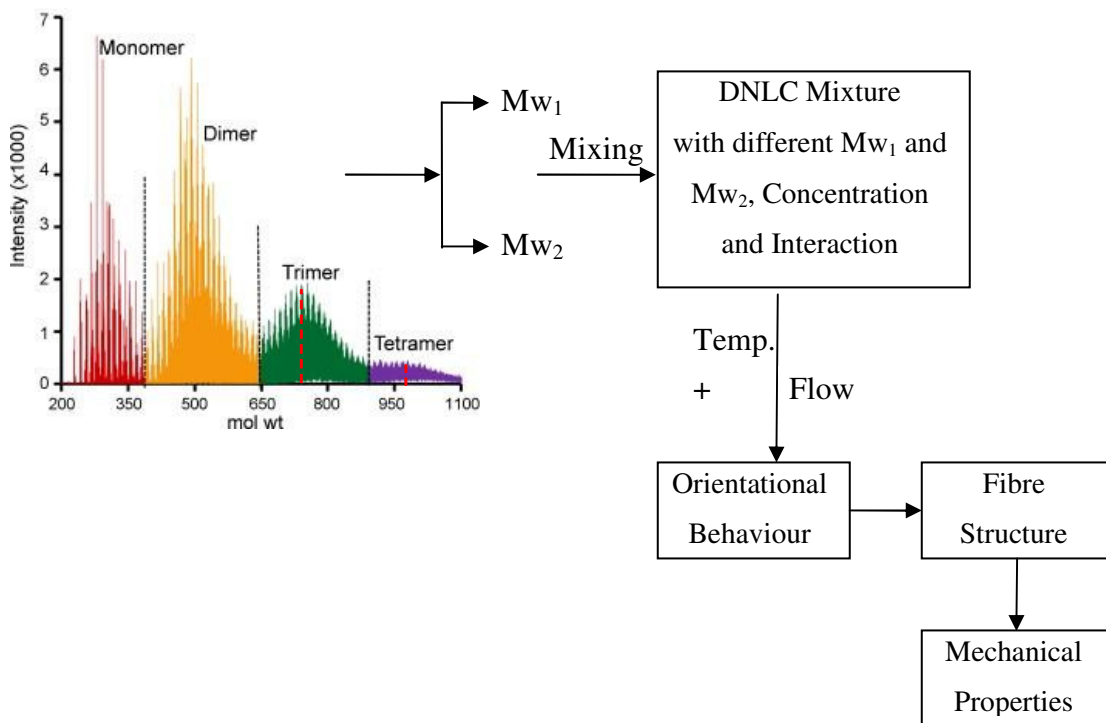
Figure 1- 10. The parameters influencing the mechanical properties of the advanced synthetic CF with a controlled design. Two monodisperse components are obtained through the separation process of the pitch and then are mixed with different concentration and are used as the raw material of the fiber spinning process. Processing temperature and extensional flow in the spinneret influence the final structure and the mechanical properties of the fiber formed in the process.

Hence to establish the link between precursor chemistry and composition with the final fibre structure (and corresponding properties) solely using experimental

approaches is very costly and inefficient. Computational simulation is a useful complement to experimental methodologies and allows the systematic study of the role of the relevant mixture variables (species' molecular weight difference, composition) on the fibre structure. The effect of operating conditions (temperature and extensional flow intensity) on the orientational behaviour of the binary mixture can also be systematically investigated. This thesis used the standard computational material science and engineering methodology[33] and includes: (i) development of thermodynamic and extensional flow theories for CM materials, (ii) modeling of the mixture's thermodynamic (molecular weight-molecular size equation, molecular weight/transition temperature equation , concentration-dependent interaction parameter equations) and rheological properties (rotational diffusivity of a discotic component in a discotic mesophase mixture) relevant to spinning processes, and (iii) accurate computational methods to solve the governing nonlinear equations obtained by integrating the theory (i) and modeling (ii) steps.

1.4.2 Theory for nematic liquid crystals applicable to CMs

1.4.2.1 Overview

Theory and simulation of liquid crystalline materials are used to capture the molecular ordering and the orientational structure of these materials under different thermal and flow conditions. The theory is based on macroscopic and mesoscopic models[12]. Macroscopic models are based on the average orientation equations using linear momentum and torque balance equations. On the other hand, mesoscopic models are based on both the average orientation and molecular ordering of the components and are based on the second moment of the orientation distribution function to describe both micro and macro phenomena. To review the theory employed in this thesis some concepts such as director field, scalar order parameter and quadrupolar tensor order parameter are explained in the next section.

1.4.2.2 Theoretical concepts

1.4.2.2.1 Director

As shown in Figure 1.11 a dimensionless unit vector **n** called the director, is introduced to represent the direction of preferred orientation of mesogenic disc-like molecules, each having an orientation shown by the unit vector **u**. In discotic

nematic liquid crystals the director is in close alignment to the molecular unit normals.
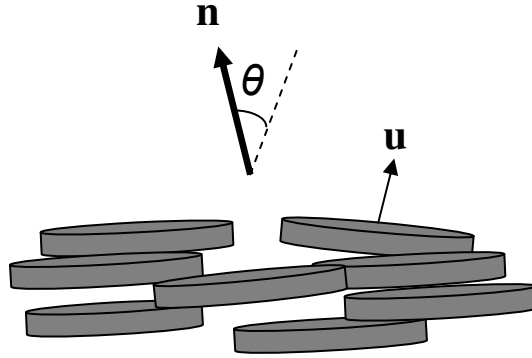
Figure 1- 11. Director of a discotic system as an average of the orientation of disc-like molecules shown by u. The population of the molecules oriented in a specific direction determines orientation distribution function, *ODF*. Scalar order parameter, S, expresses the probability of finding all the molecules parallel to the director n.

1.4.2.2.2 Scalar order parameter

The description of nematic liquid crystals involves the specification of orientational order. To make this quantitative, an orientational order parameter, *S*, is usually defined based on the average of the second Legendre Polynomial as follows:

$$S = \langle P_2 \cos\theta \rangle = \left\langle \frac{3\cos^2\theta - 1}{2} \right\rangle = \int_0^\Pi ODF(\theta)\left(\frac{3\cos^2\theta - 1}{2} \right) sin\theta d\theta \qquad (1.1)$$

where θ is the angle between the axis of each molecule, **u**, and the director **n** (see Figure 1-11) and $ODF(\theta)$ is the normalized orientation distribution function of the molecules. For a perfect orientation, *S=1*. On the other hand, for the isotropic state *S=0*. For nematic liquid crystals which exhibits partial orientation $0 < S < 1$. The temperature at which *S* shows transition from a non-zero (nematic) to zero (isotropic) value is called nematic-to-isotropic transition temperature, T_{NI}.

1.4.2.2.3 Tensor order parameter

The microstructure of liquid crystal is characterized by a second order symmetric and traceless tensor, known as the tensor order parameter **Q** [34].

$$\mathbf{Q} = \int_{\mathbb{Z}^2} ODF(\mathbf{u})\left(\mathbf{uu} - \frac{\boldsymbol{\delta}}{3} \right) dA = \left\langle \mathbf{uu} - \frac{\boldsymbol{\delta}}{3} \right\rangle$$
$$= S(\mathbf{nn} - 1/3\mathbf{I}) + 1/3P(\mathbf{mm} - \mathbf{ll}) \qquad (1.2)$$

with

$$\mathbf{Q} = \mathbf{Q}^{\mathrm{T}}; \ tr(\mathbf{Q}) = 0; \ -1/2 \le S \le 1; \ -3/2 \le P \le 3/2$$

$$\mathbf{n.n} = \mathbf{m.m} = \mathbf{l.l} = 1; \ \mathbf{nn} + \mathbf{mm} + \mathbf{ll} = \mathbf{I} = \begin{bmatrix} 1 & 0 & 0 \\ 0 & 1 & 0 \\ 0 & 0 & 1 \end{bmatrix} \tag{1.3}$$

The orientation is completely defined by the orthogonal director trial (**n**, **m**, **l**). The magnitude of the uniaxial scalar order parameter *S* is a measure of the molecular alignment along the uniaxial director **n**, as discussed in the previous section, and the magnitude of the biaxial scalar order parameter *P* is a measure of the molecular alignment in a plane perpendicular to the direction of uniaxial director **n** (**m-l**) plane.

On the principle axes, the tensor order parameter **Q** is represented as

$$\mathbf{Q} = \begin{bmatrix} -1/3(S-P) & 0 & 0 \\ 0 & -1/3(S+P) & 0 \\ 0 & 0 & 2/3S \end{bmatrix} \tag{1.4} \text{ w}$$

ith $\mu_n = 2S/3 \ \mu_m = (P-S)/3 \ \mu_l = -(P+S)/3$ being the eigenvalues of **Q**. The orientation variables describe micrometer scale phenomena as in fibre textures and are slow variables. On the other hand the scalar order parameters describe nano-scale phenomena as in interfaces and defects and are fast variables. Hence in a process flow, increasing deformation rates will first ignite orientation modes and then the molecular order modes. When studying isotropic/nematic phase transition the scalar order parameters S and P are the main variables that describe the symmetry breaking as a function of increasing temperature. If an external extensional flow is imposed the orientation of the directors (**n**, **m**, **l**) with respect to the extension axis and compression plane[35-38] must also be considered.

Typically, the director **n** is anywhere in the compression plane and this explains the widely observed 2D orientation patterns observed experimentally (see Fig 1-8 for example).

1.4.2.3 Characterization of order: experimental methods

There are several characterization methods to evaluate the nematic ordering in liquid crystalline materials including birefringence, diamagnetic susceptibility

measurements and NMR spectroscopy[39-42]. Differential scanning calorimetry (DSC) which measures the specific heat and entropy values is also a suitable method to measure the ordering as well as to distinguish the transition phenomenon like nematic to isotropic transition temperature, T_{NI} [43]. Scattering from an isotropic liquid by X-ray beam or X-ray scattering is another way of measuring the nematic ordering[40, 44]. In this thesis specific heat and X-ray intensity, as the methods to evaluate ordering, are determined computationally and can be used to compare with the experimental results. In the next section these two methods are briefly explained.

1.4.2.3.1 X-ray diffraction intensity

X-ray diffraction intensity is a method to measure the orientational order of an anisotropic liquid such as aligned nematic liquid crystal[43, 45-47]. Diffraction of an X-ray beam striking a liquid crystalline sample occurs because the wavelength of the X -ray beam is similar to the spacing of atoms in the molecules. When an X -ray beam encounters the regular arrangement of molecules most of the X -rays will destructively interfere with each other and cancel each other out, but in some specific directions they constructively interfere and reinforce one another. It is these reinforced (diffracted) X -rays that produce the characteristic X-ray diffraction patterns which represents the orientation distribution function, ODF^{48} of the nematic molecules (see equation (1.1)) [49]. The scattered intensity can give the insight to the ordering status, uniaxiality vs. biaxiality, and ordering magnitude of the molecules. X-ray intensity has been calculated for the pure nematic liquid crystals[43]. However, in this thesis the intensity is extended to the mixture of monodisperse nematic liquid crystals to obtain the orientation magnitude and its status in the CM mixtures. The details of this theory and its extension to the mixtures and its application as the characterization tool are given in chapters 2 and 4 of the thesis.

1.4.2.3.2 Calorimetry - Orientational specific heat

Specific heat calorimetry is another method to give an insight into the molecular orientation and thermal properties of the nematic liquid crystals[50]. It is the most reliable tool to detect the existence of a phase transition between the nematic and

isotropic states originating in the onset of a long range ordering. The most commonly used thermal technique for studying liquid crystals is differential scanning calorimetry (DSC)[50]. The phase sequence of a given substance is recorded by this method. The transition temperatures and qualitative enthalpy changes associated with the phase transitions are easily determined with commercially available techniques[50]. Hence, specific heat can be employed to detect the transition temperature and to quantify the effect of molecular weights, concentration, and molecular interactions. In this thesis calorimetry has been used to quantify the thermal properties and entropic behaviour of different mixtures and to classify them based on their nematic/isotropic transition trends. The details of calculating this thermodynamic quantity and its applications are given in chapter 3.

1.4.2.4 Thermodynamic of nematic liquid crystals: Maier Saupe, MS, statistical mechanics theory for equilibrium binary mixtures

The Maier Saupe theory is a statistical mechanics theory used to describe the thermodynamics of nematic liquid crystals at equilibrium, though the effect of extensional flow can also be incorporated in this model. In this theory the Helmholtz free energy per unit mole of the homogeneous mixture $A(\mathbf{Q}_1, \mathbf{Q}_2)$ is expressed as:

$$A(\mathbf{Q}_1, \mathbf{Q}_2) = -N_A \left(E_{mix}(Mw_1, Mw_2, \beta, m_1, m_2) + k_B T \ln Z(Mw_1, Mw_2, \beta, m_1, m_2) \right)$$

(1.5)

where N_A is Avogadro's number, E_{mix} is the internal energy of the mixture per molecule, k_B is the Boltzman's constant, T is the absolute temperature and Z is the partition function. Both terms on the right hand side include the effect of molecular weights of the components, Mw_1 and Mw_2, their interaction, β, and their concentrations, m_1 and m_2. By minimizing the free energy with respect to each tensor order parameter, $\mathbf{Q_i}$, the stable orientation state for each component is achieved. Hence through this theory the effect of characteristics of CM mixtures on the orientation of the components within the mixture is obtained. The Maier-Saupe theory has been explained in detail in chapters 2 and 4.

 1.4.2.5 Dynamic and rheology of nematic liquid crystals – Potential flow

A nematic liquid crystal flows in similar fashion to a conventional organic liquid with molecules of similar size. However, the flow regimes are more complex and more difficult to study than in isotropic liquids because the translational motions are coupled to inner, orientational motions of the molecules[41]; flow disturbs, enhances or induces the alignment. When the material is in the isotropic phase, flow induces orientation and produces flow-birefringence and the phase becomes paranematic[41, 51]. The paranematic phase is a non-equilibrium phase obtained when a mesogen at a temperature higher than the isotropic/nematic transition is subjected to an external field. Flow induced orientation and the formation of paranematic phase is investigated in this thesis.

Integrating thermodynamics with extensional flow-induced orientation in binary mixtures of CMs under uniaxial extensional flow merges the interplay between equilibrium uniaxial ordering and flow-induced biaxiality (see eqn. (1-3), section (1.3.2.2.3)). This combination of thermo-rheological effects will be a function of the species molecular weight asymmetry (ΔMw), their molecular interaction (β), and the concentration (m_1) (For a full discussion of the parameters see sections (1.3.2.4)). Macroscopic nematodynamics will predict flow induced orientation, *FIO,* accurately, but for binary mixtures the macroscopic material parameters will be given by unknown functions of the molecular parameters (ΔMw, β, m_1) and hence the most efficient way to include these important parameters is to use a molecular level description. For this purpose, the Maier-Saupe (MS) theory described in the previous section is extended to include the extensional flow in this thesis. In this formulation the extensional flow contributes to the partition function discussed in eqn. 1-5. The details of the extended Maier-Saupe theory with the implemented extensional flow effects to investigate the thermo-rheology of CM mixtures composing of two monodisperse components are given in chapter 4.

1.4.3 Modeling

The implementation of the Maier Saupe theory to describe orientation and order under extensional flow requires the formulation of an expression for the rotational diffusivity of the molecules. The rotational diffusivity is inversely proportional to the rotational viscosity which defines the viscous torques that act on the molecules.

The rotational diffusivity has been already derived for pure rod-like systems but no equivalent expression for discotic and discotic mixtures existed prior to this thesis.

The details of these derivations are given in chapter 4 which discusses the effect of extensional flow on the orientational behaviour of the mixture. In that chapter, first rotational diffusivity of the pure discotic nematic is modeled and then it is extended to the diffusivity of each component within the mixture. The effect of Mw of each component and its concentration and also the effect of molecular orientation of each component on the rotational diffusivity of both components is discussed in chapter 4.

1.4.4 Computation

1.4.4.1 Governing equations: algebraic integral equations

The expanded version of Maier Saupe equations (eqn. 1.5) used in this work is a set of the second type Fredholm non-linear algebraic integral equations with the following format:

$$\varphi(x) = f(x) + \lambda \int_a^b K(x,t)\varphi(t)\,dt \qquad (1.6)$$

In this type of algebraic integral equation the unknown function occurs both inside and outside of the integral. To solve this type of nonlinear equations first the integral term has to be calculated and then an iteration method to solve the nonlinear equation has to be employed. In this thesis adaptive Simson quadrature method is used for the integral evaluation and Newton-Raphson method is employed to solve the nonlinear equations. These two methods have been disscussed in detail in Appendix I.

1.4.4.2 Visualization of tensor order parameter Q

Visualization of tensor order parameter $\mathbf{Q}$ in terms of its eigenvalues is needed to characterize the structural orientation and to understand the physics behind the ordering of each species within the mixture, as mentioned in section (1.3.2.2.3). $\mu_n, \mu_m \& \mu_l$ are the eigenvalues of $\mathbf{Q}$ and obey the following restrictions: $\mu_n + \mu_m + \mu_l = 0;\quad -1/3 \le \mu_i \le 2/3$. To facilitate the visualization of the tensor $\mathbf{Q}$

it is practical to use $\mathbf{M} = \mathbf{Q} + \dfrac{\mathbf{I}}{3}$ such that $\mu_{nM} + \mu_{mM} + \mu_{lM} = 1; \quad 0 \leq \mu_{iM} \leq 1$. The eigenvalues of $\mathbf{M}$ (μ_{nM}, μ_{mM} & μ_{lM}) are used to visualize $\mathbf{Q}$, so that each eigenvalue, which is used to construct one axis of the ellipsoid, represents the extent of orientation of the molecules in the direction of its corresponding orientational axis i.e. $\mathbf{n}$, $\mathbf{m}$ and $\mathbf{l}$. Figure 1-12 shows the elliptical representation of the tensor order parameter.
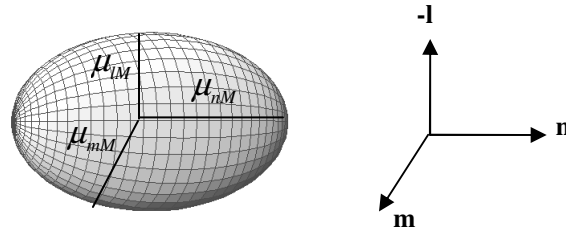
Figure 1- 12. Elliptical visualization of the tensor order parameter Q and its corresponding orientational triad system. Each dimension of the ellipsoid is composed by the eigenvalue of Q which correspond to one of its eigenvectors (n, m or l).

1.5 Need for Mesophase Mixture Modeling and Simulation

It has been shown that the effect of extensional flow, temperature and size of the fibre influence the orientational behaviour of the nematic molecules and the structure of a model fibre made of a pure DNLC system[29, 35-37, 52-57]. However, in reality anisotropic pitch- based CFs are made of CMs which are mixtures of DNLCs. Hence, there is a knowledge gap between the orientational behaviour of the pure DNLC system and the fibre structure that they form under different fibre spinning conditions, such as temperature, flow condition, size of the holes of the spinneret, and the orientational structure and the morphology of the real high modulus carbon fibres based on CM materials. As CM materials are mixtures of DNLCs, a clear understanding of the physics of discotic mixtures and their orientational behaviour at different processing conditions is essential. Figure1-15 summarizes the steps which are essential to fill the gap between the well understood system, pure DNLC, (the first circle) and the real fibre structure (final circle): (i) the thermodynamic model (Maier-Saupe model) of the pure DNLC has to be extended to the mixture to take into account the effect of temperature on the

orientational behaviour of the mixtures. (ii) In the next step the simultaneous effects of extensional flow and processing temperature on the orientational behaviour of the mixtures needs to be considered. (iii) Taking into account the simultaneous effects of temperature, flow intensity, the fibre radius and the interface between the fibre and the die mould on the orientaional behaviour of DNLC mixture is the last step to take to achieve the final structure of the fibre. This thesis focuses on the first two steps (steps (i) and (ii)), and its results can be used as the starting point for the third step (see section 6.4) .
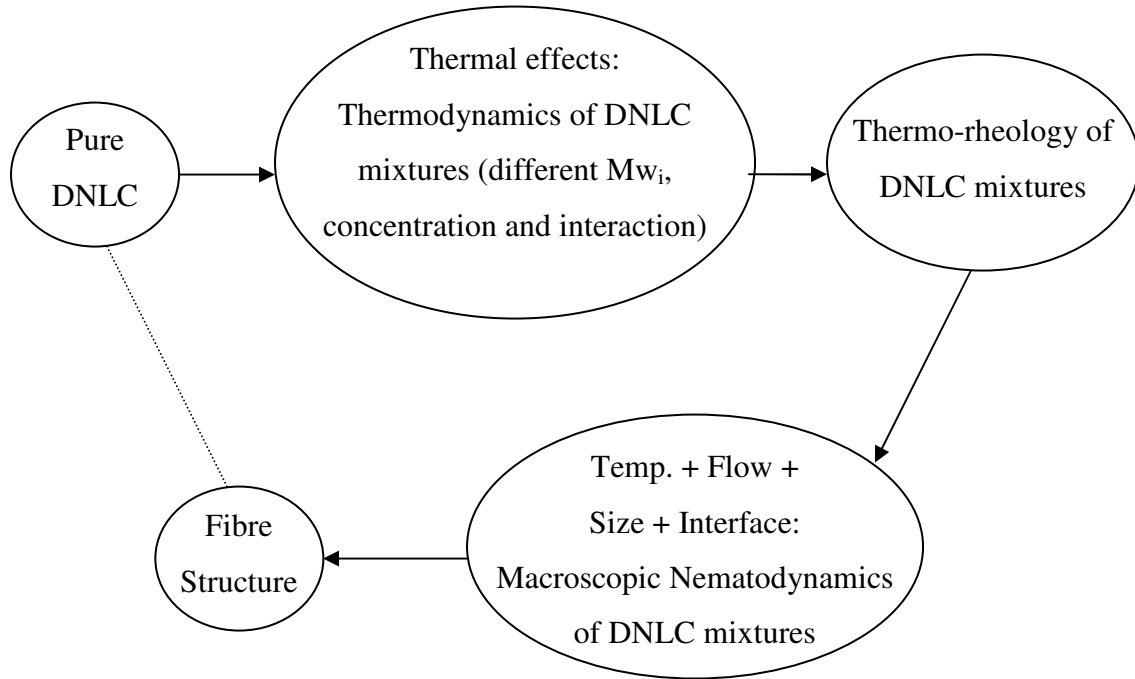
Figure 1- 13. The essential steps and parameters needed to be taken into account to describe the structure of a CM based CFs. The first circle (Pure DNLC) is well recognized and understood. The final circle (Fiber Structure) shows the final goal. The intermediate circles show the steps needed for consideration to fill this knowledge gap.

1.6 Motivations and Objectives

As mentioned in section (1.1.2) by mixing discotic liquid crystalline components different advantages to both the formation process and to the final application can be achieved. As mentioned in the previous section it has been proved that parameters such as temperature and extensional flow change the orientation of the pure nematic systems and influence the final structure of the fibres based on single

species precursors. However, in reality CMs are composed of   species with different molecular weights and concentrations. As explained in section (1.3.2.4) characteristics of these mixtures such as composition, polydispersity and molecular interaction along with the temperature and flow intensity are supposed to influence the final microstructure, final properties and final application of carbon fibres. Hence property optimization and cost reduction of high performance carbonaceous fibres require a better understanding of the thermodynamics, and thermorheology of CMs   consisting of a mixture of monodisperse disotic nematic liquid crystals. To meet these objectives this thesis concentrates on the thermodynamics of CM binary mixtures composed of two monodisperse components through the MS theory.

It is also well known that the type and extent of any kind of nematic liquid crystals, NLCs, applications are mainly determined by their thermal properties and behaviour. Hence by use of thermodynamic approach in the current thesis the thermal behaviour of the system and the macroscopic energetic and/or entropic aspects of NLC mixtures are also revealed so that comprehensive understanding of materials can be achieved[43]. For this purpose calorimetry is computed and employed to detect the entropic behaviour of the mixture as well as its transition behaviour. By use of this quantity three fundamental thermodynamic values viz. enthalpy, entropy, and free energy can be obtained; as a result, it can give   insight into the microscopic and macroscopic thermodynamic aspects of the system.

Characterization of the orientation in mixtures of NLCs needs to be further explored. As mentioned in section (1.4.2.3) characterization tools such as X-ray diffraction intensity are experimentally employed to detect the ordering behaviour and ordering magnitude. For the short range ordering the small beam size required for the experimental investigations to assess the orientational order makes the experiment unfeasible and expensive. In these cases, computational simulation of this characterization method can serve as a powerful tool to well characterize the ordering. In this thesis, theory and simulations of X-ray intensity has been performed to strengthen the link between simulation predictions and experimental observations.

Manufacturing and use of high performance liquid crystalline products and devices such as LCDs, C/C composites and CFs involves viscoelastic flows. For instance carbon fibre spinning process involves uniaxial extensional flow of liquid crystalline polydisperse CM precursors. Hence, this thesis seeks to extend the thermodynamics of carbonaceous mesophase binary mixtures with two monodisperse components to non-equilibrium states resulting from an imposed uniaxial extensional flow to investigate their thermorheological behaviour.

Another issue that requires further investigation is the orientational behaviour, phase state and structural orientation (*ODF*) of the mixture's components. As mentioned previously these mixtures are amphotropic (thermotropic/lyotropic) mixtures. In other words the orientational behaviour of the mixture is altered through the change in temperature and concentration. From point of view of application it is important to determine how each component behaves in the presence of the other at a specific temperature, concentration and flow intensity. In this thesis the effect of temperature, concentration and flow intensity on the orientational behaviour of each species and its contribution to the overall orientation of the amphotropic NLC binary mixture is also investigated.

 Lastly the orientational behaviour of NLCs in the presence of electric, magnetic and extensional flow fields follow the same physics, the observation of the orientation of the system under the extensional flow in this thesis can be used to predict its orientational patterns in the presence of the magnetic or electric fields.

The specific objectives of this thesis are:

1. to develop and solve an equilibrium thermodynamic model for binary discotic nematogens mixture based on the MS model; this model is employed to characterize the effect of intrinsic properties (molecular weight asymmetry, and molecular interactions) and concentration, on the nematic local orientation and on its local structure;

2. to extend the MS thermodynamic model to implement the extensional flow effects and then to evaluate the effect of the extensional flow on the orientational behaviour of CM binary mixtures with monodisperse components, on the phase status and on the transition behaviour of the NLC mixture;

3. to construct the thermo-rheological phase diagram of the binary DNLC mixture that reveals localized structure formation in the presence of flow;

4. to model and compute the characterization tools such as X-ray diffraction intensity and heat capacity to assess the orientational and thermo-rheological behaviour and to determine the phase diagrams of binary NLC mixtures;

5. to find, classify, characterize and explain the expected structural diversity that emerges in discotic mesogenic mixtures by regulating the thermotropic/lyotropic effects under the extensional flow of varying strength;

6. to compare MS theory to the macroscopic NLC theory (Landau de Gennes) which are used for the fibre structure modeling. This will be the start point for the structural modeling and prediction of the mechanical performance of pitch based carbon fibres which are beyond the scope of the current thesis.

1.7 Thesis Scope and Organization

A detailed description of this thesis scope and organization is shown in figure 1-14.
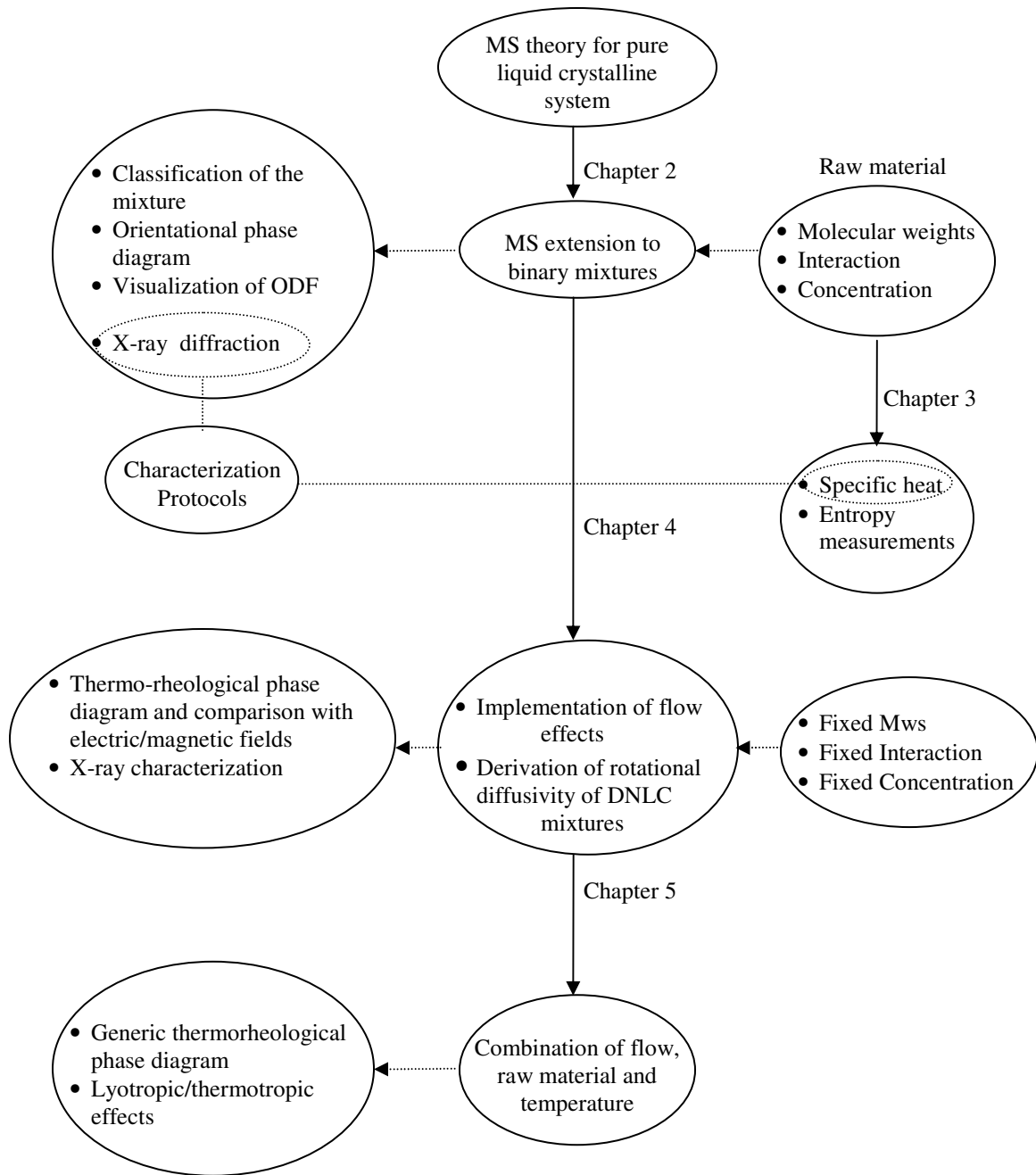
Figure 1- 14. Thesis summary and organization. Maier-Saupe theory (MS) of the pure discotic nematic liquid crystalline (DNLC) system is extended to the binary mixture of these materials. The effect of the characteristics and composition of the mixture (Mw of the components, their interaction and their concentration) on the orientational behavior of the system is studied through the extended theory. Rotational diffusivity of each discotic component within the mixture is modeled. X-ray intensity and specific heat are modeled as the characterization tools of the ordering in the system. The theory is then extended to implement the flow effects on the orientational behavior of the mixture with a fixed set of characteristics. The X-ray intensity of the system in the presence of flow is also modeled. In the last step the simultaneous effects of temperature and flow on the orientational behavior of different mixtures with different characteristics and composition are investigated.

1.7.1 Chapter 2: Thermodynamic modeling of carbonaceous mesophase mixtures

Chapter 2 studies thermodynamics of different CM binary mixtures with monodisperse components and determines how the difference between molecular weight of the components, their interaction and their concentration influence the orientational behaviour of the mixture. In this chapter MS theory which has been already used to explain and to predict the ordering behaviour and thermodynamics of the pure nematic liquid crystals[3] is first described in details and then it is extended to binary mixtures with components having different molecular weights. The extension of the theory is first validated with the observations of the pure material and then is employed to predict the thermodynamics and the equilibrium phase diagram of binary mixtures; to classify the types of the mixtures and to explain the orientational structure of the components based on their orientation distribution function, *ODF*, within the mixtures. X-ray diffraction intensity is also modeled and computed in this chapter as the characterization tool for the ordering behaviour of the mixture and for the verification of the derived model.

1.7.2 Chapter 3: Entropic behaviour of binary carbonaceous mesophases

Chapter 3 employs the MS theory derived in chapter 2 to calculate orientational entropy and orientational specific heat of the binary mixtures. These thermodynamic quantities are employed to characterize the type of the mixture as well as its characteristics such as nematic/isotropic transition temperature. Specific heat calculations provide a useful characterization tool to assess the molecular interaction, molecular weight differences and transition phenomena in the binary mixtures and are used as an appropriate verification criterion for the extended model.

1.7.3 Chapter 4: Structure and phase transitions of carbonaceous mesophase binary mixtures under uniaxial extensional flow

Chapter 4 incorporates extensional flow effects in the MS theory for binary mixtures. The rotational diffusivity of each discotic component in the CM mixture as a function of Mw of the components and their concentration is derived in this

chapter. The thermorhological phase diagram of the binary mixture in terms of temperature and flow intensity is obtained; different transition lines and different regions are characterized. The structural orientation of both components in each of the phase regions are obtained; the X-ray intensity expression derived in chapter 2 is extended to implement the flow effects and is employed to characterize the phase state and structural   of the mixture for a given temperature and flow intensity.

1.7.4 Chapter 5: Structural modeling of carbonaceous mesophase amphotropic mixtures under uniaxial extensional flow

The MS theory with the implemented flow effects is employed in this chapter to investigate the thermo-rheological phase diagram of the binary mixtures with varying concentration. For these mixtures it is found that there is a dominant and a slave component, with the former dominating the mixture structure while the latter adapts its structure by balancing thermodynamic, flow, and viscoelastic effects. It has been observed that the cooperation/competition of concentration/temperature effects single out the dominant component of the system. The most generic phase diagram in terms of temperature and flow intensity with twelve different phase regions is obtained. The structural orientation of both components in each region is characterized and can be employed to design specific orientational structure of the mixture by tuning the composition of the mixture, the temperature and the flow intensity.

1.7.5 Chapter 6: General conclusions, validations and original contribution to knowledge

Chapter 6 provides the main conclusions of the present thesis and summarizes the main accomplishments and contributions to knowledge. Validation of the models derived and the solution algorithm used in this thesis is also reviewed. Recommendations for future work are also suggested.

1.7.6 Appendix I: Numerical methods

The adaptive Simpson quadrature method to evaluate the integral terms and Newton-Raphson iteration method to solve the nonliner equation are described in detail in this appendix.

1.8 References

1. Collings, P. J.; Hird, M. *Introduction to Liquid Crystals*. Taylor & Francis: London, 1997.

2. Collings, P. J. *Liquid Crystals: Liquid crystals: natures delicate phase of matter* Princeton University Press: New Jersey, 2002.

3. Chandrasekhar, S. *Liquid crystals*. 2nd ed.; Cambridge University Press: Cambridge [England] ; New York, NY, USA, 1992.

4. Priestley, E. B.; Wojtowicz, P. J.; Sheng, P. *Introduction to liquid crystals*. Plenum Press: New York, 1975.

5. Gray, G. W. *Introduction and historical development.* In *Handbook of Liquid Crystals*, Demus, D.; Goodby, J.; Gray, G.W.; Spiess, H.W.; V.Vill, Eds. Wiley-VCH: New York, 1998; Vol. 1: Fundamentals.

6. Singh, S. *Liquid crystals*. World Scientific, London, 2002.

7. Rey, A. D. *Soft matter* **2010,** 6, 3402-3429.

8. Hurt, R. H.; Hu, Y. *Carbon* **1999,** 37, (2), 281-292.

9. Golmohammadi, M.; Rey, A. D. *Liquid Crystals* **2009,** 36, (1), 75-92.

10. Khoo, I.C. *Liquid Crystals: Physical Properties and Nonlinear Optical Phenomena*. John Wiley & Sons INC.: New York, 2007.

11. Fisch, M. R., *Liquid crystals, laptops and life*. World Scientific: London, 2004; Vol. 23.

12. Fitzer, E.; Manocha, L. M. *Carbon reinforcements and carbon/carbon composites*. *Springer*: *Berlin*, 1998.

13. Reichman, J. *Handbook of optical filters for fluorecence microscopy.* In *Chroma technology corp*.: Brattleboro, 1998.

14. Zhu, C.; Hieftje, G. M. *Applied Spectroscopy* **1989,** 43, (8), 1333-1336.

15. Ivanov, V. E.; Zolotovitskii, Y. M.; Ivanova, N. I. *Chemistry and Technology of Fuels and Oils* **1993,** 29, (1-2), 71-74.

16. Ishida, Y.; Kai, Y.; Kato, S. Y.; Misawa, A.; Amano, S.; Matsuoka, Y.; Saigo, K. *Angewandte Chemie-International Edition* **2008,** 47, (43), 8241-8245.

17. Janata, J.; Josowicz, M.; Devaney, D. M. *Analytical Chemistry* **1994,** 66, (12), R207-R228.

18. Wolinski, T. R.; Ertman, S.; Czapla, A.; Lesiak, P.; Nowecka, K.; Wdomanski, A.; Nowinowski-Kruszelnicki, E.; Dabrowski, R.; Wojcik, J. *Measurement Science & Technology* **2007,** 18, (10), 3061-3069.

19. Vorflusev, V.; Kumar, S. *Science* **1999,** 283, (5409), 1903-1905.

20. Flandrois, S. *Application of carbons.* In *Carbon molecules and materials*, Setton, R.; Bernier, P.; Lefrant, S. Taylor & Francis: London & New York, 2002; pp 458-464.

21. Yan, J. *Theory and simulation of texture formation in mesophase carbon fibers.* MS Theis, *McGill University*, Montreal, 2002.

22. http://en.wikipedia.org/wiki/Carbon_fiber.

23. http://en.wikipedia.org/wiki/Carbon_fiber#cite_note-1.

24. http://fibersource.com/f-tutor/rayon.htm.

25. http://en.wikipedia.org/wiki/Polyacrylonitrile.

26. Mushrif, S. H. *Multiscale theoritical and computational modeling of the synthesis, structure and Performance of functional carbon materials.* Ph.D. Thesis, McGill, Montreal, 2009.

27. McHugh, J. J.; Edie, D. D. *Liquid Crystals* **1995,** 18, (2), 327-335.

28. Walsh, P. J. *Carbon fibers, From ASM handbook, Vol 21: Composites*.

 29. Yan, J.; Rey, A. D. *Physical Review E* **2002,** 65, (3), 031713: 1-14.

30. Cervo, E. G.; Thies, M. C. *Journal of Supercritical Fluids* **2010,** 51, (3), 345-352.

31. Gupta, G.; Rey, A. D. *Carbon* **2005,** 43, (7), 1400-1406.

32. Cervo, E. G.; Thies, M. C. *Chemical Engineering & Technology* **2007,** 30, (6), 742-748.

33. Lezczynski, J. *Computational Materials Science* Elsevier Inc.: San Diego, 2004.

34. Golmohammadi, M.; Rey, A. D. *Journal of Non-Newtonian Fluid Mechanics* **2010,** 165, (13-14), 698-711.

35. Singh, A. P.; Rey, A. D. *Liquid Crystals* **1999,** 26, (6), 825-833.

36. Singh, A. P.; Rey, A. D. *Journal De Physique II* **1995,** 5, (9), 1321-1348.

37. Singh, A. P.; Rey, A. D. *Rheologica Acta* **1998,** 37, (4), 374-386.

38. Grecov, D.; de Andrade Lima, L. R. P.; Rey, A. D. *Plastics Rubber and Composites* **2006,** 35, (6-7), 276-286.

39. Picken, S. J. *Measurements and values for selected order parameters.* In *Physical Properties of Liquid Crystals: Nematics*, Dunmur D.; Fukuda A.; Lucchurst, G. INSPEC, The Institution of Electrical Engineers: London, 1999.

40. Collings, P.J.; Patel, J. S. *Handbook of liquid crystal research.* Oxford University Press: Oxford, 1997.

41. DeGennes, P. G.; Prost, J. *The physics of liquid crystals.* 2nd Edition ed.; Clarendon Press Oxford, 1995.

42. Nishizawa, T.; Sakata, M. *Carbon* **1992,** 30, (2), 147-152.

43. Sori, M., *Calorimetric measurments in nematics.* In *Physical Properties of Liquid Crystals: Nematics*, Dunmur, D. A.; Fukuda, A.; Luckhurst, G. R., Eds. INSPEC: London, 2001.

44. Ungar, G. *X-ray studies of nematic systems.* In *Physical Properties of Liquid Crystals: Nematics*, D. Dunmur; A. Fukuda; Lucchurst, G. INSPEC, The Institution of Electrical Engineers: London, 2002.

45. Ogale, A. A.; Lin, C.; Anderson, D. P.; Kearns, K. M. *Carbon* **2002,** 40, (8), 1309-1319.

46. Kundu, S.; Naskar, A. K.; Ogale, A. A.; Anderson, D. P.; Arnold, J. R. *Carbon* **2008,** 46, (8), 1166-1169.

47. Kundu, S.; Ogale, A. A. *Rheologica Acta* **2007,** 46, (9), 1211-1222.

48. Lhuillier, D.; Rey, A. D. *Journal of Non-Newtonian Fluid Mechanics* **2004,** 120, (1-3), 85-92.

49. Gorring, P.

http://www.csam.montclair.edu/earth/eesweb/gorring/geos443/443notes/xray.html

50. Sori, M., *Calorimetric measurments in nematics.* In *Physical Properties of Liquid Crystals: Nematics*, Dunmur, D. A.; Fukuda, A.; G.R., L., Eds. INSPEC: London, 2001; pp 14-50.

51. Rey, A. D. *Rheologica Acta* **1995,** 34, (5), 461-473.

52. Grecov, D.; Rey, A. D. *Molecular Crystals & Liquid Crystals* **2003,** 391, 57-94.

53. Doi, M. *Journal of Polymer Science: Polymer Physics Edition* **1981,** 19, 229-243.

54. Rey, A. D. *Macromolecular Theory and Simulations* **1995,** 4, (5), 857-872.

55. Hu, T. D.; Ryskin, G. *Journal of Chemical Physics* **1991,** 95, (8), 6042-6049.

56. Yan, J.; Rey, A. D. *Carbon* **2002,** 40, (14), 2647-2660.

57. Yan, J.; Rey, A. D. *Carbon* **2003,** 41, (1), 105-121.

2 Thermodynamic modeling of carbonaceous mesophase mixtures

2.1 Summary

The Maier-Saupe model is extended to the binary mixtures of uniaxial discotic nematogens to compute the equilibrium phase diagrams of carbonaceous mesophases. The ordering in the mixture is affected by temperature (thermotropic) and concentration (lyotropic). The magnitude of molecular weight asymmetry of two nematogenes and the strength of molecular interaction control the type of mixture: (a) non-ideal mixtures arise under sufficiently weak interaction and lower molecular weight differences, and (b) ideal mixtures arise under stronger molecular interaction and higher molecular weight asymmetries. Ideal mixtures have clearing (transition) temperatures that change monotonically with concentration and the higher molecular weight component has higher order parameter. Non-ideal mixtures have a minimum in the clearing temperature at a critical concentration at which the binary mixture behaves like a pure nematogen and the ordering of two species are identical; for non-ideal mixtures the relative magnitude in the species' ordering depends on the concentration; the species with lower molecular weight can have a higher order if its concentration is high enough. Characterization protocols based on x-ray computations and direct methods are proposed to detect the type of mixture and the magnitude of molecular interaction. The results provide new tools to design carbon fibers based on molecular properties.

2. 2 Introduction and literature survey

Carbonaceous mesophases (CMs), first reported by Brooks and Taylor[1], are discotic nematic liquid crystalline (DNLC) mixtures obtained from petroleum pitches and synthetic naphthalene precursors[2]. The composition, polydispersity and molecular orientation of CMs play a significant role on the final properties of cokes[3], carbon foams, carbon/carbon composites[4] and carbon fibers[5-8]. Property optimization and cost reduction of high performance carbonaceous materials require a better understanding of the thermodynamics, and dynamics of CMs

mixtures and their intrinsic properties. For instance, it is known that the final structure of the fibers based on the pure liquid crystalline materials are influenced by the temperature[9]; however, in reality CMs are not pure LCs, they are composed of the species with different molecular weights and concentrations. Several theoretical and experimental studies have been carried out on binary nematic liquid crystalline (NLC) mixtures[8, 10-14]. However, no systematic investigation has been performed to find out how the nature of the mixture and its composition control the final structure of the CM fibers and optimize product performance in structural and functional (thermal) applications. To meet this objective this paper focuses on the equilibrium thermodynamics of CM binary mixtures. As a starting point in this weakly explored area, we consider an athermal solution of two thermotropic uniaxial discotic nematogens that only differ in molecular weight thus precluding phase separation. It has been previously shown in the literature that phase separation does not play a significant role in the mixture of nematic liquid crystals differing in molecular weight. The components of some of the mixtures they have investigated also differ in the chemical structure [12, 15-17]. Based on available experimental data[10] we choose representative molecular weights of 200 to 1400.

The theory derived in this work can also be used in other nematic liquid crystalline areas. For instance, mixtures of two or more mesogens are also important in LCD (liquid crystal display) applications, where composition of the mixture is used to overcome the restrictions due to thermal operating conditions and optimization of response time by calibration of viscoelastic properties. The Maier-Saupe (MS) theory is widely used to describe the thermodynamics of nematic liquid crystals[18]. This mean field theory gives the temperature-dependence of the molecular orientation in mesogenic materials. It predicts the values of the experimentally measured scalar order parameters[19] very well and hence it has been applied to different nematic liquid crystalline systems and can be adjusted to their mixtures[12, 20]. In this paper we use the Maier-Saupe (MS) theory adjusted to binary uniaxial discotic nematogens.

The usual description of a single species discotic nematic liquid crystal[21] is based on the normalized orientation distribution function $ODF(\mathbf{u})$, where $\mathbf{u}$ is the orientation of the disk normal, given by:

$$ODF(\mathbf{u}) = \frac{1}{2\pi}f_o + \frac{3\times 5}{2\pi\times 2}Q_{ij}^2\, f_{ij}^2 + \frac{3\times 5\times 7\times 9}{2\pi\times 2\times 3\times 4}Q_{ij}^4\, f_{ij}^4 + \dots \quad (2.1)$$

where $f_o, f_{ij}^2, f_{ijkl}^4, \dots$ are orthogonal surface spherical harmonics and where the coefficients of the Fourier expansion, $\mathbf{Q}^2, \mathbf{Q}^4, \dots$ are symmetric and traceless tensors found using orthogonality. The quadrupolar tensor order parameter $\mathbf{Q}^2$ used in the Landau-de Gennes viscoelastic model[22] is:

$$\mathbf{Q} \equiv \mathbf{Q}^2 = \int_{\mathbb{Z}^2} f(\mathbf{u})\,\mathbf{f}^2\; dA = \int_{\mathbb{Z}^2} f(\mathbf{u})\left(\mathbf{uu} - \frac{\boldsymbol{\delta}}{3}\right)\; dA = \left\langle \mathbf{uu} - \frac{\boldsymbol{\delta}}{3} \right\rangle \quad (2.2)$$

where $\mathbb{Z}^2$ is half the unit sphere. For uniaxial phases $\mathbf{Q}$ is given in terms of a temperature-dependent scalar order parameter $s(T)$ and the average molecular orientation or director $\mathbf{n}$: $\mathbf{Q} = s(\mathbf{nn} - \mathbf{I}/3)$. The possible states of uniaxial discs are: (i) isotropic (I):$s=0$, and (ii) nematic $s>0$. For CMs at high temperatures the stable phase is isotropic and at sufficiently lower temperatures it is nematic; issues of stability of nematic phases in CMs are discussed in [23]. As shown in Appendix B (eqn.A2.16), for binary mixtures of uniaxial mesogens, a similar development leads to the mixture quadrupolar order parameter:

$$\mathbf{Q}_{mix} \equiv \mathbf{Q} = m_1\mathbf{Q}_1 + m_2\mathbf{Q}_2 \quad (2.3)$$

where m_i is the mole fraction of ith component. For binary discotic nematogens at equilibrium we find collinear directors $(\mathbf{n}_1 = \mathbf{n}_2)$ and the mixture uniaxial scalar order parameter then is: $s_{mix} = m_1 s_1 + m_2 s_2$. Nevertheless, since the ordering states of each species are coupled and are also dependent on temperature and dilution, we expect, based on the above observations, that binary mixture display three states:

(i) isotropic (I) : $s_1=0$, $s_2=0$;

(ii) nematic (N_{12}) with $s_1 \geq s_2$;

(iii) nematic (N_{21}) with $s_1 \leq s_2$.

For the exceptional case when $s_1 = s_2$, the nematic mixture behaves like a single component system. Previous work[24] on liquid crystalline mixtures of dissimilar mesogens focuses on phase separation effects while this paper focuses on similar mesogens under no phase separation. Figure 2-1 shows an schematic of the possible equilibrium phase diagrams for binary CMs, in terms of temperature (T) as a function of composition (m_1). The diagrams show the equilibrium phases that are possible for different degrees of interaction (β) and different degrees of molecular weight difference between the two components (ΔM_w); in this example species "1" has higher molecular weight and hence NI transition temperature than species "2". Figure 2-1a shows the thermodynamic phase diagram of a typical non-interacting ($\beta=0$) mixture. The two full lines denote the NI transition for each species; the decreasing transition temperature as dilution increases is the typical lyotropic effect. As the two transition lines cross, four phase regions are possible: I_1-I_2, I_1-N_2, I_2-N_1, N_1-N_2, where the subscript (1, 2) denotes the species. For example, when $m_1=0.6$, quenching from a sufficiently high temperature leads to the following sequence:

$$I_1, I_2 \rightarrow N_1, I_2 \rightarrow N_1, N_2$$
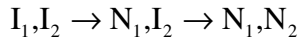
In the presence of molecular interaction ($\beta>0$), shown in figures 2-1b, 2-1c, the crossing transition lines become a single continuous isotropic-nematic transition curve, such that below (above) this curve the two species are in the nematic (isotropic) state. Depending on the nature of the mixture (i..e. molecular weight difference ΔMw and the interaction β between the components) N_{21} can show up (figure 2-1c) or it can disappear (figure 2-1b). This fact is reflected in the temperature-concentration phase diagram of the mixtures (T, m_1) which can be classified as follows:

(i) The transition temperature, T_{NI}, increases monotonically by increasing concentration; this type of behavior, which is called ideal, does not exhibit N_{21} phase (figure 2-1.b). By decreasing the temperature the only possible transition when $Mw_1 > Mw_2$ is:

$$I_1, I_2 \rightarrow N_1, N_2$$

$\beta = 0$
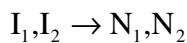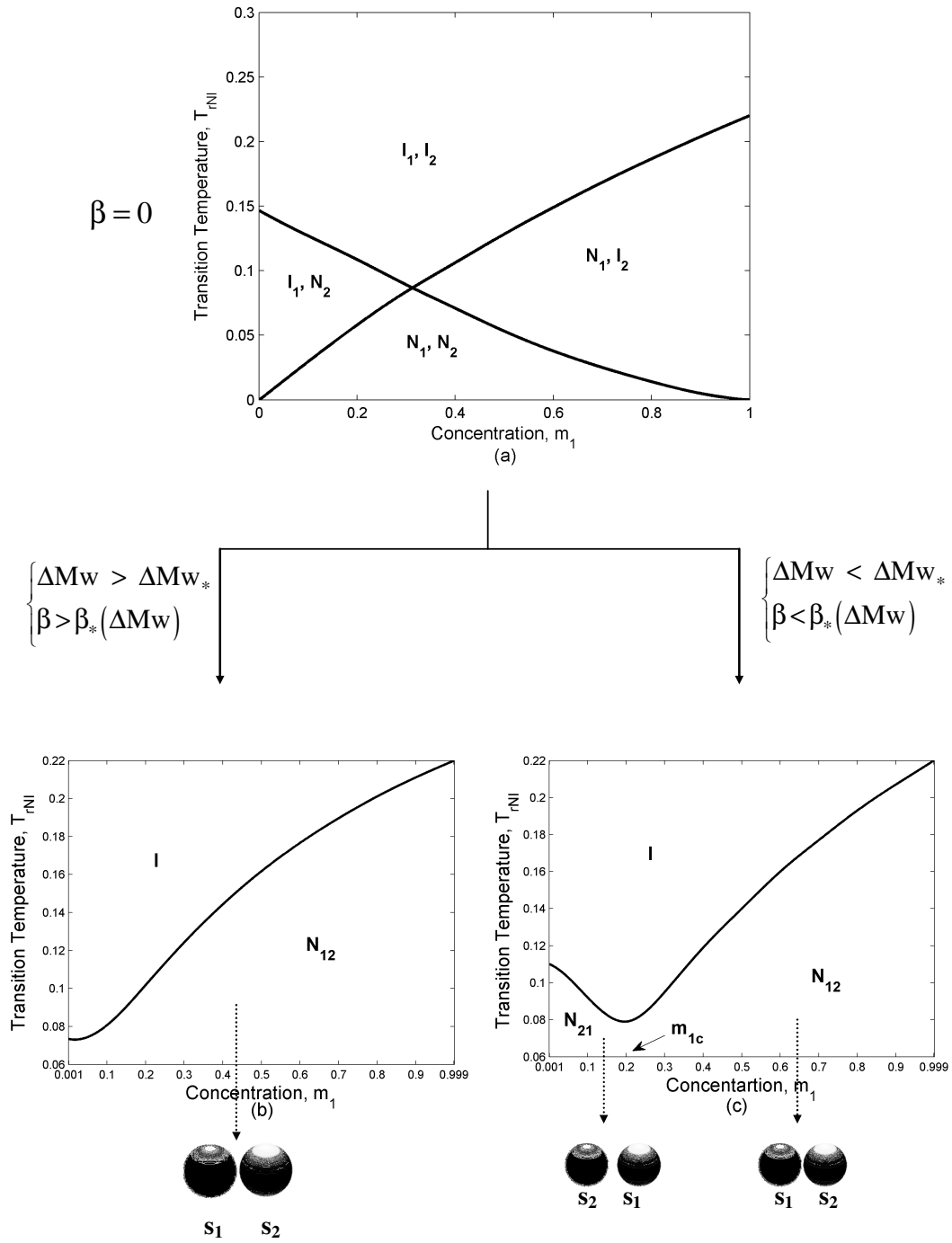
Figure 2- 1. Schematics of the expected thermodynamic phase diagrams in terms of temperature as a function of composition: (a) for non-interacting mixtures (β=0) (b) For sufficiently strongly interacting mixtures and /or sufficiently large molecular weight asymmetry (c) For weakly interacting mixtures and /or small molecular weight asymmetry.

with $s_1>s_2$. The spheres below the diagram are schematics of the orientation distribution functions of the two components on the unit sphere, where the size of the white polar cap represents the degree of molecular order; since $s_1>s_2$ the white area of "1" is smaller than the one for "2".

(ii) The transition temperature exhibits a minimum by increasing the concentration. This type of behavior, shown in figure 2-1c is called non-ideal and allows the formation of the N_{21} mixture ($s_2>s_1$) even though $Mw_2<Mw_1$. The N_{21} and N_{12} areas are separated by a vertical line that defines the critical concentration (m_{1c}) at which $s_1=s_2$ and the binary mixture behaves as single component nematogen. The critical mixture that emerges due to concentration effects is characterized by the minimum transition temperature in the temperature-composition phase diagram (T, m_1). These mixtures are formed at a specific concentration; we call it critical concentration, m_{1c}. Depending on the concentration values two cases arise:

(i) below the critical concentration, the low-molecular weight component which has higher concentration is more ordered and as a result, has a major contribution to the ordering of the mixture (lyotropic effect) so that $s_2>s_1$ (N_{21}), as shown in the orientation distribution functions below the figure;

(ii) for more concentrated systems (above critical concentration), the component with higher molecular weight makes the major ordering contribution to the mixture (Mw effect) so that $s_1>s_2$ (N_{12}), as shown in the orientation distribution function below the figure.

The specific objectives of this paper are:

(i) to develop and solve an equilibrium thermodynamic model for binary discotic nematogens athermal mixture based on the MS model;

(ii) to characterize the role of intrinsic properties (molecular weight asymmetry, and molecular interactions) and dilution, on the nematic structure;

(iii) to characterize phase transition and critical concentration in binary discotic nematogenic mixtures;

(iii) to derive an equation for the value of the interaction in the critical mixture;

(iv) to propose methods to assess the magnitude of the interaction parameter and classify mixtures.

The main focus of the paper is to describe the effect of mixing, dilution, molecular weight asymmetry on the molecular order, and phase ordering and phase transition of the mixture. Analysis of heat of transitions and related thermodynamic aspects of phase transitions are outside the scope of this paper.

The organization of this paper is as follows. Appendix A presents the single component MS model in a form compatible with the mixture model. Appendix B derives the orientation distribution of a nematic mixture in terms of the single component distributions and derives the equation for the mixture quadrupolar order parameter $\mathbf{Q}_{mix}$. Section 2.3 presents the MS binary mixture model; thermodynamic consistency and convergence to single component expression is proven. The main parameters are identified and the numerical solution scheme is defined. The thermotropic and lyotropic nature of these mixtures is discussed and the effect of molecular weight is established. Section 2.4 presents the derivation of the equation used to characterize the interaction parameter β, as well as the derivation of the X-ray intensity to determine the type of the mixture as well as the value of the critical concentration. Section 2.5 presents the numerical results and discussion: Section 2.5.1 discusses the effect of (i) the relative alignment of the components, (ii) the molecular weight asymmetry, (iii) dilution, and (iv) the interaction parameter on the molecular structure and ordering of the mixture. Section 2.5.2 discusses the effect of different parameters on the phase diagram of CM binary mixture; as mentioned above the intrinsic parameters are molecular weight asymmetry (ΔMw) and the interaction parameter (β) and the operating conditions are concentration (m_1) and temperature (T). Section 2.5.3 presents X-ray intensity and the average ordering at transition as the tools to characterize the type of the mixture as well as the value of the critical concentration. Section 2.6.5 provides the conclusions.

2.3 Maier-Saupe Binary Mixture Model

The Maier-Saupe model for a single component NLCs[25] is briefly described in Appendix A and extended below to a binary mixture of two discotic nematogens.

For a homogeneous binary mixture, the internal energy E_{mix} per molecule is given by the summation of three contributions:

$$E_{mix} = E_{11} + E_{22} + E_{12} \tag{2.4}$$

due to self (1-1, 2-2) and cross (1-2) species interactions. Figure 2-2 shows a schematic of the components in the binary mixture, where $\mathbf{u_1}$ and $\mathbf{u_2}$ are molecular unit normals and $\mathbf{n_1}$ and $\mathbf{n_2}$ are the corresponding directors with the relative alignment α. In view of eqn. (2.4), the internal energy of the mixture is (see Appendix A) generalized to:

$$E_{mix}(\mathbf{Q}) = -\frac{3}{4}W_{11}\mathbf{Q_1} : \mathbf{Q_1} - \frac{3}{4}W_{22}\mathbf{Q_2} : \mathbf{Q_2} - \frac{3}{2}W_{12}\mathbf{Q_1} : \mathbf{Q_2} \tag{2.5}$$

where the composition and molecular weight-dependent interaction parameters $\{W_{11}, W_{22}, W_{12}\}$ are:

$$W_{ii} = m_i^2 U_{ii} \; ; \; W_{12} = m_1 m_2 U_{12};$$

$$U_{ii} = \bar{U}_{ii} \frac{Mw_i}{m_1 Mw_1 + m_2 Mw_2};$$

$$U_{12} = \bar{U}_{12} \frac{\sqrt{Mw_1 Mw_2}}{m_1 Mw_1 + m_2 Mw_2}$$

where Mw_i denotes the molecular weight of the ith component, m_i its mole fraction, and $\{\bar{U}_{11}, \bar{U}_{22}, \bar{U}_{12}\}$ are the bare interaction parameters. Based on eqn.(2.5) and the MS model, the partial internal potentials (Φ_1, Φ_2) acting on each species are:
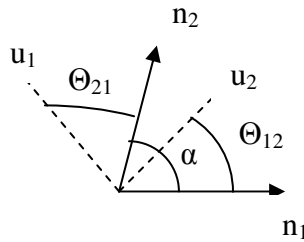
Figure 2- 2. Schematic of molecular orientation (u_1,u_2) and directors (n_1,n_2) in binary discotic nematogens which form a single nematic phase. The relative angle between the directors is α.

$$\Phi_1 = \frac{\partial E_{mix}}{\partial \mathbf{Q}_1} : \left(\mathbf{u}_1\mathbf{u}_1 - \frac{\mathbf{I}}{3}\right) = -\frac{3}{2}\left(W_{11}\mathbf{Q}_1 + W_{12}\mathbf{Q}_2\right) : \left(\mathbf{u}_1\mathbf{u}_1 - \frac{\mathbf{I}}{3}\right)$$

$$\Phi_2 = \frac{\partial E_{mix}}{\partial \mathbf{Q}_2} : \left(\mathbf{u}_2\mathbf{u}_2 - \frac{\mathbf{I}}{3}\right) = -\frac{3}{2}\left(W_{22}\mathbf{Q}_2 + W_{12}\mathbf{Q}_1\right) : \left(\mathbf{u}_2\mathbf{u}_2 - \frac{\mathbf{I}}{3}\right)$$

(2.6)

The Helmholtz free energy per unit mole of the homogeneous mixture $A(\mathbf{Q}_1, \mathbf{Q}_2)$ is:

$$A(\mathbf{Q}_1, \mathbf{Q}_2) = -N_A\left(E_{mix} + k_B T \ln Z\right)$$ (2.7)

where N_A is Avogadros number and the mixture partition function Z is factorized :

$$Z = Z_1^{m_1} Z_2^{m_2} = \left(\int e^{-\Phi_1/m_1 k_B T} d\mathbf{u}_1\right)^{m_1} \left(\int e^{-\Phi_2/m_2 k_B T} d\mathbf{u}_2\right)^{m_2}$$ (2.8)

where Z_i is the partition function of the ith species. Equations (2.5, 2.7, 2.8) are consistent with the thermodynamics[26] since they obey:

$$E_{mix} = \frac{d\beta A / N_A}{d\beta} = -E_{mix} - \frac{d\ln Z}{d\beta}$$ (2.9)

The ten equations of equilibrium are obtained by minimizing the free energy A (eqn.(2.7)) with respect to $(\mathbf{Q}_1, \mathbf{Q}_2)$.   According to the disccusion regarding eqn.(2.3) , the binary mixture displays an isotropic state and unixial nematic states. Hence we can safely reduce the solution space (from ten equations to two equations) and parametric space as follows. Scaling the Helmholtz free energy A with the bare interaction parameter $\overline{U}_{11}$, minimizing the resulting dimensionless free energy with respect to $\mathbf{Q}_1$, $\mathbf{Q}_2$, and double-contracting the tensorial equations with $\mathbf{n}_1\mathbf{n}_1$ and $\mathbf{n}_2\mathbf{n}_2$, respectively, we find:

$$m_1\varphi_1 S_1 + \frac{3}{2}\sqrt{m_1 m_2 \varphi_1 \varphi_2}\,\wp_1 S_2\left(\cos^2(\alpha) - \frac{1}{3}\right) - T_r \sum_{i=1}^{2} \frac{m_i}{Z_i}\frac{\partial Z_i}{\partial S_1} = 0$$

$$\frac{3}{2}\sqrt{m_1 m_2 \varphi_1 \varphi_2}\,\wp_1 S_1\left(\cos^2(\alpha) - \frac{1}{3}\right) + m_2\varphi_2\wp_2 S_2 - T_r \sum_{i=1}^{2} \frac{m_i}{Z_i}\frac{\partial Z_i}{\partial S_2} = 0$$

(2.10)

where the partition functions Z_i are defined in eqn.(2.6, 2.8). The asymptotic limits of eqns.(2.10) (m_1=0,1) of this expression correspond to the pure NLC. As shown

below for the present CM case, the mixture is uniaxial and $\alpha=0$. The thermodynamic of the mixture is defined by the dimensionless temperature T_r and two effective mole fractions:

$$T_r = \frac{k_B T}{\overline{U}_{11}} \quad ; \quad \varphi_i = \frac{m_i Mw_i}{\sum m_i Mw_i} \tag{2.11}$$

The two material parameters of the model are:

$$\wp_1 = \frac{\overline{U}_{12}}{\overline{U}_{11}}; \quad \wp_2 = \frac{\overline{U}_{22}}{\overline{U}_{11}} \tag{2.12}$$

The material parameters $(\wp_1, \wp_2)$ are functions of the species' molecular weights. To introduce the molecular weight dependence we use experimental data[19] in conjunction with the well-known relation $\overline{U}_{ii} = 4.542 k T_{NIi}$, where the clearing temperature T_{NIi} is a function of the molecular weight Mw_i. Experimental data on CMs suggest that this dependence is well fitted by a linear function:

$$T_{NIi} = \overline{U}_{ii}/4.542 k = a + b\, Mw_i \tag{2.13}$$

where the parameters (a,b) , based on the data of [24] are chosen as: a=-150 and b=0.75.

We choose component "1" as a representative component of a CM with Mw_1 =1400^{10} and vary the molecular weight Mw_2 of the second component so that molecular weight asymmetry $\Delta Mw = Mw_1 - Mw_2$ changes. Using eqns. (2.12, 2.13) and experimental data we find the following molecular weight dependence of $\wp_2$:

$$\wp_2 = \frac{\overline{U}_{22}}{\overline{U}_{11}} = \frac{4.542 k T_{NI2}(Mw_2)}{4.542 k T_{NI1}(Mw_1)} = \frac{c + d Mw_2}{c + d Mw_1} \tag{2.14}$$

where (c, d) are constants. Since the molecular weight dependence of $\wp_1$ is not suggested by actual data, we use:

$$\wp_1 = \beta\, \wp_2 \tag{2.15}$$

where β is a constant whose sign depends on the geometrical nature of the species: for the similar components, i.e. disks and disks or rods and rods, it is positive;

however, for dissimilar ones it is negative[27]. We note that taking β as another material parameter will not affect the essential nature of the results (i.e. presence of the ordering states (I, N)) but will only shift phase transition curves in the thermodynamic phase diagram.

The present thermodynamic model is given by the two nonlinear integral equations (eqns.(2.10)); the solution vector consists of the two scalar order parameters (s_1, s_2); the two material parameters are β and ΔMw; the thermodynamic phase diagram is obtained by sweeping over temperature T_r and concentration m_1. Equations (2.10) are solved by Newton-Raphson method, with an eight order Simpson integration method. Stability, accuracy, and convergence were ensured using standard methods. For the higher values of the molecular weight asymmetry and the higher values of the interaction parameter the numerical algorithm exhibits multiple solutions in the vicinity of the transition temperature. Depending on the values of the initial guess, the final solution vector would be different. Therefore, the values of the free energy are compared for different initial guesses and the one with the minimum energy is selected as the correct solution. Issues of metastability are not considered in this paper.

2.4 Characterization Methods

2.4.1 Computation of the Interaction Parameter for Critical Mixtures

In this section we present tools to characterize non-ideal mixtures that exhibit a minimum in the NI transition temperature corresponding to a concentration at which the two species form a pseudo-pure component nematic. Different experimental studies have reported a pronounced minimum in the transition temperature of the liquid crystalline mixtures as a function of the concentration[8, 28-30]. However, theses studies have not addressed the effect of intrinsic parameters involved in the CM mixtures, the most important one being the molecular weight asymmetry. The minimum in the phase diagram (see figure 2-1c) shows a weak interaction between the components. To calculate the values of the interaction parameter, β, of a given nematogen mixture with specific critical concentration and molecular weight asymmetry, we solve eqns.(2.10) with $s_1 = s_2$ and obtain:

$$\beta = \frac{(1-m_{lc})\left(1-\dfrac{\Delta Mw}{Mw_1}\right)\left(\dfrac{T_{rNI2}}{T_{rNI1}}\right) - m_{lc}}{(1-2m_{lc})\sqrt{\left(1-\dfrac{\Delta Mw}{Mw_1}\right)\left(\dfrac{T_{rNI2}}{T_{rNI1}}\right)}} \qquad (2.16)$$

Once we determine the value of the critical concentration (m_{1c}) for a mixture with known molecular weights (M_{w1}, M_{w2}) and transition temperatures (T_{rNI1}, T_{rNI2}), the interaction parameter β can be calculated by using eqn.(2.16). In section 4.3, we show how to determine the critical concentration and how to find the interaction parameter by using eqn.(2.16).

2.4.2 X-Ray Intensity

The solution vector (s_1, s_2) to eqns.(2.10) is used to predict X-ray intensity using previously derived equations[26]. The X-ray intensity $I_i(\theta)$ of a single component NLC when assumed to follow the MS theory, is[31]:

$$I_i(\theta) = \frac{\sqrt{\pi}}{2} ODF_i(\theta) \frac{erf\left(\sqrt{-\phi_i(\theta)/m_i kT}\right)}{\sqrt{-\phi_i(\theta)/m_i kT}} \qquad (2.17)$$

where the single species orientation distribution function is:

$$ODF_i = \exp\left(-\phi_i/m_i kT\right)/Z_i \qquad (2.18)$$

and erf is the error function. Measuring $I_i(\theta)$ is thus a useful way to determine the orientation distribution function $ODF_i(\theta)$. A review of application of eqn.(2.17) in conjunction with the MS theory is given in [32]. For a uniaxial nematic mixture ($\alpha=0$; see figure 2-2) we can safely assume that equation (2.17) holds. Using this assumption we find the mixture X-ray intensity $I_{mix}(\theta)$:

$$I_{mix}(\theta) = \frac{\sqrt{\pi}}{2} ODF_{mix} \frac{erf\left(\sqrt{-\phi_{mix}(\theta)/kT}\right)}{\sqrt{-\phi_{mix}(\theta)/kT}} \qquad (2.19)$$

where the mixture orientation function ODF_{mix} and the mixture Maier-Saupe mean field potential ϕ_{mix} are (see Appendix B):

$$ODF_{mix} = m_1 ODF_1 + m_2 ODF_2 = \exp\left(-\phi_{mix}(\theta)/kT\right)/Z_{mix}$$
$$-\phi_{mix}(\theta)/kT = \ln\left(Z_{mix}\left(m_1 ODF_1 + m_2 ODF_2\right)\right) \qquad (2.20)$$

In this work we solve eqns.(2.10) for selected areas of the (T_r, m_1) phase diagram, calculate the ODF using eqn.(2.18, 2.20), and then use the results in conjunction with eqn.(2.19) to compute $I_{mix}(\theta)$.

2.5 Results and Discussion

2.5.1 Structure of the Nematic Phase

2.5.1.1 Relative Alignment (α):

The relative alignment α defines the nature of the nematic mixture: (i) uniaxial, α=0 and (ii) biaxial, $\alpha \neq 0$. In the original tensorial formulation, minimizing A (eqn.(2.7)) with respect to (Q_1, Q_2) determines α. For mixtures of uniaxial disks differing only in molecular weight, α is zero and the nematic mixture is therefore uniaxial. (figures 2-2, 2-3). Under external fields such as confinement, flow, magnetic and electrical fields α is an unknown[33-35].
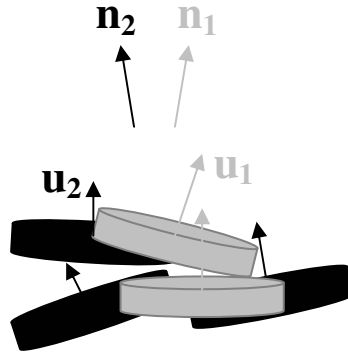
Figure 2- 3. Schematic of a binary mixture of discotic nematogens , representative of a CM mixture.

2.5.1.2 Effect of Molecular Weight Difference

This section shows how the state (I, N) and the phase transition of the binary mixture depends on the molecular weight difference $\Delta Mw = 1400 - Mw_2$.

Figure 2-4 shows the scalar order parameters s_1, s_2 and s_{mix} as a function of dimensionless temperature T_r, for $m_1 = 0.2$, $\beta = 0.1$, $\Delta Mw = 800$ (a), and $\Delta Mw = 400$ (b). At sufficiently high ΔMw (figure 2-4a), the lower molecular weight component has less ordering in spite of its higher concentration. At high enough temperatures a concavity is observed in its ordering trend. It emerges from the intrinsic tendency of the component with the lower molecular weight to be isotropic; however, due to the interaction (β) it is
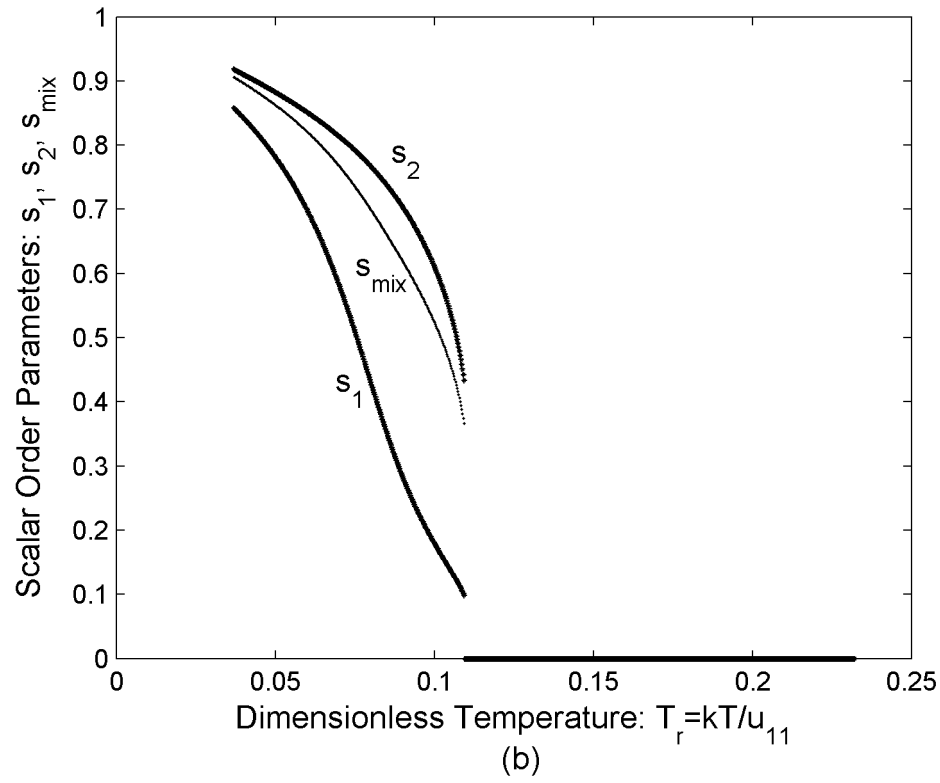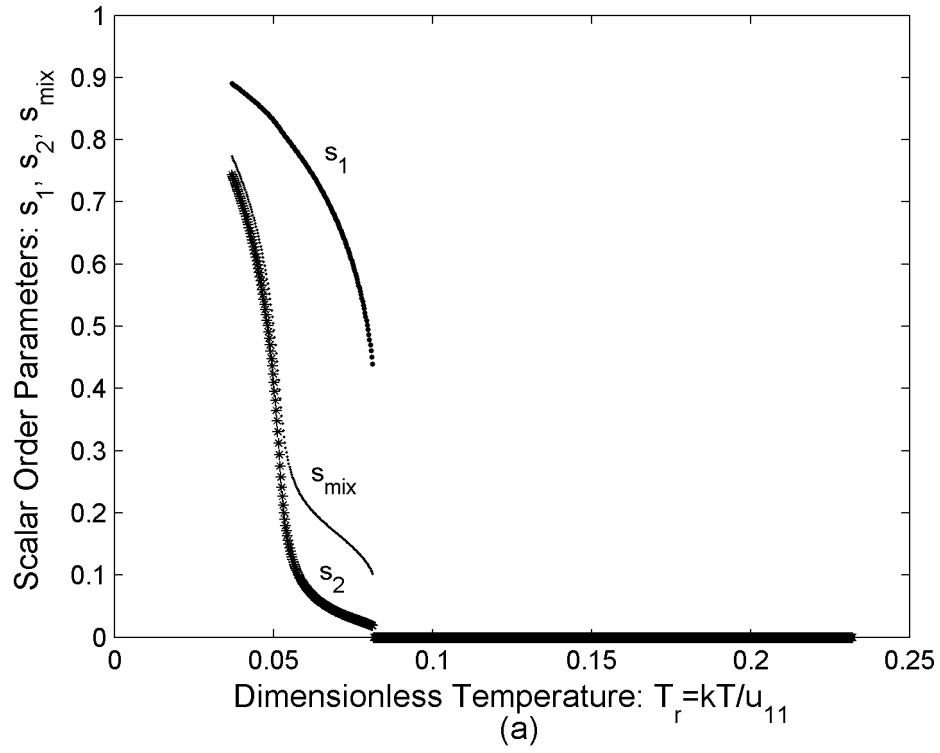
Figure 2- 4. Scalar order parameters (s_1, s_2 and s_{mix}) as a function of reduced temperature for $m_1=0.2$ and $\beta=0.1$, for $\Delta Mw=800$ ($Mw_2=600$) in (a) and $\Delta Mw=400$ ($Mw_2=1000$) in (b).

energetically preferable to be in the nematic state. The first order NI phase transition takes place at $T_r=0.095$. At lower ΔMw (figure 2-4b) the low melting component controls the ordering of the mixture due to its dominant concentration and the NI transition takes place at $T_r=0.109$.

2.5.1.3 Dilution Effect (m_1)

Mesogenic mixtures exhibit both lyotropic and thermotropic behavior: $s_i(T,m_1)$, and dilution (changes in m_1) drives the phase transition, as in other lyotropic liquid crystals[36].

Figure 2-5 shows the scalar order parameters s_1 and s_2 as a function of dimensionless temperature T_r, for $\beta=0.1$, $\Delta Mw=400$, $m_1=0.2$ (a), 0.31(b), and 0.4(c). In this case the minority component "1" has the higher molecular weight and higher T_{NI} value, but dilution introduces the lyotropic effect. At high dilution (figure 2-5a) as T_r increases the minority component has more tendency to convert to the isotropic phase. Transition takes place at $T_r=0.109$. As the concentration increases (figure 2-5b) both the minority and the majority components, exhibit a similar ordering and the mixture behaves like a pure system. The transition takes place at $T_r=0.095$ which shows a decrease compared to $m_1=0.2$. We use the term 'critical mixture' for this system and 'critical concentration' for the corresponding concentration (0.31 here). At $m_1=0.4$ (figure 2-5c) the majority component has less ordering due to its lower Mw and tends to be in the isotropic state; in this case transition takes place at $T_r=0.108$.

In partial summary, binary mixtures exhibit both lyotropic and thermotropic behavior. A minority component of relatively high M_W at low temperatures may nevertheless exhibit low ordering due to the lyotropic effect.
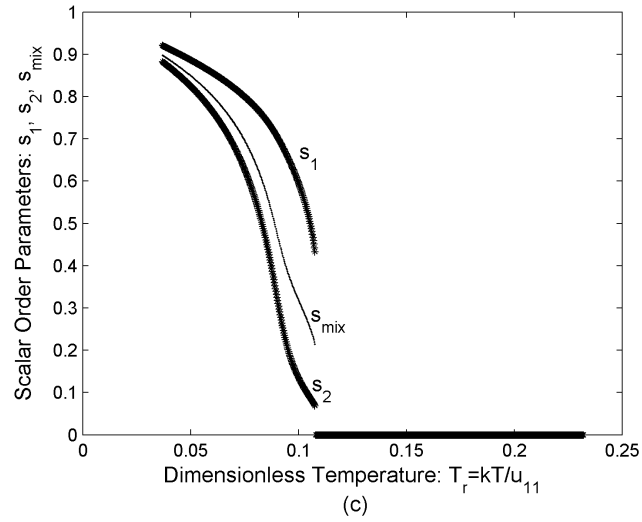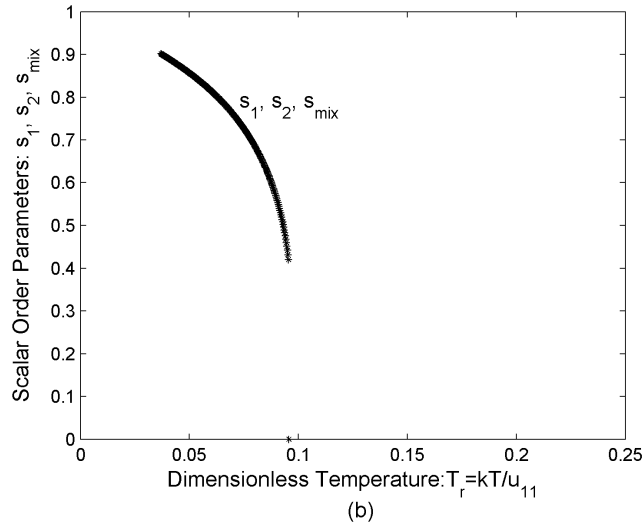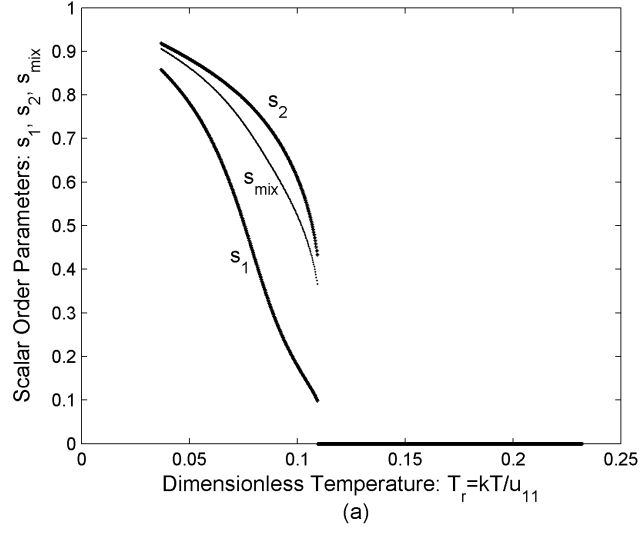
Figure 2- 5. Scalar order parameters (s_1, s_2 and s_{mix}) as a function of dimensionless temperature, for β=0.1 and ΔMw=1000 for m_1: 0.2 (a), 0.31 (b), and 0.4 (c).

2.5.1.4 Effect of Interaction Parameter (β)

In the absence of interactions, $\beta = 0$, the mixture is ideal and the two mesogens are unaffected by each other and each undergoes the clearing transition independently. Figure 2-6 shows scalar order parameters s_1, s_2, and s_{mix} as a function of dimensionless temperature T_r for $\Delta Mw=400$, $m_1=0.2$ and $\beta =0$. However, when $\beta \neq 0$ there is a single mixture clearing temperature. Figure 2-7 shows the scalar order parameters s_1, s_2, and s_{mix} as a function of dimensionless temperature T_r for $\Delta Mw=400$, $m_1=0.2$, $\beta =0.1$ (a), and 0.5(b). The figure shows that for this weakly asymmetric mixture ($\Delta Mw=400$), weak coupling (figure 2-7a) leads to coexisting nematic phases with different ordering ($s_2>s_1$), but strong coupling (figure 2-7b) leads to a critical mixture. Hence increasing the interaction enhances the effect of molecular weight asymmetry.
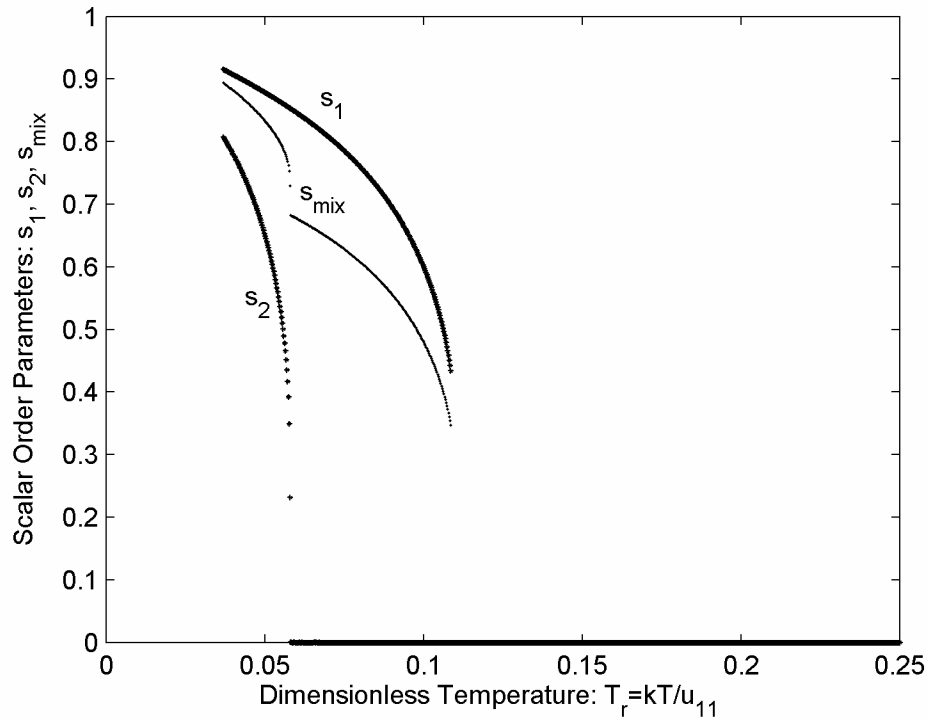
Figure 2- 6. Scalar order parameters (s1, s2 and smix) as a function of dimensionless temperature, for m1=0.2, and ΔMw=400 and β=0 (no interaction).
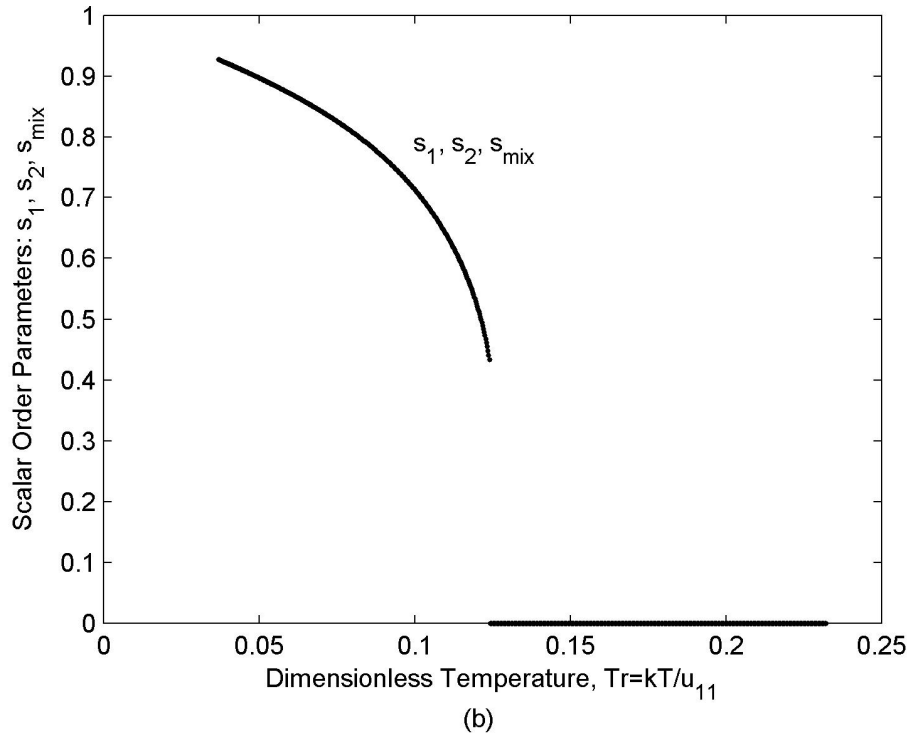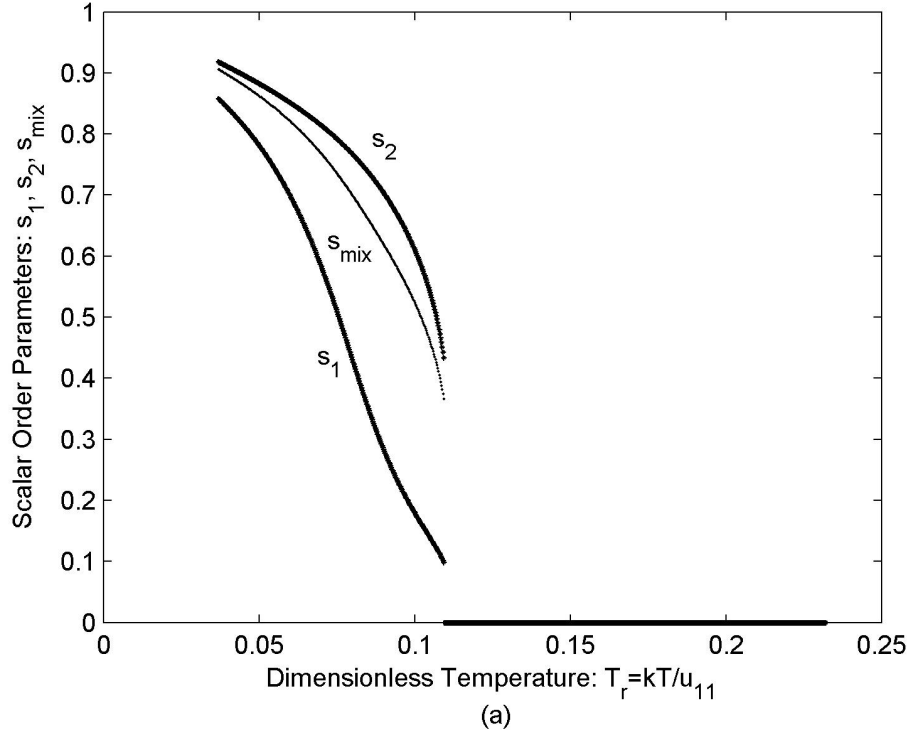
Figure 2- 7. Scalar order parameters (s_1, s_2 and s_{mix}) as a function of dimensionless temperature, for $m_1=0.2$, and $\Delta Mw=400$ for two different interaction parameters $\beta=0.1$ (a), and $\beta=0.5$ (b). For highly interacting mixtures the contribution of the higher molecular weight component "1" to the ordering becomes enhanced so that $s_1=s_2$, though $m_1<<m_2$.

50

2.5.2 Phase Diagrams

In this section we use eqn.(2.16) to classify the T-m phase diagrams. Figure 2-8 shows the classification of the mixtures in terms of molecular weight asymmetry and interaction parameter, showing the property envelopes for ideal and non-ideal mixtures. The coefficients a and b applied in eqn.(2.13) restricts the minimum value of Mw_2 as 200. Therefore, the horizontal dashed line shows the limit of ΔMw which is physically meaningful within the model (1400-200=1200). The solid curve that separates ideal from non-ideal behavior is a plot eqn.(2.16) with $m_{1c}=0$. The other distinguishing features of figure 2-8 are: (i) for equal molecular weight, non-ideality arises only under weaker interaction, (ii) as the Mw asymmetry increases, ideal behavior arises with weaker interaction.
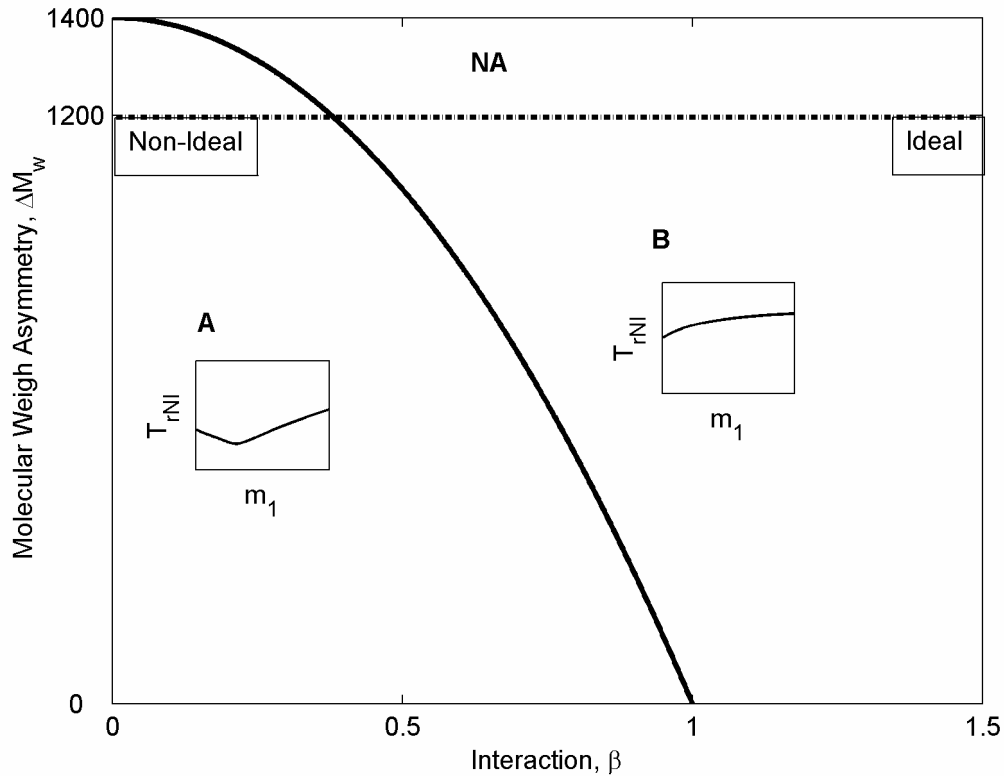
Figure 2- 8. Classification of the mixtures into two types; type A with the non-ideal behavior and type B with ideal behavior, based on their intrinsic properties: Mw asymmetry ΔMw and the interaction parameter β. For weakly interacting mixtures and /or small molecular weight asymmetry the NI transition line exhibits a minimum by increasing the concentration (region A); however, for sufficiently strongly interacting mixtures and /or sufficiently large molecular weight asymmetry the NI transition line is monotonic (region B).

Figure 2-9 shows the phase diagram of two mixtures, representing the two regions in figure 2-8, A and B. (i) the mixture in the region (A) behaves non-ideally and exhibits a minimum in its phase diagram; the mixture with the minimum transition temperature T_{NI} is the critical mixture where $s_1=s_2$ (figure 2-9a).(ii) the mixture in the region (B) which has large molecular weight asymmetry and large interaction parameter behaves ideally and shows a monotonic increase in the transition temperature T_{NI} as a function of the concentration (figure 2-9b); as a result, critical mixture can not be obtained from this region.

Figure 2-10 shows the critical concentration as a function of ΔMw and β, using eqn.(2.16). As the interaction β increases the concentration needed to obtain the critical mixture with a specific ΔMw decreases. In other words, the larger value of β enhances the effect of the component with higher molecular weight. Therefore, it controls the overall order parameter of the mixture, even at a lower concentration, contrary to the system with a smaller β. All the graphs reach the zero critical concentration. In the case of the zero critical concentration the critical mixture forms at $m_1=0$. In other words the first component (with the higher molecular weight) always controls the overall orientation of the mixture. In the other words, s_1 is always greater than s_2. The second component can control the overall orientation, only when $m_1=0$.
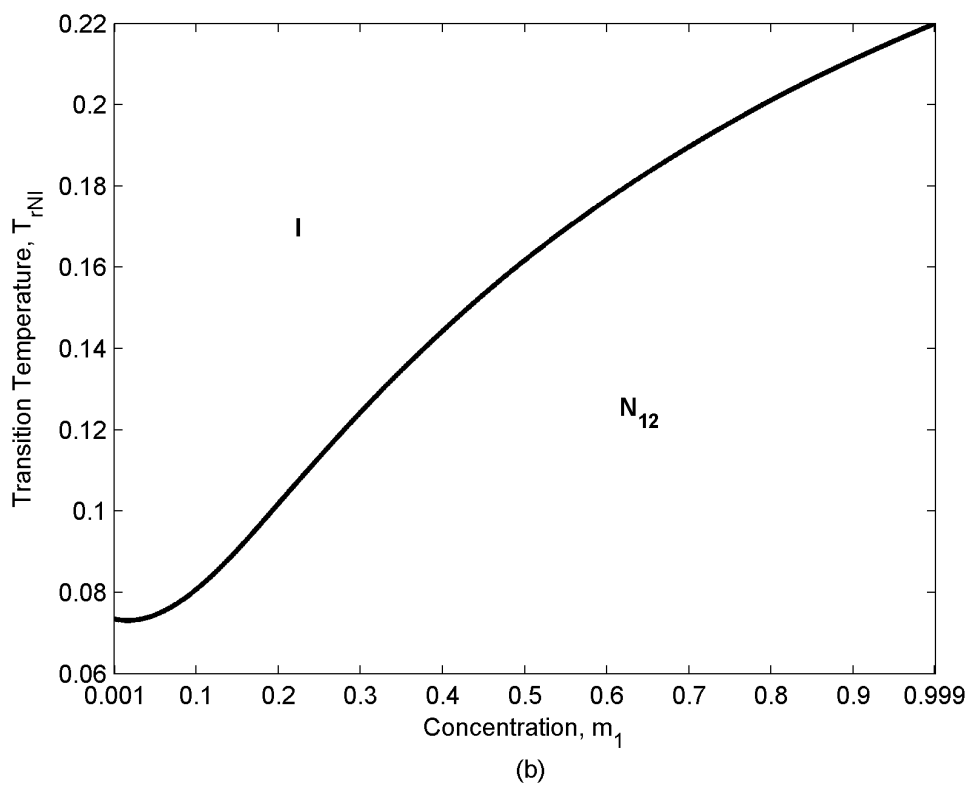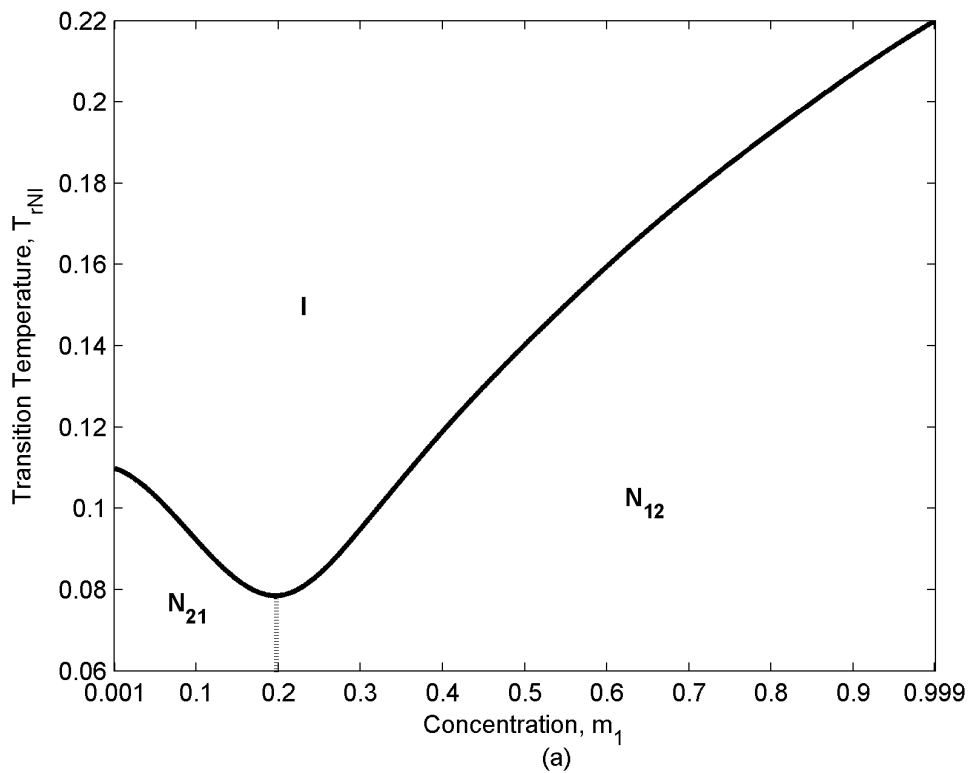
Figure 2- 9. Temperature-composition thermodynamic phase diagram for two different types of mixtures: non-ideal (with $\Delta Mw=600$ and $\beta=0.1$) (a), and ideal (with $\Delta Mw=800$ and $\beta=1$) (b).

Figures 2-11 shows the effect of β on the temperature-composition thermodynamic phase diagram for $\Delta Mw= 400$ and $\beta=0$ (no interaction) (a); $\beta=0.1$, 0.2, and 0.5 (b); I_i denotes isotropic and N_i denotes nematic. Under no interaction, (figure 2-11a) there are two clearing transition lines and in the region below the transition lines, coexisting nematic and nematic-isotropic phases are observed. As the interaction increases ($\beta\uparrow$) the crossing transition lines merge (figure 2-11b) to define the mixture isotropic-nematic transition line. The nematic region contains two parts: N_{21} with $s_2>s_1$ for the left part and N_{12} with $s_1>s_2$ for the right part. The boundary between these two regions corresponds to the critical concentration which makes critical mixture, where $s_1=s_2$ and where the transition temperature has the minimum. By increasing the interaction parameter, β, the tendency of the component with the lower Mw to remain nematic increases; as a result, transition to the isotropic phase shifts to higher temperatures.
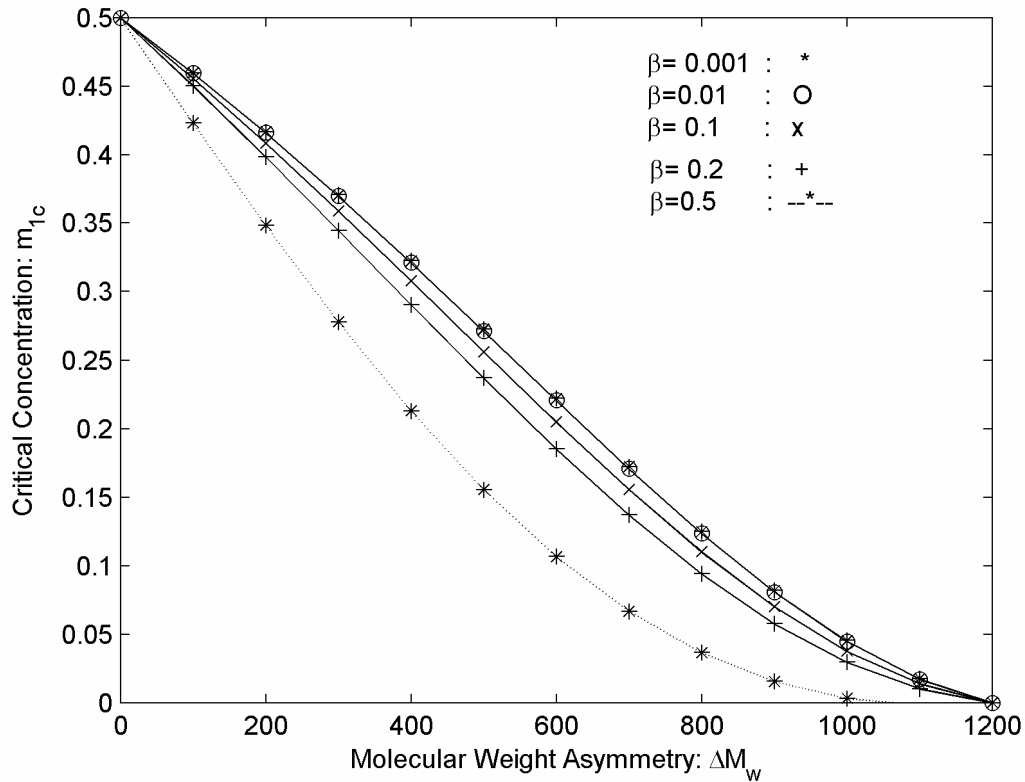
Figure 2- 10. Critical concentration as a function of the intrinsic properties: molecular weight asymmetry and the interaction parameter.

2.5.3 Critical Concentration Detection

As mentioned above, the ordering of CM mixtures are affected by the lyotropic and thermotropic effects. Concentration can shift the phase transition and any related phenomena of the mixture along the temperature axis. For instance, the final structure of the CM based fibers which is dictated by the temperature effect[21] is influenced by concentration values. Therefore, it is of key importance to determine whether a specific mixture can produce a non-ideal behavior and if it can reach a minimum transition temperature. It is also crucial to detect the critical concentration of the mixture, if it exists. In the following section, we propose predictive tools to detect the critical concentration.

2.5.3.1 X-Ray Intensity

Here we present the X-ray intensity I_{mix} calculations of the mixture using eqns.(2.19, 2.20). Figure 2-12 shows the values of the intensity parallel to the director $\theta=0$ (maximum intensity) as a function of concentration m_1, at a constant temperature T=320K for $\beta=0.1$ and molecular weight asymmetry $\Delta Mw= 400$ (a), and $\beta=1$ and molecular weight asymmetry $\Delta Mw= 800$ (b). The intrinsic properties for figure 2-12a correspond to the non-ideal region in figure 2.8. The minimum value of the intensity corresponds to the most uniform distribution function which represents the least order state. This phenomenon takes place in the vicinity of the critical concentration. Therefore, we can significantly decrease the range of the concentration in which the critical concentration exists. Figure 2-12b show the corresponding predictions for an ideal mixture and agrees with the expectation of a monotonic increase. Therefore by using X-ray intensity we can: (i) determine the mixture type and hence whether a critical concentration exists or not; (ii) estimate a range of the concentration (for non-ideal mixtures) in which the critical concentration
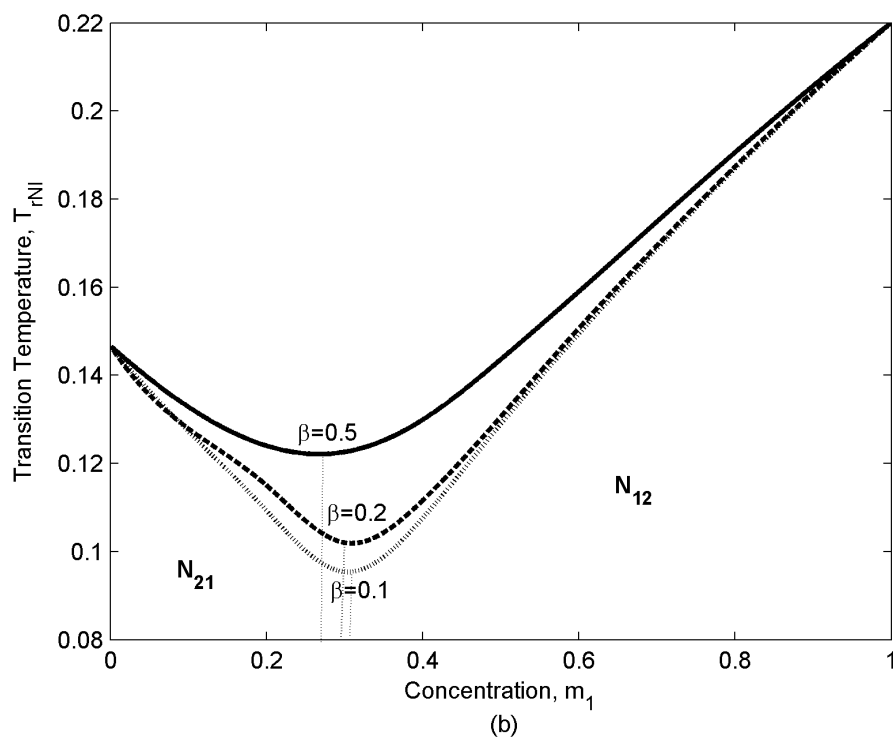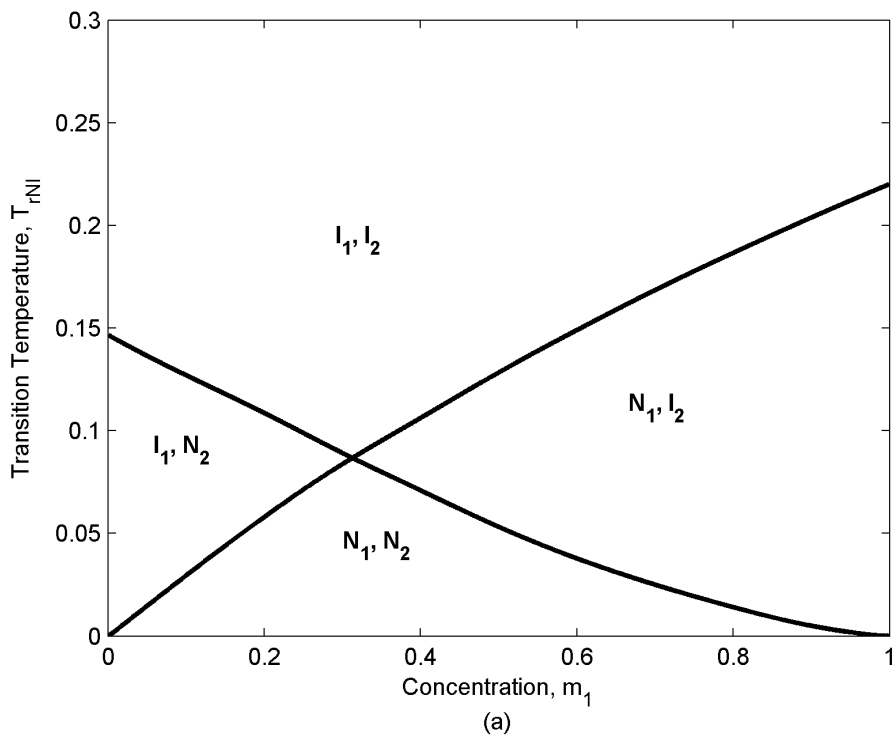
Figure 2- 11. Temperature-composition thermodynamic phase diagram for $\Delta Mw= 400$ and $\beta=0$ (no interaction) (a), $\beta=0.1, 0.2,$ and 0.5 (b). Two transition lines in the non-interaction case (11a) converts to angle nematic to isotropic transition line for the interacting cases (11b). Strong interaction results in the higher NI transition temperature.

exists. This narrowed concentration range can then be used more effectively to determine the exact value of the critical concentration, using direct methods that we mention next.

2.5.3.2 Direct Methods

Here we discuss methods that can be used to determine the critical concentration based on direct measurements of the scalar order parameter.

Figure 2-13 shows the average ordering, s_{mix}, at the transition $s_{mix}\big|_{TNI}$, as the ordering criterion, as a function of concentration for two types of behavior corresponding to figure 2-12. Figure 2-13a depicts the typical ordering trend of the mixture which behaves non-ideally. Two local minima and a local maximum are observed here. There are three regions in this graph:
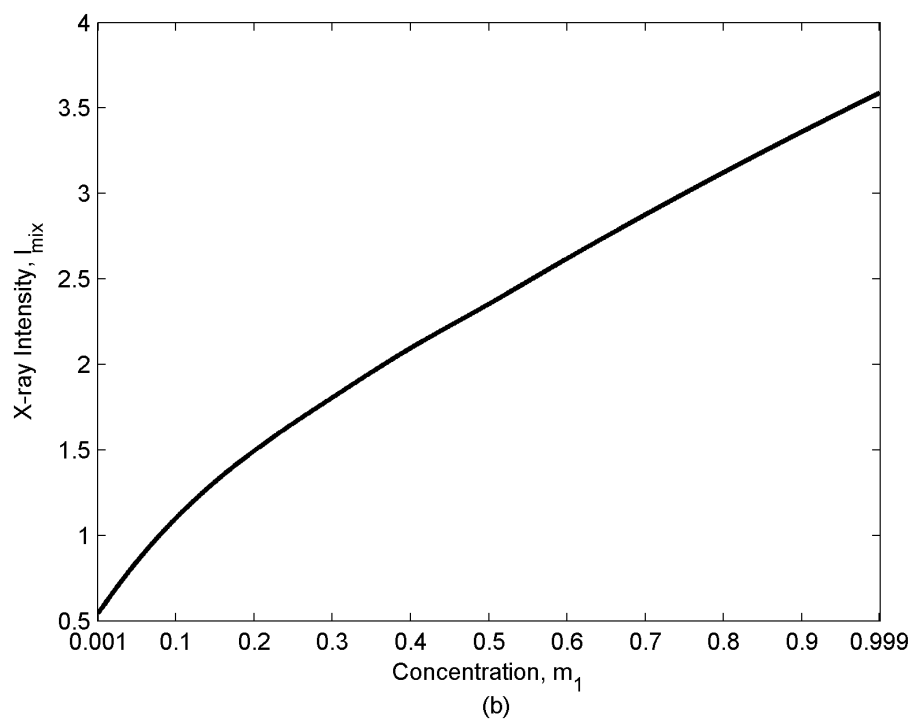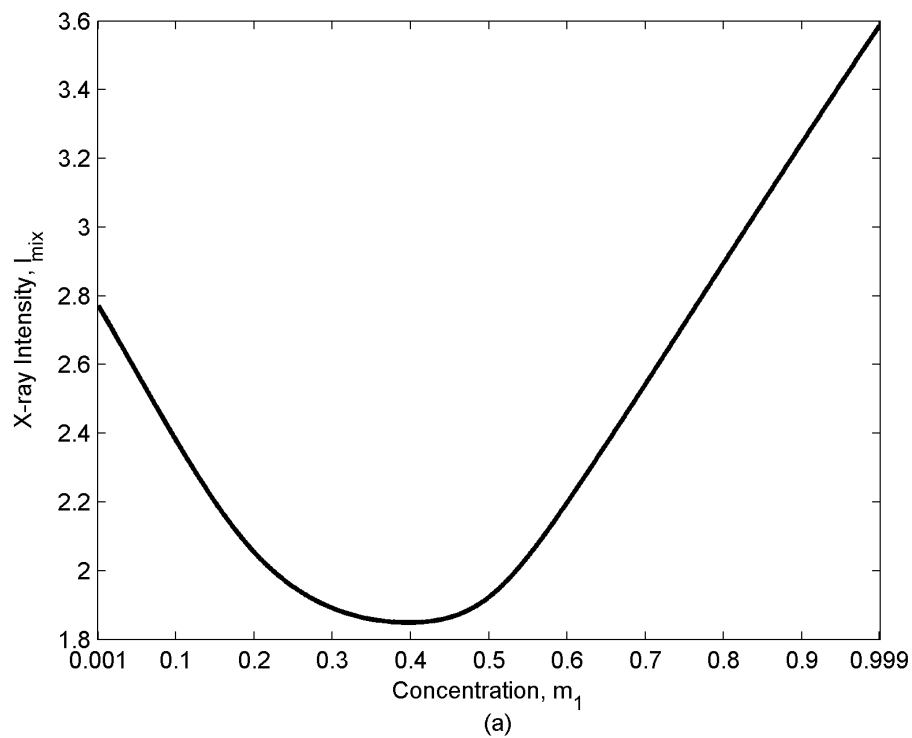
Figure 2- 12. The maximum value of the X-ray intensity as a function of the concentration at T=320K for ΔMw=400, β=0.1 (non-ideal) (a), and ΔMw=800, β=1 (ideal) (b).

Figure 2- 13. Scalar order parameter of the mixture at the transition temperature $S_{mix}|_{TNI}$ **as a function of concentration for** $\Delta Mw=400$, $\beta=0.1$(**non-ideal**) (**a**), **and** $\Delta Mw=800$, $\beta=1$ (**ideal**) (**b**). **Maximum ordering at transition is observed at the critical concentration for the non-ideal type. No maximum is observed for the ideal case.**

(i) below m_{1c}, $s_2 \gg s_1$ (which corresponds to N_{21}): In this section s_{mix} decreases by increasing concentration (as s_2 decreases); (ii) above m_{1c}, $s_1 \gg s_2$ (which corresponds to N_{12}): In this section s_1 and s_{mix} increase as concentration increases;(iii) in the vicinity of m_{1c}, $s_1 \approx s_2$ (which corresponds to the transition region): In this section the controlling component is changing and as a result, a maximum which takes place at the critical concentration appears in the graph. However, for the ideal case (figure 2-13b.), a single minimum is observed. This figure shows the typical ordering trend of the mixture which behaves ideally. In this case the maximum corresponding to the non-ideal trend moves to lower concentrations and then disappears, resulting in an ideal behavior. There is no critical concentration in this case and the component with higher molecular weight always controls the overall ordering. Therefore, experimental methods such as NMR, diamagnetic anisotropy, refractive indices which measure scalar order parameters of the mixture and its individual components[13, 19, 37, 38] can be used to detect the type of the mixture as well as the value of the critical concentration.

2.6 Conclusions

This paper extends the Maier-Saupe model to binary mixtures of discotic nematogenes. The thermotropic and lyotropic behavior of the mixtures are demonstrated by phase transitions induced by temperature and concentration changes. Based on the molecular weight asymmetry and the interaction parameter, mixtures are classified as ideal and non-ideal. Each type exhibits a distinguished temperature-concentration phase behavior, as well as a specific ordering trend: (i) non-ideal mixtures with non-monotonic NI transition temperatures and reversal of ordering $(s_1 > s_2 \rightleftarrows s_2 > s_1)$ due to the concentration effect; the value of the concentration at which this transition takes place is the critical concentration. The mixture exhibits the minimum value of the transition temperature at the critical concentration. The average ordering of this type of mixtures, at the NI transition, shows two minima and a local maximum corresponding to the critical concentration; this case is obtained for weakly interacting mixtures and its phase diagram shows lyotropic/thermotropic behavior; (ii) ideal mixtures correspond to the sufficiently strong interaction and highly asymmetric molecular weights; for

this case the NI transition temperature monotonically changes by increasing the concentration. The mixture behaves ideally and a critical concentration with ordering reversal can not be obtained. Its average ordering at the NI transition also changes monotonically with concentration. The mixture type as well as the value of the critical concentration can be determined by X-ray intensity measurements. They also can be detected by any experimental method which measures scalar order parameters.

In summary, the MS mixture model is a predictive tool that can be used to assess the nematic ordering of the mixture in response to the combined lyotropic and thermotropic effects and to control the NI transition using molecular weight asymmetry and molecular interaction as parameters.

2.7 Appendices

2.7.1 Appendix A: Maier-Saupe Model

In this section we briefly sketch the Maier-Saupe model for a single component NLCs, necessary to develop the binary mixture model. According to the Doi-Maier-Saupe model the internal potential $\Phi(\mathbf{u})$ acting on a molecule of orientation $\mathbf{u}$ in a single component LC is given by the following expression:

$$\Phi(\mathbf{u}) = -\frac{3}{2}U\mathbf{Q} : \left(\mathbf{uu} - \frac{\mathbf{I}}{3}\right) \tag{A2.1}$$

This potential is derived from an internal energy E($\mathbf{Q}$) as follow:

$$\Phi = \frac{\partial E(\mathbf{Q})}{\partial \mathbf{Q}} : \left(\mathbf{uu} - \frac{\mathbf{I}}{3}\right) = -\frac{3}{2}U\mathbf{Q} : \left(\mathbf{uu} - \frac{\mathbf{I}}{3}\right) \tag{A2.2}$$

where U has units of energy per unit volume. The entropy per molecule S is:

$$TS = -\frac{3}{2}U\mathbf{Q} : \mathbf{Q} + kT\ln Z = 2E + kT\ln Z \tag{A2.3}$$

where the partition function Z is:

$$Z = \int e^{-\Phi/k_B T} d\mathbf{u} \tag{A2.4}$$

Using eqns.(2.2) and (2.3), the molar free energy A of the system is found to be:

$$A = -N_A E - N_A k_B T \ln Z = \frac{3N_A}{4}U\mathbf{Q} : \mathbf{Q} - N_A k_B T \ln Z \tag{A2.5}$$

Now we check for the thermodynamic consistency. According to thermodynamics the relation between the internal energy E and the free energy A is given by the following expression:

$$E(\mathbf{Q}) = \frac{d\beta A}{d\beta} \tag{A2.6}$$

where $\beta = 1/k_B T$. Using equations (2.5) and (2.6) we find the consistent result:

$$E(\mathbf{Q}) = \frac{d\beta A}{d\beta} = \frac{N_A d}{d\beta}(-\beta E - \ln Z) = \left(-E - \frac{1}{Z}\frac{dZ}{d\beta}\right) = -E + 2E \tag{A2.7}$$

To find $\mathbf{Q}$ we must minimize A. By minimizing the free energy we get:

$$\frac{dA}{d\mathbf{Q}} = \frac{3}{2}UN_A\mathbf{Q} - N_A k_B T \frac{1}{Z}\frac{dZ}{d\mathbf{Q}} = 0 \tag{A2.8}$$

which yields the self-consistent relation:

$$\mathbf{Q} = \frac{1}{Z}\int\left(\mathbf{uu} - \frac{\mathbf{I}}{3}\right)e^{-\Phi/k_B T}\,d\mathbf{u} \tag{A2.9}$$

For a unixial LC ($\mathbf{Q} = S(\mathbf{nn} - \mathbf{I}/3)$), contracting eqn.(2.9) with $\mathbf{nn}$ yields:

$$S = \frac{1}{Z}\int\frac{3}{2}\left((\mathbf{u}\cdot\mathbf{n})^2 - \frac{1}{3}\right)e^{-\Phi/k_B T}\,d\mathbf{u} \tag{A2.10}$$

2.7.2 Appendix B: Orientation Distribution Function and Order Parameter for a Binary Mixture

In this Appendix we derive the orientation distribution function ODF_{mix} for a binary mixture of two discotic nematogens in terms of the single component distribution functions ODF. The orientation distribution functions and order parameter of a single component NLC were introduced in eqns.(2.1 , 2.2). Using a mass balance we find that normalized species orientation distribution functions ODF_{mix} are given by:

$$ODF_1(\mathbf{u}) = \frac{\rho_1(\mathbf{u})}{\rho_1}; \quad ODF_2(\mathbf{u}) = \frac{\rho_2(\mathbf{u})}{\rho_2} \tag{A2.11}$$

where $\mathbf{u}$ is the unit normal to a molecular disk, (ρ_1, ρ_2) are the molar densities, and ($\rho_1(\mathbf{u})$, $\rho_2(\mathbf{u})$) are the molar densities at orientation $\mathbf{u}$. Introducing the mole fraction

of the two components: $\rho_1 = m_1\rho, \rho_2 = m_2\rho$, where ρ is molar density of the mixture, eqns.(A2.11) become:

$$ODF_1(\mathbf{u}) = \frac{\rho_1(\mathbf{u})}{m_1\rho}; \qquad ODF_2(\mathbf{u}) = \frac{\rho_2(\mathbf{u})}{(1-m_1)\rho} \tag{A2.12}$$

Using a mass balance, the normalized orientation distribution function of the mixture is:

$$ODF_{mix}(\mathbf{u}) = \frac{\rho(\mathbf{u})}{\rho} = \frac{\rho_1(\mathbf{u}) + \rho_2(\mathbf{u})}{\rho} \tag{A2.13}$$

where we used the molar density of the mixture with orientation $\mathbf{u}: \rho(\mathbf{u}) = \rho_1(\mathbf{u}) + \rho_2(\mathbf{u})$. Combining eqns.(A2.12, A2.13) we find that the ODF_{mix} is a linear function of the species

$$ODF_{mix}(\mathbf{u}) = m_1 ODF_1(\mathbf{u}) + m_2 ODF_2(\mathbf{u}) \tag{A2 .14}$$

Next we define the tensor order parameter of a binary mixture $\mathbf{Q}_{mix}$. We have explained the nature, origin, and physical significance of the tensor order parameter $\mathbf{Q}$ of a single component NLC in the introduction (eqn.(2.2)). Multiplying eqn.(A2.14) with $\left(\mathbf{uu} - \dfrac{\boldsymbol{\delta}}{3}\right)$ and integrating on the unit sphere we find:

$$\int ODF_{mix}(\mathbf{u})\left(\mathbf{uu} - \frac{\boldsymbol{\delta}}{3}\right) d^2\mathbf{u} = m_1 \int ODF_1(\mathbf{u})\left(\mathbf{uu} - \frac{\boldsymbol{\delta}}{3}\right) d^2\mathbf{u} + m_2 \int ODF_2(\mathbf{u})\left(\mathbf{uu} - \frac{\boldsymbol{\delta}}{3}\right) d^2\mathbf{u}$$

$$\tag{A2.15}$$

Using eqns.(2.2, A2.15) we finally arrive at $\mathbf{Q}_{mix}$.

$$\mathbf{Q}_{mix} = m_1\mathbf{Q}_1 + m_2\mathbf{Q}_2 \tag{A2.16}$$

2.8 References

1. Singer, L. S. *Faraday Discussions* **1985**, 79, 265-272.

2. Sheikh, S. Y. *The effect of composition and shear rate on mesophase mixtures.* MS Thesis, Clemson University, Clemson, SC, 1999.

3. Marsh, H. *Fuel* **1973,** 52, (3), 205-212.

4. Gupta, G.; Rey, A. D. *Physical Review Letters* **2005,** 95, (12), 127802:1-4.

5. Edie, D. D.; Robinson, K. E.; Fleurot, O.; Jones, S. P.; Fain, C. C. *Carbon* **1994,** 32, (6), 1045-1054.

6. Hurt, R. H.; Hu, Y. *Carbon* **1999,** 37, (2), 281-292.

7. Yoon, S. H.; Korai, Y.; Mochida, I. *Carbon* **1993,** 31, (6), 849-856.

8. Nagappa, S.; Nataraju, S. K.; Marthandappa, M. *Molecular Crystals & Liquid Crystals* **1991,** 197, 15-20.

9. Yan, J.; Rey, A. D. *Physical Review E* **2002,** 65, (3), 031713: 1-14.

10. Cervo, E. G.; Thies, M. C. *Chemical Engineering & Technology* **2007,** 30, (6), 742-748.

11. Brochard, F.; Jouffroy, J.; Levinson, P. *Journal De Physique* **1984,** 45, (7), 1125-1136.

12. Humphireps, R. L.; James, G.; Luckhurst, G. R. *Symp. Faraday Society* **1971,** 5, 107-118.

13. Bates, G. S.; Beckmann, P. A.; Burnell, E. E.; Hoatson, G. L.; Palffy-Muhoray, P. *Molecular Physics* **1986,** 57, (2), 351-357.

14. PAlffy-Muhoray, P.; Dunmur, D. A.; Miller, W. H. *Liquid Crystals and Ordered Fluids* **1984,** 4, 615.

15. Beauharnois, M. E.; Edie, D. D.; Thies, M. C. *Carbon* **2001,** 39, (14), 2101-2111.

16. Yang, D. K.; Yin, Y.; Liu, H. *Liquid Crystals* **2007,** 34, (5), 605-609.

17. Barbero, G.; Evangelista, L. R. *Physical Review E* **2000,** 61, (3), 2749-2752.

18. Stephen, M. J.; Straley, J. P. *Reviews of Modern Physics* **1974,** 46, 617-702.

19. Chandrasekhar, S., *Liquid crystals*. 2nd ed.; Cambridge University Press: Cambridge [England]; New York, NY, USA, 1992.

20. Palffy-Muhoray, P.; deBruyn, J. J.; DunmurD.A. *Mol.Crys.Liq.Crys.* **1985,** 127, 301-319.

21. Yan, J.; Rey, A. D. *Carbon* **2002,** 40, (14), 2647-2660.

22. Rey, A. D.; Denn, M. M. *Annual Review of Fluid Mechanics* **2002,** 34, 233-266.

23. Zimmer, J. E.; White, J. L. *Advances in Liquid Crystals* **1982,** 5, 157-213.

24. Hu, Y.; Hurt, R. H. *Carbon* **2001,** 39, (6), 887-896.

25. Lhuillier, D.; Rey, A. D. *Journal of Non-Newtonian Fluid Mechanics* **2004,** 120, (1-3), 85-92.

26. Priestley, E. B.; Wojtowicz, P. J.; Sheng, P. *Introduction to liquid crystals.* Plenum Press: New York, 1975.

27. Bates, G. S.; Burnell, E. E.; Hoatson, G. L.; Palffy-Muhoray, P.; Weaver, A. *Chemical Physics Letters* **1987,** 134, (2), 161-165.

28. Naggapa, S.; Mahadeva, J.; Somashekarappa, H.; Somashekar, R. *Indian Journal of Physics And Proc of The Indian Assoc For The Cultivation of Science - A* **2000,** 74A, (1), 45-48.

29. Sarkar, P.; Sarkar, P. K.; Paul, S.; Mandal, P. *Phase Transitions* **2000,** 71, (1), 1-12.

30. Nagappa, S.; Jagadish, K. N.; Mahadeva, J.; Naveenkumar, S. K.; Somashekar, R. *Molecular Crystals & Liquid Crystals* **2001,** 366, 239-246.

31. Sori, M. Calorimetric Measurments in Nematics. In *Physical properties of liquid crystals: Nematics*, Dunmur, D. A.; Fukuda, A.; Luckhurst, G. R., Eds. INSPEC: London, 2001; pp 14-50.

32. Davidson, P.; Petermann, D.; Levelut, A. M. *J. Phys. II France* **1995,** 5, 113-132.

33. Rey, A. D. *Liquid Crystals* **1996,** 20, (2), 147-159.

34. Rey, A. D. *Rheologica Acta* **1995,** 34, (5), 461-473.

35. Rey, A. D. *Mol.Crys.Liq.Crys.* **1996,** 281, 155-170.

36. DeGennes, P. G.; Prost, J., *The physics of liquid crystals*. 2nd Edition ed.; Clarendon Press Oxford, 1995.

37. Delhaes, P.; Rouillon, J. C.; Fug, G.; Singer, L. S. *Carbon* **1979,** 17, (6), 435-440.

38. Hsu, M. L.; Grant, D. M.; Pugmire, R. J.; Korai, Y.; Yoon, S. H.; Mochida, I. *Carbon* **1996,** 34, 729-739.

3. Entropic Behavior of Binary Carbonaceous Mesophases

3.1 Summary

The Maier-Saupe model for binary mixtures of uniaxial discotic nematogens, formulated in a previous study[1], is used to compute and characterize orientational entropy[2] and orientational specific heat. These thermodynamic quantities are used to determine mixture type (ideal or non-ideal) which arise due to their different intrinsic properties, determined by the molecular weight asymmetry ΔMw and the molecular interaction parameter β. These molecular properties are also used to characterize the critical concentration where the mixture behaves like a single component system and exhibits the minimum nematic to isotropic (NI) transition temperature (pseudo-pure mixture). A transition within the nematic phase takes place at this specific concentration. According to the Maier-Saupe model, in a single mesogen, entropy at NI transition is a universal value; in this work we quantify the mixing effect on this universal property. The results and analysis provide a new tool to characterize molecular interaction and molecular weight differences in mesogenic mixtures using standard calorimetric measurements.

3.2 Introduction

An ideal crystalline solid (Figure 3.1a) has (i) perfect orientational order as well as (ii) perfect positional order. On the other hand, an isotropic liquid (Figure 3.1c) lacks any kind of ordering, either orientational or positional. Between these two extremes lies a nematic liquid crystal that has a partially orientational order without any positional order (Figure 3.1b)[3].

In nematic liquid crystals[4] (NLCs), the long molecular axes (u direction in Figure 3.2) are preferably oriented along a particular direction called the director n (Figure 3.2). In discotic nematic liquid crystals (DNLCs) the director n is perpendicular to the long axis of discotic molecules (Figure 3-2). In rod-like nematic liquid crystals (RNLCs) n is parallel to the long axis of the molecules (Figure 3.2). Carbonaceous mesophases (CMs), first reported by Brooks and Taylor[5], are DNLC mixtures obtained from petroleum pitches and synthetic naphthalene precursors[6]. The composition, polydispersity, and molecular orientation of CMs play a significant

role on the final properties of cokes[7], carbon foams, carbon/carbon composites[8], and carbon fibers[9-12].

(a)   **(b)**   **(c)**
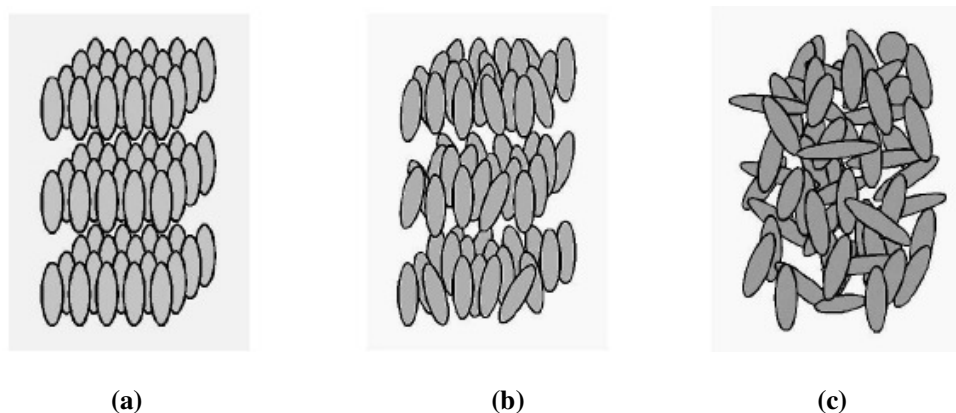
Figure 3- 1. The comparison of three states of the material: a perfect crystalline solid with positional and orientational order (a), a liquid crystal with positional disorder and partial orientational order (b) and an isotropic liquid with positional and orientational disorder (c).

Discotic Nematic Liquid Crystal
(DNLC)

Rod-like Nematic Liquid Crystal
(RNLC)
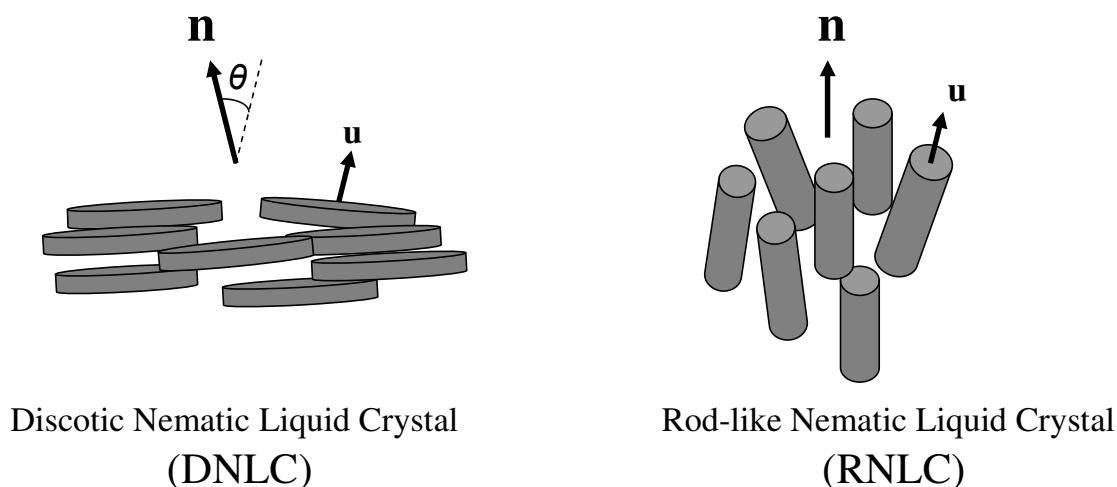
Figure 3- 2. Schematic of nematic liquid crystals (NLCs), the director n is the average of the molecular orientation u, and its classification into discotic and rod-like molecules. In discotic nematic liquid crystals the director n (average orientation) is perpendicular to the long axis of the molecules; however, in rod-like nematic liquid crystals the director n is parallel to the long axis of the molecules.

The type and extent of NLC applications[13] are mainly determined by their thermal properties. For instance, it is known that the final structure of the fibers based on the pure liquid crystalline materials is influenced by the temperature[14-17]. The results of our previous study[1] shows that the structure of the fibers based on the real

CMs which are composed of DNLC species with different molecular weights and concentrations are also influenced by the thermal effect.

By the use of thermodynamics, microscopic structure as well as macroscopic energetic and/or entropic aspects is revealed, so that comprehensive understanding of materials can be achieved[18]. One of the methods mostly used for this purpose is calorimetry. Calorimetric measurements are best suited for the recognition of phase transitions and the determination of their transition temperature. Specific heat, which can be measured by calorimetry, is one of the most useful quantities to investigate the thermal properties of LCs[18]. By use of this quantity three fundamental thermodynamic values viz. enthalpy, entropy, and free energy can be obtained; as a result, it can give an insight into the microscopic and macroscopic aspects of the system.

Theoretically, the entropic behavior and specific heat of pure NLCs are well understood by the Maier-Saupe theory[2]. For instance, this theory predicts a universal entropy value at nematic to isotropic (NI) transition for single component nematics[19]. But there is no systematic study to investigate how the composition changes the entropic value of NLC mixtures at NI transition. Experimental measurements of the entropic behavior are limited to specific nematic mixtures such as the mixtures of EPPV, PBPA and PBPA, EBBA[12, 20-22]. However, a systematic study which includes a broad range of materials and their intrinsic properties such as polydispersity and molecular interaction between the components has not been performed. Moreover, these studies are not directed to CMs which are a mixture of discotic nematogens formed by the species at a certain range of molecular weight. In this paper, we study the general thermodynamic behavior, the entropic behavior, and the characteristic features of specific heat of a mixture of two thermotropic uniaxial discotic nematogens which represents a CM that only differs in molecular weight, thus precluding phase separation. Based on our previous study[1], depending on the intrinsic properties of the system, two types of mixtures arise: ideal and non-ideal (Figure 3.3). The ultimate objective of the current study is to use thermal properties and to determine the type of the mixture

as well as its concentration that corresponds to the minimum transition temperature, critical concentration[1].

Maier-Saupe (MS) theory is widely used to describe the thermodynamics of nematic liquid crystals[23-26]. This mean field theory gives the temperature-dependence of the molecular orientation as well as macroscopic entropic aspects in mesogenic materials. It predicts the values of the experimentally measured scalar order parameters very well[24], and hence has been applied to different nematic liquid crystalline systems and can be adjusted to their mixtures[25, 27-29]. In this paper, we use the Maier-Saupe (MS) theory generalized to binary uniaxial discotic nematogens. For binary mixtures of uniaxial mesogens the mixture quadrupolar order parameter is related to that of the individual components[1]:

$$\mathbf{Q}_{mix} \equiv \mathbf{Q} = m_1 \mathbf{Q}_1 + m_2 \mathbf{Q}_2 \tag{3.1}$$

where m_i is the mole fraction of ith component. For uniaxial phase $\mathbf{Q}$ is given in terms of a temperature-dependent scalar order parameter $s(T)$ and the average molecular orientation or director $\mathbf{n}$: $\mathbf{Q} = s(\mathbf{nn} - \mathbf{I}/3)$, where $\mathbf{I}$ is the unit tensor. For binary discotic nematogens at equilibrium we find collinear directors $(\mathbf{n}_1 = \mathbf{n}_2)$ and the mixture uniaxial scalar order parameter then is:

$$s_{mix} = m_1 s_1 + m_2 s_2 \tag{3.2}$$
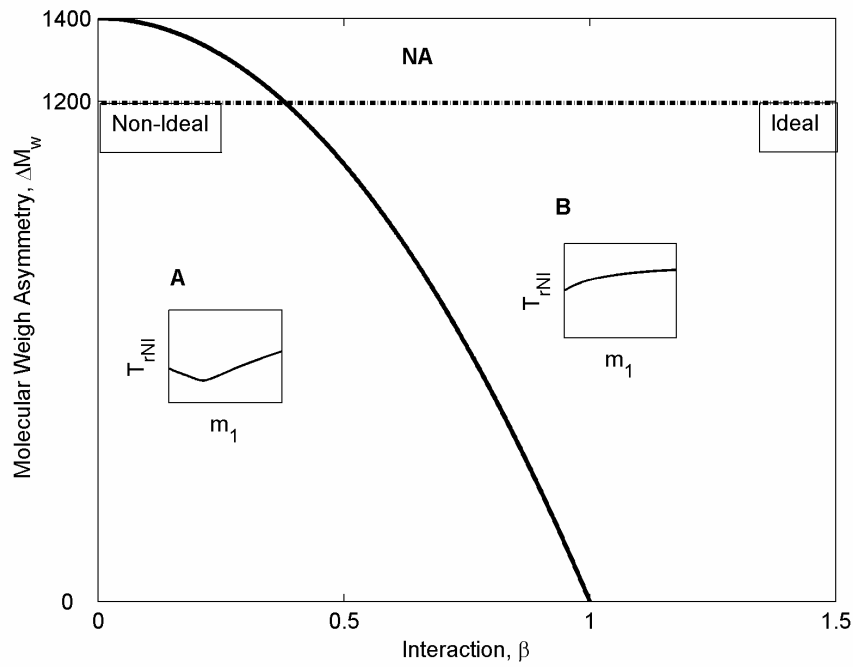
Figure 3- 3. Classification of the mixtures into two types; type A with the non-ideal behavior and type B with ideal behavior, based on their intrinsic properties: molecular weight asymmetry ΔMw and molecular interaction parameter β. For weakly interacting mixtures and /or small molecular weight asymmetry the NI transition line exhibits a minimum by increasing the concentration (region A); however, for sufficiently strongly interacting mixtures and /or sufficiently large molecular weight asymmetry the NI transition line is monotonic (region B)[1].

Nevertheless since the ordering states of each species are coupled and are also dependent on temperature and dilution, we expect, based on the above observations, that a binary mixture displays three states:

(i)   isotropic (I) : $s_1=0$, $s_2=0$;

(ii) nematic (N_{12}) with $s_1 \geq s_2$;

(iii) nematic (N_{21}) with $s_1 \leq s_2$.

Figure 3-4 shows the typical phase diagram of these mixtures. Two kinds of transition take place within mixtures: (i) Nematic to Isotropic (NI) transition due to the thermal effect , and (ii) N_{12} to N_{21} transition within the nematic phase due to the concentration effect. For the later case $s_1 = s_2$ where N_{21} converts to N_{12}; at this point nematic mixture behaves like a single component system, and the concentration corresponding to this transition is the critical concentration m_{1c} at which the NI transition temperature is a minimum. The results of our previous

study[1] show that depending on the molecular weight difference and the molecular interaction, two types of uniaxial nematic mixtures arise (Figure 3-3): (i) non-ideal mixtures; both kinds of transitions are observed within non-ideal mixtures, and (ii) ideal mixtures; only the NI transition takes place within this type of mixtures; N_{12} exists for all range of concentration; as a result, N_{21} and the critical concentration do not appear in the ideal mixture. Ideal binary mixtures arise under sufficiently strong interaction and sufficiently high molecular weight differences, while non-ideal mixtures arise under weak interaction and small molecular weight differences (asymmetries). As each carbonaceous mesophase mixture leads to different carbon fiber structure, it is of a great importance to be able to determine the type of the mixture.

(a)
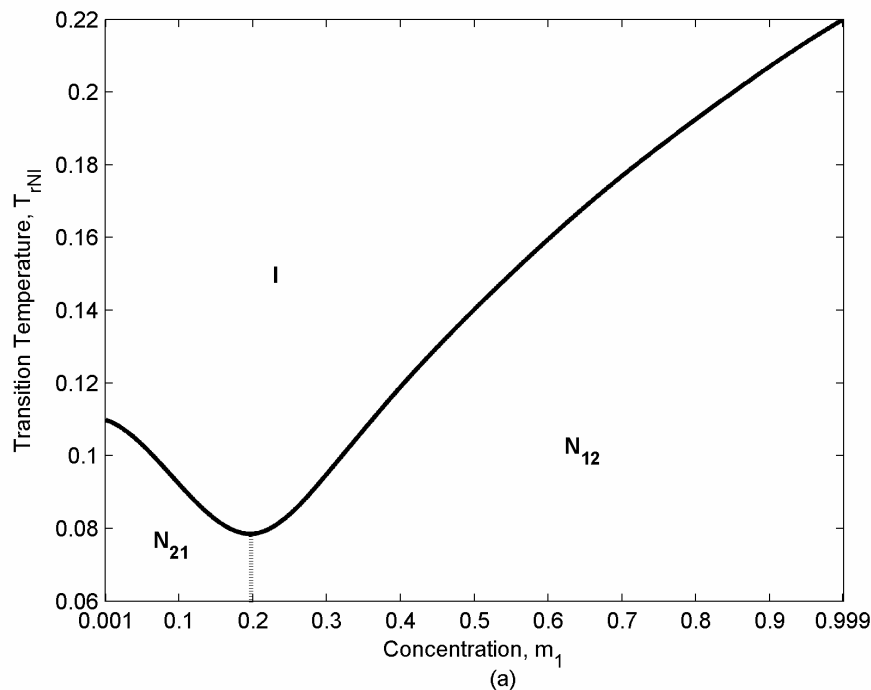
Figure 3- 4. Schematic of the phase diagram of the binary mixture which includes three states: (i) isotropic (I), (ii) nematic (N12) and, (iii) nematic (N21). In N12 (N21) the higher (lower) molecular weight species has a higher molecular order parameter than the lower (higher) molecular weight component: s1>s2 (s2>s1). Depending on the type of the mixture N21 can appear and the transition within the nematic phase between N21 and N12 takes place (for non-ideal mixtures) or it can disappear (for ideal mixtures). The concentration which corresponds to the transition within the nematic phase is the critical concentration[1].

In previous work[1] we used the values of the X-ray diffraction intensity and the average ordering to characterize the type of the mixture and its critical

concentration. In this paper we use specific heat and entropy, to characterize the binary mixtures. Figure (3-5) summarizes our objective schematically. It shows the schematic of the entropic values versus ordering for different concentration. $S_{r1(2)}$ is the value of the entropy for a single component system. This value is universal at the NI transition. Our objective is to find out the effect of concentration, molecular weight asymmetry and the interaction between the components on the (i) entropic values and the entropic jump at transition and (ii) the rate of entropy change which is needed to calculate the values of the specific heat.

The specific objectives of this paper are:

(i) to determine the entropic behavior of ideal and non-ideal mixtures,

(ii) to calculate heat capacities of the two types of mixtures, and

(iii) to determine their entropic variation at transition.

The organization of this paper is as follows:

Section 3.3 presents the essential aspects of the MS binary mixture model. Orientational entropy of the binary mixture is also introduced in this section. The main parameters influencing the thermodynamics of the system are identified and the numerical solution scheme is defined. Section 3.4 presents the derivation of the orientational specific heat. This quantity is used to characterize the type of the mixture, ideal or non-ideal, as well as the critical concentration at which a non-ideal mixture behaves as a pure mesogen. Section 3.5 presents the numerical results and discussion: Section 3.5.1 presents entropic behavior of different types of mixtures for different concentrations. Section 3.5.2 discusses the specific heat of different ideal and non-ideal mixtures as a tool to characterize the type of mixture and its critical concentration. It also shows the effect of molecular weight asymmetry on specific heat values. Section 3.5.3 presents the effect of concentration on the entropy jump at NI transition for two types of mixtures: ideal and non-ideal. Finally, the conclusions are presented in section 3.6.

3.3 Maier-Saupe Binary Mixture Model

Details of the extension of Maier-Saupe model to a binary mixture of NLCs is given in our pervious study[1]. Here we briefly present the main features of the model

which are necessary to obtain the entropic behavior and equilibrium phase diagram. The Helmholtz free energy per unit mole of the homogeneous mixture A is:

$$A(s_1, s_2) = N_A (E_{mix} - TS_{mix}) = -N_A (E_{mix} + k_B T \ln Z)$$ (3.3)

where N_A, k_B, T are the Avogadro's number, Boltzmann's constant and temperature respectively, and E_{mix}, S_{mix}, and Z are the internal energy , the orientational entropy, and the partition function of the mixture per molecule respectively. E_{mix} is given by the summation of three contributions:

$$E_{mix}(\mathbf{Q}) = -\frac{3}{4} W_{11} \mathbf{Q}_1 : \mathbf{Q}_1 - \frac{3}{4} W_{22} \mathbf{Q}_2 : \mathbf{Q}_2 - \frac{3}{2} W_{12} \mathbf{Q}_1 : \mathbf{Q}_2$$ (3.4)

where $\{W_{11}, W_{22}, W_{12}\}$ are the composition and molecular weight-dependent parameters [1]. S_{mix} as the entropy of mixing per molecule and is given by:

$$S_{mix} = \left(\frac{2E_{mix}}{T} + k_B \ln Z \right)$$ (3.5)

and Z as the mixture partition function is factorized as:

$$Z = Z_1^{m_1} Z_2^{m_2} = \left(\int e^{-\Phi_1 / m_1 k_B T} d\mathbf{u}_1 \right)^{m_1} \left(\int e^{-\Phi_2 / m_2 k_B T} d\mathbf{u}_2 \right)^{m_2}$$ (3.6)

where Z_i, Φ_i and m_i are the partition function, the partial internal potentials, and the mole fraction (concentration) of the ith species respectively.

The two equations of equilibrium are obtained by minimizing the free energy A (eqn.(3.3)) with respect to the species order parameters (s_1, s_2). Scaling the Helmholtz energy A with the bare interaction parameter $\overline{U}_{11}$, minimizing the resulting dimensionless free energy with respect to s_1, s_2 we find:

$$(a): \quad m_1 \varphi_1 s_1 + \frac{3}{2} \sqrt{m_1 m_2 \varphi_1 \varphi_2} \wp_1 s_2 \left(\cos^2(\alpha) - \frac{1}{3} \right) - T_r \sum_{i=1}^{2} \frac{m_i}{Z_i} \frac{\partial Z_i}{\partial s_1} = 0$$

(3.7)

$$(b): \quad \frac{3}{2} \sqrt{m_1 m_2 \varphi_1 \varphi_2} \wp_1 s_1 \left(\cos^2(\alpha) - \frac{1}{3} \right) + m_2 \varphi_2 \wp_2 s_2 - T_r \sum_{i=1}^{2} \frac{m_i}{Z_i} \frac{\partial Z_i}{\partial s_2} = 0$$

where φ_i and $\wp_i$ are effective mole fraction and the energetic parameter of the component "i" respectively. α is the angle between the directors of two components. The asymptotic limits of eqns.(3.6) (m_1=0,1) correspond to the pure NLC. As discussed in our pervious work [1] for the present CM case, the mixture is

uniaxial and hence the relative director aperture is $\alpha=0$. The thermodynamics of the mixture is defined by the dimensionless temperature T_r and two effective mole fractions $(\varphi_i ; i = 1,2)$:

$$T_r = \frac{k_B T}{\bar{U}_{11}} \quad ; \quad \varphi_i = \frac{m_i Mw_i}{\sum m_i Mw_i} \tag{3.8}$$

The two material parameters of the model are:

$$\wp_1 = \frac{\bar{U}_{12}}{\bar{U}_{11}}; \quad \wp_2 = \frac{\bar{U}_{22}}{\bar{U}_{11}} \tag{3.9}$$

which are functions of the molecular weights Mw_i of the two components:

$$\wp_2 = \frac{\bar{U}_{22}}{\bar{U}_{11}} = \frac{4.542 k_B T_{NI2}(Mw_2)}{4.542 k_B T_{NI1}(Mw_1)} = \frac{(a + b\, Mw_2)}{(a + b\, Mw_1)} \tag{3.10}$$

where the parameters (a, b) , based on the data of[30] are taken to be: a=-150 and b=0.75. Since the molecular weight dependence of $\wp_1$ is not suggested by actual data, we use:

$$\wp_1 = \beta \, \wp_2 \tag{3.11}$$

where β is a constant whose sign depends on the geometrical nature of the species. For similar components, such disk/disk or rods/rod mixtures, it is positive; however, for dissimilar ones it is negative[31]. As CMs are mixtures of discotic molecules the interaction parameter is positive $(\beta > 0)$. We choose component "1" as a representative higher molecular weight component of a CM with $Mw_1 = 1400$[32] and vary the lower molecular weight of the second component, Mw_2, so that the molecular weight asymmetry $\Delta Mw = Mw_1 - Mw_2 > 0$ changes.

The present thermodynamic model is given by the two nonlinear integral equations (eqns.(3.7)); the solution vector consists of the two scalar order parameters (s_1, s_2); the two material parameters are β and ΔMw; the thermodynamic phase diagram is obtained by sweeping over temperature T_r and concentration m_1. Equations (3.7 a&b) are solved by the Newton-Raphson method, using an eighth order Simpson integration method. Stability, accuracy, and convergence were ensured using standard methods[33]. In the discussion of results we use the following nomenclature for dimensionless (reduced) entropy:

$$S_r = S_{mix} / k_B \tag{3.12}$$

3.4 Specific Heat

The difference between dimensionless heat capacity of the nematic phase and that of the isotropic phase, ΔC_{pr}, can be obtained by the orientational entropy which results from the ordering of the mixture[34]:

$$\Delta C_{pr} = \Delta C_p / N_A k_B = T_r \left(\frac{\partial S_r}{\partial T_r} \right) \tag{3.13}$$

As the isotropic entropy is assumed to be zero, the value given by eqn.3.13 is the orientational part of the specific heat. Therefore, ΔC_{pr} shows the difference between C_{pr} of the nematic phase and C_{pr} of the isotropic phase. According to this equation two terms have direct contributions in the value of the specific heat: temperature, T_r, and the rate of entropy, $\left(\frac{\partial S_r}{\partial T_r} \right)$. Depending on the trend of $\left(\frac{\partial S_r}{\partial T_r} \right)$, the trend of ΔC_{pr} as a function of temperature changes. Once it increases monotonically, ΔC_{pr} increases; however, once it decreases ΔC_{pr} can either increases or decreases, depending the magnitude of each term, T_r and $\left(\frac{\partial S_r}{\partial T_r} \right)$. In this case, ΔC_{pr} does not behave monotonically and exhibits a local extremum.

3.5 Results and Discussion

The Maier-Saupe for pure mesogens, whose interaction parameter is W, predicts the following universal values:

(i) NI transition temperature: $k_B T_{NI} / W = 0.22019$

(ii) scalar order parameter in the N phase at transition: $s_{NI}=0.4289$

(iii) Latent heat at the NI transition: $\dfrac{W s_{NI}^2}{2 k_B T_{NI}} = 0.417719$

Hence, deviations form these values will provide information on the mixture, as shown below.

3.5.1 Entropic Behavior

Figure 3-5 shows the dimensionless entropy S_r as a function of ordering s, for a pure mesogen and an schematic for a generic mixture. As expected, entropy decreases with increase in ordering. At the NI transition the pure component displays the universal values (s_{NI}=0.4289, $S_{rNI} = -0.417719$), but for the generic mixture, the Figure shows a characteristic deviation for the universal transition values, which are discussed and quantified in detail in the rest of the paper.
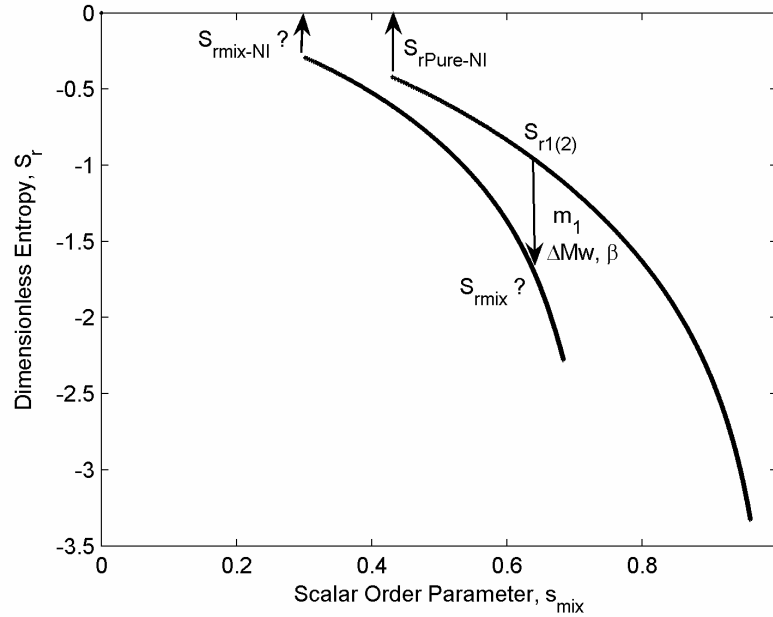
Figure 3- 5. Schematic of the effect of concentration m1, molecular weight asymmetry ΔMw and the interaction parameter β on the type, entropy and ordering of the mixture. It shows the general trend of the dimensionless entropy Sr as a function of scalar order parameter smix. As ordering increases the entropy decreases. It also shows that diluting the pure system changes the ordering and the entropy at NI transition.

Figure 3-6a shows the dimensionless entropy, S_r, as a function of temperature, for an ideal mixture with ΔMw=800 and interaction β=1 (Figure 3-3); each curve shows the entropic trend for a specific concentration m_1. The following features are observed in this figure:

(i) for any given concentration, entropy increases monotonically with increasing temperature (Figure 3-5),

(ii) for any given temperature, entropy increases with decreasing concentration: component "1" has higher Mw, so it is more ordered in the nematic range. Therefore, as the concentration m_1 increases the mixture ordering increases and entropy decreases,

(iii) entropy jumps at the nematic-isotropic first order phase transition that sets in at temperature T_{NI} (the entropy of the isotropic phase is assumed to be zero; as a result, this entropy represents the orientational entropy); the entropy jump value which is defined as (entropy of the isotropic phase) – (entropy of the nematic phase) at NI transition temperature for the almost pure mixtures (m_1=0.001,0.999) are essentially the universal value $S_{rNI} = 0.417719$, and mixing just decreases the magnitude of jump.

(iv) depending on the relative population of two components there are three distinct concentration regions: (i) $m_1 \simeq$ [0-0.1], (ii) $m_1 \simeq$ [0.2-0.3], (iii) $m_1 \simeq$ [0.4-1]. The rate of entropy change $\left(\dfrac{\partial S_r}{\partial T_r}\right)$ which corresponds to the rate of ordering change in the mixture shows a rapid decrease in region (ii). Component "2" has lower Mw; as a result, it has a lower T_{NI} (eqn.3.10). Therefore, while component "1" tends to remain nematic (N_{12} state), component "2" tends to transform to the isotropic (I) state and lose the ordering, though due to the interaction between the components it retains a low nematic ordering. As a result, when approaching the NI transition temperature of "2" the rate of ordering change in this component decreases and because of eqn.(3.2) the overall rate of change in the mixture decreases. The appearance of the inflection point in the graphs corresponds to this change in the rate of entropy trend. This phenomenon becomes enhanced when the relative concentrations of both components are significant (region (ii) $m_1 \simeq$ [0.2-0.3])

Figure 3-6b shows the entropic behavior for ΔMw=400 and interaction β=0.1 which represents a non-ideal mixture (Figure 3-3); the concentration m_1 is shown for each curve. The following features are observed in this Figure:

(i) like the ideal case increasing the temperature decreases the ordering and increases the entropy (Figure 3-3) of all the mixtures,

(ii) unlike the ideal case, the effect of concentration on the ordering and entropy is different at different temperatures, increasing concentration does not necessarily decreases the entropy. The following three distinctive dilution regions arise: (i) $m_1 \simeq$ [0-0.3], (ii) $m_1 \simeq$ [0.4-0.6], (iii) $m_1 \simeq$ [0.7-1] . Region (i) is located in N_{21} state (s_2>s_1) of the phase diagram (lower left region in Figure 3-3); in this region the

lower molecular weight species "2" is the majority component. Therefore, increasing m_1, dilutes the mixture, decreases the ordering and increases the entropy (Figure 3-5). The second and the third regions, both are located in N_{12} state ($s_1 > s_2$); therefore, the trend is opposite. As component "1" is dominant in this region, increasing its concentration makes the mixture more ordered and decreases the entropy,

(iii) there is a difference between region (ii) and region (iii). Like the ideal case, the rate of entropy change $\left(\dfrac{\partial S_r}{\partial T_r}\right)$ in the mixture shows a rapid decrease in region (ii).

When approaching the NI transition temperature of "2" the rate of ordering change in this component decreases; as a result, the overall rate of change in the mixture decreases (eqn.(3.2)). This phenomenon becomes enhanced in the region (ii), where m1= [0.4-0.6] and the concentration of both components is significant.

(iv)
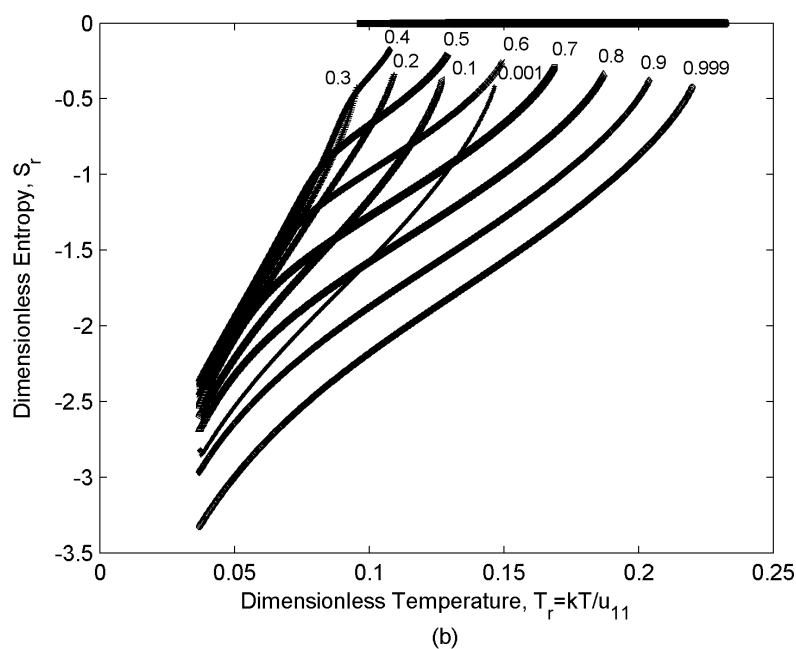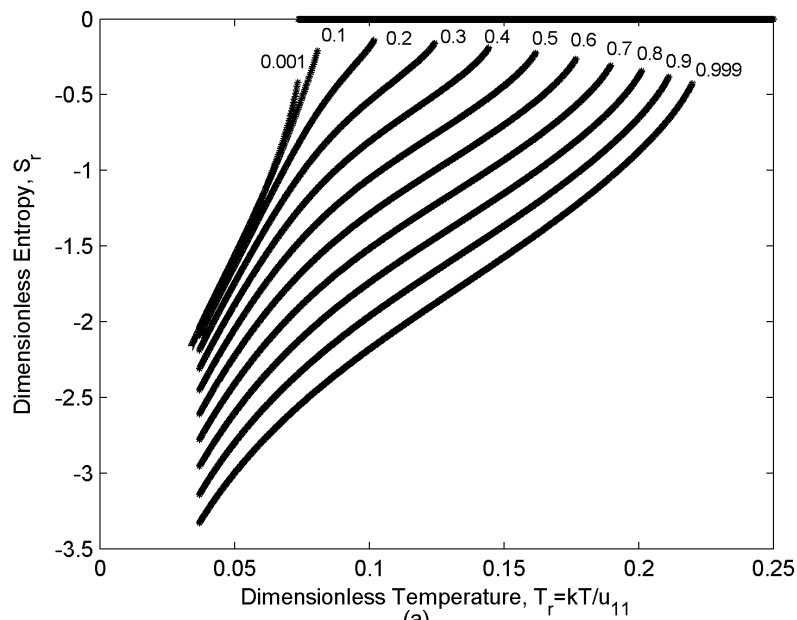
Figure 3- 6. Dimensionless entropy Sr as a function of dimensionless temperature Tr of ideal (with ΔMw= 800 and β=1) (a) and a non-ideal (with ΔMw= 400 and β=0.1) (b) mixtures for different concentrations, computed using eqns.(3.5, 3.12). Ideal mixtures show monotonic behavior with respect to dilution, while non-ideal mixtures show non-monotonicity due to the transition between N12 and N21. The entropy behavior reflects the scalar order parameters of the species and their relative concentration.

3.5.2 Specific Heat

Figure 3-7a shows the value of the specific heat versus temperature for different concentration for the ideal case with $\Delta Mw=800$ and $\beta=1$. The following significant features are observed:

(i) at any given temperature, increasing the concentration decreases the ordering and increases the specific heat.

(ii) by sweeping over temperature, specific heat behaves differently for different concentrations. Depending on the concentration region ((i) $m_1 \simeq [0\text{-}0.1]$, (ii) $m_1 \simeq [0.2\text{-}0.3]$, (iii) $m_1 \simeq [0.4\text{-}1]$, (see section 4.1) two different trends are observed in the specific heat values versus temperature: in region (i) and (iii), when the population of one of the components is insignificant, and $\left(\dfrac{\partial S_r}{\partial T_r}\right)$ changes monotonically, specific heat increases monotonically with temperature; however, in region (ii), where $m_1=[0.2\text{-}0.3]$, specific heat increases by increasing temperature and then it shows a decrease which is followed by another increase. As mentioned in section 3, the non-monotonicity of the specific heat is due to the direct contributions of the T_r and $\left(\dfrac{\partial S_r}{\partial T_r}\right)$ to its value. According to section 4.1 $\left(\dfrac{\partial S_r}{\partial T_r}\right)$ in region (ii) shows a rapid decrease in the vicinity of T_{NI} of component "2"; as a result, ΔC_{pr} decreases in this range. On the other hand, increasing temperature increases ΔC_{pr} ; as a result, a minimum appears in the ΔC_{pr} as a function of temperature.

 Figure 3-7b shows the value of the specific heat versus temperature for different concentrations for the non-ideal case with $\Delta Mw= 400$ and $\beta=0.1$ (Figure 3-3). The significant features observed are:

(i) a transition is observed in ΔC_{pr} trend vs. concentration. This transition takes place at the critical concentration where $N_{21} \rightarrow N_{12}$. Region (i) is located in N_{21} where increasing m_1 decreases the ordering and increases ΔC_{pr} ; however, regions

(ii) and (iii) are both located in N_{12} where increasing m_1 increases the ordering and decreases ΔC_{pr}.

(ii) depending on the concentration region ((i) $m_1 \simeq$ [0-0.3], (ii) $m_1 \simeq$ [0.4-0.6], (iii) $m_1 \simeq$ [0.7-1] , (see section 4.1) two different trends are observed in the specific heat values versus temperature: in region (i) and (iii), when the effect of one of the components is weak, $\left(\dfrac{\partial S_r}{\partial T_r}\right)$ changes monotonically and specific heat increases monotonically with temperature; however, in region (ii), where m_1=[0.4-0.6] and hence essentially no majority component, $\left(\dfrac{\partial S_r}{\partial T_r}\right)$ changes non-monotonically (section 4.2). As $\left(\dfrac{\partial S_r}{\partial T_r}\right)$ has a contribution to the specific heat values, ΔC_{pr} exhibits a minimum vs. temperature in this region (see section 3.3).
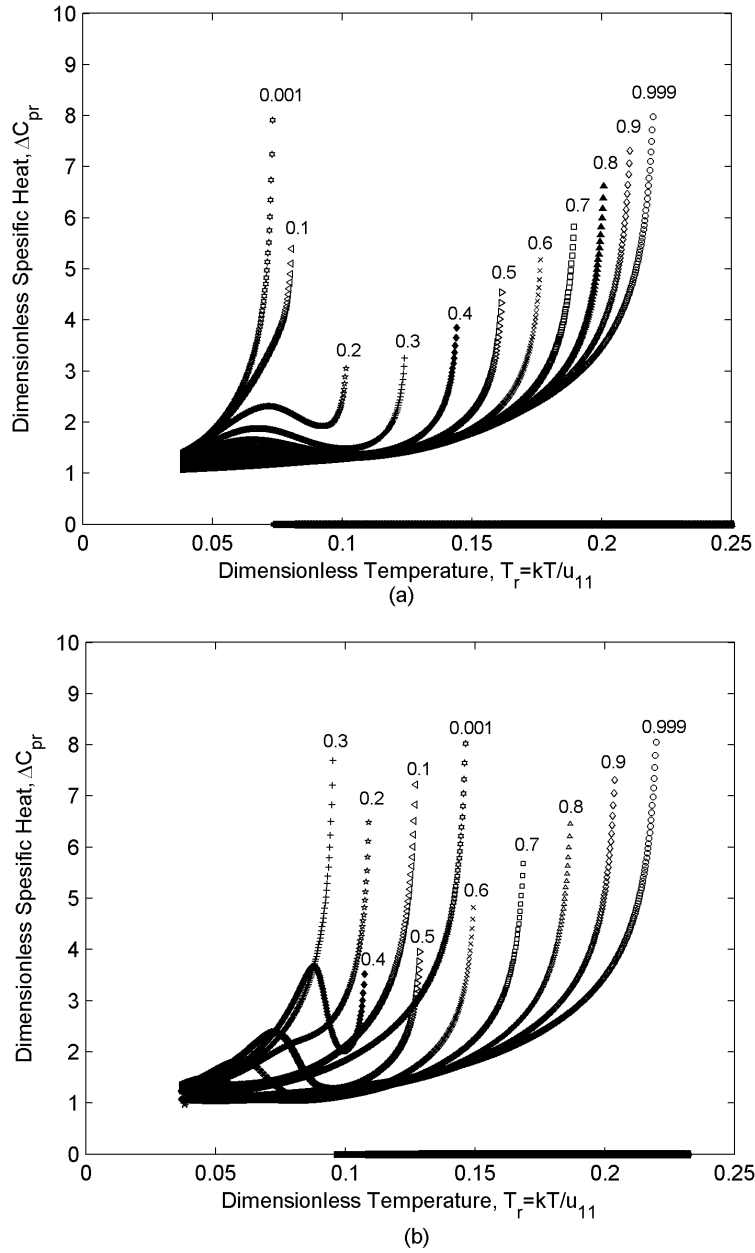
Figure 3- 7. Specific heat ΔC_{Pr} as a function of dimensionless temperature for ideal (with $\Delta Mw= 800$ and $\beta=1$) (a) and non-ideal (with $\Delta Mw= 400$ and $\beta=0.1$) (b) mixtures for different concentrations. Ideal mixtures show monotonic behavior of specific heat while non-ideal mixtures display non-monotonicity with respect to dilution. Both cases show non-monotonicity with respect to temperature whenever the relative concnetration of the components is significant.

To better understand the effect of species relative population on ΔC_{pr} values we investigate ΔC_{pr} for three mixtures with different molecular weight differences

(asymmetries) ΔMw=400 (a), 600(b), and 800(c) for m_1=0.2 and β=0.1. The results are shown in Figure 3-8. Based on Figure 3-3 all three mixtures belong to the non-ideal type. The values of the critical concentration for these mixtures are: 0.31, 0.205 and 0.11 respectively[1]. As a result, for mixtures (a) and (b) component "2" is the majority species, so they exhibit a monotonic ΔC_{pr} ; however, in mixture (c) there is no majority component and hence ΔC_{pr} exhibits an extremum.

The interaction parameter, as another intrinsic property changes the type of the mixture and the critical concentration (Figure 3-3); as a result, it also affects the ΔC_{pr} values. For brevity the related graphs are not presented here.

In partial summary, the higher Mw species always controls the overall ordering of the ideal mixture; as a result, the specific heat of ideal mixtures shows a decrease by increasing concentration at any given temperature; On the other hand, in non-ideal mixtures of weakly interacting species a transition in the trend of ΔC_{pr} versus concentration is observed. This transition takes place within the nematic phase from N_{12} to the N_{12} state. For both ideal and non-ideal type, whenever there is no majority component in the mixture, the trend of specific heat versus temperature is non-monotonic because each component tends to show different ordering at different temperature range.
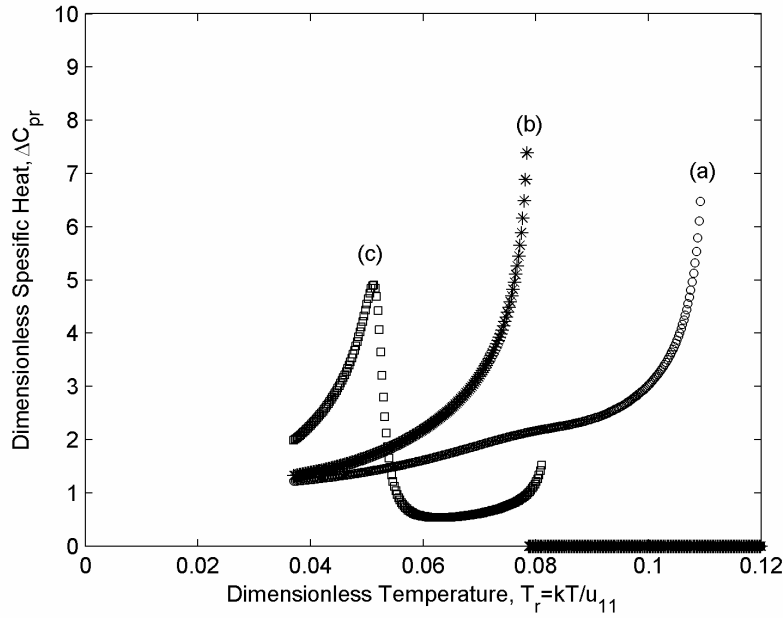
Figure 3- 8. Specific heat ΔC_{Pr} as a function of dimensionless temperature for m1=0.2 and β=0.1 for three different molecular weight asymmetries: ΔMw= 400 (a), 600 (b), and 800(c). All three cases are non-ideal mixtures; in case (c) the relative concentration of the components is significant, so it shows a non-monotonic trend with respect to temperature.

3.5.3 Entropy Jump at Transitions

Figure 3-9a shows the entropy jump at the NI transition for an ideal case, ΔMw=800 and β=1. For the pure systems (two asymptotic limits m_1=0, 1) the value of the entropy jump is the universal value 0.417[19]. On the other hand, diluting the system disturbs the orientation and increases the entropy. As a result, there is a concentration which corresponds to the minimum entropy jump at NI transition. This concentration depends on the intrinsic properties of the mixture and is about 0.2 in the present case. Increasing dissimilarity of the components (larger ΔMw) enhances the dominancy of component"1" and shifts the minimum into lower concentrations.
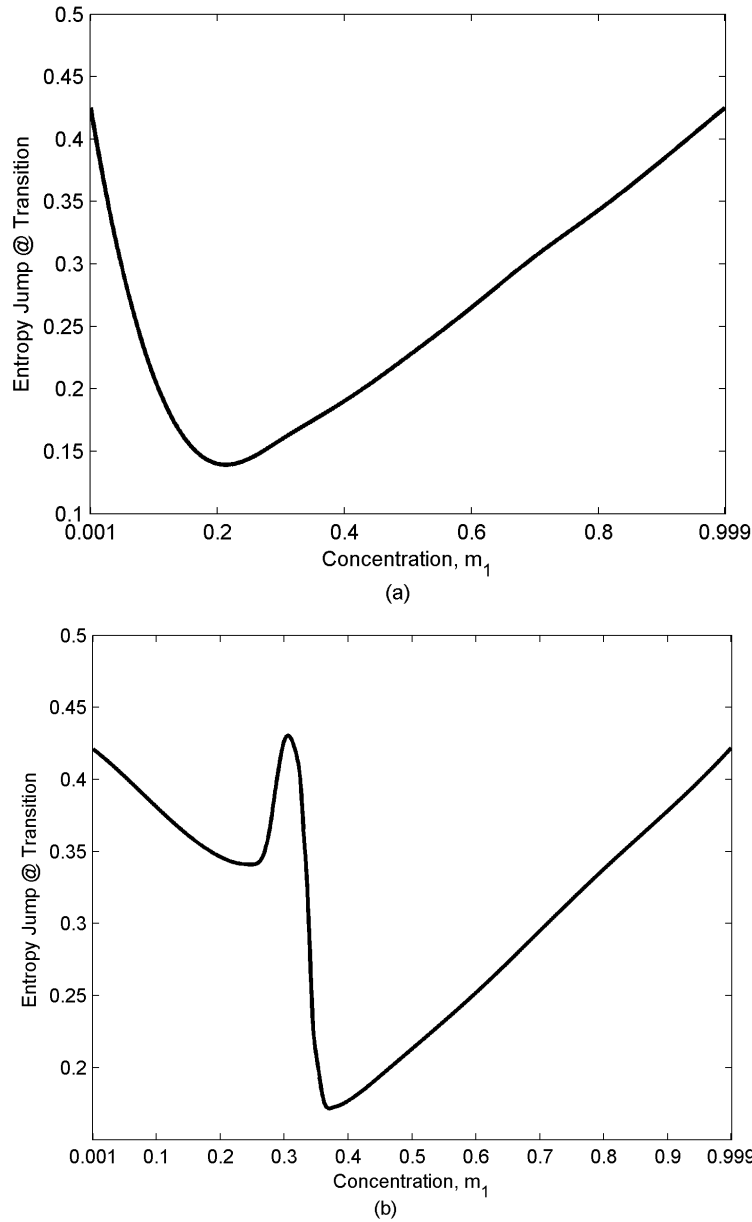
Figure 3- 9. Entropic variations at NI transition as a function of concentration for ideal (with ΔMw= 800 and β=1) (a) and non-ideal (with ΔMw= 400 and β=0.1) (b) mixtures for different concentrations. Both pure and pseudo pure mixtures have the universal entropy at NI transition. A local minimum is observed for the ideal case, where there is only N12 state; however, two local minima (one in N21 and the other in N12) and a maximum (in N12→N21 transition, which corresponds to the critical concentration) are observed for the non-ideal case.

Figure 3-9b shows the values of the entropy jump at transition for a non-ideal case, ΔMw=400 and β=0.1. In this case a local maximum is observed in the graph. The concentration corresponding to the local maximum is the critical concentration

where the mixture behaves like a single component NLC (pseudo-pure mixture). Therefore, the value of the entropy for this concentration is the universal value 0.417719 and identical to that of the pure systems. Like the ideal mixture, diluting the pure (or pseudo-pure) mixture increases the entropy. So, the first local minimum is observed between $m_1=0$ (pure system) and m_{1c} (pseudo-pure mixture) which is located in the N_{21} region and the second one is observed between $m_1 = m_{1c}$ (pseudo-pure mixture) and $m_1=1$ (pure system) which is located in the N_{12} region.

3.6 Conclusions

This paper uses the Maier-Saupe model for binary mixtures of discotic nematogenes to calculate the orientational entropy and orientational specific heat. These quantities are used to characterize the type of binary mixtures, ideal or non-ideal, which arise due to different intrinsic parameters, Mw asymmetry ΔMw and the interaction parameter β: (i) for ideal mixtures entropy and specific heat changes monotonically as a function of concentration at any given temperature. The entropic jump at NI transition exhibits a minimum for this kind of mixture. (ii) For non-ideal mixtures entropy and specific heat change non-monotonically as a function of concentration. A transition within the nematic phase from N_{21} to N_{12} is observed in this type of mixture. This transition takes place at the critical concentration and can be detected by the entropic and specific heat trend: the trend of these quantities in N_{21} is opposite to their trend in N_{12}. The entropic jump at the NI transition exhibits two local minima; one located in the N_{21} region and the other in N_{12} region. It also has a local maximum between these two regions at critical concentration, where the mixture behaves like a single component system and shows the universal entropy jump at NI transition. For both type of mixtures whenever there is a distinct majority component, ΔC_{pr} and entropy behaves monotonically versus temperature; however, when there is no majority component ΔC_{pr} and entropic trends are non-monotonic with temperature.

In the summary, heat capacity and transition entropies are shown to be useful tools to characterize the type of the discotic nematic liquid crystal and carbonaceous mesophase mixtures, to determine nematic ordering and to asses the degree of molecular interaction and molecular weights using standard calorimetric methods.

3.7 References

1. Golmohammadi, M.; Rey, A. D. *Liquid Crystals* **2009,** 36, (1), 75-92.

2. Van der Veen, J.; De Jeu, W. H.; Wannlnkhof, M. W. M.; Tlenhoven, C. A. M. *J. Phys. Chem.* **1973,** *77* (17), 2153-2155.

3. Hwang, D. K. *Computational optical science of textured liquid crystals for biosensors, rheooptics, and carbon composites.* Ph.D. Thesis, McGill University, Montreal, 2006.

4. Rey, A. D. *Soft Matter* **2007,** 3, (11), 1349-1368.

5. Singer, L. S. *Faraday Discussions* **1985**, (79), 265-272.

6. Dubois, J.; Agache, C.; White, J. L. *Materials Characterization* **1997,** 39, (2-5), 105-137.

7. Marsh, H. *Fuel* **1973,** 52, (3), 205-212.

8. Gupta, G.; Rey, A. D. *Physical Review Letters* **2005,** 95, (12), -.

9. Edie, D. D.; Robinson, K. E.; Fleurot, O.; Jones, S. P.; Fain, C. C. *Carbon* **1994,** 32, (6), 1045-1054.

10. Hurt, R. H.; Hu, Y. *Carbon* **1999,** 37, (2), 281-292.

11. Yoon, S. H.; Korai, Y.; Mochida, I. *Carbon* **1993,** 31, (6), 849-856.

12. Nagappa, S.; Nataraju, S. K.; Marthandappa, M. *Molecular Crystals & Liquid Crystals* **1991,** 197, 15-20.

13. Rey, A. D.; Denn, M. M. *Annual Review of Fluid Mechanics* **2002,** 34, 233-266.

14. Yan, J.; Rey, A. D. *Physical Review E* **2002,** 65, (3), -.

15. Yan, J.; Rey, A. D. *Carbon* **2002,** 40, (14), 2647-2660.

16. Hong, S.; Chan, P. K. *Liquid Crystals* **2006,** 33, (3), 295-306.

17. Hong, S. J.; Chan, P. K. *Computational Materials Science* **2006,** 36, (3), 310-318.

18. Sori, M., *Calorimetric measurments in nematics*. In *Physical Properties of Liquid Crystals*: Nematics, Dunmur, D. A.; Fukuda, A.; Luckhurst, G. R., Eds. INSPEC: London, 2001; pp 14-50.

19. Alapati, P. R.; Saran, D. *Physica Status Solidi B-Basic Research* **1991,** 168, (1), 39-47.

20. Naggapa, S.; Mahadeva, J.; Somashekarappa, H.; Somashekar, R. *Indian Journal of Physics And Proc of The Indian Assoc For The Cultivation of Science - A* **2000,** 74A, (1), 45-48.

21. Grasso, D.; Gandolfo, C.; Fasone, S. *Thermochimica Acta* **1984,** 77, (1-3), 413-420.

22. Nagappa, S.; Jagadish, K. N.; Mahadeva, J.; Naveenkumar, S. K.; Somashekar, R. *Molecular Crystals & Liquid Crystals* **2001,** 366, 239-246.

23. Stephen, M. J.; Straley, J. P. *Reviews of Modern Physics* **1974,** 46, 617-702.

24. Chandrasekhar, S., *Liquid crystals*. 2nd ed.; Cambridge University Press: Cambridge [England]; New York, NY, USA, 1992.

25. Humphireps, R. L.; James, G.; Luckhurst, G. R. *Symp. Faraday Society* **1971,** 5, 107-118.

26. Lhuillier, D.; Rey, A. D. *Journal of Non-Newtonian Fluid Mechanics* **2004,** 120, (1-3), 85-92.

27. Bates, G. S.; Beckmann, P. A.; Burnell, E. E.; Hoatson, G. L.; Palffy-Muhoray, P. *Molecular Physics* **1986,** 57, (2), 351-357.

28. PAlffy-Muhoray, P.; Dunmur, D. A.; Miller, W. H. *Liquid Crystals and Ordered Fluids* **1984,** 4, 615.

29. P.Palffy-Muhoray, J. J. d., D.A.Dunmur. *Mol.Crys.Liq.Crys.* **1985,** 127, 301-319.

30. Hu, Y.; Hurt, R. H. *Carbon* **2001,** 39, (6), 887-896.

31. Bates, G. S.; Burnell, E. E.; Hoatson, G. L.; Palffy-Muhoray, P.; Weaver, A. *Chemical Physics Letters* **1987,** 134, (2), 161-165.

32. Cervo, E. G.; Thies, M. C. *Chemical Engineering & Technology* **2007,** 30, (6), 742-748.

33. Huebner, K. H.; Dewhirst, D. L.; Smith, D. E.; Byrom, T. G., *The Finite Element Methods for Engineers*. John Wiley & Sons, INC.: New York, 2001.

34. Prausnitz, J. M.; Lichtenthaler, R. N.; Azevedo, E. G. *Molecular Thermodynamics of Fluid-Phase Equilibrium*. Prentice Hall Inc.: Englewood Cliffs, 1986.

4. Structure and Phase Transitions of Carbonaceous Mesophase Binary Mixtures Under Uniaxial Extensional Flow

4.1 Summary

The Maier-Saupe model for binary mixtures of uniaxial discotic nematogens, formulated in previous studies[1], is extended to simulate the effect of uniaxial extensional flow on the phase behavior and structure. The rotational diffusivity of each disk-like component in the mixture of a high molecular weight (Mw) and a low molecular weight species, is derived based on: (i) a power law that relates molecular size to molecular weight and (ii) the excluded volume of binary disc-like molecules. The thermo-rheological phase diagram of a 50/50 mixture, given in terms of temperature (T) and Deborah (De) number show the existence of four T-De regions and six solutions: oblate($\perp,\parallel$), prolate ($\perp,\parallel$) and scalene($\perp,\parallel$), where the symbols ($\perp,\parallel$) indicate alignment of the tensor order ellipsoid with respect to the extension axis. It is found that, with increasing T, the higher molecular weight component exhibits weak deviations from the well-known pure species response to uniaxial extensional flow $\left(\text{uniaxial} \perp \text{nematic} \rightarrow \text{biaxial nematic} \rightarrow \text{uniaxial} \parallel \text{paranematic}\right)$. In contrast, the low molar mass component is always uniaxial and the orientation of the oblate or prolate states is dictated by the coupling effects emanating from the high molar mass component. Analysis of the coupling effects reveals that the changes in conformation $\left(\text{oblate} \rightleftarrows \text{prolate}\right)$ and orientation $\left(\perp \rightleftarrows \parallel\right)$ is effected through changes in pairs of eigenvalues. At high temperature, extensional flow acting on an isotropic phase produces an oblate paranematic state in the high Mw species and a prolate paranematic state in the low Mw species. Finally we show that X-ray intensity calculations are able to detect the different regions of the thermo-rheological phase diagram characterized by the presence of oblate, prolate, scalene nematic and paranematic states.

4.2 Introduction

Carbonaceous mesophases (CMs), first reported by Brooks and Taylor[2], are discotic nematic liquid crystalline (DNLC) mixtures obtained from petroleum pitches and synthetic naphthalene precursors[3]. Manufacturing of high performance carbon fibers by melt-spinning is one of the major applications of these precursor materials. Carbon fiber spinning process involves unixial extensional flow of liquid crystalline polydisperse CM precursors. As a result, the final structure of the fiber depends not only on the precursor chemistry, but also, on the uniaxial extensional flow which is applied during the process. This paper seeks to extend the thermodynamics of carbonaceous mesophase binary mixtures[1] to non-equilibrium states produced by an imposed uniaxial extensional flow.

The thermodynamics of binary carbonaceous mesophase mixtures composed of two mono-disperse components was described in[1] using the Maier-Saupe liquid crystal model adapted to discotic mesogens. Here we summarize the main findings[1, 4] relevant to the current paper. Since the only difference between the mixture components is their molecular weight, phase separation does not have to be considered in this case. The state of the mesogenic mixture depends on the quadrupolar order parameters[5] of the mixture. The mixture quadrupolar order parameter $\mathbf{Q}_{\text{mix}}$[1] is:

$$\mathbf{Q}_{mix}\left(\Delta\text{Mw},\beta,m_1,T\right) = m_1\mathbf{Q}_1 + (1-m_1)\mathbf{Q}_2 \tag{4.1}$$

where $\Delta\text{Mw} = M_{w1} - M_{w2}$ is molecular weight asymmetry given by the difference of the molecular weights of each component, β is the molecular interaction parameter , m_1 is the mole fraction of component "1", and T is the temperature; $\mathbf{Q}_1$ and $\mathbf{Q}_2$ are the quadrupolar tensor order parameters of each component:

$$\mathbf{Q}_1 = S_1(\mathbf{n}_1\mathbf{n}_1 - \frac{\mathbf{I}}{3}) + \frac{P_1}{3}\left(\mathbf{m}_1\mathbf{m}_1 - \mathbf{l}_1\mathbf{l}_1\right), \mathbf{Q}_2 = S_2(\mathbf{n}_2\mathbf{n}_2 - \frac{\mathbf{I}}{3}) + \frac{P_2}{3}\left(\mathbf{m}_2\mathbf{m}_2 - \mathbf{l}_2\mathbf{l}_2\right) \tag{4.2}$$

where {S_i ; i=1,2 and P_i ; i=1,2 } are the pure component scalar order parameters and {$\mathbf{n}_i$; i=1,2, $\mathbf{m}_i$; i=1,2 and $\mathbf{l}_i$; i=1,2 } are the orientation unit vectors; each orientation triad is orthogonal: $\mathbf{n}_1\cdot\mathbf{m}_1 = \mathbf{n}_1\cdot\mathbf{l}_1 = \mathbf{n}_2\cdot\mathbf{m}_2 = \mathbf{n}_2\cdot\mathbf{l}_2 = 0$. Using eqns.(4.2) we find the scalar order parameters (S_{mix}, P_{mix}) for the mixture:

$$S_{mix} = \frac{3}{2}\left(m_1\mathbf{Q}_1 : \mathbf{nn} + (1-m_1)\mathbf{Q}_2 : \mathbf{nn}\right); P_{mix} = \frac{3}{2}\left(m_1\mathbf{Q}_1 + (1-m_1)\mathbf{Q}_2\right):\left(\mathbf{mm} - \mathbf{ll}\right) \tag{4.3}$$

where **n**, **m** and **l** form the director triads of the mixture. A binary mesogenic mixture is uniaxial only when $P_1=P_2=0$ or $P_i = \pm 3S_i$ $(i = 1 \& 2)$ and $\mathbf{n} = \mathbf{n}_1 = \mathbf{n}_2$. Biaxiality then can arise through orientation differences ($\mathbf{n}_1 \neq \mathbf{n}_2$) or through single species   biaxiality$\left(P_1 > 0, P_2 > 0\right)$ & $P_i \neq \pm 3S_i$ $(i = 1 \& 2)$.   Under   the   uniaxial extensional flow it is shown below that the latter case takes place.

When mixing mesogens, uniaxial or biaxial phases may arise, such as when mixing rods$\left(\mathbf{n}_1\right)$ with disks$\left(\mathbf{n}_2\right)$[6], when the director are normal to each other: $\mathbf{n}_1 \perp \mathbf{n}_2$.   In addition, mesogenic mixtures are simultaneously lyotropic and thermotropic (amphotropic materials)[7,1,4], such that isotropic-nematic transitions can be affected by changes in temperature and concentration. For binary CMs at equilibrium we find collinear directors $\left(\mathbf{n}_1 = \mathbf{n}_2\right)$, no biaxiality is observed and the mixture uniaxial scalar order parameter then is[1]:

$$S_{mix} = m_1 S_1 + m_2 S_2 \tag{4.4}$$

Nevertheless since the ordering states of each species are coupled and are also dependent on temperature and dilution, we find[1], based on the above observations, that a binary mixture at equilibrium can display three possible states:

(i) isotropic (*I*) : $S_1=0$, $S_2=0$;

(ii) nematic (N_{12}) with $S_1 \geq S_2$;

(iii) nematic (N_{21}) with $S_1 \leq S_2$.

In our previous thermodynamic work[1] two kinds of transitions take place within mixtures of two components with the first one being the higher molecular weight component and the second one being the lower molecular weight component: (i) Nematic to Isotropic (*NI*) transition due to the thermal (thermotropic) effect, and (ii) N_{12} to N_{21} transition within the nematic phase due to the concentration (lyotropic) effect. For the later case $S_1 = S_2$ where N_{21} converts to N_{12}; at this point a nematic mixture behaves like a single component system, and the concentration corresponding to this transition is the critical concentration m_{1c} at which the *NI* transition temperature is an absolute minimum. The results of our previous study[1] show that depending on the molecular weight difference and the molecular interaction, two types of uniaxial nematic mixtures arise: (i) non-ideal mixtures;

both kinds of transitions are observed within non-ideal mixtures, and (ii) ideal mixtures; only the *NI* transition takes place within this type of mixtures; N_{12} exists for all range of concentration and as a result N_{21} and the critical concentration do not appear in the ideal mixture. Ideal binary mixtures arise under sufficiently strong interaction and sufficiently high molecular weight differences, while non-ideal mixtures arise under weaker interaction and relatively smaller molecular weight differences (asymmetries). As each carbonaceous mesophase mixture leads to different carbon fiber structure, it is of a great importance to be able to determine the type of the mixture. In this paper we show that under so called non-ideal mixture conditions, when the molecular weight asymmetry is ΔMw=1200-600=800, the interaction parameter is β=0.5 and the concentration is above the critical concentration m_{1c} (m_1=0.5 in this work), the high Mw species responds to extensional flow essentially as a pure mesogen, but the low Mw species, being subjected to strong enough coupling effects from the high Mw component, does not. The range of interaction parameter, β, which creates a non-ideal behavior out of this mixture (ΔMw=800, m1=0.5) is (0, 0.65). The effect of the interaction parameter on the ordering behavior is studied in the current work. The response of the mixture with the concentration below the critical concentration to the extensional flow, however, will be investigated in our future work.

Nematodynamics of single component liquid crystals has been extensively studied at the macro, meso, and molecular level[8-11]. Below we refer to order parameter and alignment interchangeably.

When the material is in the isotropic phase, flow induced alignment, *FIA*, (see Appendix A) produces flow-birefringence and the phase is paranematic[5, 12]. The paranematic phase is a non-equilibrium phase obtained when a mesogen at a temperature higher than the isotropic/nematic transition is subjected to an external field; under uniaxial extensional flow the paranematic phase adopts a prolate state with its unique axis along the extension direction. In addition to flow-induced alignment, flow-induced orientation (*FIO*) arises through the action of viscous torques on the eigenvectors of **Q**.

For single component discotic nematics under uniaxial extensional flow in the z-direction, the result of dual *FIO* and *FIA* effects is a stationary **Q**-tensor that is biaxial[13]:

$$\mathbf{Q} = S(\dot{\varepsilon})(\mathbf{nn} - \frac{\mathbf{I}}{3}) + \frac{P(\dot{\varepsilon})}{3}(\mathbf{mm} - \mathbf{ll}); \quad \mathbf{l} = -\boldsymbol{\delta}_z \qquad (4.5)$$

where $(\dot{\varepsilon})$ is the extension rate and the directors **n** and **m** are in the compression x-y plane. The exact spatial distribution depends on the geometry and boundary condition[14-17]. The flow-induced biaxiality arises because the deformation rate on the plane normal to **n** (**m-l** plane) is anisotropic. The degree of biaxiality was found to increase with increasing $(\dot{\varepsilon})$.[13]

A brief review of the macroscopic nematodynamics description of binary mesophases has been given in Appendix B. Through the review we can see that under uniaxial extensional flow both directors $\mathbf{n}_1$, $\mathbf{n}_2$ align in the compression plane and in the absence of gradient elasticity (spatially homogenous case) they will coincide: $\mathbf{n}_1 = \mathbf{n}_2$. (For the heterogeneous case one has to consider elasticity gradient, boundary conditions and possible defect formation[18-20])

Integrating the thermodynamics with the flow-induced orientation and flow-induced alignment in binary mixtures of CMs under uniaxial extensional flow merges the interplay between equilibrium uniaxial ordering and flow-induced biaxiality, which will be a function of the species molecular weight asymmetry (ΔMw), their interaction (β), and concentration (m_1). Macroscopic nematodynamics (eqns.((A4.1-A4.4))) will predict *FIO* and *FIA* accurately, but for binary mixtures the macroscopic material tensors (see tensors $\left(\mathbb{R}^{21}, \mathbb{R}^{22}, \mathbb{R}^{31}, \mathbb{R}^{33}\right)$ in Appendices B and C) will be given by unknown functions of the molecular parameters ($\Delta Mw, \beta, m_1$) and hence the most efficient way to include these important parameters is to use a molecular level description.

 The Maier-Saupe (MS) theory, the theory for the molecular level description, is widely used to describe the thermodynamics of nematic liquid crystals[1,21, 22]. It predicts the values of experimentally measured scalar order parameters of a pure system very well[23], and hence has been applied to different nematic liquid

crystalline systems and can be adjusted to model their mixtures[1]. In the presence of uniaxial extensional flow, both, the flow potential and the molecular potential contribute to the total potential, which is one of the key elements of the MS theory[24]. In other words, the extensional flow effects can be implemented through a flow potential. The flow can be considered as potential flow if the torque $\boldsymbol{\tau}$ can be expressed by the potential $H(\mathbf{u})$ of an external field[25]:

$$\boldsymbol{\tau} = -\boldsymbol{\Omega} H \tag{4.6}$$

where $\mathbf{u}$ is the unit molecular normal to the discs, $\boldsymbol{\Omega}$ is the rotational operator and given by

$$\boldsymbol{\Omega} = \mathbf{u} \times \frac{\partial}{\partial \mathbf{u}} \tag{4.7}$$

The details of this theory will be given in the next section. When comparing the MS and Landau-de Gennes nematodynamics approaches, we see that eqn.(4.12) corresponds to eqns.((A4.1-A4.3)), as previously demonstrated[21] and hence the predictions for single component CMs under extensional flow[26] serve as guidance. Finally, since X-ray is a useful tool to determine the orientation distribution function[27], and the latter is easily computed by the MS model[1], the modeling results can be verified by experimental data and inversely, X-ray experimental data can be converted into useful nematic order information.

The specific objectives of this work are:

(i) to evaluate the effect of the extensional flow on biaxiality and on the orientational behavior of CM binary mixtures,

(ii) to investigate the effect of extensional flow on the nematic to the paranematic/isotropic transition behavior of the NLC mixture;

7. to evaluate the effect of extensional flow on the structure of paranematic phase;

8. to construct the thermo-rheological phase diagram of the binary DNLC mixture in the presence of flow;

9. to use X-ray intensity calculations to determine the thermo-rheological phase diagram.

The organization of this paper is as follow. Section 4.3 presents the MS binary mixture model; the flow effect is introduced through the flow potential; the rotational diffusivity is derived for discotic nematogens and then it is extended to binary mixtures; the numerical solution scheme is also defined. Section 4.4 presents the derivation of the orientation distribution function, *ODF*, and the X-ray intensity of the mixture with the flow effects. Section 4.5 presents the results. Section 4.5.1 classified the type of solutions obtained for the ordering and the structural behavior of the components within the mixture. Section 4.5.2 reports the orientational and structural behavior of the mixture under the flow and the temparature effects. Section 4.5.3 shows the effect of flow and temperature on the X-ray intensity of the mixture as the characterization tool to asses its distribution function and nematic ordering. Section 4.5.4 discusses the effect of the interaction parameter between the components on their molecular ordering. Section 4.6 presents the conclusions. Appendix A describes flow-induced orientation (*FIO*) and flow-induced alignment (*FIA*) which are the important issues relevant to fiber spinning and to this paper. Appendix B reviews the macroscopic nematodynamics description of binary mesophases briefly and Appendix C explains how the viscoelastic coupling between two components influences their orientation.

4.3 Maier-Saupe Binary Mixture Model

The Maier-Saupe model for a single component NLCs[22] and its extension to model the binary mixture of two discotic nematogens has been described in our previous study[1, 4]. For a homogeneous binary mixture, the internal energy E_{mix} per molecule, due to self (1-1, 2-2) and cross (1-2) species interactions, is given by the sum of three contributions:

$$E_{mix}\left(\mathbf{Q}\right) \ = -\frac{3}{4}W_{11}\mathbf{Q}_1 : \mathbf{Q}_1 - \frac{3}{4}W_{22}\mathbf{Q}_2 : \mathbf{Q}_2 - \frac{3}{2}W_{12}\mathbf{Q}_1 : \mathbf{Q}_2 \tag{4.8}$$

The composition and molecular weight-dependent interaction parameters $\{W_{11}, W_{22}, W_{12}\}$ are as follows:

$$W_{ii} = m_i^2 U_{ii} \ ; \ \ W_{12} = m_1 m_2 U_{12} ; \text{i=11,22} \tag{4.9}$$

where

$$U_{ii} = \bar{U}_{ii} \; \frac{Mw_i}{m_1 Mw_1 + m_2 Mw_2}; \quad U_{12} = \bar{U}_{12} \tag{4.10}$$

and Mw_i denotes the molecular weight of the ith component, m_i its mole fraction, and $\{\bar{U}_{11}, \bar{U}_{22}, \bar{U}_{12}\}$ are the bare interaction parameters. Based on eqn.(4.8) and the MS model, the partial internal molecular potentials (Φ_1, Φ_2) acting on each species are:

$$\Phi_1 = \frac{\partial E_{mix}}{\partial \mathbf{Q}_1} : \left(\mathbf{u}_1 \mathbf{u}_1 - \frac{\mathbf{I}}{3} \right) = -\frac{3}{2}\left(W_{11}\mathbf{Q}_1 + W_{12}\mathbf{Q}_2 \right) : \left(\mathbf{u}_1 \mathbf{u}_1 - \frac{\mathbf{I}}{3} \right)$$

$$\Phi_2 = \frac{\partial E_{mix}}{\partial \mathbf{Q}_2} : \left(\mathbf{u}_2 \mathbf{u}_2 - \frac{\mathbf{I}}{3} \right) = -\frac{3}{2}\left(W_{22}\mathbf{Q}_2 + W_{12}\mathbf{Q}_1 \right) : \left(\mathbf{u}_2 \mathbf{u}_2 - \frac{\mathbf{I}}{3} \right) \tag{4.11}$$

where $\mathbf{u_1}$ and $\mathbf{u_2}$ are the molecular unit normal vectors of the two disc-like components as shown in Figure 4-1.
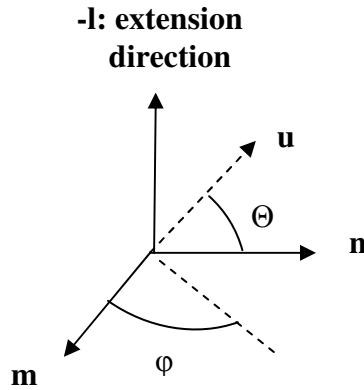
Figure 4- 1. Schematic of the molecular orientation u and the directors (n, m and l) for discotic nematogens. The extension direction is always along the l eigenvector of Q (see eqn.(4.8)). In general, imposition of extensional flow tends to increase φ and orient the molecules in the compression n-m plane.

The Helmholtz free energy per unit mole of the homogeneous mixture is:

$$A(\mathbf{Q}_1, \mathbf{Q}_2) = -N_A \left(E_{mix} + k_B T \ln Z \right) \tag{4.12}$$

where N_A is the Avogadros number and the mixture partition function Z is factorized as:

$$Z = Z_1^{m_1} Z_2^{m_2} = \left(\int e^{-J_1/k_B T} d\mathbf{u}_1 \right)^{m_1} \left(\int e^{-J_2/k_B T} d\mathbf{u}_2 \right)^{m_2} \tag{4.13}$$

where Z_i is the partition function of the ith species. In the absence of any external potential, such as flow, the total potential J contains only the internal potential Φ accounting for the molecular interactions. In the presence of any external field like electric field or magnetic field or a potential flow (such as a steady uniaxial extensional flow) the field or the flow potential also contributes to the total potential. As a result, the partition function (eqn. (4.13)) is expressed as:

$$Z = Z_1^{m_1} Z_2^{m_2} = \left(\int e^{-\Phi_1/m_1 k_B T - H_1/k_B T} d\mathbf{u}_1 \right)^{m_1} \left(\int e^{-\Phi_2/m_2 k_B T - H_2/k_B T} d\mathbf{u}_2 \right)^{m_2} \tag{4.14}$$

where the dimensionless flow potential $H_i / k_B T$ is given by [24]:

$$\frac{H_i}{k_B T} = -\frac{3\dot{\varepsilon}}{4\bar{D}_{ri}} (\mathbf{u}.\mathbf{e_z})^2 R \tag{4.15}$$

where $\dot{\varepsilon}$ is the steady rate of uniaxial extension, $\bar{D}_{ri}$ is the rotational diffusivity of the ith component, $\mathbf{u}$ is the molecular unit normal, $\mathbf{e_z}$ the flow (extension) direction, and R is the rheological effective shape factor which is negative for disk-like molecules[10]. From eqn.(4.15) it is seen that the flow potential is proportional to R , but in contrast to shear flow , there are no stability issues if $|R| < 1$ since extensional flow is irrotational[10]. The relationship between the rotational diffusivity and the Mw of a system containing a single species of rod like molecules is known to be[28]:

$$D_r \sim Mw^a \tag{4.16}$$

$a < 0$ and depends on the concentration regime ($a \simeq$ -9 for the concentrated solutions where liquid crystals can exist).   However, such a relationship for mixtures of discotic molecules needs to be derived. Using the generalized expression for the rotational diffusivity[25] we find:

$$D_r \sim D_{r0} \left(\frac{1}{\nu V_{exc}} \right)^2 \tag{4.17}$$

where D_{r0} is the rotational diffusivity in the dilute media, ν is the number density and V_{exc} is the excluded volume. For a single discotic species of molecular diameter D, it is known[29, 30].that $V_{exc} \sim D^3$ and $D_{r0} \sim D^{-3}$ [29, 30]. Using these results we expect that the expression of D_r for a single species is:

$$D_r \sim \frac{1}{v^2 D^9} \tag{4.18}$$

Next we extend the diffusivity expression (18) to binary mixtures in terms of concentration and molecular weights. To find the relationship between the Mw and its diameter D we have used a model discotic molecule of the chemical compound circumcircumcoronene[31], shown in figure 4-2.
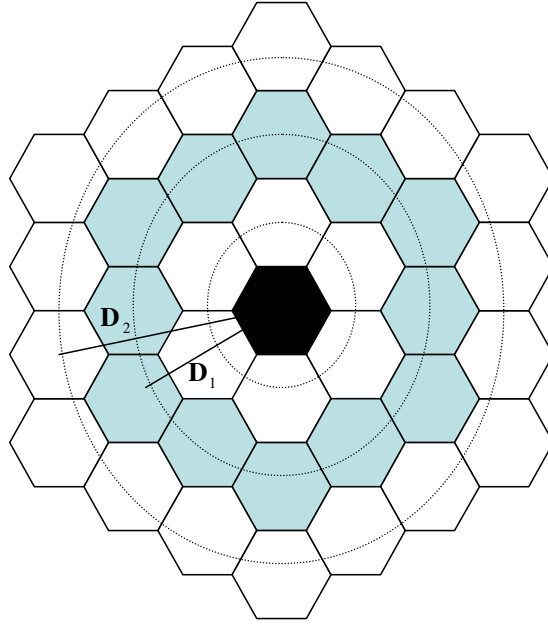
Figure 4- 2. The aromatic molecule, circumcircumcoronene, used to derive (eqn.(4.24)) the relationship between the rotational diffusivity Dr of each species and its corresponding Mw. As in rod-like nematics Dr is a strong function of Mw. A topological calculation gives a power law expression (eqn.(4.24)) in agreement with experiments[29].

By using this representative molecular structure we obtain the following power law between molecular weight and diameter:

$$M_{w1} \sim D_1^{1.65} , \qquad \frac{M_{w1}}{M_{w2}} = \left(\frac{D_1}{D_2}\right)^{1.65} \tag{4.19}$$

To obtain the relationship between the molecular weight Mw and the diameter D the layers are added to the core molecule and the Mw of the carbon atoms of the overall structure is calculated (the Mw of the hydrogen atoms are insignificant). In other words, the core molecule (benzene molecule) has the diameter $1D$ with six carbon atoms. When the first layer is added up to the core a molecule with $3D$ in diameter and 24 carbon atoms forms. Addition of the second layer to the core forms

a molecule with a diameter $5D$ and 54 carbon atoms, and so on. We then plotted the molecular weight Mw as a function of the diameter D in the logarithmic scale and measure the slope. This power law relationship between molecular weight and diameter agrees very well with the data available for the circumcoronene and circumcircumcoronene molecules[29]. As the starting point of the derivation of the rotational diffusivity of the discotic mixtures we assume that it follows a similar relationship as equation (4.17). The excluded volume of the ith component with diameter D_i in a binary mixture of discotic nematogens is given as follows[32]:

$$V_{exc\,i} \sim m_i D_i^3 + m_j D_i D_j \frac{\left(D_i + D_j\right)}{2}$$

(4.20)

Using eqns.(4.18 to 4.20), the rotational diffusivity of the ith component in the binary mixture is found to be:

$$D_{ri} = C\left(\frac{m_i}{m_1 Mw_1 + m_2 Mw_2}\right)^{-2} M_{wi}^{-\frac{3}{p}} \left(m_i M_{wi}^{\frac{3}{p}} + m_j M_{wi}^{\frac{1}{p}} M_{wj}^{\frac{1}{p}} \frac{\left(M_{w1}^{\frac{1}{p}} + M_{w2}^{\frac{1}{p}}\right)}{2}\right)^{-2} \quad ; p = 1.65$$

(4.21)

where C is the correlation coefficient with units of $\left(Kgmole / Kg\right)^{2-\frac{9}{P}} S^{-1} K^{-1}$.

Figure 4-3 shows the effect of m_1 on D_{r1}/C. As component "1" has a higher molecular weight than "2", increasing its concentration decreases the ability of the molecules to rotationally diffusivity within the mixture. The function is well fitted in the double logarithmic scales with a line of slope m= -1.94. Eqn. (4.21) defines D_r as a function of the Mw and concentration in isotropic media. To include the effect of anisotropic media we use the correction factor[33]:

$$\left(1 - \frac{3}{2}\mathbf{Q}_{mix} : \mathbf{Q}_{mix}\right)^{-2}$$

(4.22)

The complete rotational diffusivity of each component in the anisotropic media now reads:
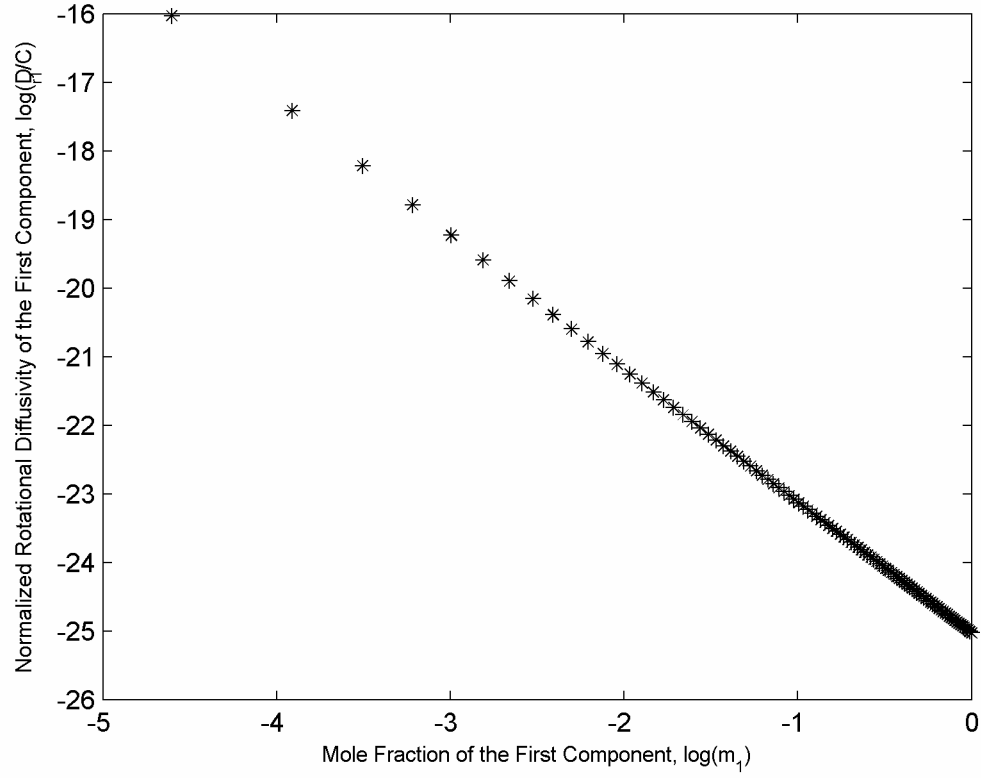
Figure 4- 3. Effect of concentation on the normalized rotational diffusivity of the high molecular weight species. The diffussivity is well fitted with $\log\left(Dr/C\right) = -1.94\log m_1$. See eqn.(4.26).

$$D_{ri} = C\left(\frac{m_i}{m_1 Mw_1 + m_2 Mw_2}\right)^{-2} Mw_i^{-\frac{3}{p}}\left(m_i M_{wi}^{\frac{3}{p}} + m_j M_{wi}^{\frac{1}{p}} M_{wj}^{\frac{1}{p}}\frac{\left(M_{w1}^{\frac{1}{p}} + M_{w2}^{\frac{1}{p}}\right)}{2}\right)\left(1 - \frac{3}{2}\mathbf{Q}_{\mathbf{mix}}:\mathbf{Q}_{\mathbf{mix}}\right)^{-2}$$

(4.23)

By replacing D_r in eqn. (4.23) by its expression in eqn. (4.15) we obtain the flow potential (of the first component) as

$$\frac{H_1}{k_B T} = -\frac{3}{4}(\mathbf{u}.\mathbf{e_z})^2 RDe\left(1 - \frac{3}{2}\mathbf{Q}_{mix} : \mathbf{Q}_{mix}\right)^2 \frac{\left(\dfrac{m_1}{m_1 Mw_1 + m_2 Mw_2}\right)^2}{\left(\left(\dfrac{m_1}{m_1 Mw_1 + m_2 Mw_2}\right)_{ref}\right)^2} \frac{M_{w1}^{\frac{3}{p}}}{\left(M_{w1}^{\frac{3}{p}}\right)_{ref}}$$

$$\frac{\left(m_1 M_{w1}^{\frac{3}{p}} + (1-m_1) M_{w1}^{\frac{1}{p}} M_{w2}^{\frac{1}{p}} \dfrac{\left(M_{w1}^{\frac{1}{p}} + M_{w2}^{\frac{1}{p}}\right)}{2}\right)^2}{\left(\left(m_1 M_{w1}^{\frac{3}{p}} + (1-m_1) M_{w1}^{\frac{1}{p}} M_{w2}^{\frac{1}{p}} \dfrac{\left(M_{w1}^{\frac{1}{p}} + M_{w2}^{\frac{1}{p}}\right)}{2}\right)_{ref}\right)^2} \tag{4.24}$$

where *De* is the dimensionless Deborah number given by :

$$De = \frac{\dot{\varepsilon}}{Dr_{ref}} = \frac{\dot{\varepsilon}}{CkT_{ref}}\left(\left(\frac{m_1}{m_1 Mw_1 + m_2 Mw_2}\right)_{ref}\right)^2 \left(M_{w1}^{\frac{3}{p}}\right)_{ref} \times$$

$$\left(\left(m_1 M_{w1}^{\frac{3}{p}} + (1-m_1) M_{w1}^{\frac{1}{p}} M_{w2}^{\frac{1}{p}} \frac{\left(M_{w1}^{\frac{1}{p}} + M_{w2}^{\frac{1}{p}}\right)}{2}\right)_{ref}\right)^2 \tag{4.25}$$

The expression for $\dfrac{H_2}{k_B T}$ is found by using the same steps. Finally replacing

eqns.(4.24) into eqn.(4.12) we find the extended free energy for a binary CM

mixture under steady uniaxial extensional flow in the "z" direction. The ten steady

state governing equations for the binary mixture are obtained by minimizing the

extended free energy *A* (eqn.(4.12)) with respect to $(\mathbf{Q}_1, \mathbf{Q}_2)$. According to the

discussion regarding eqn. (4.3), the binary mixture displays isotropic, uniaxial and

biaxial nematic states. Hence we can safely reduce the solution space (from ten

equations (in terms of tensor order parameters) to four scalar equations) and

parametric space as follows. According to the discussion of *FIO* in the introduction

and in appendix A, for steady uniaxial extensional flow along the "z" direction, the two director triads are proved to be congruent (see Appendix B),

n=n₁=n₂, m=m₁ = m₂, δ_z =-l₁ = -l₂ (4.26)

where δ_z is the unit vector along "z" (extension axis). In the computations described below we fixed the orientation triad as per eqn. (4.26). Since the compression plane normal to the stretching direction is isotropic the orientation of the **n-m** axes within this plane is irrelevant. Scaling the extended Helmholtz free energy A (eqn.(4.12)) with the bare interaction parameter $\bar{U}_{11}$, minimizing the resulting dimensionless free energy with respect to **Q₁**, **Q₂**, and double-contracting the tensorial equations with **nn** and **mm** we find the governing equations for the scalar order parameters S_1, S_2, P_1, P_2:

$$m_1\varphi_1 S_1 + \sqrt{m_1\varphi_1 m_2\varphi_2}\, L_1 S_2 - T_r \sum \frac{m_i}{Z_i}\frac{\partial Z_i}{\partial S_1} = 0$$

$$m_2\varphi_2 L_2 S_2 + \sqrt{m_1\varphi_1 m_2\varphi_2}\, L_1 S_1 - T_r \sum \frac{m_i}{Z_i}\frac{\partial Z_i}{\partial S_2} = 0$$

$$\frac{1}{3}m_1\varphi_1 P_1 + \sqrt{m_1\varphi_1 m_2\varphi_2}\, L_1 \frac{P_2}{3} - T_r \sum \frac{m_i}{Z_i}\frac{\partial Z_i}{\partial P_1} = 0$$

$$\frac{1}{3}m_2\varphi_2 L_2 P_2 + \sqrt{m_1\varphi_1 m_2\varphi_2}\, L_1 \frac{P_1}{3} - T_r \sum \frac{m_i}{Z_i}\frac{\partial Z_i}{\partial P_2} = 0$$

(4.27)

where the partition functions Z_i are given in eqn.(4.13). The asymptotic limits of eqns.(4.27) (m_1=0,1) correspond to the pure NLC, and in the absence of flow eqns.(4.27) reduce to the equilibrium thermodynamics case[1]. The thermodynamics of the mixture is defined by the dimensionless temperature T_r and two effective mole fractions as follows:

$$T_r = \frac{k_B T}{\bar{U}_{11}} \quad ; \quad \varphi_i = \frac{m_i M w_i}{\sum m_i M w_i}$$

(4.28)

The two material parameters of the model are:

$$L_1 = \frac{\bar{U}_{12}}{\bar{U}_{11}}; \quad L_2 = \frac{\bar{U}_{22}}{\bar{U}_{11}}$$

(4.29)

The material parameters (L_1, L_2) are functions of the species' molecular weights. To approximate real CMs we fix the *Mw* of the first and the second species as 1400

and 600, respectively[34]. The concentration m_1 and m_2 are also fixed as 0.5. By using the molecular weight dependency of the transition temperatures and the material parameter L_2 [1, 4], we obtain T_{N1}, T_{N2} and L_2 as 900 K, 300 K and 0.3333. Since the molecular weight dependency of L_1 is not suggested by actual data[1], we use:

$$L_1 = \beta L_2 \tag{4.30}$$

where β is the interaction coefficient and is positive for mixtures of similar molecules (disk/disk). In this study we fix β as 0.5.

The present model is given by the four nonlinear integral equations (eqns.(4.27)); the solution vector consists of four scalar order parameters (S_1, S_2, P_1, P_2); The flow effect is obtained by changing the *De* number and the phase ordering effect by sweeping over temperature T_r. The equations are solved using Newton-Raphson method, with an eight order Simpson integration method. Stability, accuracy, and convergence were ensured using standard methods. Issues of multistability and bifurcations are not considered in this paper. Numerical accuracy was established using the known pure component limits.

We use the results given by eqns. (4.27) to construct an atlas of orientation states in the scalar order parameter P-S triangle, similar to the one reported by[35]. The atlas, given in figure 4-4, is used to describe the orientational behavior of each component in the mixture. It defines the nomenclature of various steady state solutions presented in the next section, and indicates the sign of the corresponding eigenvalues[35].

To better understand the results in terms of the orientational structures we have also illustrated the orientation of the discotic molecules with respect to the major director of the system (**n**) (4-5.a) and the biaxial directors (**m** and **l**) for the uniaxial (4-5.b) and biaxial (4-5.c) cases in figure 4-5. In figure (4-5.b), the uniaxial case, the orientation distribution of the molecules in **m-l** plane (perpendicular to the major director) is isotropic and the projection of the oriented discs on **m-l** plane is a circle with two identical eigenvalues. On the other hand in figure (4-5.c), biaxial case, the orientation distribution of the molecules in **m-l** plane is anisotropic and
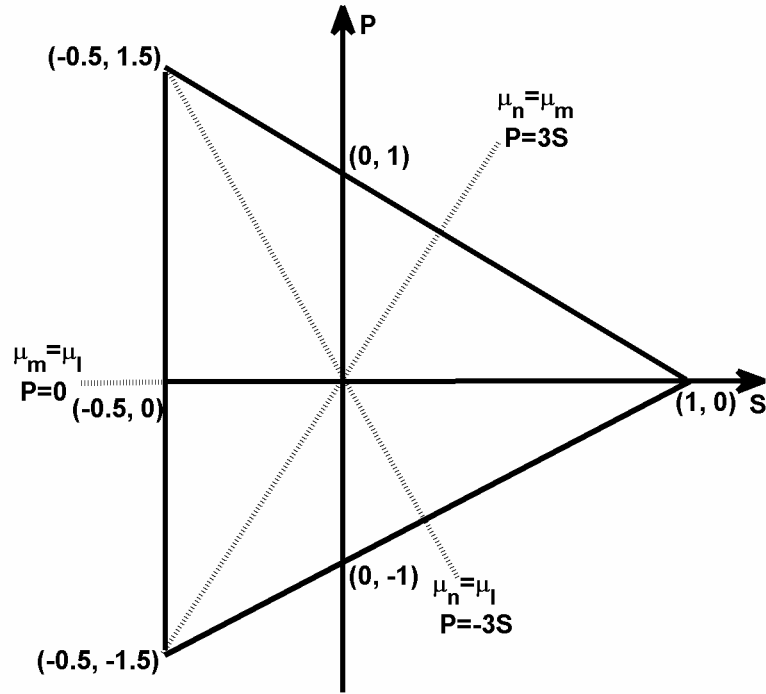
Figure 4- 4. Atlas of the orientation in terms of the scalar order parameters *S* and *P* and their corresponding eigenvalues, adapted from[35]. The dashed lines denote uniaxial states. Changing the temperature and/or extensional flow rate produces a trajectory in the (*S, P*) phase plane, usually across the biaxial regions. In the present model, the low molar mass component is always confined to the *P=0* (uniaxial line) while the state of high Mw species, under continuous increase in temperature, moves from the *P=0* line across the upper biaxial region to end up in the *P=3S* uniaxial line. See Figure 4-7 for exact details.

the projection of the oriented discs on **m-l** plane is an ellipsoid with two distinct eigenvalues.

4.4 Characterization Method: X-ray Intensity

The angular dependence of the X-ray intensity $I_i(\theta)$ of a binary nematic mixture in the absence of flow has been already derived in previous work[1]. Here we extend the calculation to take flow into account and find:

$$I_i(\alpha) = \frac{\sqrt{\pi}}{2} ODF_i \frac{erf\left(\sqrt{-J_i(\mathbf{n})/kT}\right)}{\sqrt{-J_i(\mathbf{n})/kT}}$$
(4.31)

where the single species orientation distribution function is:

(b) Uniaxial: $\mu_n > \mu_m = \mu_l$

(a)

(c) Biaxial: $\mu_n > \mu_m > \mu_l$
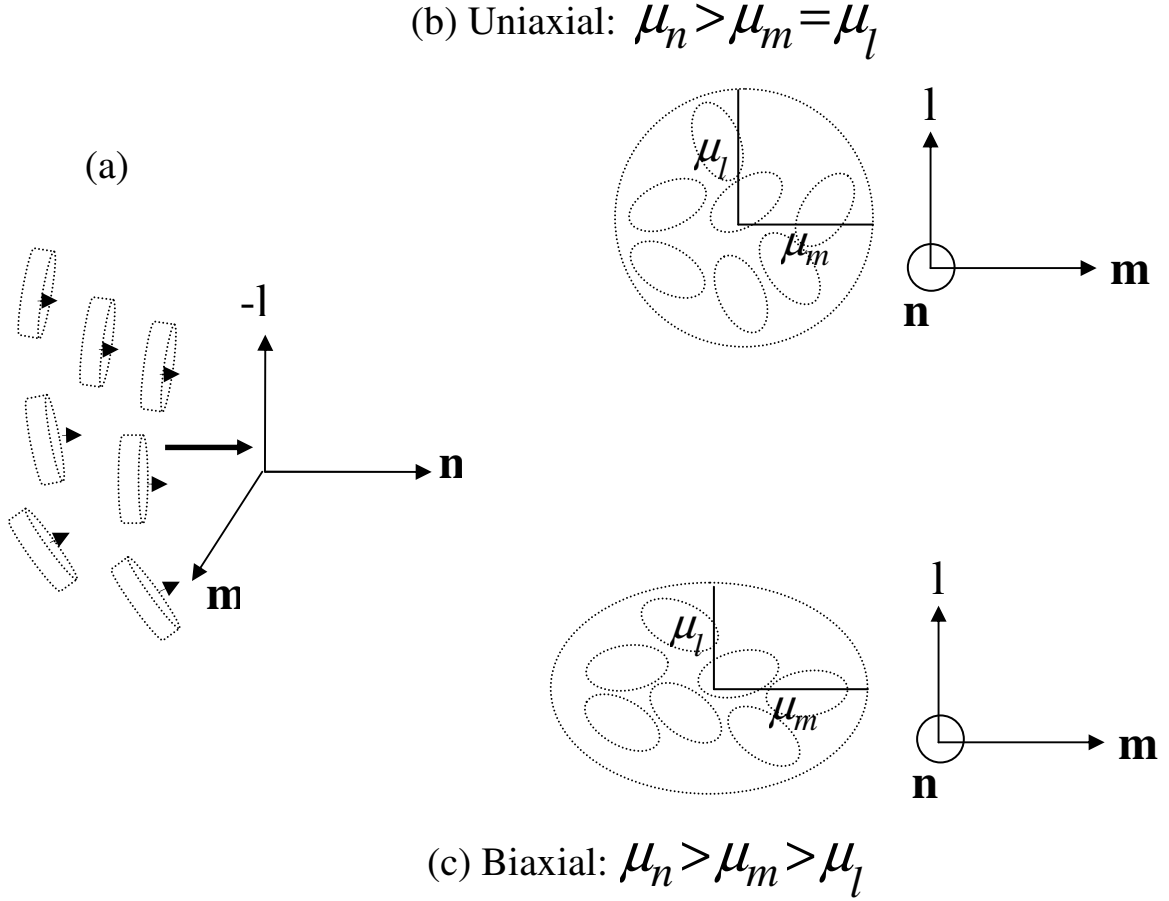
Figure 4- 5. Orientation of the discotic molecules with respect to the major director of the system (n) (5.a) and the biaxial directors (m and l) for the uniaxial (5.b) and biaxial (5.c) cases. In the uniaxial case, the projection of the orientation distribution of the molecules on m-l plane is a circle with two identical eigenvalues. On the other hand in the biaxial case, the projection of the orientation distribution of the molecules on m-l plane is an ellipsoid with two distinct eigenvalues.

$$ODF_i(\mathbf{n},\mathbf{m}) = \exp\left(-J_i(\mathbf{n},\mathbf{m})/k_B T\right)/Z_i, \quad J_i(\mathbf{n},\mathbf{m}) = \left(\frac{\Phi_i}{m_i} + H_i\right),$$

(4.32)

$$Z_i = \int e^{-J_i/k_B T} d\Omega_i$$

and *erf* is the error function. Measuring $I_i(\theta,\varphi)$ is thus a useful way to determine the orientation distribution function $ODF_l(\theta,\varphi)$ and the ordering magnitude. For a nematic mixture where the intermolecular angles are zero (α, β & $\gamma=0$; see figure 4-6) we can safely assume that equation (4.31) holds. Using this assumption we find the mixture X-ray intensity $I_{mix}(\theta,\varphi)$:
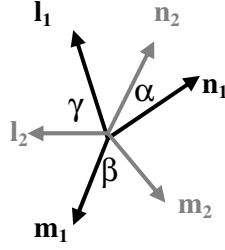
Figure 4- 6. Orientation coordinates of the two ("1" and "2") components. The angles between the two coordinate systems, α, β and γ, are assumed to be zero.

$$I_{mix}\left(\theta,\varphi\right) = \frac{\sqrt{\pi}}{2} ODF_{mix} \frac{erf\left(\sqrt{-J_{mix}\left(\mathbf{n},\mathbf{m}\right)/k_B T}\right)}{\sqrt{-J_{mix}\left(\mathbf{n},\mathbf{m}\right)/k_B T}} \tag{4.33}$$

where the mixture orientation function ODF_{mix} and the mixture Maier-Saupe mean field potential J_{mix} are

$$\begin{aligned} ODF_{mix} &= m_1 ODF_1 + m_2 ODF_2 \\ &= exp\left(-J_{mix}\left(\theta,\varphi\right)/k_B T\right)/Z_{mix} \end{aligned} \tag{4.34}$$

$$-J_{mix}\left(\theta,\varphi\right)/kT = ln\left(Z_{mix}\left(m_1 ODF_1 + m_2 ODF_2\right)\right)$$
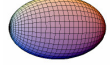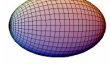
Below we use eqn.(4.33) to predict the mixture structure using X-ray measurements.

4.5 Results and Discussion

4.5.1 Solution Classification

Table 4-1 presents the six classes of steady state solutions to equations (4.27) using the sign and the ordering of the eigenvalues of $\mathbf{Q}_1$ and $\mathbf{Q}_2$ and the orientation of the dominant eigenvector with respect to the extension direction. Although stability was not investigated, the correspondence of these solutions with the well-known stable solutions to the single component case provides indirect evidence of their stability.

Table 4- 1. Solution Classification

Solution symbol	Solution symmetry	Sign of $\mu_n = 2S/3$	Sign of $\mu_m = (P-S)/3$	Sign of $\mu_l = -(P+S)/3$	Eigenvalues ordering	Corresponding structures
N_U^+	*Uniaxial Nematic*	+	-	-	$\mu_n > \mu_l = \mu_m$	Prolate ⊥
N_U^-	*Uniaxial Nematic*	-	+	+	$\mu_n < \mu_l = \mu_m$	Oblate ⊥
N_B^+	*Biaxial Nematic*	+	-	-	$\mu_n \rangle \mu_m \rangle \mu_l$	Scalene ⊥
PN_U^+	*Uniaxial Paranematic*	+	-	-	$\mu_n > \mu_l = \mu_m$	Prolate ⊥
PN_U^-	*Uniaxial Paranematic*	+	-	+	$\mu_l < \mu_n = \mu_m$	Oblate ||
PN_B^-	*Biaxial Paranematic*	+	*- or +*	-	$\mu_l < \mu_m < \mu_n$	Scalene ||

The first two columns give the symbols and names of the solution, the 3th-5th column give the sign of the three eignevalues, the 6th the ordering, and the 7th the visualization of the tensor ellipsoid using the usual **Q+I**/3 unit trace quadrupolar tensor, i.e. each axis of the ellipsoid corresponds to one eigenvalue of the tensor **Q+I**/3 (see figure 4-5); the symbols ⊥,|| denote perpendicular or parallel alignment of the unique axis of the tensor order parameter ellipsoid or the axis which

corresponds to the eigenvalue with the largest absolute value with respect to the extension axis, which is always along the **l** eigenvector.   These six solutions are

N_U^+ : Uniaxial Nematic with $\quad\quad \mu_n > \mu_l = \mu_m$

N_U^- : Uniaxial Nematic with $\quad\quad \mu_n < \mu_l = \mu_m$

N_B^+ : Biaxial Nematic with $\quad\quad \mu_n \rangle \mu_m \rangle \mu_l$

PN_U^+ : Uniaxial Paranematic with $\mu_n > \mu_l = \mu_m$

PN_U^- : Uniaxial Paranematic with $\mu_l < \mu_n = \mu_m$

PN_B^- : Biaxial Paranematic with $\quad \mu_n \rangle \mu_m \rangle \mu_l$

where the superscripts refer to the sign of the largest absolute eigenvalue and the subscript refers to the state (*U*: uniaxial, *B*: biaxial) . If there are two identical eigenvalues the state is uniaxial, otherwise it is biaxial. The corresponding ellipsoidal structures are prolate, oblate and scalene. Each radii of the ellipsoid refers to one eigenvalue. We use standard nomenclature: prolate is a rugby ball shaped ellipsoid with two identical eigenvalues; oblate is a disk-shaped ellipsoid with two identical eigenvalues and a scalene ellipsoid represents a structure with three different eigenvalues.

4.5.2 Orientational and Structural Behavior

Figure 4-7 shows the phase diagram of the binary system obtained as the solutions to equations (4.27). The lower Mw component ("2") is always uniaxial while the high Mw component "1" may be uniaxial or biaxial; below when referring to biaxial state it is understood to refer to the higher Mw component "1". The phase diagram contains four regions separated by four distinct transition lines. Each
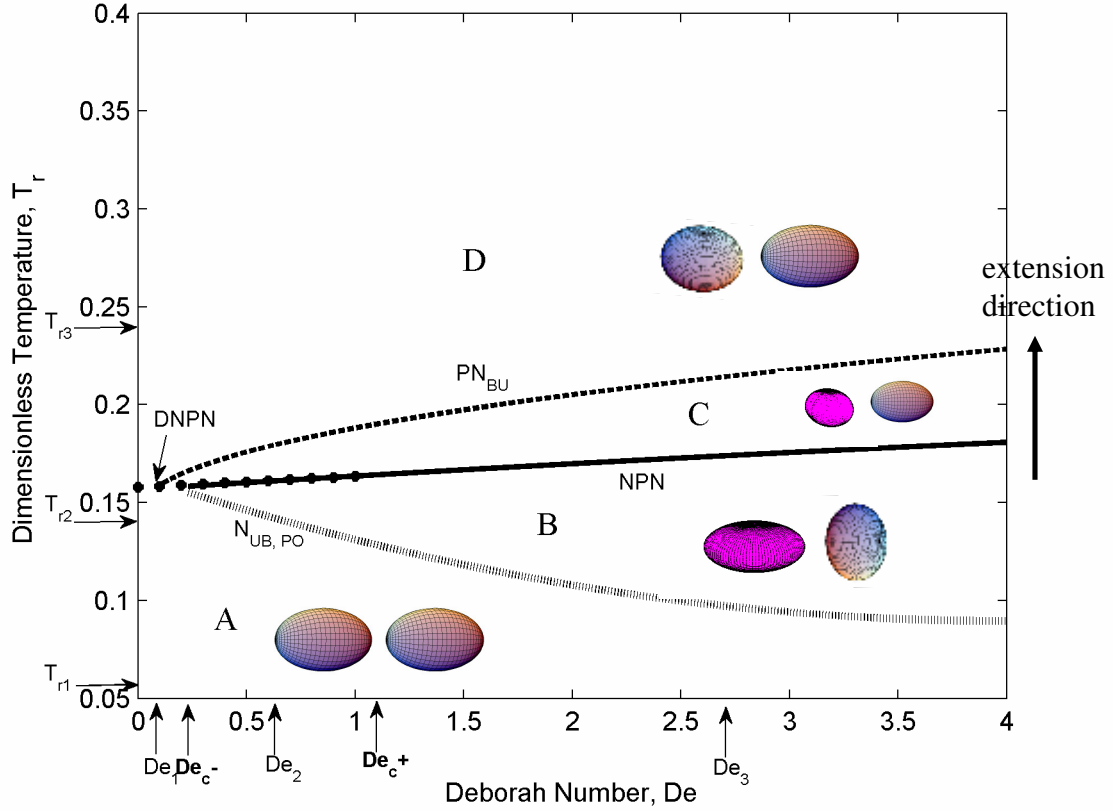
Figure 4- 7. Thermo-rheological phase diagram of the binary mixture in terms of dimensionless temperature T_r and Deborah (De) number. The phase diagram is vided into four regions and the state of each species is defined by the Q+I/3 tensor ellipsoid. The corresponding orientational/order parameter structures: region A with N_{U1}^+ and N_{U2}^+, region B with N_{B1}^+ and N_{U2}^-, region C with PN_{B1}^- and PN_{U2}^+ and region D with PN_{U1}^- and PN_{U2}^+, where the symbols are defined in Table (4-1). The temperatures in the y-axis are used in Fig.4-13 to 4-15. The De number in the x-axis are used in Figs.(4-8, 4-9).

region is characterized by a phase and a structural state of the two components. In each region, the structure on the left corresponds to the first component and the one on the right corresponds to the second component. The regions are:

Region A: $N_{U1}^+ / N_{U2}^+ \Rightarrow prolate \perp / prolate \perp$

Region B: $N_{B1}^+ / N_{U2}^- \Rightarrow scalene \perp / oblate \perp$

Region C: $PN_{B1}^- / PN_{U2}^+ \Rightarrow scalene \parallel / prolate \perp$

Region D: $PN_{U1}^- / PN_{U2}^+ \Rightarrow oblate \parallel / prolate \perp$

where the subscript i=1, 2 refers to the component number. The low temperature nematic region A contains two prolate $\perp$ states; in both components the director **n**

is normal to the extension direction. The high temperature paranematic region *D* contains the oblate ∥ and prolate ⊥ states. Transitional regions *B* and *C* contain mixed states in terms ordering: scalene /oblate ⊥ and scalene/prolate⊥, respectively. The four transition lines that define the four regions are:

(1) $N_{UB,PO}$: Nematic Uniaxial-Biaxial and Prolate-Oblate transition line which separates region *A* from region *B* (horizintal dashed line)

(2) $DNPN$: Discontinous Nematic − Paranemtaic transition line which separates regions *A* and *B* from regions *C* and *D* (dotted and full line with superposed dotts)

(3) NPN : Nematic − Paranemtaic transition line which separates region *B* from region *C*(full line)

(4) PN_{BU} : Paranematic Biaxial-Uniaxial transition line which separates region *C* from region *D*(dashed line)

The DNPN line that describes the discontinuous transition between nematic and paranematic states is itself divided into two segments:

(i) $0 < De < De_{c-} = 0.3$: here the discontinuous transition is between uniaxial nematic/ uniaxial nematic (*A*) and uniaxial paranematic/uniaxial paranematic (*D*) or biaxial paranematic/uniaxial paranematic (*C*).

(ii) $De_{c-} = 0.3 < De < De_{c+} = 1.3$: here the discontinuous transition is between biaxial nematic (*B*) and biaxial paranematic/uniaxial paranematic (*C*).

For $De > De_{c+} = 1.3$ the nematic/paranematic transition (full line) is always continuous.

Next we discuss the phase and structural behavior of the component within the mixture by imposing the extensional flow on the homogeneous mixture and by increasing the dimensionless temperature T_r at three different constant *De* numbers as follows (see labels on y and x axes of Fig.4-7):

$De_1 = 0.1 < De_{c-} = 0.3$
$De_{c-} = 0.3 < De_2 = 1 < De_{c+} \simeq 1.3$
$De_3 > De_{c+} \simeq 1.3$

and then (Figs.4-13 to 4-15) we discuss the X-ray intensity profile of the mixture at different *De* numbers at three temperatures T_{r1}, T_{r2} and T_{r3}.

Figure 4- 8 shows the components and mixture scalar order parameters $(S_1, S_2, S_{mix}, P_1, P_2, P_{mix})$ and the corresponding components' eigenvalues (μ_n, μ_m, μ_l) as a function of dimensionless temperature, for $De_1 = 0.1 < De_{c_-}$, corresponding to the discontinuous nematic/paranematic transition.
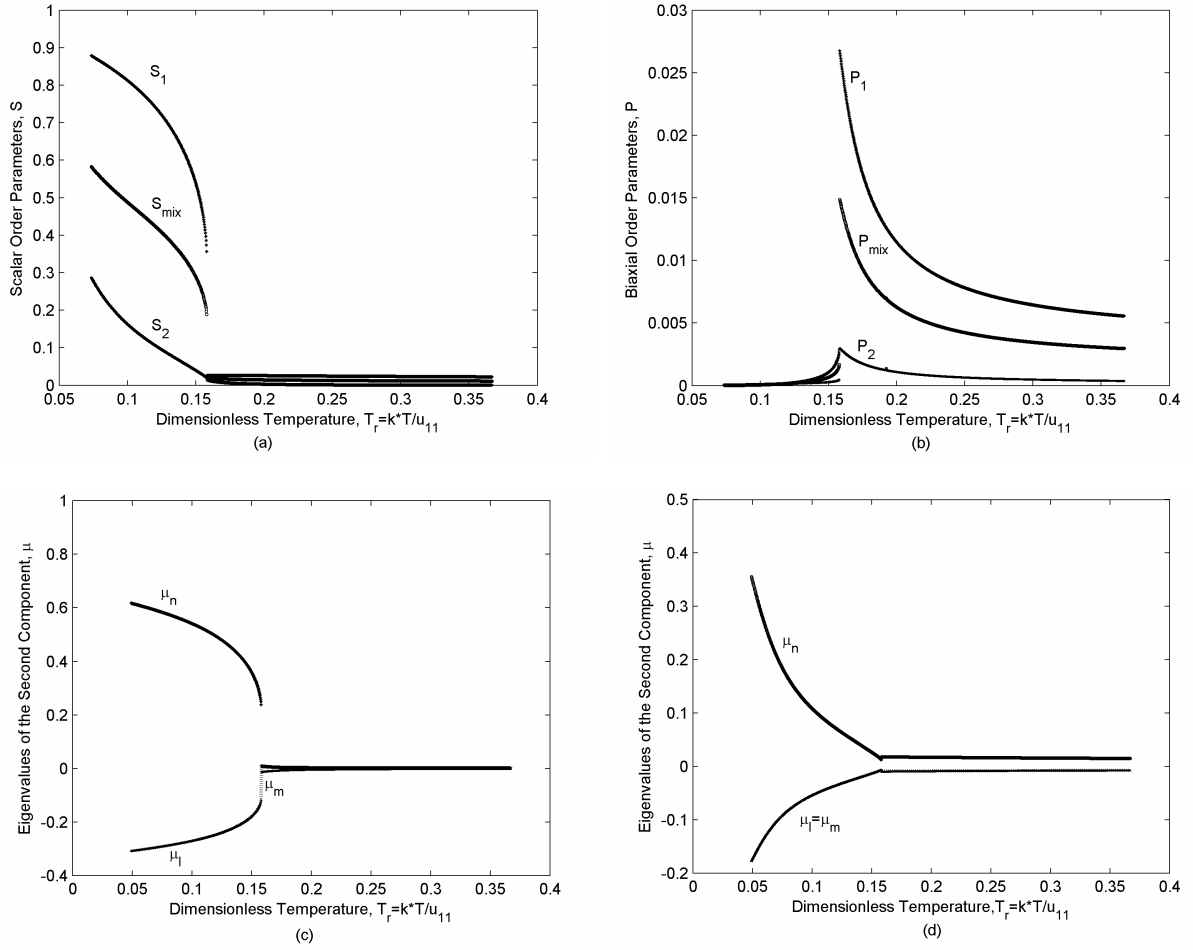
Figure 4- 8. Scalar order parameters (S and P) (a,b) and the eigenvalues (μ_n, μ_m & μ_l) (c,d) of the components as a function of dimensionless temperature for De=De$_1$=0.1. As temperature increases at this De, regions A and D of the phase diagram (Fig.4-7) are traversed.

By increasing the dimensionless temperature two regions *A* and then *D* emerge. In region *A*, the stable phases are uniaxial nematic, N_U^+, for both components, the scalar order parameters are positive and the biaxial order parameters are negligible. For each component, there are two identical eigenvalues, $\mu_n > \mu_l = \mu_m$, and the unique value, μ_n, is positive. Hence, the corresponding structures are both

prolate $\perp$. By increasing temperature at this *De* a discontinuous transition from nematic to paranematic phase takes place and region *D* is reached. This region is paranematic which is obtained by subjecting the isotropic phase to a uniaxial extension. In region *D* the stable phases are both uniaxial paranematic with positive scalar order parameters and negligible biaxiality. The stable phase is PN_{U1}^- for the first component with two identical eigenvalues, $\mu_{l1} < \mu_{n1} = \mu_{m1}$, composing a parallel oblate. For the second component however, the stable phase is PN_{U2}^+ again with two identical egienvalues, but this time $\mu_{n2} > \mu_{l2} = \mu_{m2}$, composing a perpendicular prolate. At sufficiently low *De*, then the main effect of temperature is to transform prolate/prolate nematic state into an oblate/prolate paranematic state. Figure 4-9 shows the scalar order parameters $(S_1, S_2, S_{mix}, P_1, P_2, P_{mix})$ and the corresponding components' eigenvalues (μ_n, μ_m, μ_l) for $De_{c-} = 0.3 < De_2 = 1 < De_{c+} \simeq 1.3$, corresponding to discontinuous transition between nematic and paranematic states. By increasing the dimensionless temperature from zero four regions *A*, *B*, *C* and *D* appear. In region *A*, (like in the pervious case, Fig.4-8) the stable phases are both uniaxial nematic, N_U^+, and the corresponding structures are both prolate $\perp$. By increasing temperature at this *De*, a transition within the nematic phase takes place and region *B* is reached. In region *B* the stable phase for the first component is biaxial nemtaic, N_{B1}^+, its scalar order parameter is positive and its biaxiality is significant. There are three distinct eigenvalues, $\mu_{n1} \rangle \mu_{m1} \rangle \mu_{l1}$ with μ_{n1} being positive and the largest value; the corresponding structure is scalene $\perp$. For the second component, however, the stable phase is uniaxial nemtic, N_{U2}^-, with negative scalar order parameter and two identical eigenvalues, $\mu_{n2} < \mu_{l2} = \mu_{m2}$, which denote a perpendicular oblate state. By further increasing the temperature, a nematic to paranematic discontinuous
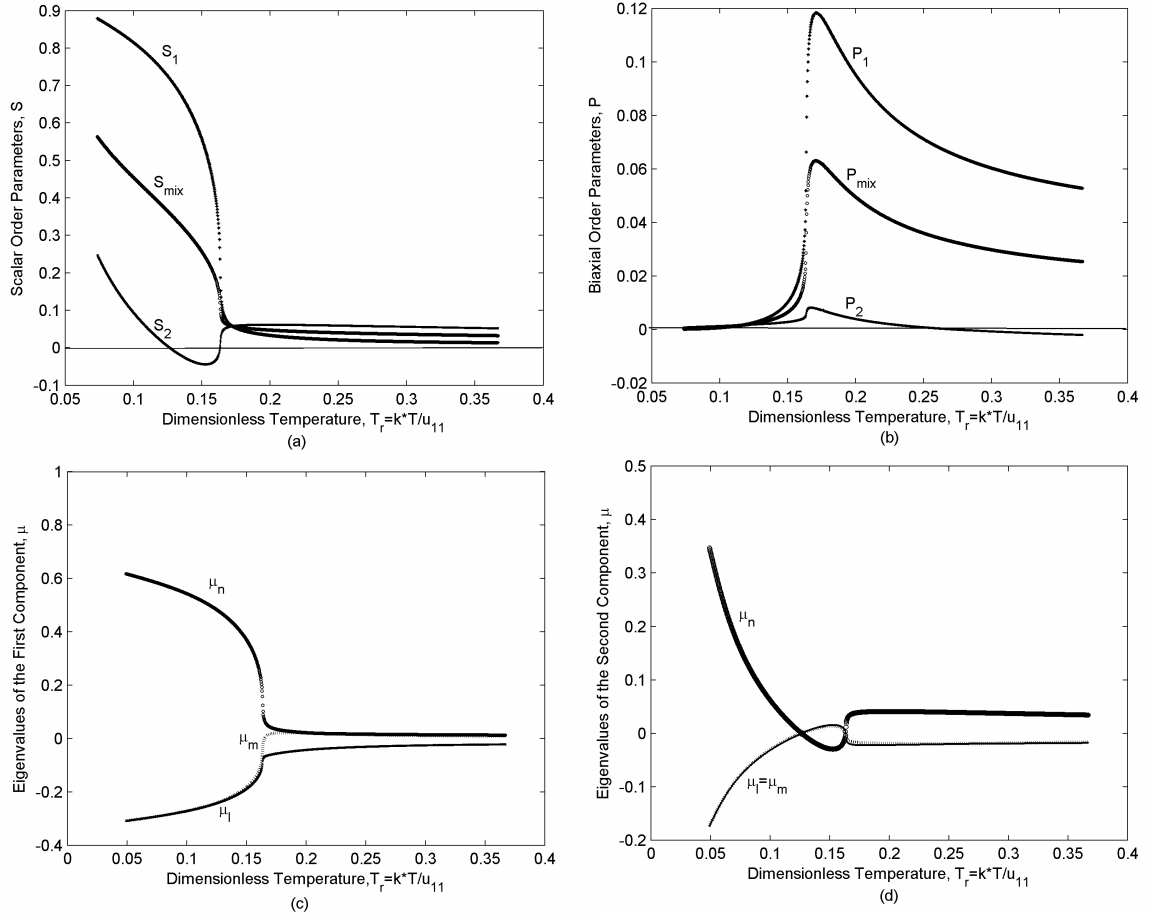
Figure 4- 9. S calar order parameters (S and *P*) (a,b) and the eigenvalues (μ_n, μ_m & μ_l) (c,d) of the components as a function of dimensionless temperature for *De=De₂=1*. As temperature increases at this *De*, regions *A*, *B*, *C* and *D* of the phase diagram are traversed.

transition takes place and region *C* emerges. In region *C* the stable phase for the first component is uniaxial paranematic, PN_{U1}^{-}, its scalar order parameter is positive and its biaxiality is significant. There are three distinct eigenvalues, $\mu_{n1} > \mu_{m1} > \mu_{l1}$ with μ_{l1} being negative and of largest value, and the corresponding structure is the parallel scalene. For the second component, however, the phase is uniaxial paranematic, PN_{U2}^{+}, with two identical eigenvalues, $\mu_{n2} > \mu_{l2} = \mu_{m2}$, denoting a prolate $\perp$. By increasing temperature in the paranematic phase at this *De* a continuous transition within the paranematic phase takes place and region *D* is reached. In region *D* the stable phases are uniaxial paranematic, PN_{U1}^{-}, for the first component and uniaxial paranematic, PN_{U2}^{+}, for the second component. The

corresponding structures are a oblate // and prolate⊥, respectively. For $De_3 > De_{c+} \simeq 1.3$ the phase and structural transitions of the component are identical to the second case, $De_{c-} = 0.3 < De = 1 < De_{c+} \simeq 1.3$, the only difference is the continuous nematic to paranematic transition which takes place at De_3. In the other words the De_{C+} is the last point of the *DNPN* transition line in the phase diagram (figure 4-7).

To better understand the phase and structural behavior of our discotic mixture we have also reproduced orientational behavior[36] and the phase diagram of the pure system (figure 4-10). The phase diagram has three regions: (i) unxial nematic (N_U^+), (ii) biaxial nematic (N_B^+) and (iii) uniaxial paranematic $\left(PN_U^-\right)$. There are three transition lines: N_{UB}, *DNPN* and *NPN*. The transition lines emerge at $T_r \simeq 0.22$, *De=0*. (i) continuous uniaxial nematic(N_U^+)/biaxial nematic(N_B^+) (N_{UB}: dashed line), (ii) nematic biaxial(N_B^+)/uniaxial paranematic (PN_U^+); for $0 < De < De_c \simeq 0.55$ the transition is discontinuous (*DNPN* : dotted line) and when $De > De_c = 0.55$ the transition is continuous.

At low temperatures (region N_U^+) there is thermodynamic and flow cooperation. Thermodynamics favors the uniaxial orientation N_U^+ while extensional flow also favors orientation along **n** with **n** along the compression plane and hence there is no competing effect. At higher temperatures and higher *De*, the thermodynamic uniaxial alignment along **n** now competes with the biaxial flow alignment producing the biaxial nematic state (region N_B^+) with **n** along the compression plane. Further temperature increase eventually leads to the biaxial nematic/ uniaxial paranematic transition. In the paranematic state (region PN_B^-) the oblate state has the unique axis (**l** vector) along the extension direction; here the competition of thermodynamics that prefers an isotropic state and the flow effect that seeks molecular alignment along the compression plane results in the oblate state. A simple first order estimate that captures the competition is
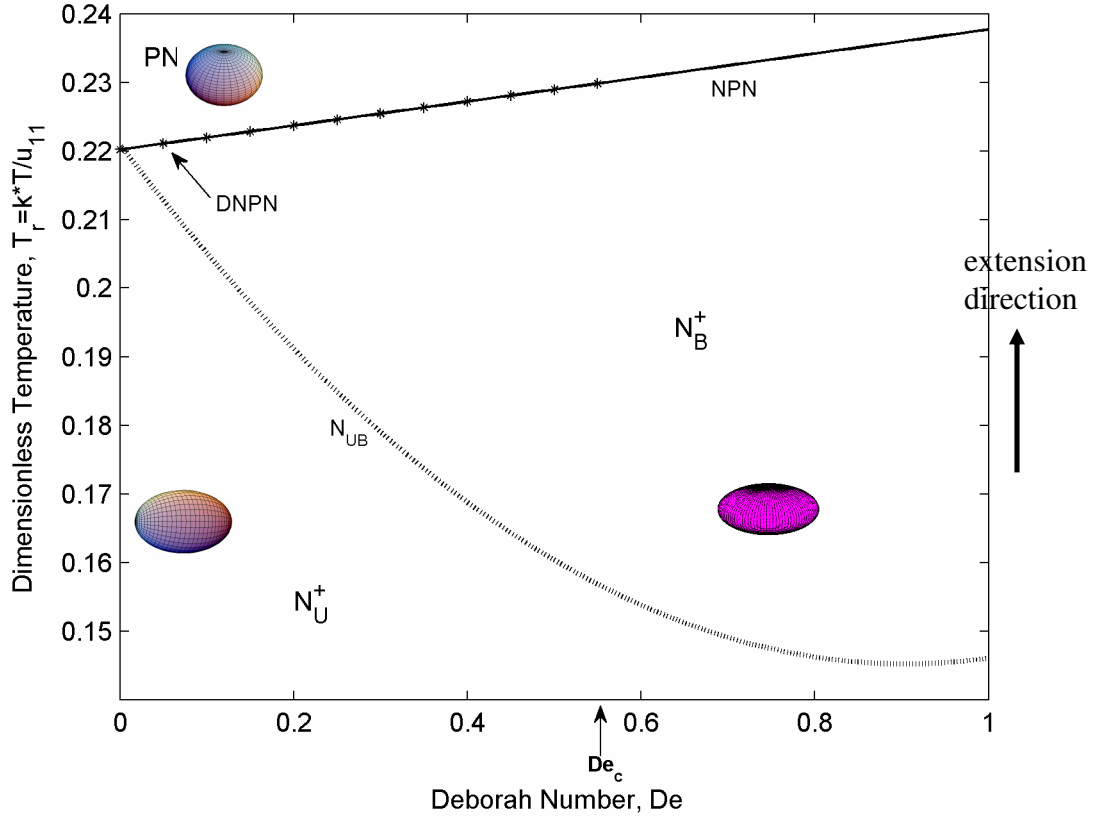
Figure 4- 10. Thermo-rheological phase diagram of a single discotic nematogen with its corresponding orientational/order parameter structures: N_U^+ **at low temperatures,** N_B^+ **at medium temperatures and** *De* **numbers and** PN_B^- **at high temperatures. Comparing Figs. 4-7 and 4-10 we see that the high Mw species follows essentially the pure species response but that low molar mass component exhibits new behavior.**

$$\mathbf{Q} = \alpha_1 \begin{bmatrix} -\dot{\varepsilon}/2 & 0 & 0 \\ 0 & -\dot{\varepsilon}/2 & 0 \\ 0 & 0 & \dot{\varepsilon} \end{bmatrix} \tag{4.35}$$

where α_1 is a ratio of viscosity to thermodynamic coefficients or relaxation time. The resulting eigenvalues of $\mathbf{Q}$

$$\mu_n = \frac{\alpha_1 \dot{\varepsilon}}{2}; \mu_m = \frac{\alpha_1 \dot{\varepsilon}}{2}; \mu_l = -\alpha_1 \dot{\varepsilon} \tag{4.36}$$

capture the oblate PN_B^- state (see Fig.4-10).

According to Figures (4-7 to 4-9) the dominant component ("1") in the mixture essentially follows the standard behavior of the pure mesophase (Fig.4-10) with a small perturbation which is the formation of the biaxial paranematic (PN_{B1}^-, region

116

C). The second low molar mass component, however, behaves differently. Although at low temperatures it shows the standard phase state which is uniaxial nematic N_{U2}^+, at medium and high temperatures and also at high *De* numbers (*B*, *C* and *D* regions) it adopts different orientational and structural states. Extension affects the molecules of the second low molar mass component differently. For instance, in region *D*, flow tends to align the molecules of species "1" in the compression (**n**-**m**) plane to form a parallel oblate but it aligns the molecules of the second component in a prolate $\perp$ structure. This phenomenon is due to the coupled viscoelastic forces generated within the mixture, as illustrated in Fig.4-11 and discussed in the introduction.

Figure 4-11 shows an input (temperature (*T*), Deborah number (*De*))-output (tensor order parameters $\mathbf{Q}_1$, $\mathbf{Q}_2$, $\mathbf{Q}_{\text{mix}}$) model of the mixture's nemato-rheology. The viscoelastic coupling VE indicates how the nematodynamics of the high Mw ("1") and low Mw ("2") components are mutually affected by viscoelastic (VE) effects. In what follows we concentrate on elastic (E) effects since they explain the observed results (Figs. 4-7 to 4-9)).
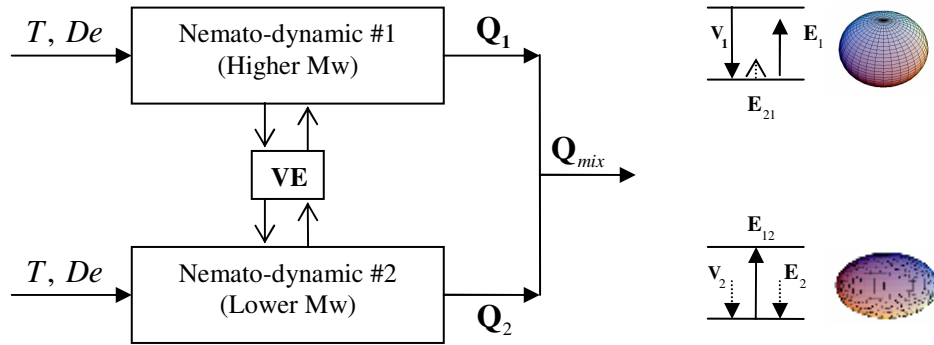
Figure 4- 11. Block diagram of coupled nematodynamics. The thermo-rheological input (*T*, *De*) results in a tensor order parameter output ($\mathbf{Q}_1$, $\mathbf{Q}_2$, $\mathbf{Q}_{\text{mix}}$) under action of the nematodynamics and viescoleastic (VE) coupling effects (see eqns.(4.35)). The model is used to explain the deviations of the low Mw species from the standard behaviour (Fig.4-10); see upper and lower right schematics. In region *D*, the high Mw species adopts the usual oblate $\parallel$ state (upper schematic) under the balance between viscous ($\mathbf{V}_1$) and thermodynamic ($\mathbf{E}_1$) and weak coupling ($\mathbf{E}_{21}$) effects. The low molar mass species meanwhile adopts a prolate $\perp$ state under viscous ($\mathbf{V}_2$), thermodynamic ($\mathbf{E}_2$) and strong coupling ($\mathbf{E}_{12}$). See text for details.

To explain the complex structures found in Region D (oblate parallel for "1" and prolate perpendicular for "2") we need to consider two factors: (i) the molecular weight asymmetry leads to asymmetric coupling effect, such that the influence of "1" on "2" is significant but the influence of "2" on "1" is insignificant; (ii) coupling effects from "1" on "2" change the usual structures of pure mesogens shown in Fig.(4-10). The terminology of the schematics on the right Fig.4-11 is: (A) Vi: viscous effect, Ei: elastic effect, Eij: elastic coupling effect of "i" on "j", (B) up-ward arrow $\left(\uparrow\right)$ indicates that the effect tends to align the unit normals along the extension axis, down-ward arrow $\left(\downarrow\right)$ indicates that the effect tends to align the unit normals along the compression plan; at steady state all the effects must balance. First we note (downward arrow in upper right Fig.4-11) that the extensional force within nematodynamics "1", V_1, aligns the molecules of component 1 preferentially in the compression (**n-m**) plane, reduces μ_{l1} and forms the parallel oblate, as predicted in eqn.(4.36) . At steady state this force is balanced with an elastic force, E_1, which tends to align the molecular unit normals back to the extension direction (upward arrow in upper right Fig. 4-11). The viscoelastic coupling effect of the low Mw component "2" on "1", denoted E_{21}, sensed by the high molecular weight component, #1, is not significant due to the molecular weigh asymmetry. However, the low molar mass component #2 is significantly affected by "1". The viscoelastic force generated by "2", V_2, (downward arrow in lower right Fig. 4-11) tends to align its director to the compression plane and to reduce μ_{l2} like the standard (pure or component 1) case. However, the coupling effect which tends to align the director to the extension direction, E_{21} (upward arrow in upper right Fig.4-11) is large enough to orient the molecules of "2" back to the extension direction and to increase μ_{l2}. As the relationship $\mu_{n2} + \mu_{m2} + \mu_{l2} = 0$ has to be satisfied, $\mu_{n2} + \mu_{m2}$ has to decrease to compensate for the increase of μ_{l2}. The decrease in $\mu_{n2} + \mu_{m2}$ can be achieved in several ways (i.e both decrease, one increases and the other decreases, and so on). The self-selected approach observed in Fig.4-7 is to pick the solution with the minimum number of

eigenvalues exchanges such that μ_{n2} remains almost constant and μ_{m2} decreases to compensate for the μ_{l2} increment. The net result is that $\mu_{l2} = \mu_{m2} < 0, \quad \mu_{n2} > 0$ and a prolate $\perp$ forms. The formation of different structures in regions B and C follows the same physics.

4.5.3 Effect of Flow (*De*) on the ODF and X-ray Intensity

In this section we present the simultaneous effect of thermodynamic, temperature, and *De* number, on the molecular alignment of our mixture in terms of X-ray intensity, I_{mix}, computed using eqn.(4.33). As the second term in eqn. (4.33) is a weak function of the polar angle θ and of the azimutual angle φ, the shape of X-ray intensity and *ODF* are essentially the same. Hence, for brevity, we only report the X-ray intensity plot and not the *ODF*. As the *ODF* is a representative of the uniaxial and biaxial ordering within the system, to better understand what X-ray intensity characterizes we first present the effect of *De* number on the ordering of the system as temperature increases. Figure 4-12 shows the effect of *De* on the scalar order parameters of the first component, S_1 and P_1 as the representative of the system. The parabola formed in figure (4-12.a) is similar to the one exhibited by single component mesogens subjected to a magnetic field[37] or an external stress[38] which have the similar effect as that of the uniaxial extensional flow. This result is also a validation for our computations. Likewise in Fig.4-12b a tilted parabola is well fitted to the P_1 values, a result that appears to be observed for the first time. The vertexes of both parabolas denote the critical point at which discontinuous and continuous transitions meet. Increasing *De* at a constant temperature, enhances the uniaxial ordering S which is due to their orientation along **n** (polar angle θ $=90; 0 \leq \theta \leq 180$) and also the asymmetry of their orientation in the **m-l** plane (along azimuthal angle $\varphi; 0 \leq \varphi \leq 360$) so that greater $P = 3/2(\mu_m - \mu_l)$ values are obtained. *ODF* and X-ray characterize these orderings, they characterize distribution of the molecular (unit normals) orientation with respect to the major director **n** through the polar angle θ and the asymmetry of their orientation in the **m-l** plane through the azimuthal angle φ. Figure 4-13 shows the X-ray intensity versus θ and φ for low temperature *T₁=200K (Tᵣ₁=0.0489 see figure 4-7)*,
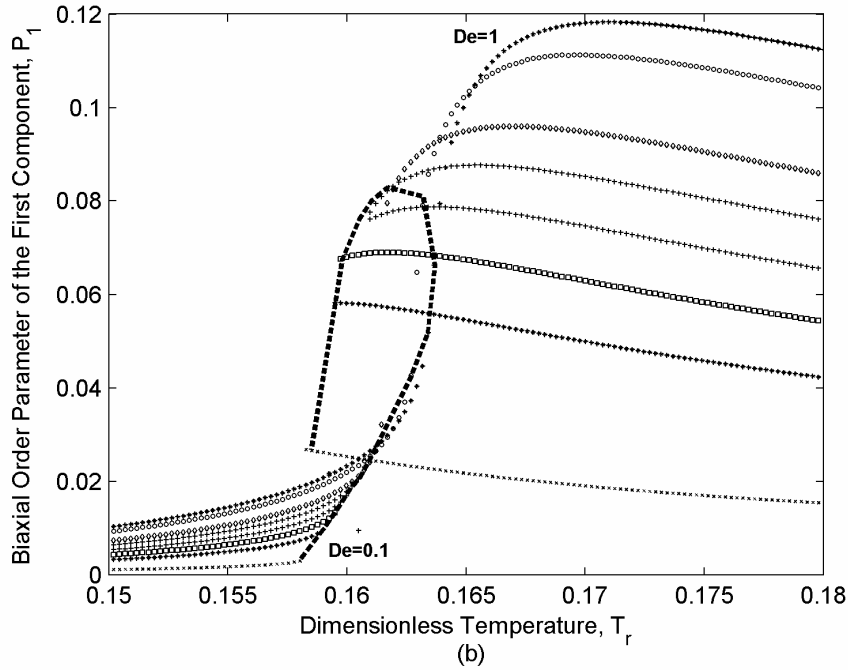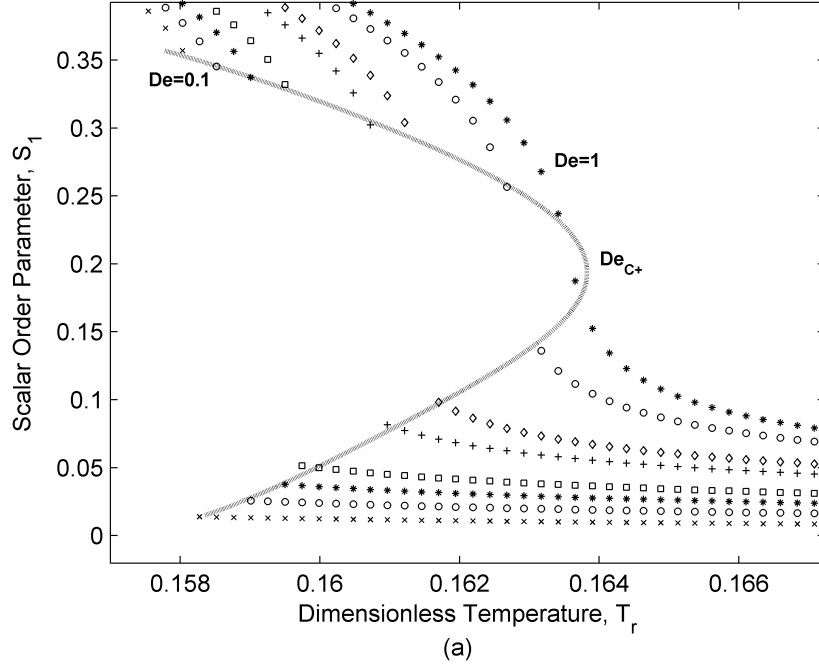
Figure 4- 12. Uniaxial and biaxial order parameters of the first component (S_1, P_1) as a function of the reduced temperature in a narrower range of *De* numbers (from 0.1 to 1). Fig. 4-12a shows that the nematic/paranematic transition is discontinuous for low *De* but becomes continuous at $De_{c+}=1.3$. The transition coordinates describe a parabola whose vertex denote the critical point at which discontinuous and continuous transitions meet. Likewise Fig.4-12b shows that the transition coordinates forming a tilted parabola whose vertex again denote the critical point at which discontinuous and continuous transitions meet.; the tilted P-parabola is an additional way to characterize the change between continuous and discontinuous nematic/paranematic transitions.

corresponding to region *A* of Fig.4-7. Regardless of the *De* number, the X-ray intensity values are identical. They show a bell shape distribution along the polar angle θ and a constant value along the azimuthal angle φ. In the other words, at low enough temperatures thermodynamic effects always dictates the orientation and yields N_U^+ with the standard bell shape X-ray intensity (along θ) and no asymmetry (no variation along φ)in the **m-l** plane.
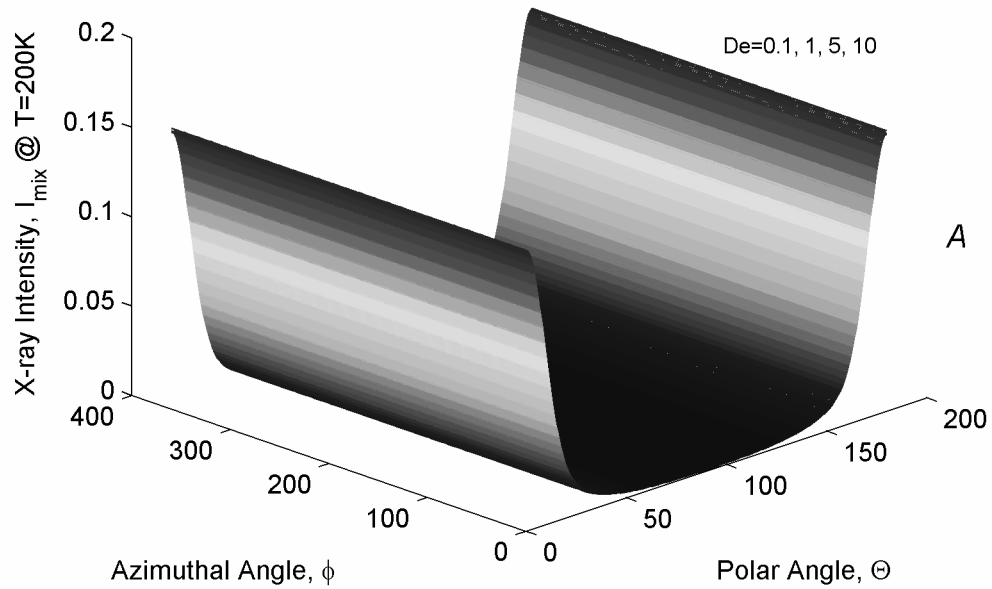
Figure 4- 13. The effect of *De* number on the X-ray intensity of the mixture, I_{mix}, at low temperatures, $T=T_1=200K$ ($T_{r1}=0.0489$) corresponding to Region *A* in Fig.4-7. Regardless of the *De* number the X-ray intensity follows the same forms of the standard pure N_U^+.

Figure 4-14 shows the X-ray intensity at intermediate temperature $T_2=600K$ ($T_{r2}=0.1467$ see figure 4-7*)* for different *De* numbers, corresponding to a trajectory across regions A and B of Fig.4-7. The intensity surfaces start to peel off; there is still no significant asymmetry in the **m-l** plane (no significant change along the azimuthal angle φ) but *De* changes the intensity along the polar angle θ. At this temperature, low *De* numbers generate a broad bell shape distribution (standard shape). But as *De* increases the uniaxial ordering increases and *ODF* and X-ray

intensity profiles become narrower. It is noted that at this *T*, the transition between regions A and B at $De \simeq 0.6$ is detected by the X-ray signal since the surface shows distinct separation sensitivity for $De > 0.6$.
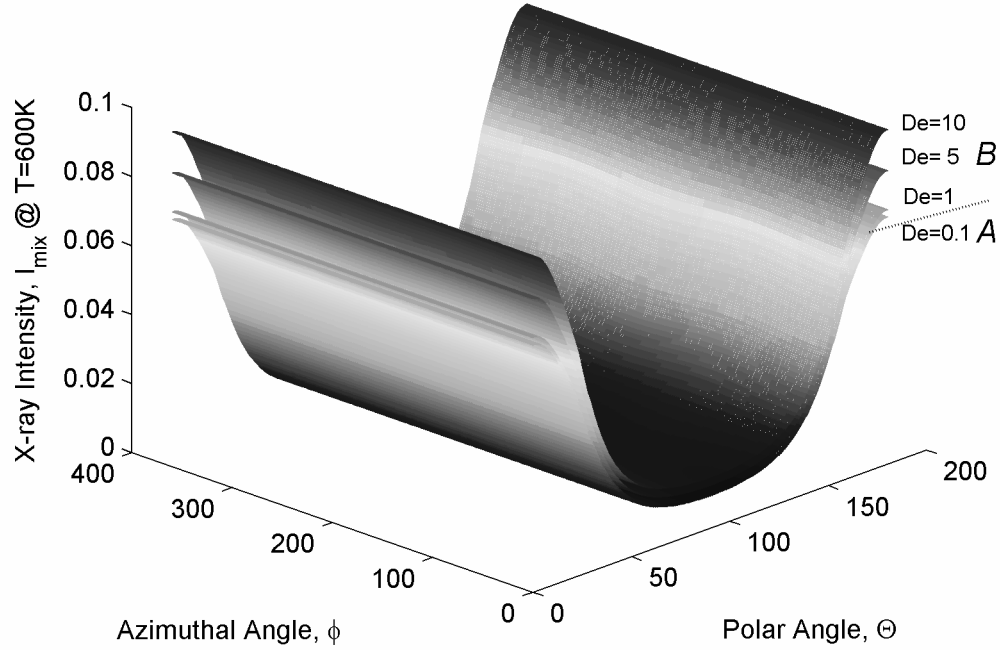
Figure 4- 14. The effect of *De* number on the X-ray intensity of the mixture, I_{mix}, at medium temperature, $T= T_2=600K$ ($T_{r2}=0.1467$); as *De* increase regions *A* and *B* are traversed in Fig.4-7. The intensity surfaces start to peel off; there is still no significant asymmetry in the m-l plane (along φ direction) but as *De* increases the intensity along the polar angle θ becomes narrower.

At high temperatures ($T_3=1000K$, $T_{r3}=0.2445$ see figure 4-7) , corresponding to a trajectory across regions *D* and *C* of Fig.4-7, there is a significant change along both axes; the surfaces separate and oscillate and the X-ray intensity profile becomes narrower along θ as *De* increases (figure 4-15). A significant asymmetry in the **m-l** plane is also formed in the system; this can be observed through the non-constant values of the intensity along the azimuthal angle φ. It is noted that at this *T*, the transition between regions *D* and *C* occurs at $De \simeq 5.3$ and that the shape of the X-ray surface clearly detects this transition.
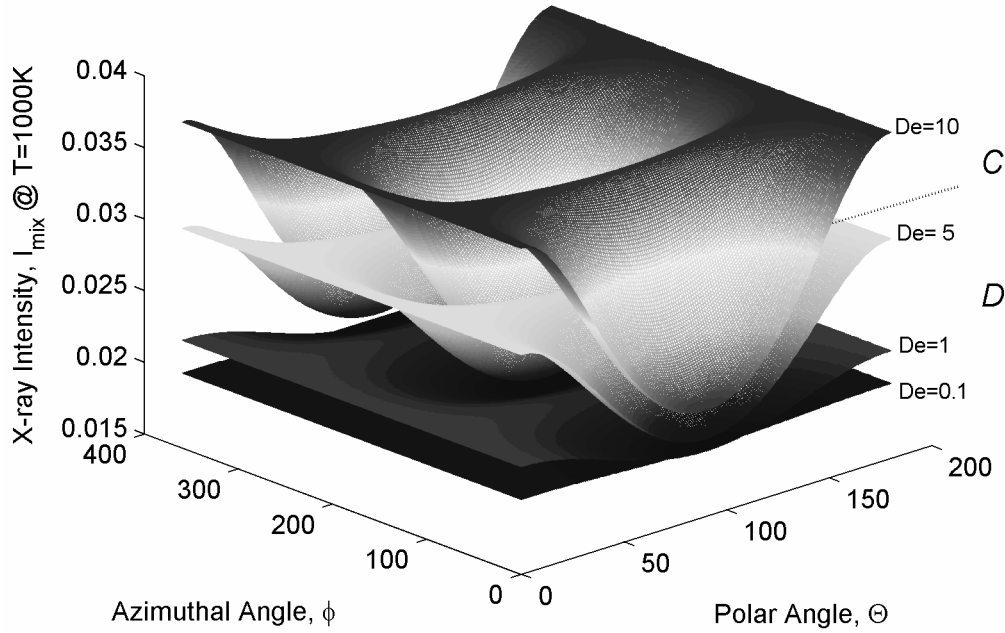
Figure 4- 15. The effect of *De* number on the X-ray intensity of the mixture, *I$_{mix}$*, at high temperature, *T= T$_3$=1000K (T$_{r3}$=0.2445)*; as *De* increases regions *D* and *C* are traversed in Fig.4-7. There is a significant change along both axes for this case; the surfaces separate and oscillate and the X-ray intensity profile becomes narrower along *θ* as *De* increases. A significant asymmetry in the m-l plane (along φ direction) is also observed.

4.5.4 Effect of Interaction Parameter on Molecular Ordering

In this work we study a representative non-ideal mixture. For the specific molecular weight asymmetry (ΔMw=800) and the concentration m$_1$=0.5 of the mixture β has to be in the range of (0, 0.65) to keep the non-ideality (see figure 4-16). We characterize the effect of β in this range on the species' order parameters (see the following figure) for De=1. The results of the simulations shown in Fig. 4-16 indicate:

1. increasing β closes the order parameter gap (i.e difference between the order parameters of the two components) in the nematic phase;

2. increasing β opens the order parameter gap in the paranematic phase;

3. increasing β increases the Nematic to Isotropic transition temperature, *T$_{NI}$*.

Our coupled nematodynamic model explains these features. In the nematic phase, with thermodynamic/flow cooperation, increasing β closes the order parameter gap. In the paranematic phase, with thermodynamic/flow competition, $\mathbf{Q_1}$ exerts a substantial thermodynamic force on $\mathbf{Q_2}$ opening the order parameter gap.
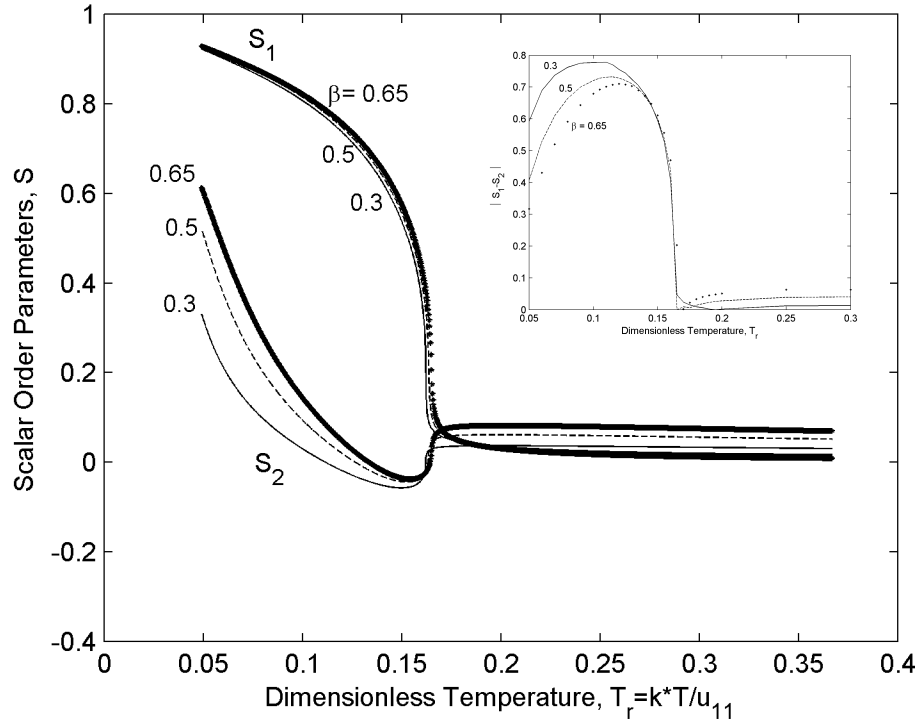
Figure 4- 16. Efffect of interaction parameter, *β*, on the uniaxial order parameter of the two components (S_1, S_2) as a function of the reduced temperature. The mixtures with the selected *β*s (0.3, 0.5 and 0.65) all behave non-ideally [1]. The insert in this figure shows $\left| S_1 - S_2 \right|$ as a function of the reduced temperature for the same β values. In the nematic phase increasing β, narrows the difference between the two order parameters. However, in the paranematic phase, increasing β increases difference between the two order parameters. At low temperatures, thermodynamic and flow cooperate and increasing interactions leads to the closer values of the order parameters. At high temperatures in the isotropic state, imposed flow creates flow-induced birefringence that competes with the thermodynamically preferred random order; hence increasing interaction leads to a strong thermodynamic effect that increases the difference between order parameters of the two species.

At low β the order parameter gap is in the nematic phase but there is no gap in the paranematic phase. At high β there is no gap in nematic phase, but a large order

parameter gap in the paranematic phase. In partial summary, under thermodynamic/flow cooperation (nematic phase) increasing β closes order parameter gap, under thermodynamic/flow competition (paranematic phase) increasing β opens the order parameter gap. The intermediate NI transition region interpolates between these two effects.

4.6 Conclusions

This paper uses the extended Maier-Saupe model for binary mixtures of discotic nematogenes to investigate the effect of steady uniaxial extensional flow on the orientational structure and molecular order of carbonaceous mesophase mixtures. The flow contribution is incorporated through a flow potential term. The concentration and molecular weight dependence of the rotational diffusivity of each component in a mixture is formulated using the excluded volume of discotics in a binary mixture (eqns.(4.17, 4.20)) and a novel power law scaling relation between molecular size and molecular weight (eqn.(4.19)). This work shows that mixing high and lower molecular weight nematogenic species introduces asymmetric coupling effects, such that the higher molecular weight component changes the flow-induced structures of the lower molecular weight component, but that the converse is not true. Comparing the thermo-rheological phase diagram of single component (Fig.4-10) with the binary one (Fig.4-7) results in the following observations:

1. Increasing the temperature in the high molecular weight species results in the following structure/orientation sequences (Fig.4-7):

$0 < \text{De} < 0.3 : \text{N prolate} \perp \xrightarrow{\text{discont}} \text{PN oblate} \parallel$

$0.1 < \text{De} < 1.3 : \text{N prolate} \perp \xrightarrow{\text{cont}} \text{N scalene} \perp \xrightarrow{\text{discont}} \text{PN scalene} \parallel \xrightarrow{\text{cont}}$
$\text{PN oblate} \parallel$

$\text{De} > 1.3 : \text{N prolate} \perp \xrightarrow{\text{cont}} \text{N scalene} \perp \xrightarrow{\text{cont}} \text{PN scalene} \parallel \xrightarrow{\text{cont}}$
$\text{PN oblate} \parallel$

where the text over the arrows refer to the continuous or discontinuous nature of the transition, and $\parallel$ $(\perp)$ denotes parallel to the extension axis. The main difference with the flow-response of the pure system is the presence of a direct uniaxial

nematic/paranematic transition for *0<De<0.3* and the presence of temperature/*De* region with a biaxial paranematic state (Region C in Fig.4-7). The thermorheological behaviour of the low molecular weight component in a binary mixture is starkly different than for the pure system. Increasing the temperature in the low molecular weight species results in the following structure/orientation sequences (Fig.4-7):

$0 < \mathrm{De} < 0.3:$ N prolate $\perp \xrightarrow{\text{discont}}$ PN prolate $\perp$

$0.1 < \mathrm{De} < 1.3:$ N prolate $\perp \xrightarrow{\text{cont}}$ N oblate $\perp \xrightarrow{\text{discont}}$ PN prolate $\perp \xrightarrow{\text{cont}}$ PN prolate $\perp$

$\mathrm{De} > 1.3:$ N prolate $\perp \xrightarrow{\text{cont}}$ N oblate $\perp \xrightarrow{\text{cont}}$ PN prolate $\perp \xrightarrow{\text{cont}}$ PN prolate $\perp$

The deviations from the pure species response to extensional flow are due to coupling effects (Fig.4-11). New expressions for *ODF* and X-ray intensity in binary mesogenic mixtures are derived (eqns.4.32 to 4.34)) and used (Figs.4-13 to 4-15) to map the different regions of the thermo-rheological phase diagram (Fig.4-7)). It is shown (Figs. 4-13 to 4-15) that X-ray intensity clearly detects the different paranematic states found at higher temperatures and varying Deborah numbers as well as the various oblate and prolate nematic states found at lower temperatures. The present work provides a foundation in mixing to manipulate extensional flow-induced structures in carbon fiber-forming processes.

4.7 Appendices

4.7.1 Appendix A

One of the important issues relevant to fiber spinning and this paper is flow-induced orientation (*FIO*) and flow-induced alignment (*FIA*), which can be gleaned by considering the dissipation function D[12, 39]:

$$D = \underbrace{\mathbf{T}^s : \mathbf{F}}_{\psi^V \text{:Viscous flow}} - \underbrace{\left(\frac{\delta A}{\delta \mathbf{Q}}\right)^{[s]} : \overset{\mathrm{o}}{\mathbf{Q}}}_{\psi^E \text{:Elastic term}} \quad , \quad \overset{\mathrm{o}}{\mathbf{Q}} = \frac{d\mathbf{Q}}{dt} + \mathbf{W} \cdot \mathbf{Q} - \mathbf{Q} \cdot \mathbf{W} \qquad (A4.1)$$

where $\mathbf{T}^s$ is the symmetric extra stress tensor, $\mathbf{F}$ is the rate of deformation tensor, $(\delta A / \delta \mathbf{Q})^{[s]}$ is the symmetric traceless variational derivative, A is the Helmholtz free energy, $\overset{\mathrm{o}}{\mathbf{Q}}$ is Zaremba-Jaumann co-rotational derivative and $\mathbf{W}$ is the vorticity

tensor. The linear expansion of the fluxes $(\mathbf{T^s}, \overset{\circ}{\mathbf{Q}})$ in terms of forces $(\mathbf{F}, -\delta A/\delta \mathbf{Q})$ gives

$$\begin{bmatrix} \overset{\circ}{\mathbf{Q}} \\ \mathbf{T}^s \end{bmatrix} = \begin{bmatrix} \mathbb{R}_1 & \mathbb{R}_2 \\ \mathbb{R}_3 & \mathbb{R}_4 \end{bmatrix} \begin{bmatrix} \mathbf{F} \\ -\delta A/\delta \mathbf{Q} \end{bmatrix} \tag{A4.2}$$

From eqn. (A4.2) the kinetics of $\mathbf{Q}$ is:

$$\overset{\circ}{\mathbf{Q}} = \left\{ \mathbb{R}_1 : \mathbf{F} - \mathbb{R}_2 : \left(\frac{\delta A}{\delta \mathbf{Q}} \right) \right\}^{[s]} \tag{A4.3}$$

where [s] denotes symmetric traceless, $\left(\mathbb{R}_1, \mathbb{R}_2 \right)$ are $\mathbf{Q}$ and $\mathbf{I}$-dependent fourth order tensors, and the first term is the flow-induced orientation; $\mathbf{I}$ is the 3x3 unit tensor. From eqns. (A4.1) and (A4.3) we find that the flow-induced orientation (*FIO*) and flow-induced alignment (*FIA*)[40]:

$$FIO: \mathbf{\Gamma_n} = \left(\underbrace{\frac{\mathbb{R}_1 : \mathbf{F} \cdot \mathbf{n}}{\mathbf{\psi}^V}}_{\text{viscous torque}} \right) \times \mathbf{n}, \quad \mathbf{\Gamma_m} = \left(\frac{\mathbb{R}_1 : \mathbf{F} \cdot \mathbf{m}}{\mathbf{\psi}^V} \right) \times \mathbf{m}$$

$$FIA: \mathfrak{I}_s = \underbrace{\left(\mathbb{R}_1 : \mathbf{F} \right)}_{\mathbf{\psi}^V} : \mathbf{nn}, \quad \mathfrak{I}_p = \underbrace{\left(\mathbb{R}_1 : \mathbf{F} \right)}_{\mathbf{\psi}^V} : \left(\mathbf{mm} - \mathbf{ll} \right) \tag{A4.4}$$

where $\left(\mathbf{\Gamma_n}, \mathbf{\Gamma_m} \right)$ are the flow torques acting on $\mathbf{n}$ and $\mathbf{m}$, and $\left(\mathfrak{I}_s, \mathfrak{I}_p \right)$ are the flow potentials acting on S and P. Since the directors are the slow variables and the scalar order parameters are the fast ones, increasing flow intensity will first modify orientation and then order.

4.7.2 Appendix B

The macroscopic nematodynamics of binary mesophases has been studied at the director level in the absence of elasticity gradient, and mainly under shear flows[12]. Again, the *FIO* and *FIA* for the two director $(\mathbf{n}_1, \mathbf{n}_2)$ model can be gleaned from the dissipation function *D*:

$$D = \mathbf{T}^s : \mathbf{F} - m_1(\mathbf{I} - \mathbf{n}_1\mathbf{n}_1) \cdot \left(\frac{\delta A}{\delta \mathbf{n}_1} \right) \cdot \mathbf{N}_1 - (1 - m_1)(\mathbf{I} - \mathbf{n}_2\mathbf{n}_2) \cdot \left(\frac{\delta A}{\delta \mathbf{n}_2} \right) \cdot \mathbf{N}_2 \tag{A4.5}$$

where $\mathbf{N}_1, \mathbf{N}_2$ are the Zaremba-Jaumann co-rotational derivative vectors for $\mathbf{n}_1$ and $\mathbf{n}_2$[41]. Again linear expansion of the fluxes $(\mathbf{T}^s, \mathbf{N}_1, \mathbf{N}_2)$ in terms of forces $(\mathbf{F}, -(\mathbf{I} - \mathbf{n}_1\mathbf{n}_1) \cdot \delta A/\delta\mathbf{n}_1, -(\mathbf{I} - \mathbf{n}_2\mathbf{n}_2) \cdot \delta A/\delta\mathbf{n}_2)$ gives[11, 12, 39]:

$$
\begin{bmatrix} \mathbf{T}^s \\ \mathbf{N}_1 \\ \mathbf{N}_2 \end{bmatrix} = \begin{bmatrix} \mathbb{R}^{11} & \mathbb{R}^{12} & \mathbb{R}^{13} \\ \mathbb{R}^{21} & \mathbb{R}^{22} & 0 \\ \mathbb{R}^{31} & 0 & \mathbb{R}^{33} \end{bmatrix} \begin{bmatrix} \mathbf{F} \\ -(\mathbf{I} - \mathbf{n}_1\mathbf{n}_1) \cdot \left(\dfrac{\delta A}{\delta\mathbf{n}_1} \right) \\ -(\mathbf{I} - \mathbf{n}_2\mathbf{n}_2) \cdot \left(\dfrac{\delta A}{\delta\mathbf{n}_2} \right) \end{bmatrix}
\tag{A4.6}
$$

Using eqn. (A4.6) $\mathbf{N}_1, \mathbf{N}_2$ are found to be

$$
N_{1i} = \mathbb{R}^{21}_{ijk} F_{jk} - \mathbb{R}^{22}_{ij} \left(I_{jk} - n_{1j} n_{1k} \right) \underbrace{\left(\frac{\delta A}{\delta n_{1k}} \right)}_{\text{elasticity gradien}} \quad , N_{2i} = \mathbb{R}^{31}_{ijk} F_{jk} - \mathbb{R}^{33}_{ij} \left(I_{jk} - n_{2j} n_{2k} \right) \underbrace{\left(\frac{\delta A}{\delta n_{2k}} \right)}_{\text{elasticity gradien}}
$$

$$
\tag{A4.7}
$$

Since the third order tensors $\mathbb{R}^{21}, \mathbb{R}^{31}$ are different, shear flow leads to biaxiality $\mathbf{n}_1 \neq \mathbf{n}_2$[40]. On the other hand under uniaxial extensional flow $(\mathbf{N}_1 = \mathbf{N}_2 = 0)$ both directors $\mathbf{n}_1$, $\mathbf{n}_2$ align in the compression plane and in the absence of gradient elasticity (we are considering the spatially homogenous case; for heterogeneity one has to consider gradient elasticity, boundary conditions and possible defect formation.[18-20]) they will coincide: $\mathbf{n}_1 = \mathbf{n}_2$[12,39]. Hence under spatially homogenous conditions, biaxiality in CM mixtures under uniaxial extensional flow arises from *FIA* generated by the anisotropy in the deformation rate in the plane containing the stretching direction (**l-m** plane); in a cylindrical (r, φ, z) coordinate system with stretching along z, the deformation rate anisotropy in the (φ, z) plane produces biaxiality.

4.7.3 Appendix C

Another important aspect of flow of mixtures is viscoelastic coupling[39]. Considering the tensor order parameter steady state version of the second eqn. (A4.6) we write:

$$\frac{\delta A\left(\mathbf{Q}_1,\mathbf{Q}_2\right)}{\delta \mathbf{Q}_2}=\left\{\left(\mathbb{R}^{33}\right)^{-1}\left(\mathbf{Q}_1,\mathbf{Q}_2\right):\mathbb{R}^{31}\left(\mathbf{Q}_1,\mathbf{Q}_2\right):\mathbf{F}\right\}^{[s]} \qquad \text{(A4.8)}$$

where we indicate the tensor $\left(\mathbf{Q}_1,\mathbf{Q}_2\right)$ dependencies explicitly. Hence to characterize the response of species "2" to flow and temperature changes we have to consider the thermodynamic and viscous effects of component "1" on "2" that appear in $\left(A,\mathbb{R}^{31},\mathbb{R}^{33}\right)$. For example, whenever extensional flow $\left(\dot{\varepsilon}\right)$ changes an eigenvalue, such as $\mu_{1l}\left(\dot{\varepsilon}\right)<\mu_{1l}\left(\dot{\varepsilon}=0\right)$, there will be an additional thermodynamic force from species "1" onto species "2" along the **l** direction that changes the balance between flow and thermodynamics effects of a pure "2" species in that direction. In general this coupling effect is asymmetric and significant when considering the effect of the higher molecular weight component on the lower molecular weight component, since within relevant temperature intervals, mesophase ordering increases with increasing molecular weight.

4.8 References

1. Golmohammadi, M.; Rey, A. D. *Liquid Crystals* **2009**, 36, (1), 75-92.

2. Singer, L. S. *Faraday Discussions* **1985**, 79, 265-272.

3. Sheikh, S. Y. *The effect of composition and shear rate on mesophase mixtures.* MS Thesis, Clemson University, Clemson, SC, 1999.

4. Golmohammadi, M.; Rey, A. D. *Entropy* **2008,** 10, (3), 183-199.

5. DeGennes, P. G.; Prost, J., *The physics of liquid crystals.* 2nd Edition ed.; Clarendon Press Oxford, 1995.

6. Palffy-Muhoray, P.; deBruyn, J. J.; Dunmur, D.A. *Molecular Crystals & Liquid Crystals* **1985,** 127, 301-319.

7. Dierking I., *Textures of liquid crystals.* Wiley-VCH: Weinheim, 2003.

8. Larson, R. L. *The structure and rheology of complex fluids.* Oxford University Press: New York, 1999.

9. Forest, M. G., Wang Q., Zhou H. *Liquid Crystals* **2001**, 28, (5), 717-720.

10. Rey, A. D.; Denn, M. M. *Annual Review of Fluid Mechanics* **2002,** 34, 233-266.

11. Tsuji, T.; Rey, A. D. *Journal of Non-Newtonian Fluid Mechanics* **1997,** 73, (1-2), 127-152.

12. Rey, A. D. *Rheologica Acta* **1995,** 34, (5), 461-473.

13. Singh, A. P.; Rey, A. D. *Journal De Physique II* **1995,** 5, (9), 1321-1348.

14. Wang, L.; Rey, A. D. *Liquid Crystals* **1997,** 23, (1), 93-111.

15. Wang, L.; Rey, A. D. *Modeling and Simulation in Materials Science and Engineering* **1997,** 5, (1), 67-77.

16. Yan, J.; Rey, A. D. *Carbon* **2002,** 40, (14), 2647-2660.

17. Yan, J.; Rey, A. D. *Physical Review E* **2002,** 65, (3), 031713: 1-14.

18. Rey, A. D. *Soft Matter* **2007,** 3, (11), 1349-1368.

19. Wincure, B. M.; Rey, A. D. *Nano Letters* **2007,** 7, (6), 1474-1479.

20. Rey, A. D. *Journal of Chemical Physics* **1999,** 110, (19), 9769-9770.

21. Lhuillier, D.; Rey, A. D. *Journal of Non-Newtonian Fluid Mechanics* **2004,** 120, (1-3), 85-92.

22. Priestley, E. B.; Wojtowicz, P. J.; Sheng, P. *Introduction to liquid crystals.* Plenum Press: *New York*, 1975.

23. Chandrasekhar, S., *Liquid crystals.* 2nd ed.; Cambridge University Press: Cambridge [England]; New York, NY, USA, 1992.

24. Ziabicki, A.; Jarecki, L. *Journal of Non-Newtonian Fluid Mechanics* **2001,** 97, (1), 31-52.

25. Doi, M.; Edwards S. F., *The theory of polymer dynamics*, Oxford University Press: New York, 1987.

26. Singh, A. P.; Rey, A. D. *Liquid Crystals* **1999,** 26, (6), 825-833.

27. Sori, M., Calorimetric Measurments in Nematics. In Physical Properties of Liquid Crystals: Nematics, Dunmur, D. A.; Fukuda, A.; Luckhurst, G. R., Eds. INSPEC: London, 2001; pp 14-50.

28. Acevedo, A.; Cotts, P. M.; Shine, A. D. *Macromolecules* **2005,** 38, (15), 6648-6655.

29. Xu, R. L.; Chu, B. J. *Journal of Colloid and Interface Science* **1987,** 117, (1), 22-30.

30. Perrin, F. *Journal De Physique Et Le Radium* **1934,** 5, 497-511.

31. Soncini, A.; Steiner, E.; Fowler, P. W.; Havenith, R. W. A.; Jenneskens, L. W. *Chemistry-a European Journal* **2003,** 9, (13), 2974-2981.

32. Wensink, H. H.; Vroege, G. J. *Journal of Physics-Condensed Matter* **2004,** 16, (19), S2015-S2027.

33. Grecov, D.; de Andrade Lima, L. R. P.; Rey, A. D. *Plastics Rubber and Composites* **2006,** 35, (6-7), 276-286.

34. Hurt, R. H.; Hu, Y. *Carbon* **1999,** 37, (2), 281-292.

35. Rey, A. D. *Macromolecular Theory and Simulations* **1995,** 4, (5), 857-872.

36. Maïcssa, P.; Ten Bosch, A.; Sixou, P. *Journal of Polymer Science Part C-Polymer Letters* **1983,** 21, **757-765**.

37. Wojtowic. P.J.; Sheng, P. *Physics Letters A* **1974,** A 48, (3), 235-236.

38. Schatzle, J.; Kaufhold, W.; Finkelmann, H. *Makromolekulare Chemie-Macromolecular Chemistry and Physics* **1989,** 190, (12), 3269-3284.

39. Rey, A. D. *Liquid Crystals* **1996,** 20, (2), 147-159.

40. Farhoudi, Y.; Rey, A. D. *Rheologica Acta* **1993,** 32, (3), 207-217.

41. Grecov, D.; Rey, A. D. *Journal of Rheology* **2005,** 49, (1), 175-195.

5. Structural Modeling of Carbonaceous Mesophase Amphotropic Mixtures under Uniaxial Extensional Flow

5.1 Summary

The extended Maier-Saupe model for binary mixtures of model carbonaceous mesophases (uniaxial discotic nematogens) under externally imposed flow, formulated in previous studies[1, 2], is used to characterize the effect of uniaxial extensional flow and concentration on phase behavior and structure of these mesogenic blends. The generic thermo-rheological phase diagram of the single-phase binary mixture, given in terms of temperature (T) and Deborah (De) number shows the existence of four T-De transition lines that define regions that correspond to the following quadrupolar tensor order parameter structures:(i) oblate($\perp, \parallel$) , (ii) prolate ($\perp, \parallel$), (iii) scalene O($\perp, \parallel$) and (iv) scalene P($\perp, \parallel$), where the symbols ($\perp, \parallel$) indicate alignment of the tensor order ellipsoid with respect to the extension axis. It is found that with increasing T the dominant component of the mixture exhibits weak deviations from the well-known pure species response to uniaxial extensional

flow $\left(\text{uniaxial} \perp \text{nematic} \rightarrow \text{biaxial nematic} \rightarrow \text{uniaxial} \parallel \text{paranematic} \right).$ In contrast, the slaved component shows a strong deviation from the pure species response. This deviation is dictated by the asymmetric viscoelastic coupling effects emanating from the dominant component. Changes in conformation $\left(\text{oblate} \rightleftarrows \text{prolate} \right)$ and orientation $\left(\perp \rightleftarrows \parallel \right)$ are affected through changes in pairs of eigenvalues of the quadrupolar tensor order parameter. The complexity of the structural sensitivity to temperature and extensional flow is a reflection of the dual lyotropic/thermotropic nature (amphotropic nature) of the mixture and their cooperation/competition. The analysis demonstrates that the simple structures (biaxial nematic and uniaxial paranematic) observed in pure discotic mesogens under uniaxial extensional flow are significantly enriched by the interaction of the lyotropic/thermotropic competition with the binary molecular architectures and with the quadrupolar nature of the flow.

Key Words: discotic nematic liquid crystals, carbonaceous mesophases, thermodynamics of mesophase mixtures, uniaxial extensional flow, binary mesogenic mixtures, thermo-rheological phase diagram, concentration, amphotropic, lyotropic, thermotropic.

5.2 Introduction

Carbonaceous mesophases[3] (CMs) are discotic nematic liquid crystalline (DNLC)[4] mixtures obtained from petroleum pitches and synthetic naphthalene precursors[5]. The thermodynamics of binary carbonaceous mesophase mixtures composed of two mono-disperse components was previously described[1] using the Maier-Saupe liquid crystal model[6] adapted to discotic mesogens. Since the only difference between the mixture components is their molecular weight, phase separation does not have to be considered in this case. For binary CMs at equilibrium it was found that the ordering states of each species is the result of thermotropic, lyotropic, and coupling effects. We found[1], based on the above observations, that a binary mixture at equilibrium can display three possible states:

(i) isotropic (I) : $S_1=0$, $S_2=0$;

(ii) nematic (N_{12}) with $S_1 \geq S_2$;

(iii) nematic (N_{21}) with $S_1 \leq S_2$.

with S_i being the scalar order parameter of the ith component, where the first component ("1") has the higher molecular weight (M_W). In our thermodynamic study[1] two kinds of transitions take place within mixtures of two components: (i) Nematic-to-Isotropic (NI) transition due to the thermal (thermotropic) effect, and (ii) N_{12} to N_{21} transition within the nematic phase due to the concentration (lyotropic) effect. In the later transition, where N_{21} converts to N_{12}, $S_1 = S_2$, and at this point a nematic mixture behaves like a single component system; the concentration corresponding to this transition is the critical concentration m_{1c} at which the NI transition temperature is an absolute minimum.[1]

At higher concentrations of the higher Mw (first) component ($m_1 > 0.5$) thermotropic and lyotropic effects[7, 8] cooperate and ensure that the higher Mw component controls the overall orientation of the system and becomes the dominant component. At low concentrations ($m_1 < m_{1c}$), on the other hand, lyotropic effects

are dominant and promote the lower Mw species to become the dominant component. In the intermediate regime, though, thermotropic and lyotropic effects compete and the dominant effect determines the dominant component; if temperature effects overcome dilution effects the high Mw component becomes dominant, otherwise the one with lower Mw becomes dominant. It will be demonstrated below that the dominant component of a binary mesogenic mixture follows closely the behavior of a single species mesophase under external flows, and that the slaved component adapts by displaying a rich set of orientation and ordering states, according to the prevailing dilution and temperature conditions.

Uniaxial extensional flow of carbonaceous mesophases is used for the formation of carbon fiber precursors and due to the molecular discotic shape and the uniaxial quadrupolar nature of the flow results in structures different than those observed in rod-like nematics. Figure 5-1 summarizes structural transformations of discotic mesogens under uniaxial extensional flow above the isotropic/nematic transition temperature T_{NI} (top) and below T_{NI} (bottom). The mesogenic discs are subjected to uniaxial extensional flow that contains a stretching axis (vertical) and a planar compression plane (horizontal plane). The ellipsoids represent[9] the nematic quadrupolar tensor order parameter **Q** plus the dyadic **I**/3. The full-line arrows are the flow deformations (axial stretching and planar compression), the dashed arrows denote the effect of flow on the quadrupolar tensor ellipsoids, and the double-line arrows denote the unique axis of the ellipsoids. Above T_{NI} extensional flow transforms the isotropic state into a paranematic uniaxial state through an axial compression of the tensor ellipsoid, with its unique axis along the vertical stretching direction. The stable state is a balance between compression flow effects and thermodynamic resistance along the stretching axis of the flow. Below T_{NI} extensional flow transforms the uniaxial nematic state into a biaxial nematic state through anisotropic compression and re-orients the director **n** towards the compression plane; the cross-section of the ellipsoid is subjected to a flow-compression along the stretching direction and hence there is a thermodynamic response along this direction. In this paper we seek to extend the basic understanding of these viscoelastic processes for a binary mixture, and determine if
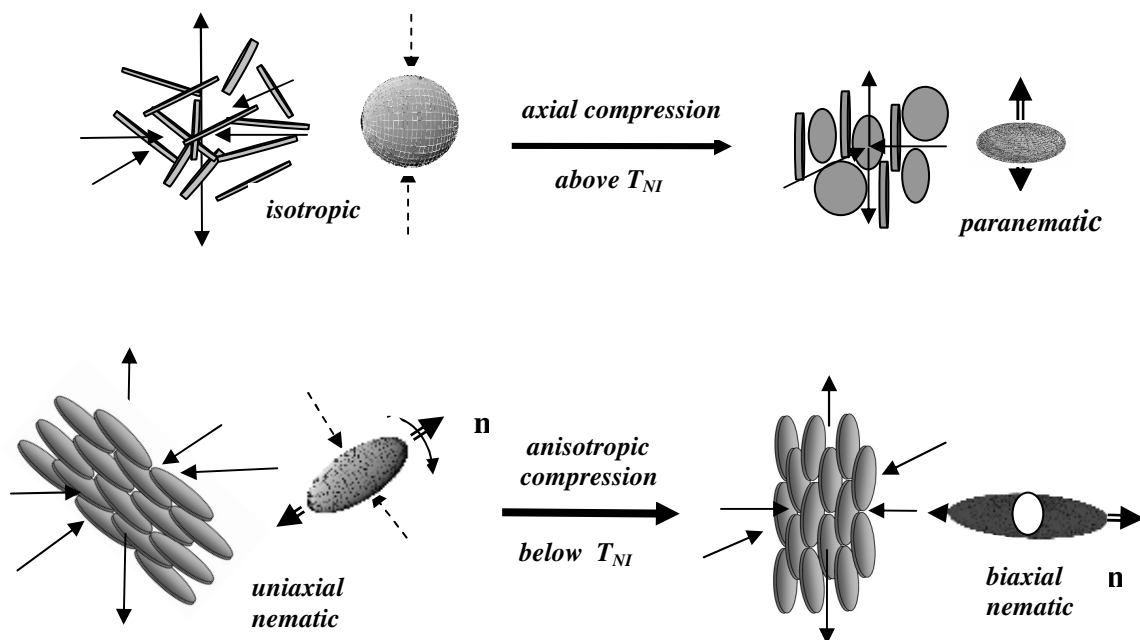
Figure 5-1. Schematic of structural transformation of single component discotic mesogens under a uniaxial extensional flow above the nematic/isotropic transition temperatute T_{NI} (top) and below T_{NI} (below). Above T_{NI} extensional flow transforms the isotropic state into a paranematic uniaxial state with its unique axis along the stretching direction. Below T_{NI} extensional flow transforms the uniaxial nematic state into a biaxial nematic state through anisotropic compression and re-orients the director n towards the compression plane. The full-line arrows are the flow deformations (axial stretching and planar compression), the dashed arrows denote the effect of flow on the quadrupolar tensor ellipsoids, and the double-line arrows denote the unique axis of the ellipsoids.

the basic structures (paranematic and biaxial nematic) are enriched through lyotropic effects and cross-couplings.

Integrating the thermodynamics with flow-induced orientation and flow-induced alignment in binary mixtures of CMs under uniaxial extensional flow merges the interplay between equilibrium uniaxial ordering and flow-induced biaxiality, which will be a function of the species molecular weight asymmetry (ΔMw), their interaction (β), and concentration (m_1). Macroscopic nematodynamics will predict flow induced orientation and flow induced alignment[9-12] accurately, but for binary mixtures the macroscopic material tensors that form part of the formulation will be given by unknown functions of the molecular parameters (ΔMw,β,m_1)[9, 13-16] and hence the most efficient way to include these important parameters is to use a molecular level description. For this purpose, the Maier-Saupe (MS) theory is

extended to incorporate the flow effects; in the presence of uniaxial extensional flow (a potential flow) both the flow potential and the molecular potential contribute to the total MS potential and make it appropriate to describe the non-equilibrium thermodynamics of different nematic liquid crystalline systems[1, 9, 17]. In this work we use the extended MS theory with the implemented flow effects to investigate the thermorheological phase diagram of the binary mixture (ordering and structuring as functions of temperature and Deborah number, *De*).

The specific objectives of this paper are: (i) to find, classify, characterize and explain the expected structural diversity that emerges in discotic mesogenic mixtures by regulating the thermotropic/lyotropic effects under a uniaxial quadrupolar extensional flow of varying strength; (ii) to present thermo-rheological phase diagrams that reveal localized structure formation through anisotropic viscoelasticity; (iii) to extend the basic understanding of flow induced structures shown in Figure 5-1 to mesogenic mixtures. Since uniaxial extensional flow of discs is equivalent to biaxial extensional flow of rods, the results of this work are applicable to these systems as well[18].

The organization of this paper is as follow. Section 5.3 presents the extended MS binary mixture model with the implemented uniaxial extensional flow obtained in our pervious work[9]; the numerical solution scheme is also defined in this section. Section 5.4 presents the results. Section 5.4.1 classifies the type of solutions obtained for the ordering and the structural behavior of the components within the mixture. Section 5.4.2 reports the orientational and structural behavior of the mixture under flow and the temperature effects. Section 5.4.3 presents the effect of concentration on the phase diagram. Section 5.5 presents the conclusions.

5.3 Maier-Saupe Binary Mixture Model

Details of the extension of Maier-Saupe model to a binary mixture of NLCs under the uniaxial extentional flow is given in our pervious studies[1, 2, 9]. The discotic nematic mixture is characterized by the usual quadrupolar tensor order parameters:[1]

$$\mathbf{Q}_i = S_i \left(\mathbf{n}_i \mathbf{n}_i - \mathbf{I}/3 \right) + \frac{P_i}{3} \left(\mathbf{m}_i \mathbf{m}_i - \mathbf{l}_i \mathbf{l}_i \right); i = 1, 2; \quad \mathbf{Q}_{mix} = \sum_{i=1} m_i \mathbf{Q}_i \qquad (5\text{-}1)$$

where (S_i, P_i) are the uniaxial and biaxial molecular order parameters, $(\mathbf{n}_i, \mathbf{m}_i, \mathbf{l}_i)$ are the directors, m_i are the species' mole fractions and $\mathbf{Q}_{mix}$ is the quadrupolar order parameter of the mixture. In this paper the biaxial directors $\mathbf{l}_i$ are along the extensional flow direction ("z") and the directors $\mathbf{n}_i, \mathbf{m}_i$ are always in the compression plane ("x-y"). The rate of deformation tensor $\mathbf{A}$ for uniaxial extensional flow and corresponding $\mathbf{Q}_i$ are:

$$\mathbf{A} = \begin{bmatrix} -\dot{\varepsilon}/2 & 0 & 0 \\ 0 & -\dot{\varepsilon}/2 & 0 \\ 0 & 0 & \dot{\varepsilon} \end{bmatrix}, \quad \mathbf{Q}_i = \begin{bmatrix} \mu_{in} & 0 & 0 \\ 0 & \mu_{im} & 0 \\ 0 & 0 & \mu_{il} \end{bmatrix} \tag{5-2}$$

with $\dot{\varepsilon}$ being the rate of deformation and μ_i s the eigenvalues of the tensor order parameter $\mathbf{Q}_i$. Equations (5.2) indicate the correspondence between stretching direction/compression plane and orientation. For this particular flow and mixture it has been shown that the two director triads are congruent[9] and hence only equations for the scalar order parameters S_i, P_i are needed. The governing equations for the scalar order parameters S_1, S_2, P_1, P_2 are[1]:

$$m_1\varphi_1 S_1 + \sqrt{m_1\varphi_1 m_2\varphi_2}\, L_1 S_2 - T_r \sum \frac{m_i}{Z_i}\frac{\partial Z_i}{\partial S_1} = 0$$

$$m_2\varphi_2 L_2 S_2 + \sqrt{m_1\varphi_1 m_2\varphi_2}\, L_1 S_1 - T_r \sum \frac{m_i}{Z_i}\frac{\partial Z_i}{\partial S_2} = 0$$

$$\frac{1}{3}m_1\varphi_1 P_1 + \sqrt{m_1\varphi_1 m_2\varphi_2}\, L_1 \frac{P_2}{3} - T_r \sum \frac{m_i}{Z_i}\frac{\partial Z_i}{\partial P_1} = 0 \tag{5-3}$$

$$\frac{1}{3}m_2\varphi_2 L_2 P_2 + \sqrt{m_1\varphi_1 m_2\varphi_2}\, L_1 \frac{P_1}{3} - T_r \sum \frac{m_i}{Z_i}\frac{\partial Z_i}{\partial P_2} = 0$$

where $\varphi_i = \dfrac{m_i Mw_i}{\sum m_i Mw_i}$ is the effective mole fraction of the ith component, T_r is the dimensionless temperature, L_1 and L_2 are the material parameters give by the following expressions:

$$L_1 = \frac{\overline{U}_{12}}{\overline{U}_{11}}; \quad L_2 = \frac{\overline{U}_{22}}{\overline{U}_{11}}; \quad L_1 = \beta L_2 \tag{5-4}$$

where $\bar{U}_{11}, \bar{U}_{22}$ and $\bar{U}_{12}$ are the interaction parameters between the pair of (1,1), (2,2) and (1,2) molecules, β is the interaction coefficient and is positive for mixtures of similar molecules (disk/disk); in this study we fix β as 0.1 and $Z_{i,}$ is the partition function of the ith component given by the following expression[10]:

$$Z_i = \left(\int e^{-\Phi_i/m_i k_B T - H_i/k_B T} d\mathbf{u}_i \right) \tag{5-5}$$

with Φ_i being the molecular potential of the ith component given by the following expressions:

$$\frac{\Phi_1}{m_1 k_B T} = -\frac{1}{m_1 T_r} \frac{3}{2} \left(\begin{array}{l} m_1 \varphi_1 \left(S_1 (Cos^2\theta - \frac{1}{3}) + \frac{P_1}{3} Sin^2\theta \left(Sin^2\mu - Cos^2\mu \right) \right) \\ + \sqrt{m_1 \varphi_1 m_2 \varphi_2} L_1 \left(S_2 (Cos^2\theta - \frac{1}{3}) + \frac{P_2}{3} Sin^2\theta \left(Sin^2\mu - Cos^2\mu \right) \right) \end{array} \right)$$

$$\frac{\Phi_2}{m_2 kT} = -\frac{1}{m_2 T_r} \frac{3}{2} \left(\begin{array}{l} m_2 \varphi_2 L_2 \left(S_2 (Cos^2\theta - \frac{1}{3}) + \frac{P_2}{3} Sin^2\theta \left(Sin^2\mu - Cos^2\mu \right) \right) \\ + \sqrt{m_1 \varphi_1 m_2 \varphi_2} L_1 \left(S_1 (Cos^2\theta - \frac{1}{3}) + \frac{P_1}{3} Sin^2\theta \left(Sin^2\mu - Cos^2\mu \right) \right) \end{array} \right)$$

$$\tag{5-6}$$

where θ and μ are the polar and azhimutal angles in the director **n-m-l** triad system and H_i the flow potential of the ith component :

$$\frac{H_i}{k_B T} = -\frac{3\dot{\varepsilon}}{4} De \left(\mathbf{u}.\mathbf{e_z} \right)^2 R f \left(S_1, S_2, P_1, P_2, m_1, m_2, Mw_1, Mw_2 \right)$$

$$\tag{5-7}$$

where **u** is the molecular unit normal, $\mathbf{e_z}$ is the flow (extension) direction, R is the rheological effective shape factor and f is a complex function of ordering, molecular weight and concentration of the components given in [9] . The Deborah number De appearing in eqn.(5.7) is :

$$De = \frac{\dot{\varepsilon}}{D_{ref}} \tag{5-8}$$

where $\dot{\varepsilon}$ is the steady rate of uniaxial extension rate, D_{ref} is the rotational diffusivity of the discotic higher molecular weight component at a reference temperature[9]. To approximate the present model to real CMs we take the Mw of

the first and the second species to be 1400 and 1000, respectively[1, 9, 19]. The interaction parameter β is also fixed as 0.1[1].

The present model is given by the four nonlinear integral equations (eqns.(5.3)); the solution vector consists of four scalar order parameters (S_1, S_2, P_1, P_2). The relative thermo-rheological effects are calibrated as follows: (i) the flow effect is modified by changing the De number, (ii) the phase ordering is affected by sweeping over temperature T_r and (iii) the extent of mutual coupling by sweeping over concentration of the first component, m_1. The equations are solved using the Newton-Raphson method, with an eight order Simpson integration method. Stability, accuracy, and convergence were ensured using standard methods. Issues of multistability and bifurcations are not considered in this paper. Numerical accuracy was established using the known pure component limits[1]. Next we present the possible ordering states (Fig. 5-2, 5-3) based on the system phase space that is needed to classify the solutions (see Tables 5-1, 5-2).

We use the results given by eqns. (5.3) to construct an atlas of ordering states in the scalar order parameter P-S triangle, similar to the one reported by [18, 20]. The phase space given in Fig. 5-2 is used to describe the ordering behavior of each component in the mixture, to define the nomenclature of various steady state solutions presented in the next section, and to indicate the sign of the corresponding eigenvalues[9]. The unit sphere description of the director triad (**n**, **m**, **l**) in this figure is used to explain the alignment characteristics at different limiting points on the alignment phase plane. The dashed lines denote the uniaxial states and it starts at a corner with perfect ordering along one of the eigenvectors (**n,m,l**) and ends with a planar state at the midpoint of each triangle side. The table indicates transitions and regions defined in Fig. 5-3. Changes in temperature or extension rate define a trajectory in this phase space that may cross the transition lines (α, γ, ξ). Figure 5-3 shows the orientation of the discotic molecules with respect to the dominant director of the system (**n**) (5-3a) and the biaxial directors (**m** and **l**) and the corresponding eigenvalues of the tensor order parameters of the first and second component ($\mathbf{Q}_1$ and $\mathbf{Q}_2$) for the uniaxial (Fig. 5-3b), degenerated uniaxial (Fig. 5-3c) and biaxial (Fig. 5-3d) states; as noted above **l** is along the extension direction
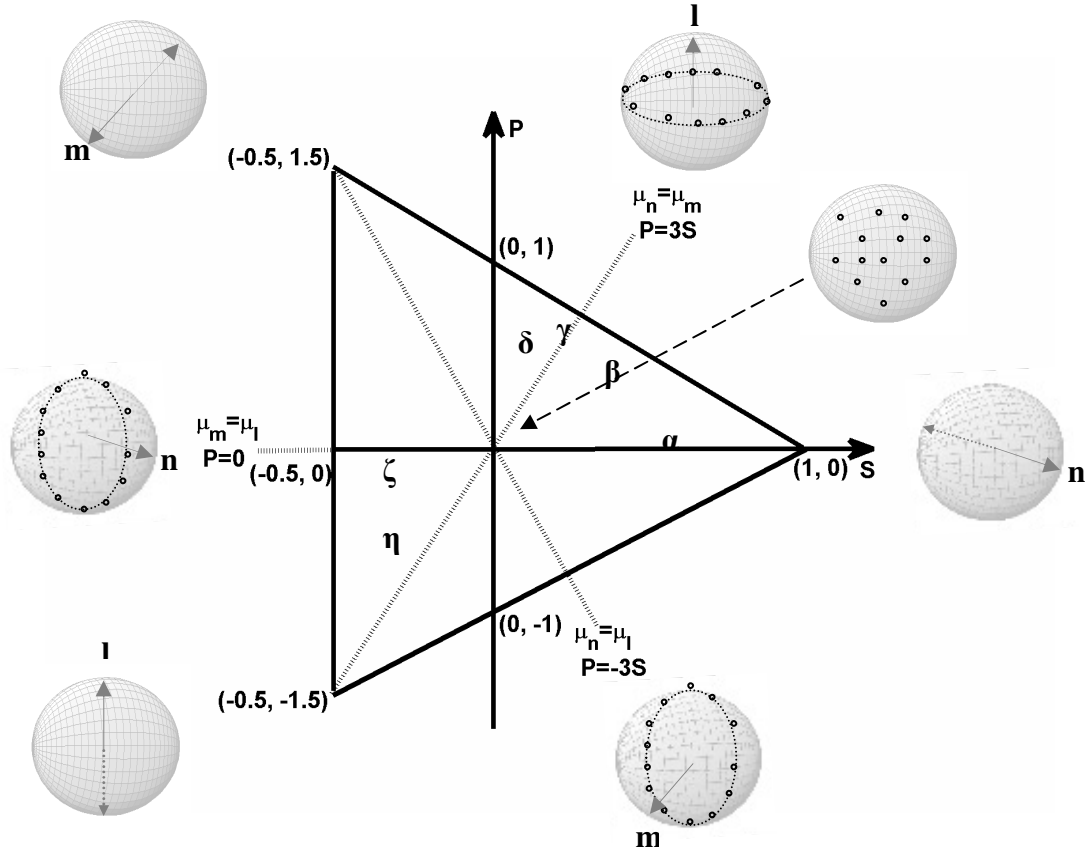
$$\begin{cases} \text{Line } \alpha: & \mu_n > \mu_l = \mu_m, \quad N_U^+, PN_U^+ \\ \text{Region } \beta: & \mu_n \rangle \mu_m \rangle \mu_l, \quad\quad N_B^+, PN_B^+ \\ \text{Line } \gamma: & \mu_l < \mu_n = \mu_m, \quad PN_{U\parallel}^- \\ \text{Region } \delta: & \mu_l < \mu_m < \mu_n, \quad PN_{B\parallel}^- \\ \text{Line } \xi: & \mu_n < \mu_l = \mu_m, \quad PN_U^-, N_U^- \\ \text{Region } \eta: & \mu_l \rangle \mu_m \rangle \mu_n \ N_B^-, \quad PN_{B\perp}^- \end{cases}$$

Figure 5- 2. Atlas of the orientation in terms of the scalar order parameters *S* and *P* and their corresponding eigenvalues, adapted from [9, 18]. The unit sphere description of the director triad (n, m, l) is used to explain the alignment characteristics at different limiting points on the alignment phase plane. The dashed lines denote uniaxial states. Changing the temperature and/or extensional flow rate produces a trajectory in the (*S, P*) phase plane, usually across the biaxial regions. Under continuous increase in temperature, the change from uniaxial to biaxial state takes place by moving from the *P=0* line across the upper biaxial region to end up in the *P=3S* uniaxial line. The table summarizes the transition lines, regions, and orientation states given in terms of eigenvalues. See   figure (5-4) for terminology of the various nematic (N) and paranematic (PN) states.

(b) Uniaxial: $\mu_n > \mu_m = \mu_l$

Prolate

extension direction

(c) Biaxial: $\mu_n > \mu_m > \mu_l$

Scalane P

(a)

(d) Biaxial: $\mu_n = \mu_m > \mu_l$
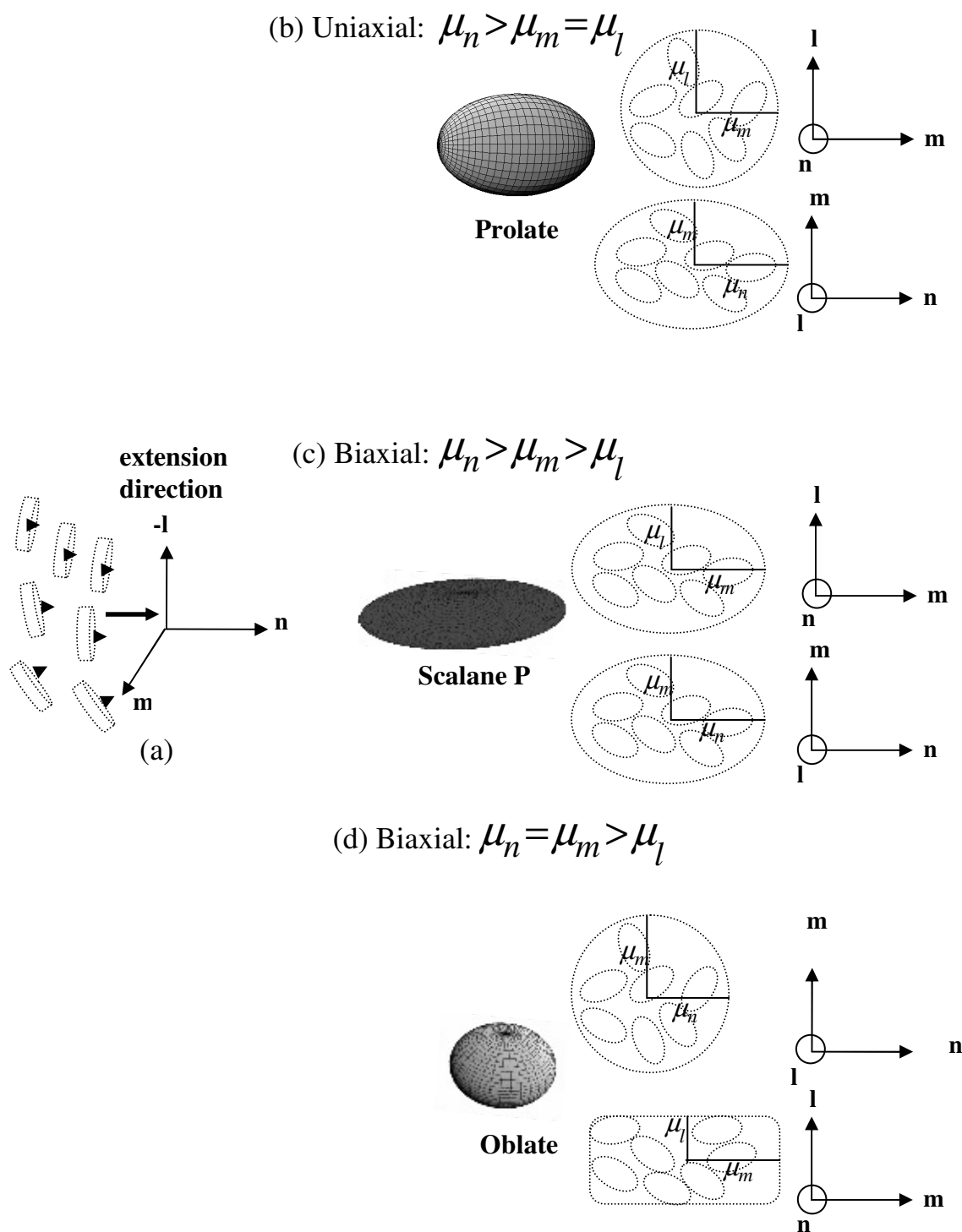
Oblate

Figure 5- 3. Orientation of discotic molecules with respect to the dominant director of the system (n) (a) and the biaxial directors (m and l) for the uniaxial, prolate (b), degenerated uniaxial, oblate (c) and biaxial, scalene P (d) cases. In the uniaxial case, the projection of the orientation distribution of the molecules on m-l plane is a circle with two identical eigenvalues. On the other hand in the biaxial case, the projection of the orientation distribution of the molecules on m-l plane is an ellipsoid (or an ellipsoid with corners) with two distinct eigenvalues.

141
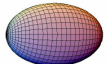
and **n-m** are anywhere in the compression plane. In Fig.5-3b the uniaxial case, the orientation distribution of the molecules in **m-l** plane (perpendicular to the dominant director) is isotropic and the projection of the oriented discs on **m-l** plane is a circle with two identical eigenvalues. On the other hand in Fig.5-3c a degenerate case, the orientation distribution of the molecules is isotropic in **n-m** plane but it composes a shape similar to an ellipsoid with the added corners in **m-l** plane; this generates a result similar to the occurrence of compression in the flow (**l**) direction. In Fig. 5-3d biaxial case, the orientation distribution of the molecules in **m-l** plane is anisotropic and the projection of the oriented discs on **m-l** plane is an ellipsoid with two distinct eigenvalues. Other structures are also made based on the eigenvalues in the three directions.
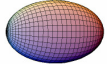
5.4 Results and Discussion

5.4.1 Solution Classification

Table 5-1 presents the ten steady state solutions to equations (5.3) using the sign and the ordering of the eigenvalues of tensor order parameters ($\mathbf{Q}_1$ and $\mathbf{Q}_2$) of the components #1 and #2 and the orientation of the dominant eigenvector with respect to the extension direction[9]. Although stability was not investigated, the correspondence of these solutions with the well-known stable solutions to the single component case provides indirect evidence of their stability.

Table 5- 1. Solution Classification

Solution symbol	Solution symmetry	Sign of $\mu_n = 2S/3$	Sign of $\mu_m = (P-S)/3$	Sign of $\mu_l = -(P+S)/3$	Eigenvalues ordering	Corresponding structures
N_U^+	*Uniaxial Nematic*	+	-	-	$\mu_n > \mu_l = \mu_m$	Prolate $\perp$
N_U^-	*Uniaxial Nematic*	-	+	+	$\mu_n < \mu_l = \mu_m$	Oblate $\perp$

Symbol	Name				Ordering	Visualization
N_B^+	*Biaxial Nematic*	+	-	-	$\mu_n \rangle \mu_m \rangle \mu_l$	ScaleneP ⊥
N_B^-	*Biaxial Nematic*	-	+	+	$\mu_l \rangle \mu_m \rangle \mu_n$	ScaleneO ⊥
PN_B^+	*Biaxial Nematic*	+	-	-	$\mu_n \rangle \mu_m \rangle \mu_l$	ScaleneP ⊥
PN_U^+	*Uniaxial Paranematic*	+	-	-	$\mu_n > \mu_l = \mu_m$	Prolate ⊥
$PN_{U\perp}^-$	*Uniaxial Nematic*	-	+	+	$\mu_n < \mu_l = \mu_m$	Oblate ⊥
$PN_{U\parallel}^-$	*Uniaxial Paranematic*	+	+	-	$\mu_l < \mu_n = \mu_m$	Oblate ‖
$PN_{B\perp}^-$	*Biaxial Nematic*	-	+	+	$\mu_l \rangle \mu_m \rangle \mu_n$	ScaleneO ⊥
$PN_{B\parallel}^-$	*Biaxial Paranematic*	+	-	-	$\mu_l < \mu_m < \mu_n$	ScaleneO ‖

The first two columns of Table 5-1 give the symbols and names of the solution, the 3th-5th column give the sign of the three eignevalues, the 6th the ordering, and the 7th the visualization of the tensor ellipsoid using the usual **Q+I/3**   unit trace quadrupolar tensor[9] (see figures (5-2) and (5-3)); the symbols ⊥,‖ denote

perpendicular or parallel alignment of the unique axis of the tensor order parameter ellipsoid or the axis which corresponds to the eigenvalue with the largest absolute value with respect to the extension axis, which is always along the **l** eigenvector. These ten solutions are

N_U^+ : *Uniaxial Nematic with* $\mu_n > \mu_l = \mu_m$

N_U^- : *Uniaxial Nematic with* $\mu_n < \mu_l = \mu_m$

N_B^+ : *Biaxial Nematic with* $\mu_n \rangle \mu_m \rangle \mu_l$

N_B^- : *Biaxial Nematic with* $\mu_l \rangle \mu_m \rangle \mu_n$

PN_B^+ : *Biaxial Nematic with* $\mu_n \rangle \mu_m \rangle \mu_l$

PN_U^+ : *Uniaxial Paranematic with* $\mu_n > \mu_l = \mu_m$

$PN_{U\perp}^-$: *Uniaxial Paranematic with* $\mu_n < \mu_l = \mu_m$

$PN_{U\|}^-$: *Uniaxial Paranematic with* $\mu_l < \mu_n = \mu_m$

$PN_{B\perp}^-$: *Biaxial Paranematic with* $\mu_l \rangle \mu_m \rangle \mu_n$

$PN_{B\|}^-$: *Biaxial Paranematic with* $\mu_l < \mu_m < \mu_n$

where the superscripts refer to the sign of the largest absolute eigenvalue and the subscripts refer to the state (*U*: uniaxial, *B*: biaxial). If there are two identical eigenvalues the state is uniaxial, otherwise it is biaxial. The corresponding ellipsoidal structures are prolate, oblate and scalene. It is seen from Table 5-1 that sweeping over temperature and concentration, leads to trajectories that sample regions β, δ, and η in Fig.5-2.

5.4.2 Orientational and Structural Behavior

Figure (5-4) shows a schematic of the generic phase diagram of the binary system by solving eqn. (5.3) and by sweeping over *De*, *T* and m_1. The phase diagram contains twelve regions separated by four distinct transition lines. Each region is characterized by a phase and a structural state of the two components. Table 5-2 summarizes the salient characteristics of each region.
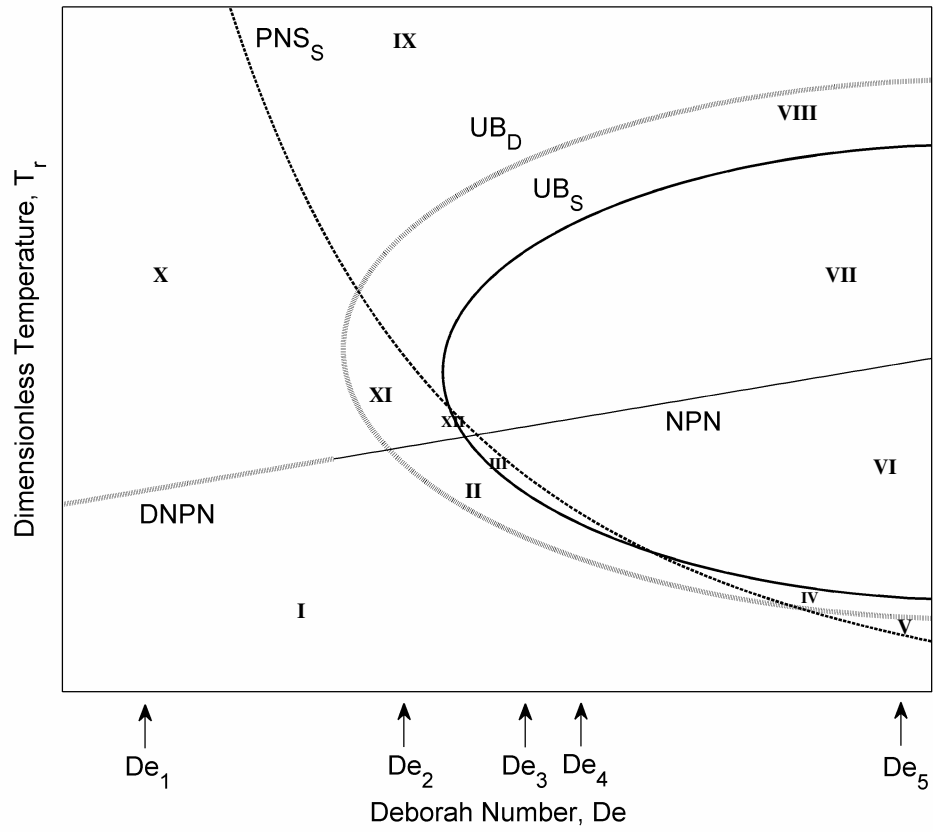
Figure 5- 4.Schematic of a generic thermo-rheological phase diagram of the binary mixture in terms of dimensionless temperature T_r and Deborah De number. The phase diagram is divided into twelve regions by four transition lines ($DNPN\text{-}NPN$, UB_D, UB_S and PNS_S); the state of each species (see Table 5-2) is defined by the Q+I/3 tensor ellipsoid. The behavior of the mixture is explained at the De numbers indicated on the x-axis of the figure.

Table 5- 2. Characteristics of the Regions of Phase Diagram

Region	Solution Symbol of the Dominant Component	Solution Symbol of the Slaved Component	Corresponding Transition Lines
I	N_U^+ Prolate $\perp$	N_U^+ Prolate $\perp$	NPN, UB_D & PNS_S
II	N_B^+ ScaleneP $\perp$	N_U^+ Prolate $\perp$	UB_D, NPN, UB_S & PNS_S
III	N_B^+ ScaleneP $\perp$	N_B^+ ScaleneP $\perp$	UB_S, NPN & PNS_S
IV	N_B^+ ScaleneP $\perp$	N_U^- Oblate $\perp$	PNS_S, UB_S & UB_D
V	N_U^+ Prolate $\perp$	N_U^- Oblate $\perp$	PNS_S & UB_D
VI	N_B^+ ScaleneP $\perp$	N_B^- ScaleneO $\perp$	PN_S, NPN & UB_S
VII	PN_B^+ ScaleneP $\perp$	$PN_{B\perp}^-$ ScaleneO $\perp$	PNS_S, UB_S & NPN

VIII	PN_B^+ *ScaleneP* $\perp$	$PN_{U\perp}^-$ *Oblate* $\perp$	$PNS_S,\ UB_D\ \&$ UB_S
IX	PN_U^+ *Prolate* $\perp$	$PN_{U\perp}^-$ *Oblate* $\perp$	$PNS_S,\ \&\ UB_D$
X	$PN_{U\parallel}^-$ *Oblate* $\parallel$	PN_U^+ *Prolate* $\perp$	$NPN,\ UB_D\ \&$ PNS_S
XI	$PN_{B\parallel}^-$ *ScalaneO* $\parallel$	PN_U^+ *Prolate* $\perp$	$UB_D,\ PNS_S,$ $NPN\ \&\ UB_S$
XII	PN_B^+ *ScalaneP* $\perp$	PN_B^+ *ScalaneP* $\perp$	$UB_S,\ NPN\ \&$ PNS_S

The first column of Table 5-2 gives the numbers associated with each region, the 2nd and 3rd columns give the names of the solution and the corresponding ellipsoidal structures and the 4th column gives the transition lines which marks the basin of each region. These transition lines are:

$(1, 2)$ UB_D, UB_S : uniaxial-biaxial transition lines (of the dominant and slaved components) which are structural (uniaxial vs. biaxial) transition lines;

(3) *DNPN-NPN* : discontinuous-continuous Nematic-Paranematic transition line which is a phase transition line;

(4) PNS_S : positive to negative ordering transition line of the slaved component which is a structure transition line.

The *DNPN-NPN* line which separates nematic from paranematic phase is the phase transition line; in the first section (lower *De* numbers) a discontinuous transition takes place, however in the second section (higher *De* numbers) a continuous transition takes place. The remaining three lines are structural transition lines which define the formation/disappearance of biaxiality in the dominant (UB_D uniaxial-biaxial transition in the dominant component) and slaved (UB_S uniaxial-biaxial transition in the slaved component) components and the formation of the degenerated phase with a negative ordering in the slaved component (PNS_S: positive to negative ordering transition in the slaved component).

We study the phase diagram at five fixed different *De* numbers and increase T, and observe the following transformations (see schematic in Fig. 5-4):

(i) By increasing temperature at $De=De_1$ region *I* and region *X* emerge. In region *I*, the stable phases are uniaxial nematic, N_U^+, for both components, meaning that the scalar order parameters are positive and the biaxial order parameters are negligible. For each component, there are two identical eigenvalues, $\mu_n > \mu_l = \mu_m$, and the unique value, μ_n, is positive. Hence, the corresponding structures are both prolate $\perp$. By increasing temperature at this *De*, the nematic to paranematic phase transition takes place and region *X* is reached. This region is paranematic which is obtained by subjecting the isotropic phase to a uniaxial extension. In region *X* the stable phases are both uniaxial paranematic with positive scalar order parameters and negligible biaxiality. The stable phase is $PN_{U\|D}^-$ for the dominant component with two identical eigenvalues, $\mu_{lD} < \mu_{nD} = \mu_{mD}$, composing a parallel oblate. For the slaved component however, the stable phase is PN_{US}^+ again with two identical egienvalues, but this time $\mu_{nS} > \mu_{lS} = \mu_{mS}$, resulting in a perpendicular prolate. At sufficiently low *De*, hence the main effect of temperature is:

prolate/prolate nematic state →oblate/prolate paranematic state

(ii) By increasing the dimensionless temperature at $De=De_2$ five regions *I*, *II*, *XI*, *VIII* and *IX* appear. In region *I*, like the pervious case, the stable phases are both uniaxial nematic, N_U^+, and the corresponding structures are both prolate $\perp$. By

increasing temperature at this *De*, a transition within the nematic phase takes place and region *II* is reached. In region *II* the stable phase for the dominant component is biaxial nemtaic, N_{BD}^+, its scalar order parameter is positive and its biaxiality is significant. There are three distinct eigenvalues, $\mu_{nD} \rangle \mu_{mD} \rangle \mu_{lD}$ with μ_{nD} being positive and the largest value; the corresponding structure is scalene P$\perp$. For the slaved component, however, the stable phase is still uniaxial nematic, N_{US}^+, with a perpendicular prolate structure. By further increasing the temperature, a nematic-to-paranematic transition takes place and region *XI* emerges. In region *XI* the stable phase for the dominant component is biaxial paranematic, $PN_{B\|D}^-$, its scalar order parameter is positive and its biaxiality is significant. There are three distinct eigenvalues, $\mu_{nD} > \mu_{mD} > \mu_{lD}$ with μ_{lD} being negative and of largest value, and the corresponding structure is the parallel scalene O. For the slaved component, however, the phase is uniaxial paranematic, PN_{US}^+, with two identical eigenvalues, $\mu_{nS} > \mu_{lS} = \mu_{mS}$, denoting a prolate $\perp$. By increasing temperature in the paranematic phase at this *De* a continuous transition within the paranematic phase takes place and region *VIII* is reached. In region *VIII* the stable phase for the dominant component is biaxial paranematic, PN_{BD}^+, its scalar order parameter is positive and its biaxiality is significant. There are three distinct eigenvalues, $\mu_{nD} > \mu_{mD} > \mu_{lD}$ with μ_{nD} being positive and of largest value, and the corresponding structure is the scaleneP$\perp$. For the slaved component, however, the phase is uniaxial paranematic, $PN_{U\perp S}^-$, with two identical eigenvalues, $\mu_{nS} < \mu_{lS} = \mu_{mS}$, and a negative scalar order parameter denoting an oblate$\perp$. By increasing temperature even more, region *IX* is reached. The stable phases in this region are PN_{UD}^+ for the dominant component and $PN_{U\perp S}^-$ for the slaved component and the corresponding structures are prolate$\perp$ and oblate$\perp$ respectively. Hence at this *De*, the effect of temperature is not only to transform nematic state into the paranematic state but it is also to induce biaxiality in the dominant component and a degenerated phase (negative ordering /oblate structure) in the slaved component.

(iii) By increasing the dimensionless temperature at $De=De_3$ seven regions *I*, *II*, *III*, *XII*, *VII*, *VIII* and *IX* appear. The new regions appearing here are regions *III* and *XII*. In region *III* the stable phases for both of the components are biaxial nemtaics, N_B^+, and the corresponding structures are scalene P$\perp$. In region *XII*, similar to region *III*, the structures are scalene P$\perp$ but the stable phases are biaxial paranematics, PN_B^+. A temperature increase transforms the nematic phase in region *III* to the paranematic phase in region *XII*. The overall effect of increasing temperature increase at this *De* is the following sequence:

inducing biaxiality in the dominant component $\rightarrow$ *inducing biaxiality in the slaved component* $\rightarrow$ *transforming the nematic phase to the paranematic phase* $\rightarrow$ *forming the degenerated phase (negative ordering) in the slaved component* $\rightarrow$ *reconverting the slaved and then dominant component to the uniaxial structure*

(iv) By increasing the dimensionless temperature at $De=De_4$ seven regions *I*, *II*, *III*, *VI*, *VII*, *VIII* and *IX* appear. The new region appearing in this case is region *VI*. In this region the stable phase for the dominant component is biaxial nemtaic, N_{BD}^+, and its corresponding structure is scaleneP$\perp$. For the slaved component, the stable phase is biaxial nemtic, N_{BS}^-, with negative scalar order parameter, $\mu_{lS}\rangle\mu_{mS}\rangle\mu_{nS}$, which denote a scalaneO$\perp$. So the overall effect of the temperature increase at this *De* is:

inducing biaxiality in the dominant component $\rightarrow$ *inducing biaxiality in the slaved component* $\rightarrow$ *forming the degenerated phase (negative ordering) in the slaved component* $\rightarrow$ *transforming the nematic phase to the paranematic phase* $\rightarrow$ *reconverting the slaved and then dominant component to the uniaxial structure*

(v) By increasing the dimensionless temperature at $De=De_5$ seven regions *I*, *V*, *IV*, *VI*, *VII*, *VIII* and *IX* appear. The new region appearing in this case is region *V*. In this region the stable phase for the dominant component is uniaxial nematic, N_{UD}^+, and its corresponding structure is Prolate$\perp$. For the slaved component, the stable phase is uniaxial nematic, N_{US}^-, with negative scalar order parameter,

$\mu_{nS} < \mu_{lS} = \mu_{mS}$, which denote an oblate $\perp$. So the overall effect of the temperature increase at this *De* is:

forming the degenerated phase (negative ordering) in the slaved component $\rightarrow$ *inducing biaxiality in the dominant component* $\rightarrow$ *inducing biaxiality in the slaved component* $\rightarrow$ *transforming the nematic phase to the paranematic phase* $\rightarrow$ *reconverting the slaved and then dominant component to the uniaxial structure.*

To better understand the phase and structural behavior of our discotic mixture we also report the computed orientational behavior and the phase diagram (Figure 5-5) of the pure system reproduced in our previous work[9].
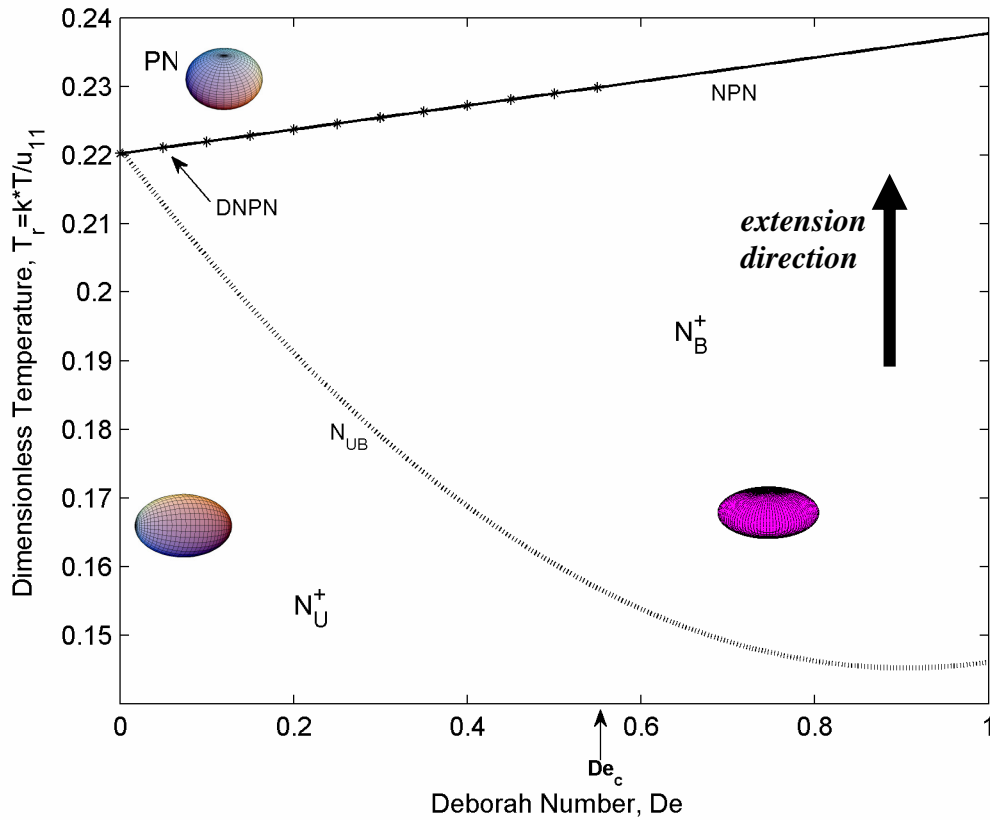
Figure 5- 5.Thermo-rheological phase diagram of a single discotic nematogen with its corresponding orientational/order parameter structures: N_U^+ **at low temperatures,** N_B^+ **at medium temperatures and *De* numbers and** PN_B^- **at high temperatures adapted from [9]. Comparing Figs. (5-4) and (5-5) we see that the dominant component follows essentially the pure species response but that other component exhibits starkly new behavior.**

The phase diagram (Figure 5-5) of a pure mesogen has three regions: (i) uniaxial nematic (N_U^+), (ii) biaxial nematic (N_B^+) and (iii) uniaxial paranematic $\left(PN_U^-\right)$. There are two dominant transition lines: N_{UB}, and *DNPN-NPN*; these two transition lines emerge at $T_r \simeq 0.22$, *De=0*. (i) N_{UB} (dashed line) is the continuous uniaxial nematic(N_U^+)/biaxial nematic(N_B^+) transition , and (ii) *DNPN-NPN* (dotted line) is the nematic biaxial(N_B^+) /uniaxial paranematic (PN_U^+) transition; for $0 < De < De_c \simeq 0.55$ the transition is discontinuous and when $De > De_c = 0.55$ the transition is continuous. At low temperatures (region N_U^+) there is thermodynamic and flow cooperation. Thermodynamics favors the uniaxial orientation N_U^+ while extensional flow also favors orientation along **n** with **n** along the compression plane and hence there is no competing effect. At higher temperatures and higher *De*, the thermodynamic uniaxial alignment along **n** now competes with the biaxial flow alignment producing the biaxial nematic state (region N_B^+) with **n** along the compression plane. Further temperature increase eventually leads to the biaxial nematic/ uniaxial paranematic transition. In the paranematic state (region PN_B^-) the oblate state has the unique axis (**l** vector) along the extension direction; here the competition of thermodynamics that prefers an isotropic state and the flow effect that seeks molecular alignment along the compression plane results in the oblate state. Referring to figure (5-2) it is observed that the responses of the pure system to extensional flow are always along the line α, in the region β or along the line γ of the P-S triangle. Below we refer to a component of a mixture that closely follows the pure species as "dominant" and the other as "slaved", as explained in what follows.

Comparing Figs. (5-4) and (5-5) it follows that the dominant component in the binary mixture essentially follows the standard behavior of the pure mesophase with a small perturbation, which is the formation of the biaxial paranematic ($PN_{B\|D}^-$, region *XI*) and uniaxial paranematic (PN_{UD}^+, region *IX*), region . Hence, it shows the additional responses in the region δ of the P-S triangle (figure (5-2)). The slaved component, however behaves starkly differently. Although at low

temperatures and low *De* values it shows the standard phase state which is uniaxial nematic N_{US}^+, at moderate and high temperatures and also at high *De* values (regions *IV* to *XII)* it adopts different orientational and structural states. Extension affects the molecules of the second (slaved) component differently. For instance, in region *X*, flow tends to align the molecules of the dominant species in the compression (**n-m**) plane to form a parallel oblate but it aligns the molecules of the slaved component in a prolate ⊥ structure. Hence, the slaved component responses to the flow with the structures along the line α, in the region β, along the line ζ or in the region η of the P-S triangle (figure (5-2)). This phenomenon is due to the coupled viscoelastic forces generated within the mixture, as illustrated in figure (5-6) (adapted from [9]). Figure 5-6 shows an input (temperature (*T*), Deborah number (*De*))-output (tensor order parameters $\mathbf{Q}_D$, $\mathbf{Q}_S$, $\mathbf{Q}_{mix}$) model of the mixture's nemato-rheology. The viscoelastic coupling VE indicates how the nematodyanmics of the dominant and slaved components are mutually affected by viscoelastic (*VE*) effects. In the following we concentrate on elastic (*E*) effects since they explain the observed results in the phase diagram.
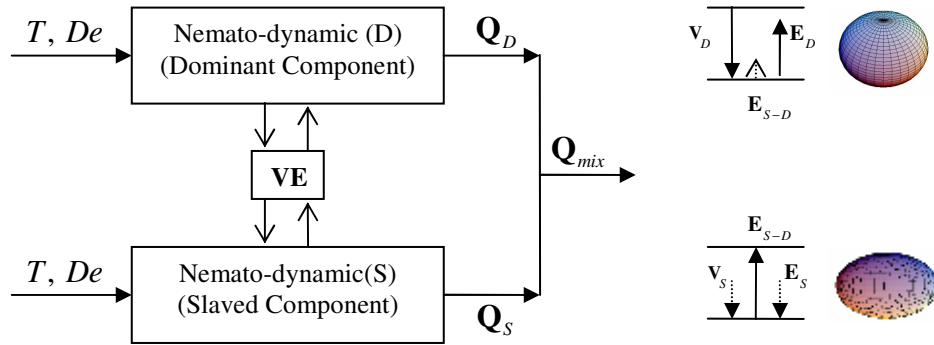
Figure 5- 6. Block diagram of coupled nematodynamics adopted from [9]. The thermorheological input (*T, De*) results in a tensor order parameter output (Q₁, Q₂, Qmix) under action of the nematodynamics and viescoleastic (*VE*) coupling effects. The model is used to explain the deviations of the slaved species from the standard behavior (Fig.(5-5)); see upper and lower right schematics. In region *X*, the dominant component adopts the usual oblate ‖ state (upper schematic) under the balance between viscous (V_D) and thermodynamic (E_D) and weak coupling ($E_{S\text{-}D}$ effects. The slaved component meanwhile adopts a prolate ⊥ state under viscous (V_S), thermodynamic (E_S) and strong coupling ($E_{D\text{-}S}$). See text for details.

To explain the complex structures found in Region X (oblate parallel for the dominant component and prolate perpendicular for the slaved one) we need to consider two factors: (i) the combination of the molecular weight asymmetry ΔMw and dilution effects lead to asymmetric coupling effects, such that the influence of the dominant component on the slaved one is significant while the converse effect is much weaker. The result of lyothropic-thermotropic cooperation/competition singles out the dominant that behaves essentially as the pure mesogen and delegates the other component to the slaved state. Figure (5-7) shows an schematic of the

C: Lyotropic-
Thermotropic
Cooperation

m_{1c}

B: Lyotropic-
Thermotropic
Competition

A: Lyotropic
Dominancy

Mole Fraction of the First Component, m_1

Molecular Weight Asymmetry, ΔM_w
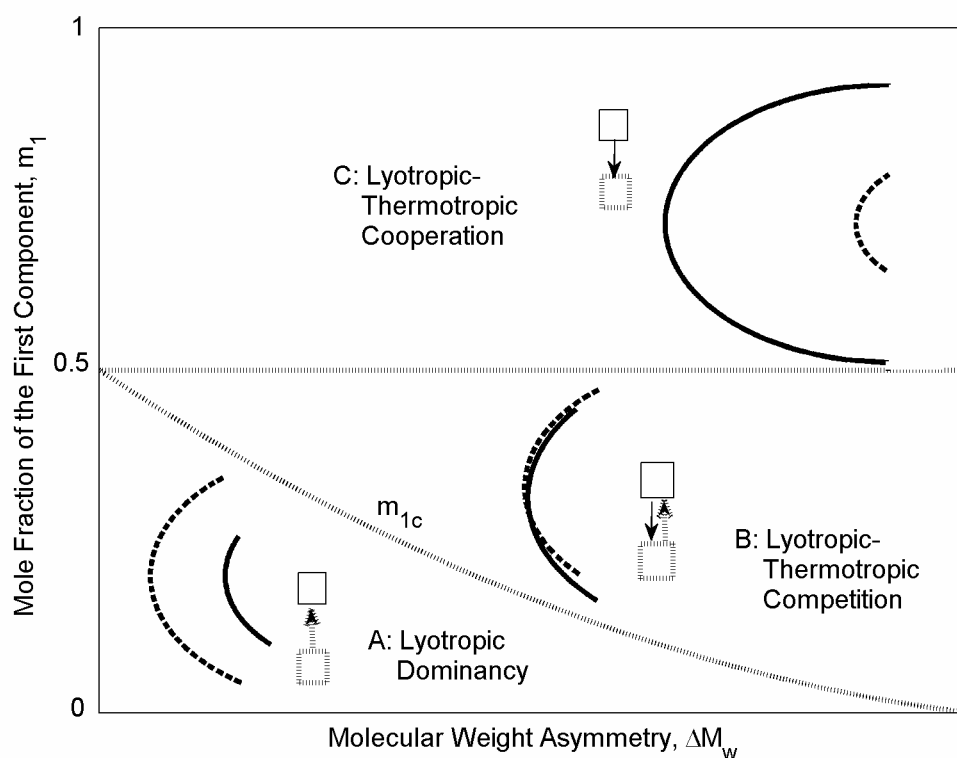
Figure 5- 7. Schematic of thermotropic and lyotropic effects on the dominant and slaved components in terms of concentration m_1 and molecular weight asymmetry ΔMw. The arrows connecting the boxes denote the coupling effects between the individual nematodynamics (square boxes). The full and dashed lines represent the typical biaxiality regions for the higher Mw (first) and lower Mw (second) components respectively. The plot has three regions. In region C ($m_1>0.5$) thermotropic and lyotropic effects cooperate and make the higher Mw component controls the overall orientation of the system and it becomes the dominant (master) component. In region A ($0<m_1<m_{1c}$) dilution effects is always dominant which makes the lower Mw species dominant. In region B ($m_{1c}<m_1<0.5$) temperature effects and dilution effects compete and the prevailing effect determines the dominant component.

lyotropic/thermotropic cooperation/competition that exists in coupled nematodynamics, in terms of concentration and molecular asymmetry.

The full (dashed) line represents the typical boundary of the biaxial region of the component with the higher Mw (lower Mw). The dotted line m_{1c} defines the critical line for lowest possible NI transition. The small square boxes represent the two nematodynamic processes and the vertical arrow(s) indicate how couplings operate in the three regions of the phase diagram; the top (bottom) box correspond to the higher (lower) molecular weight species. At higher concentrations of the higher Mw (first) component (region C: $m_1 > 0.5$) thermotropic and lyotropic effects cooperate and ensure that the higher Mw component controls the overall orientation of the system and it becomes the dominant component (downward arrow). At low concentrations ($m_1 < m_{1c}$: region A), on the other hand, the dilution effects are dominant and lytropicity elevates the lower Mw component to the dominant status (up-ward arrow). In the intermediate regimes ($m_{1c} < m_1 < 0.5$: region B), however, thermotropic and lyotropic effects compete and the controlling effect determines the dominant (major) component (up/down arrows) ; if temperature effects overcome dilution effects the high Mw component becomes dominant otherwise the lower Mw becomes dominant;

(ii) the second factor is that the coupling effects from "dominant" on "slaved" change the usual structures of pure mesogens shown in figure (5-5). The terminology of the schematics on the right Fig.(5-6) is: (A) V_i: viscous effect, E_i: elastic effect, E_{ij}: elastic coupling effect of "i" on "j", (B) up-ward arrow $(\uparrow)$ indicates that the effect tends to align the unit normals to the disks along the extension (**l**) axis, the down-ward arrow $(\downarrow)$ indicates that the effect tends to align the unit normals along the compression (**n-m**) plane; at steady state all the effects must balance. First we note (downward arrow in upper right Fig. (5-6)) that the extensional force within nematodynamics of the dominant component V_D aligns the molecules of the this component preferentially in the compression (**n-m**) plane, reduces μ_{lD} and forms the well-known parallel oblate state, as predicted in eqn.(5.3). At steady state this force is balanced with an elastic force, E_D, which

155

tends to align the molecular unit normals back to the extension direction (upward arrow in upper right Fig. (5-6)). The viscoelastic coupling effect of the "slaved" component on the "dominant" component, denoted $E_{S\text{-}D}$, sensed by dominant component, D, is not as significant as the converse effect. However, the slaved component is significantly affected. The viscoelastic force generated by "slaved" species, V_S, (downward arrow in lower right Fig. (5-6)) tends to align its director to the compression plane and to reduce μ_{lS} like the standard (pure or dominant component) case. However, the coupling effect which tends to align the director to the extension direction, $E_{S\text{-}D}$ (upward arrow in upper right Fig. (5-6)) is large enough to orient the molecules of "slaved" species back to the extension direction and to increase μ_{lS}. As the relationship $\mu_{nS} + \mu_{mS} + \mu_{lS} = 0$ has to be always be satisfied, $\mu_{nS} + \mu_{mS}$ has to decrease to compensate for the increase of μ_{lS}. The decrease in $\mu_{nS} + \mu_{mS}$ can be achieved in several ways (i.e both decrease, one increases and the other decreases, etc.). The self-selected approach observed in Fig. (5-4) is to pick the solution with the minimum number of eigenvalues exchanges such that μ_{nS} remains almost constant and μ_{mS} decreases to compensate for the μ_{lS} increment (see fig. (5-2)). The net result is that $\mu_{lS} = \mu_{mS} < 0, \quad \mu_{nS} > 0$ and a prolate $\perp$ forms. The formation of different structures in the other regions follows the same physics.

5.4.3 Effect of Concentration on the Phase Diagram

To show how the dilution and thermotropic effects choose the dominant component and influence the phase diagram we present the thermorheological behavior at three specific concentrations: (i) at critical concentration $m_1=m_{1c}$, (ii) below critical concentration $m_1<m_{1c}$, region A and (iii) above critical concentration $m_1>m_{1c}$, region C. The intermediate region, region B, exhibits the behavior between the region A and C with more complex behavior. The investigation of this region is beyond the scope of this work. We recall that $m_{1c}=0.308$ is the critical concentration with the lowest nematic/isotropic phase transition.

Figure (5-8) shows the phase diagram at the concentration below critical concentration $m_1=0.1<m_{1c}$ representing regime (A) in figure 5-7. Only regions I,

IV, *V*, *VI*, *VII*, *IX* and *XI* of the generic phase diagram (see Fig. 5-4) appear in this phase diagram. At this concentration, the dilution effect overcomes the thrmotropic effect and turns the second component with the lower Mw (but higher concentration: $m_2=0.9$) into the dominant species. As a result weak flows induce biaxiality only in the second component and it aligns the molecules of the first (slaved) component preferentially in the compression (**n-m**) plane to form a perpendicular oblate (negative ordering) even at low temperatures. As mentioned above this effect corresponds to the asymmetric viscoelastic coupling effect.
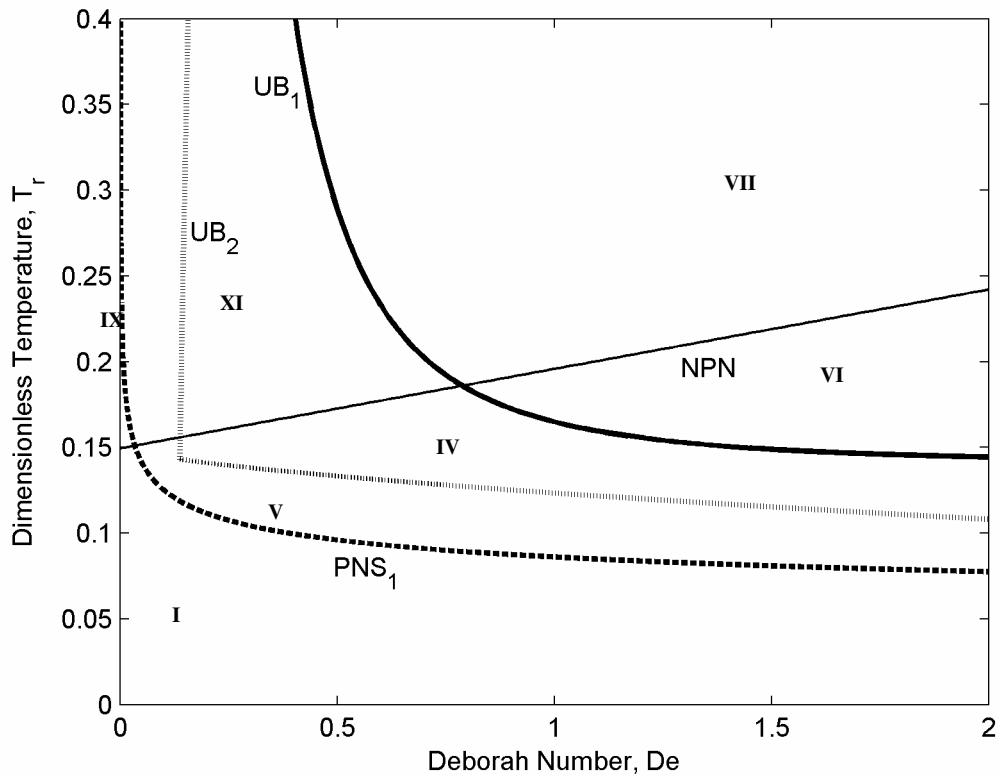
Figure 5- 8. Thermo-rheological phase diagram of the binary mixture at $m_1=0.1<m_{1c}$ in terms of dimensionless temperature T_r and Deborah (De) number. Dilution effect overcomes the thermotropic effect at this concentration and makes the second component with lower Mw and higher concentration ($m_2=0.9$) the dominant component of the system.

Figure (5-9) shows the phase diagram at $m_1=m_{1c}=0.308$ representing line $m_1=m_{1c}$ in figure (5-7). At this concentration the strengths of the dilution and the thermotropic effects are very close and as a consequence more regions of the

generic phase diagram (Regions *I*, *II*, *III*, *VI*, *VII*, *VIII*, *X*, *XI*, and *XII*) appear in this phase diagram. Still the dilution effect is more significant and favors the second component to be dominant. As a result weak flows induce biaxiality only in the second component but slightly stronger flows induce biaxiality in the first (slaved) one. There is a mutual viscoelastic coupling effect, though it is still asymmetric and as a result the second component aligns the molecules of the first (slaved) component back to the extension direction and forms a prolate. Another important observation is that by increasing concentration UB_D and PNS_S move toward each other.
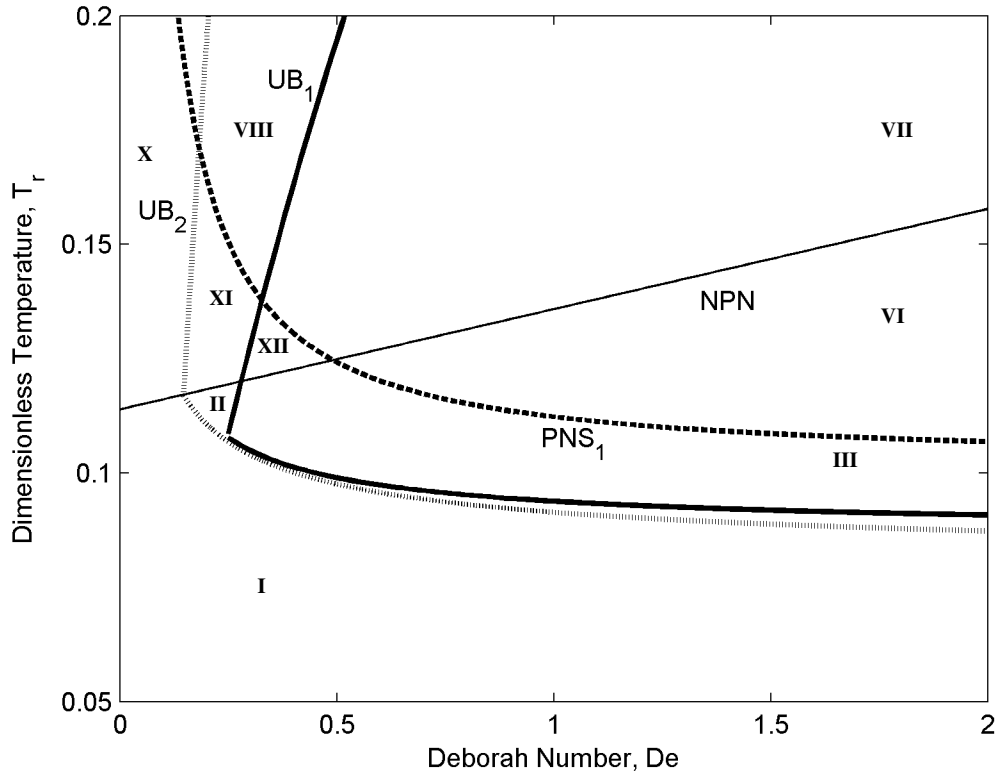
Figure 5- 9. Thermo-rheological phase diagram of the binary mixture at $m_1=0.308=m_{1c}$ representing the line $m_1=m_{1c}$ of figure (5-7) in terms of dimensionless temperature T_r and Deborah (De) number. Dilution effect and thermotropic effect have almost similar contributions and a mutual viscoelastic coupling effect exists in this case, though the dilution effect is still dominant and makes the lower Mw component the dominant one.

Figure (5-10) shows the phase diagram at $m_1=0.7>m_{1c}$ representing regime (C) of figure (5-7).
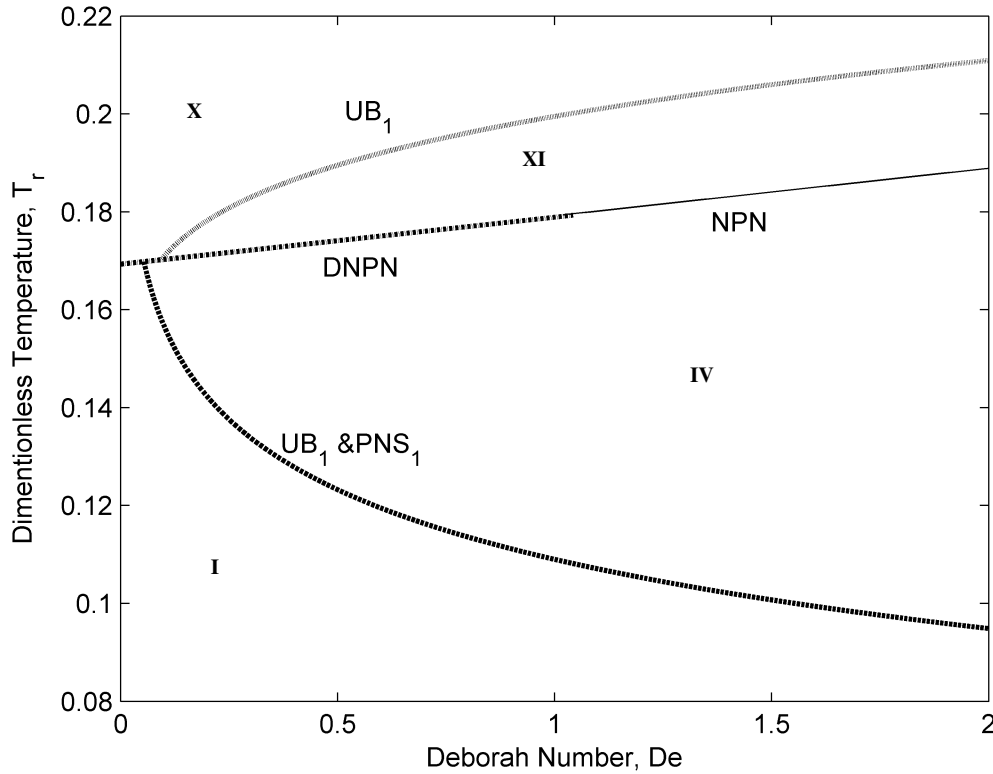
Figure 5- 10. Thermo-rheological phase diagram of the binary mixture at $m_1=0.7>m_{1c}$ representing region C of figure (5-7) in terms of dimensionless temperature T_r and Deborah (De) number. Dilution effect and thermotropic effect both promote the dominancy of the higher Mw component. Viscoelastic coupling effect is strongly asymmetric so that first component influences the structure of the second one but the converse effect is insignificant. Due to the strong asymmetric coupling effect only regions I, IV, X and XI appear in this phase diagram.

At this concentration both the lyotropic and thermotropic effects cooperate and dominant component of the system is the majority high molecular weight species. The viscoelastic coupling effect is almost one way i.e. only the dominant component influences the slaved one and the converse is not true. So only four regions appear in this phase diagram; UB_S line of the generic phase diagram (figure

(5-4)) which shows the formation of biaxiality in the slaved component moves to much stronger flow intensities to the right side of the diagram so that the slaved component is always uniaxial for the range of De investigated. UB_D and PNS_S in this phase diagram have also merged.

5.5 Conclusions

This paper uses the extended Maier-Saupe model for binary mixtures of discotic nematogenes to investigate the effect of steady uniaxial extensional flow and concentration of the components on the orientational structure and molecular order of carbonaceous mesophase mixtures. Through solving the governing equations obtained in our previous work[9] a generic thermo-rheological phase diagram containing four transition lines and twelve orientational and structural regions are obtained (Figs. 5-4, 5-8 to 5-10, Tables 5-1 and 5-2). The computational results show that depending on the concentration of the system an asymmetric viscoelastic coupling is generated between the components such that the dominant component changes the flow-induced structures of the slaved component, but that the converse is not very significant. Comparing the thermo-rheological phase diagram of single component (Fig. 5-5) with the binary one (Fig. 5-4) shows that the flow-response of the dominant component is close to the pure system but the behavior of the slaved one is very different. The deviations from the pure species response to extensional flow are due to coupling effects (Fig. 5-6). The dominant component is selected by the combination of thermotropic and lyotropic (dilution) effects (Fig. 5-7). At high concentration of the higher Mw component (m_1) thermotropic and lyotropic effects cooperate and make the higher Mw component the dominant one. At low m_1s, the dilution effects overcome and make the lower Mw component the dominant one. In the intermediate regimes, however, thermotropic and dilution effects compete and the controlling effect determines the dominant component. When thermotropic effects are controlling the higher Mw component becomes dominant otherwise the overcoming dilution effect makes the lower Mw component dominant. Depending on the relative concentrations of the component the viscoelastic coupling effects shown in figure (5-6) can be absolutely one way (for a large difference between the concentrations) and results in the formation of only uniaxial slaved structure or it

can be mutual (for the smaller concentration differences) and allows biaxiality be induced in both components. The present work provides a foundation in mixing to tune extensional flow strength and concentration to achieve tailored induced structures in carbon fiber-forming processes that are dominated by extensional deformation. Finally, the results can also be applied to rod-like nematics[15], fiber dispersions, and main-chain liquid crystal polymers under biaxial compressional flow.

5.6 References

1. Golmohammadi, M.; Rey, A. D. *Liquid Crystals* **2009,** 36, (1), 75-92.
2. Golmohammadi, M.; Rey, A. D. *Entropy* **2008,** 10, (3), 183-199.
3. Singer, L. S. *Faraday Discussions* **1985**, (79), 265.
4. Ho, A. S. K.; Rey, A. D. *Rheologica Acta* **1991,** 30, (1), 77-88.
5. Sheikh, S. Y. *The Effect of Composition and Shear rate on Mesophase Mixtures.* Clemson University, Clemson, SC, 1999.
6. Chandrasekhar, S. *Liquid crystals.* 2nd ed.; Cambridge University Press: Cambridge [England] ; New York, NY, USA, 1992.
7. Dierking, I. *Textures of liquid crystals.* Wiley-VCH: Weinheim, 2003.
8. Wang, L.; Rey, A. D. *Liquid Crystals* **1997,** 23, (1), 93-111.
9. Golmohammadi, M.; Rey, A. D. *Journal of Non-Newtonian Fluid Mechanics* **2010,** 165, (13-14), 698-711.
10. Rey, A. D. *Rheologica Acta* **1995,** 34, (5), 461-473.
11. Rey, A. D. *Liquid Crystals* **1996,** 20, (2), 147-159.
12. Han, W. H.; Rey, A. D. *Journal of Rheology* **1994,** 38, (5), 1317-1334.
13. Larson, R. L. *The Structure and Rheology of Complex Fluids.* Oxford University Press: New York, 1999.
14. Forest, M. G.; Wang, Q.; Zhou, H. *Liquid Crystals* **2001,** 28, (5), 717-720.
15. Rey, A. D.; Denn, M. M. *Annual Review of Fluid Mechanics* **2002,** 34, 233-266.
16. Tsuji, T.; Rey, A. D. *Journal of Non-Newtonian Fluid Mechanics* **1997,** 73, (1-2), 127-152.

17. Ziabicki, A.; Jarecki, L. *Journal of Non-Newtonian Fluid Mechanics* **2001,** 97, (1), 31-52.

18. Singh, A. P.; Rey, A. D. *Journal De Physique II* **1995,** 5, (9), 1321-1348.

19. Hurt, R. H.; Hu, Y. *Carbon* **1999,** 37, (2), 281-292.

20. Rey, A. D. *Macromolecular Theory and Simulations* **1995,** 4, (5), 857-872.

6. Conclusions and Contributions to Original Knowledge

6.1 General Conclusions

6.1.1 Overview

Bridging the gap between the current knowledge on the ordering behavior of pure DNLCs and the morphology and mechanical properties of carbon fibers based on CMs requires a fundamental understanding of the orientational behavior of DNLC mixtures under varying temperatures and extensional flow rates. The present thesis models the thermodynamics and thermo-rheological behavior of DNLCs binary mixtures by using a statistical mechanics approach. It investigates the effect of characteristics of the mixture i.e. molecular weight of each component, their interaction and concentration as well as the effect of processing conditions i.e. temperature and flow intensity on the molecular orientation and order of each component within the mixture. It also formulates and solves X-ray diffraction intensity and specific heat models to assess the degree of ordering and the level of biaxiality within the mixture. These structural characterization tools are also employed to validate the modeling algorithm as well as the structural predictions of the thesis. The key findings of the thermodynamics, thermo-rheology and characterization predictions are summarized in the following subsections:

6.1.2 Thermodynamic modeling of carbonaceous mesophase mixtures (Chapter 2)

The Maier-Saupe thermodynamic model which predicts the orientational behavior and phase diagram of pure DNLCs is extended to binary mixtures of discotic nematogenes as representative of CMs formed by pure mesogens. The dual thermotropic and lyotropic behavior of the mixtures are demonstrated by phase transitions induced by temperature and concentration changes. Based on the intrinsic properties of the mixture, i.e. molecular weight asymmetry and the interaction between the components, two classes of mixtures are predicted: ideal and non-ideal. Each type exhibits a distinguished temperature-concentration phase behavior, NI transition temperature trend as well as a specific ordering trend: (i)

non-ideal mixtures with non-monotonic NI transition temperatures and reversal of component ordering ($s_1 > s_2 \rightleftarrows s_2 > s_1$) due to the concentration effect; the value of the concentration at which this transition takes place is a critical concentration. The mixture exhibits the minimum value of the transition temperature at the critical concentration; this case is obtained for weakly interacting mixtures and its phase diagram shows lyotropic/thermotropic behavior; (ii) ideal mixtures correspond to the sufficiently strong interaction and highly asymmetric molecular weights; for this case the NI transition temperature monotonically changes by increasing the concentration. The mixture behaves ideally and a critical concentration with ordering reversal can not be obtained. The mixture type as well as the value of the critical concentration can be determined by X-ray intensity measurements and can be also predicted by this characterization tool which is derived mathematically in our work. Experimentally, they also can be detected by any experimental method which measures scalar order parameters.

6.1.3 Entropic Behavior of Binary Carbonaceous Mesophases (Chapter 3)

The extended Maier-Saupe model for binary mixtures of discotic nematogens is used to calculate the orientational entropy and orientational specific heat. These quantities are shown to be useful tools to characterize the type of the discotic nematic liquid crystal and carbonaceous mesophase mixtures, ideal or non-ideal, and to determine nematic ordering and to asses the degree of molecular interaction and molecular weights using standard calorimetric methods: (i) for ideal mixtures entropy and specific heat changes monotonically as a function of concentration at any given temperature. (ii) For non-ideal mixtures entropy and specific heat change non-monotonically as a function of concentration. The critical concentration can be detected by the entropic and specific heat trend: the trends of these quantities before and after this concentration are opposite. For both type of mixtures whenever there is a distinct majority component, orientational specific heat, ΔC_{pr}, and entropy behaves monotonically versus temperature; however, when there is no majority component ΔC_{pr} and entropic trends are non-monotonic with temperature.

6.1.4 Structure and Phase Transitions of Carbonaceous Mesophase Binary Mixtures Under Uniaxial Extensional Flow (Chapter 4)

The extended Maier-Saupe model for binary mixtures of discotic nematogens incorporates the effect of steady uniaxial extensional flow on the orientational structure and molecular order of carbonaceous mesophase mixtures. The concentration and molecular weight dependence of the rotational diffusivity of each component in a mixture, which has a contribution to the flow term, is formulated using the excluded volume of discotics in a binary mixture and a novel power law scaling relation between molecular size and molecular weight. The thermo-rheological phase diagram of each component within the mixture is obtained and indicates that mixing high and lower molecular weight nematogenic species introduces asymmetric coupling effects, such that the higher molecular weight component changes the flow-induced structures of the lower molecular weight component, but that the converse is not true. Comparing the thermo-rheological phase diagram of single component with the binary one shows that the behavior of high molecular weight component is close to the pure system. However, the thermorheological behavior of the low molecular weight component is starkly different than for the pure system. The deviations from the pure species response to extensional flow are due to viscoelastic coupling effects. New expressions for *ODF* and X-ray intensity in binary mesogenic mixtures are also derived and are used to map the different regions of the thermo-rheological phase diagram. The results provide a foundation in mixing to manipulate extensional flow-induced structures in carbon fiber-forming processes.

6.1.5 Structural Modeling of Carbonaceous Mesophase Amphotropic Mixtures under Uniaxial Extensional Flow (Chapter 5)

The extended Maier-Saupe model for binary mixtures of discotic nematogens is used to investigate the effect of steady uniaxial extensional flow and concentration of the components on the orientational structure and molecular order of carbonaceous mesophase mixtures. Through solving the governing equations obtained in this work a generic thermo-rheological phase diagram containing four transition lines and twelve orientational and structural regions are obtained. The

computational results show that depending on the concentration of the system an asymmetric viscoelastic coupling is generated between the components such that the dominant component changes the flow-induced structures of the slaved component, but that the converse is not very significant. Comparing the thermo-rheological phase diagram of single component with the binary one shows that the flow-response of the dominant component is close to the pure system but the behavior of the slaved one is very different. The deviations from the pure species response to extensional flow are due to coupling effects. The dominant component is selected by the combination of thermotropic and lyotropic (dilution) effects. The present work provides a rational approach to tune extensional flow strength and concentration to achieve tailored induced structures in carbon fiber-forming processes.

6.2 Contributions to Original Knowledge

1. The statistical mechanics-based Maier-Saupe model was extended to the binary DNLC mixtures.

2. The effect of molecular weight, molecular interaction and composition of carbon fiber precursors on structural order has been characterized;

3. The presence of ideal and non-ideal binary mixtures has been identified and explained in terms of molecular interaction and molecular weight asymmetry.

4. The critical concentration corresponding to the minimum transition temperature for each ideal mixture is reported.

5. The mathematical model to evaluate the molecular interaction between the components is derived.

6. The model of X-ray diffraction intensity as a function of the orientation distribution function is derived and used to assess orientation and order in the mixture.

7. The equations of orientational specific heat and entropic behavior of DNLC mixtures are derived. These quantities are used to evaluate the transition temperature of each mixture and to determine the type of mixture behavior (ideal and non-ideal).

8. The molecular weight dependency of the rotational diffusivity of discotic mesogens within the mixture through the excluded volume of each component is derived.

9. The thermodynamic Maier-Saupe mixture model is extended to incorporate uniaxial extensional flow. The extended model is used to construct thermo-rheological phase diagrams that predict the structural features of a mesogenic mixture at given temperatures and extension rates.

10. X-ray diffraction intensity of each component in the presence of extensional flow is modeled; this quantity is then employed to evaluate the degree of biaxiality and the ordering structure of each component at different temperatures and flow intensities.

11. Thermotropic/lyotropic cooperation/competition effects of the DNLC mixture at different temperatures and flow intensities are evaluated.

12. The effect of concentration on the thermo-rheological phase diagram of each component within the mixture is investigated; the generic thermo-rheological phase diagram which can serve as the orientational map of the binary mixture to select the proper raw material, processing temperature and flow conditions for a specific application is obtained.

6.3 Validations

The derived theoretical models, the solution algorithm and some of the computational predictions of this work are validated by theoretical, numerical and experimental observations previously reported in the literature. The validations include the following predictions:

- The thermodynamic behavior of the pure system (in terms of S-T_r) obtained in chapter 2 (Figure 2-6) agrees quantitatively with both numerical[1, 2] and experimental[1-3] observations.

- The nematic/isotropic transition temperature (T_{NI}) depression due to the mixing effect predicted for non-ideal mixtures in chapter 2 (Figures 2-8 and 2-9), is qualitatively consistent with both numerical [2, 4] and experimental[2] observations.

- The X-ray intensity-based prediction of the *ODF* reported in chapter 2 (Figure 2-12) is quantitatively verified by both numerical[5] and experimental[5, 6] X-ray trends.

- Heat capacity trends predicted in chapter 3 (Figure 3-7) are qualitatively validated with experimental observations[7-9].

- The Mw dependency of the rotational diffusivity of the discotic components reported in chapter 4 is validated qualitatively with experimental observations[10].

- The formation of the field-induced paranematic phases reported in chapter 4 (in Figure 4-8 for instance) is validated qualitatively with both numerical[11-18] and experimental[12] results.

- The ordering trend in the vicinity of the transition temperature and the formation of the characteristic parabola composed of phase transition points for different field intensities reported in chapter 4 (Figure 4-12a) is validated with the numerical[11, 12, 14] and experimental[12] observations.

- The formation of the uniaxial oblate structure in the paranematic phase under extensional flow effects observed in chapters 4 and 5 (in Figure 4-7 and 4-10 for instance) is validated by the formation of the oblate structure under the extensional and compressional flow in pure discotic systems reported[19] and agrees with random planar structure observed in CM based CFs[20].

- The fact that the director **n** is restricted to the compression plane, reported in chapters 4 and 5, is validated with the reported numerical results[21] and agrees with the 2D orientation patterns in CM based CFs observed experimentally[9, 22].

- The X-ray intensity observation, as the representation of *ODF*, in the presence of external field reported in chapter 4 (Figures 4-13 to 4-15) is quantitatively verified by both numerical investigation of *ODF* of the pure system under the electric field[23] and experimental[24] X-ray trends.

6.4 Recommendations for future work

1. The thermo-rheological behavior of DNLC mixtures in the intermediate concentration region can be studied. Competitive ordering structures are expected to be observed in this region.

2. To achieve the final structure of carbon fibers in the fiber spinning process mesoscopic theories such as Landau de Gennes theory[1, 25] have to be employed. Mesoscopic theories have parameters that are difficult to measure. The Maier Saupe model used in this thesis can be used to predict these model parameters.

3. Thermodynamic and thermo-rheology investigations of the mixture of dissimilar molecules (discs and rods) can be investigated by the present Maier-Saupe theory. Mixtures of rods and disks can represent carbon nanotube/liquid crystalline composites. The current model can be used to describes rod/disc mixtures with the following changes : (i) a negative interaction parameter has to be used as β (see chapter 2, section 2.2), (ii) the rheological shape factor of rods is positive (see chapter 4, section 4.3), and (iii) in the excluded volume of each component in the mixture of dissimilar molecules in the rotational diffusivity model a new expression for the excluded volume of each component has to be derived (see chapter 4, section 4.3).

4. The molecular dynamic, stress tensor and rheological behavior [26] of DNLC mixtures can be obtained by using the orientation distribution function (see chapter 2, section 2.4.2 and section 2.7.2 and chapter 4, section 4.4), tensor order parameter (see chapter 4, section 4.2) and nematic potentials (see chapter 4, section 4.3) obtained in the present thesis.

6.5 Refrences

1. Chandrasekhar, S. *Liquid crystals*. 2nd ed.; Cambridge University Press: Cambridge [England] ; New York, NY, USA, 1992.

2. Nagappa, S.; Nataraju, S. K.; Marthandappa, M. *Molecular Crystals & Liquid Crystals* **1991,** 197, 15-20.

3. Kuczynski, W.; Zywucki, B.; Malecki, J. *Molecular Crystals & Liquid Crystals* **2002,** 381, 1-19.

4. PAlffy-Muhoray, P.; Dunmur, D. A.; Miller, W. H. *Liquid Crystals and Ordered Fluids* **1984,** 4.

5. Ungar, G., *X-ray studies of nematic systems.* In *Physical Properties of Liquid Crystals: Nematics*, Dunmur D.; Fukuda A.; Lucchurst, G., INSPEC, The Institution of Electrical Engineers: London, 2002.

6. Kundu, S.; Naskar, A. K.; Ogale, A. A.; Anderson, D. P.; Arnold, J. R. *Carbon* **2008,** 46, (8), 1166-1169.

7. Sori, M. *Calorimetric measurments in nematics.* In *Physical Properties of Liquid Crystals: Nematics*, Dunmur, D. A.; Fukuda, A.; Luckhurst, G. R., INSPEC: London, 2001; pp 14-50.

8. Yokoyama, H. *Interfaces and thin films.* In *Handbook of liquid crystal research* Collings, P. J.; Patel, J. S., Oxford University Press: New York, 1997; p 196.

9. Lu, S.; Blanco, C.; Appleyard, S.; Hammond, C.; Rand, B. *Journal of Materials Science* **2002,** 37, (24), 5283-5290.

10. Acevedo, A.; Cotts, P. M.; Shine, A. D. *Macromolecules* **2005,** 38, (15), 6648-6655.

11. Maïcssa, P.; Ten Bosch, A.; Sixou, P. *Journal of Polymer Science Part C-Polymer Letters* **1983,** 21, 757-765.

12. Gramsbergen, E. F.; Longa, L.; Dejeu, W. H. *Physics Reports-Review Section of Physics Letters* **1986,** 135, (4), 195-&.

13. P.Palffy-Muhoray, J. J. d., Dunmur, D.A. *Molecular Crystals & Liquid Crystals* **1985,** 127, 301-319.

14. Yamashita, M. *Molecular Crystals & Liquid Crystals* **2003,** 398, 75-85.

15. Popa-Nita, V.; Gerlic, I.; Kralj, S. *International Journal of Molecular Sciences* **2009,** 10, (9), 3971-4008.

16. Matsuda, H.; Koda, T.; Nishioka, A.; Ikeda, S. *Journal of the Physical Society of Japan* **2004,** 73, (10), 2753-2758.

17. Varga, S.; Szalai, I. *Physical Chemistry Chemical Physics* **2000,** 2, (9), 1955-1959.

18. Rey, A. D. *Macromolecular Theory and Simulations* **1995,** 4, (5), 857-872.

19. Forest, M. G.; Wang, Q.; Zhou, H. *Liquid Crystals* **2001,** 28, (5), 717-720.

20. Chung, D. D. L. *Carbon Fiber Composites*. Butterworth-Heinemann: Boston, 1994.

21. Singh, A. P.; Rey, A. D. *Journal De Physique II* **1995,** 5, (9), 1321-1348.

22. Cho, T.; Lee, Y. S.; Rao, R.; Rao, A. M.; Edie, D. D.; Ogale, A. A. *Carbon* **2003,** 41, (7), 1419-1424.

23. Ziabicki, A.; Jarecki, L. *Journal of Non-Newtonian Fluid Mechanics* **1994,** 54, 269-283.

24. Kundu, S.; Ogale, A. A. *Rheologica Acta* **2007,** 46, (9), 1211-1222.

25. DeGennes, P. G.; Prost, J. *The Physics of Liquid crystals*. 2nd Edition ed.; Clarendon Press Oxford, 1995.

26. Larson, R. G. *The Structure and rheology of complex fluids*, Oxford University Press, Inc., Oxford, 1999.

A. Appendix I: Numerical methods

A1.1 Integral evaluation (Simson Quadrature)

In numerical analysis, Simpson's rule is a method for numerical integration, the numerical approximation of definite integrals. Specifically, it is the following approximation:

$$\int_a^b f(x)dx \approx \frac{b-a}{6}\left[f(a)+4f\left(\frac{a+b}{2}\right)+f(b)\right] \tag{A.1}$$

Figure A-1 shows the integrand $f(x)$ which is approximated by the quadratic interpolant $P(x)$, $[a, b]$ as the interval and m the mid point of this interval.
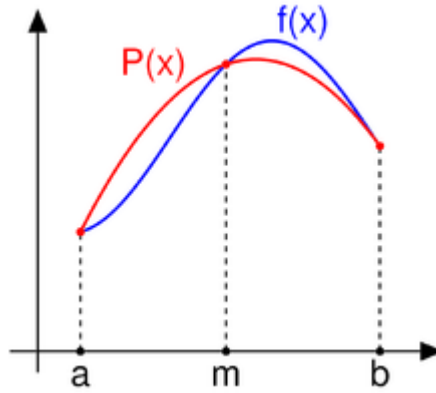
Figure A- 1. **Simpson's rule can be derived by approximating the integrand $f(x)$ by the quadratic interpolant $P(x)$ [1].**

If the interval of integration $[a, b]$ is in some sense "small", then Simpson's rule will provide an adequate approximation to the exact integral. By small, what we really mean is that the function being integrated is relatively smooth over the interval $[a, b]$. For such a function, a smooth quadratic interpolant like the one used in Simpson's rule will give good results. However, it is often the case that the function we are trying to integrate is not smooth over the interval. Typically, this means that either the function is highly oscillatory, or it lacks derivatives at certain points. In these cases, Simpson's rule may give very poor results. One common way of handling this problem is by breaking up the interval $[a, b]$ into a

number of small subintervals. Simpson's rule is then applied to each subinterval, with the results being summed to produce an approximation for the integral over the entire interval. This sort of approach is termed the composite Simpson's rule. Suppose that the interval *[a, b]* is split up in *n* subintervals, with *n* an even number. Then, the composite Simpson's rule is given by

$$\int_a^b f(x)dx \approx \frac{h}{3}\left[f(x_0) + 2\sum_{j=1}^{n/2-1} f(x_{2j}) + 4\sum_{j=1}^{n/2} f(x_{2j-1}) + f(x_n) \right] \qquad (A.2)$$

where *h* is the interval between each two x_j and x_{j+1} points. This method has been employed for the integral evaluation in this thesis[1].

A.2 Newton-Raphson as an iteration method to solve nonlinear equations

Newton-Raphson iterative method is considered as a very powerful method with fast convergence, yet not fool-proof[2] to solve non-linear equations. Here this method is explained. For a single equation:

f(x)=0

the problem is to find $x = \alpha$ such that $f(\alpha) = 0$. Assume that a Taylor series expansion of *f(x)* follows: (the function is regular at $x = \alpha$)

$$f(x+\delta) = f(x) + f'(x)\delta + \frac{f''(x)}{2}\delta + ... \qquad (A.3)$$

For small values of δ and for well behaved functions, the terms beyond linear are not important, hence $f(x+\delta) = 0$ implies

$$\delta = \frac{-f(x)}{f'(x)} \qquad (A.4)$$

so the recursion relation is $x_{i+1} - x_i = -\frac{f(x_i)}{f'(x_i)}$ with i being the iteration number and

the new iteration becomes $x_{i+1} = x_i - \frac{f(x_i)}{f'(x_i)}$.

For a system of non-linear equations:

$$\begin{cases} f_1(x_1, x_2, x_3, \dots x_n) = 0 \\ f_2(x_1, x_2, x_3, \dots x_n) = 0 \\ \vdots \\ f_n(x_1, x_2, x_3, \dots x_n) = 0 \end{cases} \qquad (A.5)$$

or $\underline{f}(\underline{x}) = \underline{0}$

or $f_i(x_j) = 0 \qquad i,\ j=1,2,\dots n$

To apply Newton-Raphson we expand $\underline{f}$ around the Kth iterative

$$f_i(x_j^{K+1}) = f_i(x_j^k) + \sum_{j=1}^{n} \left. \frac{\partial f_i}{\partial x_j} \right|_{x^K} (x_j^{K+1} - x_j) + \dots$$

$$\underline{f}(\underline{x}^{K+1}) = \underline{f}(\underline{x}^K) + \left. \frac{\partial \underline{f}}{\partial \underline{x}} \right|_{x^K} \bullet (\underline{x}^{K+1} - \underline{x}^K) + \dots \qquad (A.6)$$

where $\dfrac{\partial f_i}{\partial x_j} = \dfrac{f_i(x_j + \Delta x_j) - f_i(x_j)}{\Delta x_j}$ is the numerical differentiation and is called the
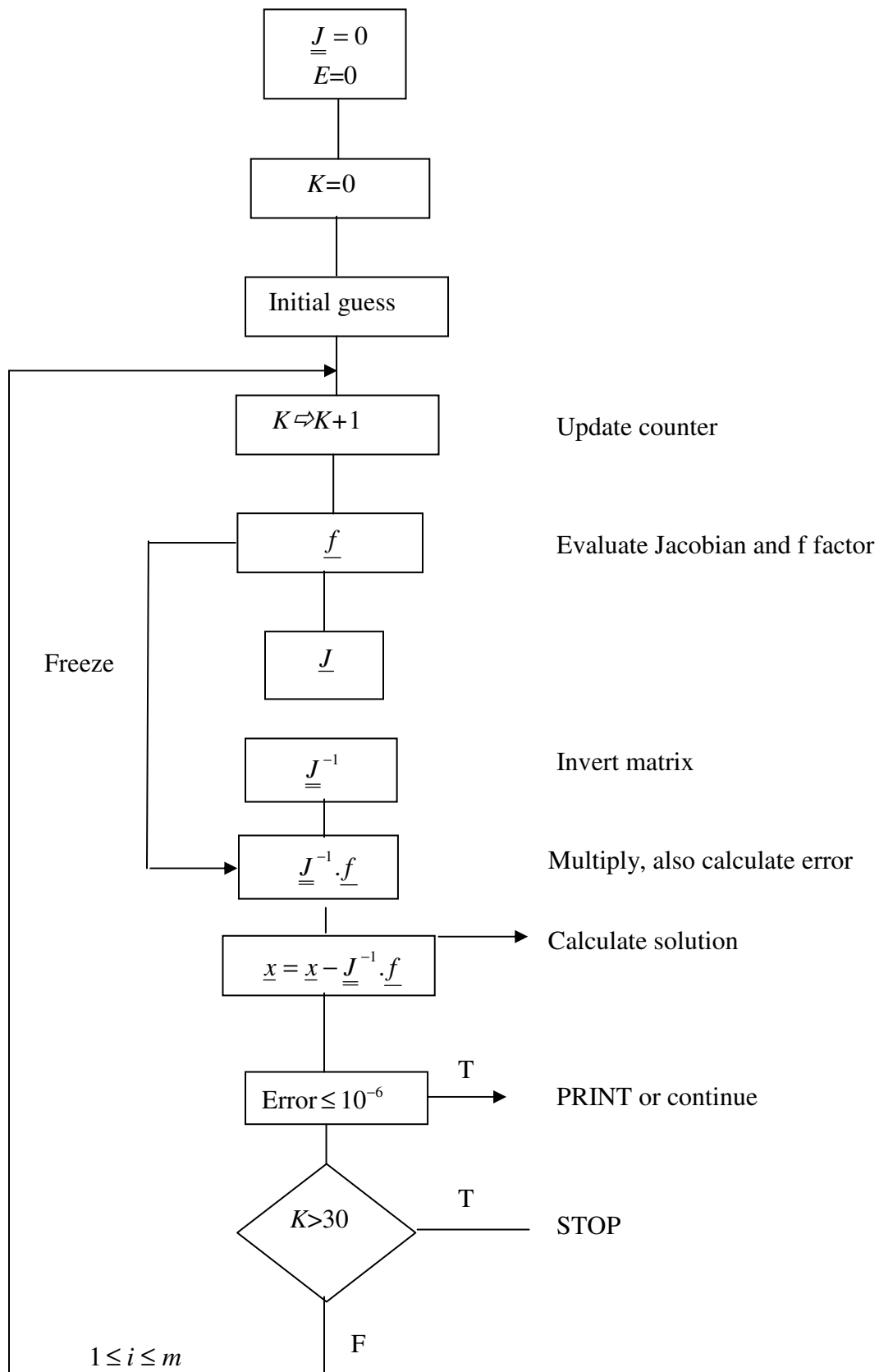
Jacobian Matrix, $J_{ij} = \dfrac{\partial f_i}{\partial x_j}$. To find the solution:

$$x_j^{K+1} = x_j^k - \sum_{j=1}^{n} \left. J_{ji}^{-1} \right|_{\underline{x}^K} f_i(x_j^k)$$

$$\underline{x}^{K+1} = \underline{x}^K - \underline{\underline{J}}^{-1} . f \qquad (A.7)$$

To check the convergence the value of $\underline{f}$ and the difference between successive

values of $\underline{x}$ are used:

$\|x_{i+1} - x_i\|_2 < \varepsilon$ is the convergence criterion where $\varepsilon \sim 10^{-6}$ is usually assumed.

The algorithm of this method is given in Figure A-2.

Figure A- 2. Newton-Raphson Algorithm.

The Newton-Raphson method has been used in this thesis to solve nonlinear algebraic equations. At a specific temperature, an initial guess is assumed and fed

175

to the integral term. The integral term is then evaluated by the Simpson method and then the equation is solved by the Newton-Raphson algorithm, as in figure A-2. The zeroth order continuation method is employed to obtain the initial guess at a specific temperature. For the first temperature, an initial guess is assumed but for the next ones the solution achieved at T_0 is used as the initial guess for the next temperature T_1. Simply

$$\mathbf{u}_{\text{initial}}\left(T_1\right) = \mathbf{u}\left(T_0\right) = \mathbf{u}\left(T_1\right) + \left.\frac{d\mathbf{u}}{dT}\right|_{T_0}\left(T - T_0\right) + HOT \tag{A.8}$$

So in the zeroth order continuation:

$$\mathbf{u}_{\text{initial}}\left(T_1\right) - \mathbf{u}\left(T_1\right) = 0\left[\left.\frac{d\mathbf{u}}{dT}\right|_{T_0}\left(T_0 - T_1\right)\right] \tag{A.9}$$

1. Postolache, M. Metode Numerice, http://en.wikipedia.org/wiki/Simpson's_rule <http://en.wikipedia.org/wiki/Simpson&>.
2. Balagurusamy, E. *Numerical Methods*. McGraw-Hill: New Delhi, 2007.